LARGE DEFORMATION ANALYSIS OF CONTINUUM COMPLIANT MECHANISMS

by

AKANO, Theddeus Tochukwu

(Matriculation Number: 059047004)

B.Eng (Owerri), M.Sc (Lagos), R.Engr, MNSE, MNIMECH

Thesis submitted to School of Postgraduate Studies, University of Lagos, in Partial fulfilment of the requirement for the award of the degree of Doctor of Philosophy

in

Systems Engineering

Department of Systems Engineering
Faculty of Engineering
University of Lagos, Nigeria
2014

CERTIFICATION

SCHOOL OF POSTGRADUATE STUDIES
UNIVERSITY OF LAGOS, AKOKA, LAGOS, NIGERIA

CERTIFICATION

This is to certify that the thesis

"**LARGE DEFORMATION ANALYSIS OF CONTINUUM COMPLIANT MECHANISMS**"

Submitted to School of Postgraduate Studies, University of Lagos for the award of the degree of

Doctor of Philosophy in Systems Engineering
is a record of original research work carried out

by

AKANO, Theddeus Tochukwu
in Department of Systems Engineering

Theddeus T. Akano
--------------------------------------   ----------------------------   ----------------
Authors Name   **Signature**   **Date**

Professor O. A. Fakinlede
--------------------------------------   ----------------------------   ----------------
1st Supervisor's Name   **Signature**   **Date**

Emeritus Prof. V. O. S. Olunloyo.
--------------------------------------   ----------------------------   ----------------
2nd Supervisor's Name   **Signature**   **Date**

Professor O.M. Sadiq
--------------------------------------   ----------------------------   ----------------
1st Internal Examiner's Name   **Signature**   **Date**

Professor A. A. Oyediran
--------------------------------------   ----------------------------   ----------------
2nd Internal Examiner's Name   **Signature**   **Date**

Professor M. A. Waheed
--------------------------------------   ----------------------------   ----------------
External Examiner's Name   **Signature**   **Date**

Professor D. E. Esezobor
--------------------------------------   ----------------------------   ----------------
SPGS Representative   **Signature**   **Date**

DEDICATION

This thesis is dedicated to:

God The Father, The Son and The Holy Ghost. The God who is the creator of the universe and its fullness thereof. May His great name be praised, exalted and glorified now and forever more. AMEN.

ACKNOWLEDGEMENTS

The author wishes to acknowledge the gracious support of the many people that contributed to this work both directly and indirectly. I need to acknowledge Professor O.A Fakinlede that has been a superb and dedicated research supervisor. His mentoring and example have been and will yet be invaluable. I like to acknowledge his moral and financial support. His vision and broad knowledge play an important role in this research work. I also like to thank him for pushing me to the stage that I thought I never could accomplish. I also like to thank my research co-supervisor, Distinguished Professor Emeritus V. O. S. Olunloyo for his continuous moral support and contributions to this success. It is my honour to have had opportunity to work with these great minds and their great characters. Their supports, commitments and contributions have been an inspiration. I am indebted to my vibrant Head of Depaertment, Dr T. A Fashanu and dynamic Departmental Postgraduate Coordinator, Dr F. O. Ogunwolu. These two great men threw in all energies to ensure that thesis was adequately processed. I need also to express my gratitude to the entire academic staff of Department of Systems Engineering: Distinguished Professor Oye Ibidapo-Obe, Dr S. O Asaolu, Dr O. A. Ajofoyinbo, Dr O. O. E. Ajibola, Dr M. K. O.Ayomoh, Dr O. A. Alli, Dr O. P. Popoola, Engr O. A. Adeleye, Engr A. A. Sosimi, Engr J. Ogbehme, Surv C. Onyedikam, Mr O.I. Oluwasuji and Mr K.O. Orolu. I will also not forget the cooperation of the departmental administrative staff: Mrs F. M. Ayoade, Mrs A. Ajayi, Mrs S.Sanusi, Mrs M.Oseni and Mr O. F. Oladipupo.

I consider my family to be my greatest blessing. A special thanks goes to my wife Sandra. Her sacrifices for our family while I struggled with the details of this work are

the main reason this thesis was ever finished. My mothers' continual support and prayers in behalf of my schooling has provided me with motivation and the encouragement to go on. Thanks to my little angels, Olivia and Angelia for singing songs to cheer me up. A worthy thanks equally goes to my elder sister Philomena for her immeasurable support.

I like to thank the following people that have shared their research experience: Professor M. A. Salau, Professor F. N. Okafor, Professor D.E Esezobor, Professor A. A. Oyediran, Dr. M. A. Bodude and Dr M. A. Amuda. Allow me to also acknowledge Dr S.O. Adeosun for sharing his expertise in fatigue prediction and test. Again, I appreciate the moral support from Dr. C.A. Osheku during my very first years of study. I also like to thank the entire staff of Dean's office, especially, Mrs Adaobi Ihedewa and Mr Gbenga. Many thanks also go out to my colleagues in the faculty that have contributed significantly their expertise to help me completing the experiment results presented in this thesis. Also I like to express my gratitude to Dr J.S. Ajiboye and Dr S. J. Ojolo for their supports and contributions that play important role in this thesis.

I also appreciate the supports from these my students: Oba Tobechukwu, Odunjinrin Tolulope, Egbetakin Akintade and Ogundero Micheal. I like also to acknowledge the Sub-Dean, Mr Agbetile, Mr Kingsley, Mr Geoffrey and Mrs Shade Ogunkoya, all from School of Postgraduate Studies for their patience in answering all of my questions.

These token of appreciations should not be complete if I don't mention the sprirtual backing of my spiritual father, His Grace, The Most Rev Professor Daddy Hezekiah MFR. The Annoited Prophet of The Most High God. The Lion of The Tribe of Ibo.

I apologize to every other person who has contributed to the success of this work but has not been recognized. Please, accept my apology and see the omission as unintentional.

ABSTRACT

Compliant mechanisms (CMs) above the traditional rigid-body mechanisms have the sole merit of no relative moving parts hence preventing any form of wear, backlash, noise and need for lubrication. Its applications are versatile and fully domicile in such sectors as medicine, robotics, aerospace, biomechanics, food processing and automotive industries to mention a few. The Pseudo Rigid Body (PRB) equivalence of compliant mechanisms have been the conventional approach used by earlier researchers to analyse compliant mechanisms. Attempts at direct analyses often assume linearity and static conditions. These are justifiable in several situations where compliant mechanisms have been successful in replacing materials with several moving parts. The application domain of compliant mechanisms is widening to dynamic environment where the deformations are relatively large. It is therefore necessary to consider nonlinearities resulting from geometry and hyperelasticity. This work presents a systematic model for the analyses of compliant mechanisms. Methods of continuum mechanics and finite element method were used to model compliant mechanisms. Static and dynamic analyses were carried out using the proposed model. Compliant mechanism (CM) examples are presented. Results from linear, geometric nonlinear together with combined geometric and material nonlinearities assumptions were compared with published laboratory investigated compliant mechanisms. It is revealed that while geometric nonlinear or even linear model could capture the CM output displacement when input load or displacement is 20% of the total input, the results obtained herein have shown that for large input load or displacement, the only reliable result is that from hyperelasticity. The dynamic analysis of CMs show that neglecting material nonlinearity could lead to failure due to end point effect. A Continuum Damage Mechanics (CDM) model is also proposed to assess the fatigue life of polymeric compliant material. The elastic strain energy is computed on the basis of a nearly incompressible hyperelastic constitutive relation. The damage evolution equation is used to develop a Mathematical formula that describes the fatigue life as a

function of the nominal strain amplitude. Fatigue tests experiment were conducted on polymeric compliant materials. The result from the prediction formula shows a strong agreement with that of experiment. It was established that for strain amplitude lower than 0.100 mm/mm, the developed model is more appropriate to predict the fatigue life of polymeric CMs than other compared models. It is expected that the models and results presented here will have a wide spectrum of applications and will effectively facilitate the process of design and optimization of compliant mechanisms.

TABLE OF CONTENTS

CHAPTER 1: INTRODUCTION---1

CHAPTER 2: LITERATURE REVIEW--13

LIST OF FIGURES

LIST OF TABLES

NOMENCLATURES

Ω Domain

$\boldsymbol{X}$ Position vector in reference coordinate

$\boldsymbol{x}$ Position vector in current coordinate

u_{in} displacement at the input boundary

Γ_{in} input boundary

F_{in} applied force

F_{out} virtual force at the output boundary

Γ_{out} output boundary

u_{out} displacement at the output boundary

Γ_g support boundary

Ω_r reference configuration

Ω_c current configuration

$\boldsymbol{E}_i$ unit vector in reference configuration

$\boldsymbol{e}_i$ unit vector in current configuration

F deformation gradient

C Right Cauchy-Green tensor

b Left Cauchy-Green tensor

J determinant of the deformation gradient

u displacement

Ψ strain energy density function

$\boldsymbol{S}$ second Piola-Kirchhoff stress tensor

$U(J)$ dilatation part of the strain energy density function of a nearly
           incompressible material

$\Psi(C)$	deviatoric part of the strain energy density function of a nearly incompressible material
p	hydrostatic pressure
Π_{ext}	functional for effects of body forces and surface tractions
F^{vol}	dilatation part of the deformation gradient
F^{iso}	isochoric part of the deformation gradient
$\bar{C}$	mixed right Cauchy-Green deformation tensor
$\bar{S}$	second Piola-Kirchhoff stress tensor from the mixed right Cauchy-Green deformation tensor
δ	variation
$\delta\Pi_{inner}$	the inner virtual work
$\otimes$	tensor product
$\bar{\tau}$	Kirchhoff stress
tr	trace
N_r	isoparametric interpolations function
B_u	strain displacement matrix
$\bar{p}$	mean stress
$\bar{\mathbb{C}}$	material tangent moduli
$\hat{\mathbb{C}}$	spatial tangent moduli
$\bar{D}$	transformation of spatial tangent moduli
∇N	spatial gradient of the shape function
$\delta\Pi_{internal}$	the internal virtual work
$\delta\Pi_{inertial}$	the inertial virtual work
$\delta\Pi_{ext}$	the external virtual work
t	contact force
b	body force

R	radius of curvature of the beam
a, b	coordinates of end of a beam element
S_x	displacement vector in x coordinate
S_z	displacement vector in z coordinate
T_p	kinetic energy of the beam particles
T_s	kinetic energy associated with transverse shear
α	measure of transverse shear angle
V_a	angular velocity
T_R	kinetic energy due to rotatory inertia
T	total kinetic energy of the beam element
h	thickness of beam element
u_x, u_y, u_z	displacements of the member at any point in the x, y and z directions
τ_{xz}	shear stress
γ_{xz}	shear strain
G_{xy}	shear modulus
A_{xz}	x-z plane area
A_s	shear area
N_{xx}	axial force in the beam
M_{xx}	bending moment in the beam
L_f	Lagrangian function
g_u	Lagrange interpolation function
$\mathcal{G}_i$	first derivative of Lagrange interpolation function
$\Delta_{1\ldots\ldots,6}$	Hermite polynomials
$\lambda_1, \lambda_2, \lambda_3$	principal stretches

LIST OF ACRONYMS

AIDS	Acquired Immunodeficiency Syndrome
CBMM	Compliant Bistable Micromechanism
CDM	Continuum Damage Mechanics
CM	Compliant Mechanism
CMs	Compliant Mechanisms
CMA	Compliant Mechanical Amplifier
CNC	Computer Numeric Controlled
CNT	Carbon Nanotube
CSA	Compliant Stroke Amplifier
DFA	Design for Assembly
DFM	Designs for Manufacture
DNA	Deoxyribonucleic Acid
EDM	Electrical Discharge Machining
ELF	ElectroForce
EFGM	Element-Free Galerkin Method
ESO	Evolutionary Structural Optimisation
FDM	Finite Difference Method
FE	Finite Element
FEA	Finite Element Analysis
FEM	Finite Element Method
GNL	Geometric Nonlinearity
HiL	Hardware in the Loop

HP	Human Plasminogen
HSA	Human Serum Albumin
Hyper	Hyperelasticity
I – DEAS	Integrated Design Engineering Analysis Software
LDPE	Low Density Polyethylene
LDPP	Low Density Polypropylene
MEMS	Micro-Electro Mechanical Systems
MIS	Minimally Invasive Surgery
NASA	National Aeronautics and Space Administration
NCF	Near-Constant-Force
PID	Proportional-Integral-Derivative
PRBM	Pseudo Rigid Body Model
PSA	Prostate Specific Antigen
RVE	Representative Volume Element
SIMP	Solid Isotropic Microstructure with Penalization
SMA	Shape-Memory-Alloys
UFC	Unified Form-assembly
2-D	Two Dimensional
3-D	Three Dimensional

CHAPTER 1: INTRODUCTION

A mechanism is defined as a mechanical device that transfers forces and motions from an input source to output link (Erdman and Sandor, 1991). As shown in Fig. 1.1(a), a conventional rigid-link mechanism is designed to obtain mobility exclusively from rigid body translations and rotations using revolute joints, prismatic joints, and higher order pairs which couple the relative motions of the members. Fig. 1.1(b) is its compliant counterpart that has one of its links sensibly deformable.
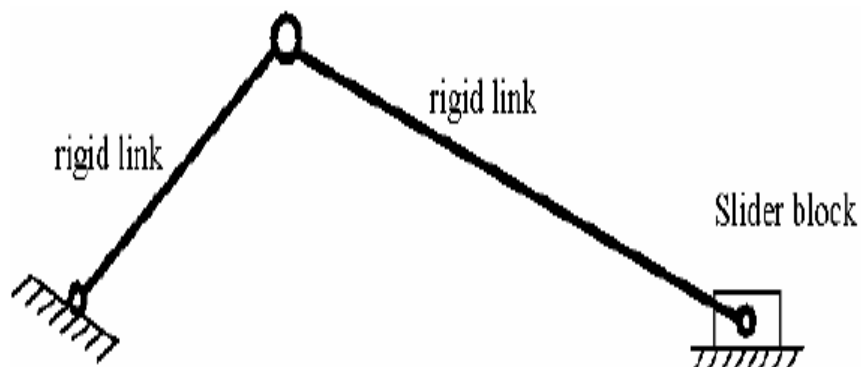
Fig. 1.1(a): A Conventional Rigid Link Mechanism
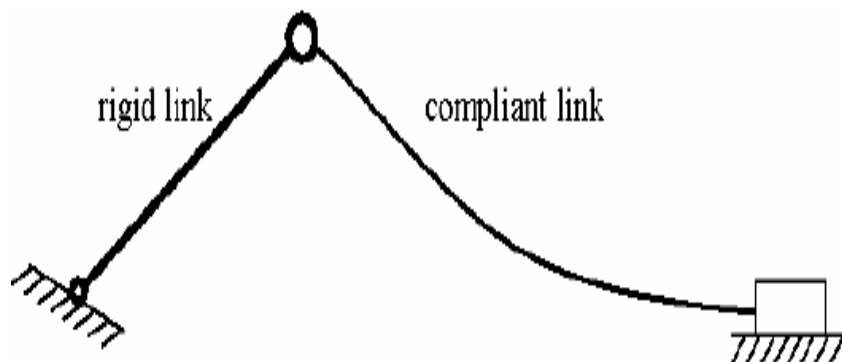
Fig. 1.1 (b): Compliant Mechanism

Traditional mechanisms are engineered to be strong and rigid. The use of flexibility has primarily been avoided due to the increased difficulty in accounting for flexibility and the large potential or performance degradation, such as decreased efficiency, positional inaccuracies, and structural instabilities. In contrast, biological designs such as the thorax of a honeybee or the leg of a grasshopper are *strong and compliant*. By opposing traditional engineering techniques, nature has found clever methods to produce "bio-mechanical devices" which achieve functionality by taking advantage of structural compliance (Vogel, 1998). To parallel biological design, a *compliant mechanism* is defined as a mechanism which exploits flexibility from one or more of its members to achieve controlled transmission of forces and motions. Fig. 1.2 illustrates a monolithic compliant gripper which closes and exerts force on an object in response to an applied input force. The main challenge in designing a compliant mechanism is to effectively synthesize the most efficient structural form (topology, size, and shape) given the functional requirements.
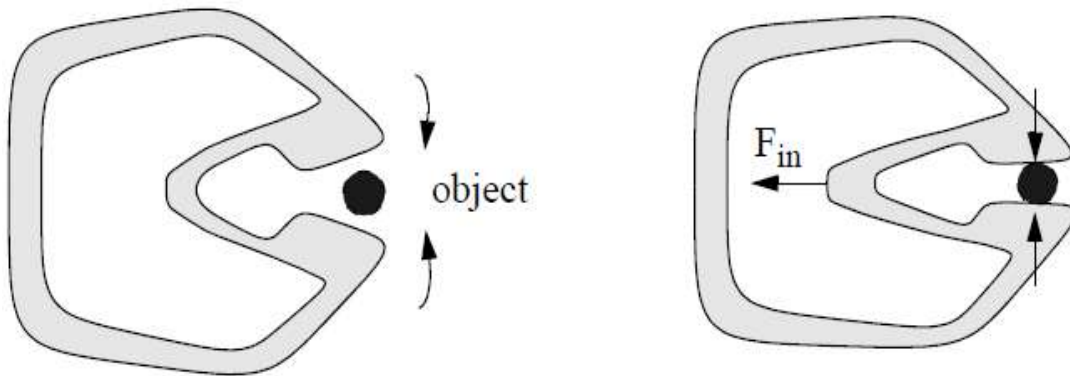
Fig. 1. 2: Illustration of a Compliant Gripper Mechanism

1.1 Background to the Study

Fully compliant mechanisms can be viewed as flexible continua and can be treated as such in their synthesis and analysis (Ananthasuresh and Frecker, 2001). Large and small

deformations of a flexible body can be modelled in the body's actual continuum form instead of Pseudo Rigid Body Models. As such compliant mechanisms can be modelled using the methods of continuum mechanics (Ananthasuresh and Frecker, 2001).The basic idea in the design of compliant mechanism is to recast the design problem as an optimal material distribution problem so that the resulting continuum structure can fulfil the requirements of a mechanism and thus, it is called continuum compliant mechanism (Wang and Cheng, 2009). In this work, we modelled compliant mechanisms using the methods of continuum mechanics. Since the material comprising compliant mechanisms will generally undergo finite strains, displacements, and rotations when the mechanism functions under normal design actuation forces, the analysis and design framework must be general enough to treat finite deformation effects (Swan and Rahmatalla, 2004).

In recent years, the research on the design and analysis of compliant mechanisms has made great progress, at the same time, it has faced many challenges. Compliant mechanisms rely on elastic deformation to achieve force and motion transmission, such deformations are not necessarily small (Howell, 2001). When a structure undergoes sufficiently large deformation, the structure exhibits nonlinear behaviour. This nonlinear behaviour comes from two different sources, namely geometry and material. The former makes it necessary to include nonlinear terms in the displacement-strain relations and the latter results in the failure of linear material model. Although most successful examples of compliant mechanism design and analysis by nonlinear formulation were reported, majority of the designs were based only on nonlinearity due to geometry. The use of linear material model may not be valid in practice because materials with large compliance are often nonlinear materials (Sigmund, 2001a and

2001b). Most engineering materials exhibit nonlinear behaviour when the deformation is sufficiently large. The design and analysis of compliant mechanism should take the material nonlinearity into account because the functionalities of the complaint mechanism are accomplished from its large deformation (Jung and Gea, 2002).

Polymers are commonly used in the design of compliant mechanisms (Howell, 2001). It is important to use the nonlinear characteristics of polymers to analyse the performance of compliant mechanism. Thermoplastic polymers like polypropylene exhibit a viscoelastic material response (Mankame and Ananthasuresh, 2004). It has been frequently noted that with certain constitutive laws, such as those of viscoelasticity and associative plasticity, the material behaves in a nearly incompressible manner (Zienkiewicz and Taylor, 2000). Polymers have small volumetric changes during deformation and as such are incompressible or nearly-incompressible materials (ANSYS, 2012). In general, the response of a typical polymer is strongly dependent on temperature (Bower, 2010). At low temperatures, polymers deform elastically, like glass; at high temperatures the behaviour is viscous, like liquids; at moderate temperatures, the behaviour is like a rubbery solid. Hyperelastic constitutive laws are intended to approximate this rubbery behaviour. Polymers are capable of large deformations and subject to tensile and compression stress-strain curves (Gong and Moe, 2002). The simplest, yet relatively precise description for this type of material is isotropic hyperelasticity (Gong and Moe, 2002). Nearly incompressible hyperelasticity model is employed to reproduce the elastic responses for the constitutive theory of finite viscoelasticity (Marvalova, 2006)

.

1.2   Statement of the Problem

Designing a compliant mechanism (CM) for a specific application can be a complex problem. The basic trade-off is between the flexibility to achieve deformed motion and the rigidity to sustain external load (Li and Kota, 2002). Many researchers have proposed various synthesis techniques for creating a viable CM, including topology and shape optimization methods. Many of these methods for topology and dimensional synthesis were based on kinetostatic design specifications and do not consider the dynamic effects in the design stage. The resulting designs are therefore valid for static or low frequency applications. The dynamic effects can be significant and for instance, a CM may exhibit a very different mechanical advantage at high frequencies compared to what it was designed for under static situations (Li and Kota, 2002). In fact, the impact of dynamic behaviour is of great importance in improving the design of CMs, especially for complex mechanisms such as aircraft systems and micro-electro mechanical systems (MEMS). To improve on the performance and operation accuracy of such compliant mechanisms, the dynamic and static analysis of CMs need to be further studied. However, to get the most reliable result, both the material and geometric nonlinearities must be incorporated into the model.

1.3   Aim and Objectives of the Research

This research is aimed at reducing risk of failure of compliant mechanisms due to improper analysis. The objectives of the research are:

    i.   To develop a model that can adequately capture the effect of geometric and material nonlinearities to the analysis of CMs.

    ii.   To investigate the combined effect of geometric and material nonlinearities to the analysis of CM.

iii. To investigate the influence of shear deformation in the nonlinear analysis of CMs.

iv. To develop a mathematical model for the fatigue failure prediction of polymeric CMs at any strain cycle.

1.4 Scope of the Research

This research is concerned with the incorporation of both geometric and material nonlinearity to the analysis of compliant mechanisms. Throughout this work, compliant mechanisms with the following characteristics are considered:

- Since most compliant mechanisms are designed for planar manipulation, we will focus on two dimensional problems in this research.
- Compliant mechanisms idealized as flexible continuum
- The material response is considered as being isotropic.
- The operating condition is moderate temperature.

1.5 Significance of the Study

When compliant mechanisms are used over time, they have tendency to deform as a result of stress, fatigue, temperature and other mechanical and environmental factors. Compliant mechanisms are used by different industries for different tasks. Different applications of compliant mechanisms have different deformation limit. It is important for the users of such systems to have indicators of the permissible deformation limit of such systems in order to avoid catastrophic failure especially in mission critical systems/industries such as aerospace systems, surgery in medicine etc. Our proposed model will help the developers of compliant mechanisms to incorporate sensor based indicators capable of predicting the deformation limit which can guide the users of such

systems to understand the deformation behaviour of the compliant mechanism. This work will show great significance in reliability and safety of CMs using proper methodology.

1.6   Definition of Terms

Anisotropy   Variation of material properties with direction. Both global and local user defined coordinate systems can be used to define anisotropic material properties.

Body Forces   Forces distributed through the volume of a body.

Cauchy Stress   The most fundamental stress measure defined as force/deformed area in fixed directions not following the body.

Compliant Mechanism Flexible mechanisms that transfer an input force or displacement to another point through elastic body deformation.

Constitutive Equations The equations formulating the stress-strain relationship of a material.

Constraint   Constrains the displacement or rotations to zero or a specified value.

Contact Model   The Mathematical method to model bodies that come into contact with each other.

Continuum   A body that can be continually sub-divided into infinitesimal elements with properties being those of the bulk material.

Continuum Damage Mechanics	Concerned with the representation, or modelling, of damage of materials that is suitable for making engineering predictions about the initiation, propagation, and fracture of materials.
Continuum Mechanics	A branch of mechanics that deals with the analysis of the kinematics and the mechanical behaviour of materials modelled as a continuous mass rather than as discrete particles.
Coordinate System	Global Cartesian, local geometrical, application specific, and user-defined coordinate systems. Loads, constraints, material properties, and variables are defined in a specific coordinate system.
Cycle Counting	Method that transforms an arbitrary load cycle into a well-defined stress description.
Cycles to Failure	Limiting number of repeatable load cycles that will cause fatigue.
Damage	Accumulated state in the material that degrades the performance of the structure. A microstructural change that results in a deterioration of material properties
Damage Parameter	Explains how much of the material that is damaged
Deformation	The change in shape and/or size of the body from an initial or undeformed configurations.
Deformation Gradient	Tensor containing the complete information about the local straining and rotation of the material. It is a positive definite second rank tensor.

Endurance Limit / Fatigue Limit	The highest repeatable stress a material can be subjected to and not experience any fatigue. An attention should be made to weather the endurance limit is the maximum stress or the amplitude stress. Both stress measures are given by material data providers.
Elasticity Matrix	The matrix relating strain to stresses.
Equilibrium Equation	The equation expressing the equilibrium formulated in the stress components.
Eulerian	Model described and solved in a coordinate system that is fixed (spatial frame).
Fatigue	A term describing the phenomena where a component fails after repeated loadings and unloadings. The progressive and localized structural damage that occurs when a material is subjected to cyclic loading.
Fatigue Life	The number of applied repeated stress cycles a material can endure before failure.
Geometric Nonlinearity	In solid mechanics, the deformation state characterized by finite (or large displacements) but small to moderate strains. Sometimes referred to as nonlinear geometry.
Green-Lagrange Strain	Nonlinear strain measure used in large-deformation analysis.
Hyperelasticity	A constitutive relation used to model rubbers and rubbery materials.

Isotropic Material	A material where the material properties are independent of direction.
Lagrangian	Model described and solved in a coordinate system that moves with the material.
Large Deformation	The deformations are so large so that the nonlinear effect of the change in geometry or stress stiffening need to be accounted for.
Load Cycle	A well-defined load history that after sufficient number of repetitions can lead to fatigue.
Mechanism	A system of moving parts that changes an input motion and force into a desired output motion and force.
Mixed Formulation	A formulation used for nearly incompressible materials, where the mean stress have been added as a dependent variable to avoid numerical problems.
Material Nonlinearity	The type of nonlinearity that arises when a material exhibits non-linear stress-strain relationship.
Principle of Virtual Work	States that the variation in internal strain energy is equal to the work done by external forces.
Pseudo Rigid Body Model	A way of representing CMs using their rigid body components that have equivalent force-deflection characteristics.
Rubbery	A way of depicting nonlinear materials that exhibit nonlinear constitutive characteristics of rubber.

Second Piola-Kirchhoff Stress	Conjugate stress to Green-Lagrange strain used in large deformation analysis.
Strain Energy	The energy stored by a structure as it deforms under load.
Strain	Relative change in length, a fundamental concept in structural mechanics.
Stress	Internal forces in the material, normal stresses are defined as forces/area normal to a plane, and shear stresses are defined as forces/area in the plane.
Time-Dependent Study	A time-dependent or transient study shows how the solution varies over time, taking into account mass, mass moment of inertia, and damping.

1.7   Organisation of the Thesis

This thesis consists of six chapters and each chapter is divided into sections and subsections. These provide a detailed description of the subject matter and make for easy reading and referencing. The chapters of the thesis are itemised below:

- Chapter One introduces the constructal theory and presents the motivation, justification and background of the study.

- Chapter Two provides literature reviews on the subject of basic theory with the focus on the assumptions taken in the analysis of compliant mechanism by early researchers.

- Chapter Three contains the detailed methodology for the problem to be solved. This includes the nonlinear finite element and detailed continuum mechanics formulations.

- Chapter Four deals with the experimental set up for the fatigue prediction test that includes the test sample, Electroforce machine and Wintest interface.

- Chapter Five shows the results generated from the respective models and the validation from laboratory published results.

- Chapter Six provides a general summary of the findings of the study. It also presents the conclusions and contributions, as well as recommendations for future work.

CHAPTER 2: LITERATURE REVIEW

The literature review is divided into many parts. First the history, classification, applications and other preliminary review of compliant mechanisms, methodology and solution are introduced. Finally, review of prior and related works on compliant mechanisms were carried out.

2.1 History of Compliant Mechanism

Mother Nature has used compliance since the beginnings of life in things such as plants, bird wings and legs of small insects. Inventions inspired from nature, have used deflections in their mechanism designs. For example, bows (Fig. 2.1) and catapults rely on the energy stored in a deflected beam to propel their missiles across long distances. Tweezers grasp small objects between two flexible beams. Various types of springs and some hinges also use deflections to achieve the motion desired.

Fig. 2.1: Historical Bow

The ability of mankind to synthesize the design of compliant mechanism has only existed for a short time. Euler was the first to quantify the deflection of flexible beams with the development of the Bernoulli-Euler equation (Howell, 2001).

A compliant mechanism can be defined as single piece flexible structure, which uses elastic deformation to achieve force and motion transmission (Frecker *et al.,* 1997; 1999). It gains some or all of its motion from the relative flexibility of its members rather than from rigid body joints alone (Howell, 2001). Such mechanism, with built-in flexible segments, is simpler and replaces multiple rigid parts, pin joints and add-on springs. Hence, it can often save space and reduce costs of parts, materials and assembly labour. Fig. 2.2 illustrates a monolithic compliant gripper which closes and exerts force on an object in response to an applied input force. The main challenge in designing a compliant mechanism is to effectively synthesize the most efficient structural form (topology, size, and shape) given the functional requirements.
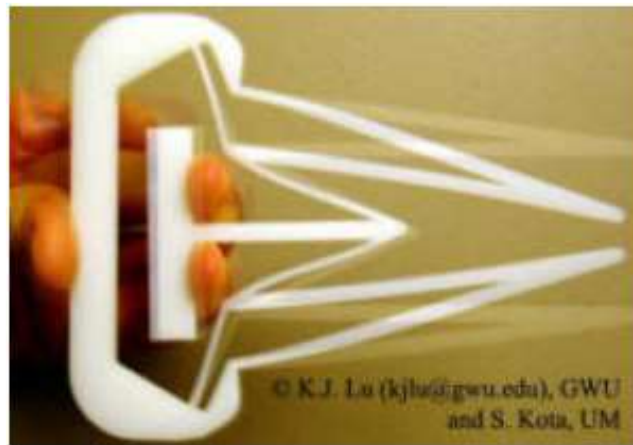
Fig. 2.2: Compliant gripper mechanism

Other possible benefits of designing compliance into devices may be reductions in weight, friction, noise, wear, backlash and importantly, maintenance. There are many familiar examples of compliant mechanisms designed in single-piece that has replaced rigid-link mechanisms, which will be highlighted in other section in this study. Fig. 2.3, shows examples of compliant mechanisms commonly used.

14
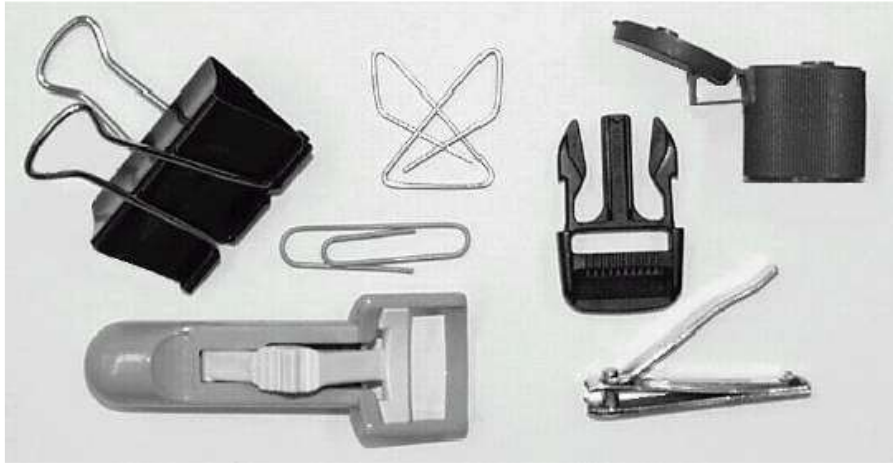
**Fig. 2.3: Common compliant devices; a binder clip, paper clip,
backpack latch, lid, eyelash curler and nail clippers**

We can simply manufacture a single-piece fully compliant mechanism via injection moulding, extrusion and rapid prototyping for medium size devices (Mortensen *et al.,* 2000), or using silicon surface micromachining (Larsen *et al.,* 1997) and electroplating techniques (Chen, 2001) for compliant micromechanisms. Although a compliant mechanism gives numerous advantages, it is difficult to design and analyse. Much of the current compliant mechanism design, however, must be performed without the aid of a formal synthesis method and is based on designer's intuition and experience (Sigmund, 1997; Frecker, 1997; Solehuddin *et al.,* 2002). Several trial and error iterations using finite element models are often required to obtain the desired mechanism performance.

2.2   Classification of Compliant Mechanisms

Compliant mechanisms can be classified by the various rigid and flexural elements which make up the device (Ananthasuresh *et al.,* 1994) as shown in Fig. 2.4. *Partially compliant mechanisms* contain rigid mechanical members and conventional joints combined with compliant members. *Fully compliant mechanisms* contain no mechanical joints and gain mobility strictly from elastic deformation.

**(a) Partially Compliant Mechanism
Lumped Compliance**

**(b) Partially Compliant Mechanism
Distributed Compliance**

**(c) Fully Compliant Mechanism
Lumped Compliance**

**(d) Fully Compliant Mechanism
Distributed Compliance**
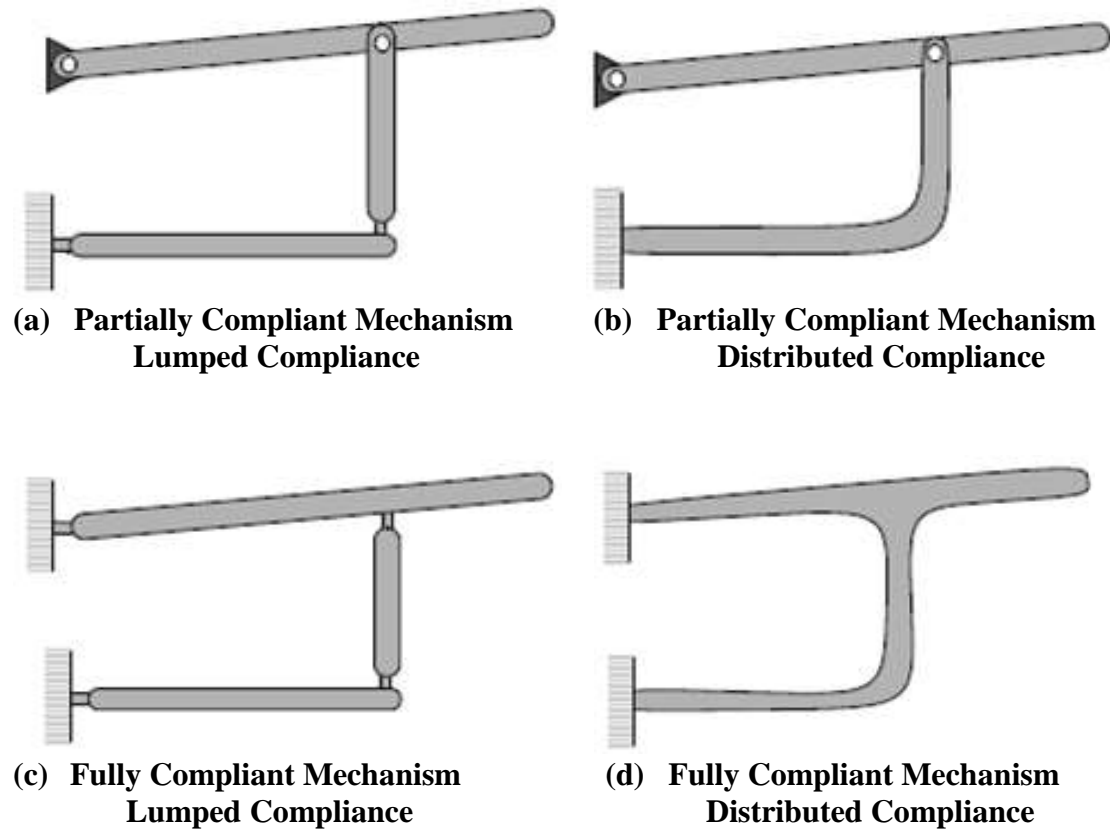
Fig. 2.4: Classification of Compliant mechanism

A compliant member can facilitate elastic deformation by concentrating strains in small regions or more evenly distributing strains throughout the structure. *Lumped compliant mechanisms* which concentrate strains in small regions are characterized by thin flexural segments which can model the behaviour of revolute joints. *Distributed compliant mechanisms* do not contain the characteristic thin flexible segments, but rather distribute the strain more-or-less uniformly along the flexible members. Distributed compliant mechanisms are advantageous over lumped compliant mechanisms in that stress concentrations are generally avoided.

2.3   Applications of Compliant Mechanisms

New competitive products must meet the growing demands of the market. They must be light-weighted, resource efficient, durable, stable and have a low noise emission. At

the same time, the products must be introduced quickly into the market. For the fulfilment of these demands, it is necessary to use the advantages of compliant mechanisms. Compliant mechanisms are applicable in various fields such as adaptive structures, components in transportations, hand-held tools, electronics, robotics, medical, etc. for numerous reasons.

2.3.1 Adaptive Structures

Adaptive structures have the ability to adapt, evolve or change their properties or behaviour in response to the environment around them. The analysis and design of adaptive structures requires a highly multi-disciplinary approach which includes elements of structures, materials, dynamics, control, design and inspiration taken from biological systems. Development of adaptive structures has been taking place in a wide range of industrial applications, but is particularly advanced in the aerospace and space technology sector with morphing wings, deployable space structures; piezoelectric devices and vibration control of tall buildings.
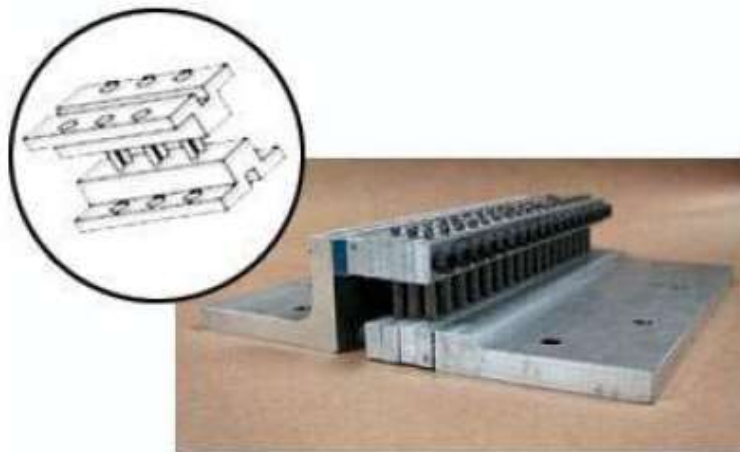
Fig. 2.5: Basic Building Block for NASA Goddard's Compliant Mechanisms

Example include Compliant Cable Technology that was developed by National Aeronautics and Space Administration (NASA) Goddard Space Flight Centre. In

structural connections, these mechanisms provide compliance and dampening. They permit motion in the primary direction and selective motion in other directions. This provides subtle cushioning, twisting and realignment, which allows mating and contact surfaces to conform to each other. The essential functional element-the bending element-of NASA Goddard's compliant mechanism consists of a short cable section.

The configuration and material are varied according to the specific application requirements (Barghout, 2003). The bending element is constrained at each end in cantilever fashion (Fig. 2.5). A snap-fit mechanism can be engaged by simply pushing the two counter parts together. However, it is not a favoured choice in design for disassembly since it is often difficult to disengage without making any destruction to the components. Li *et al.* (2002) have demonstrated the design of reversible snap-fit compliant mechanism, which actuated with localized thermal expansion of materials through time transient heat transfer within the structure. Compliant mechanical amplifiers are used for piezoelectric actuators to increase effective stroke of the actuator (Canfield and Frecker, 2000; Frecker and Canfield, 2000). Furthermore, the actuators designed may be used in smart structures applications such as helicopter rotor blade control.

2.3.2 Biomechanical Application

Motivated by the successful application of compliant mechanisms in robotics and automation, its extension to biomechanics are now emerging and several cutting-edge research topics are currently been studied. We introduce some of these topics in the following sections.

2.3.2.1 Compliant Prosthetic Sockets

The geometry of the residual limb, liner and socket were acquired from computed tomography (CT) data of a transtibial amputee. The compliant features consisted of thin-wall sections and two variations of spiral slots integrated within the socket wall (Fig. 2.6).

<div align="center">

(a) Side View   **(b) Frontal View**
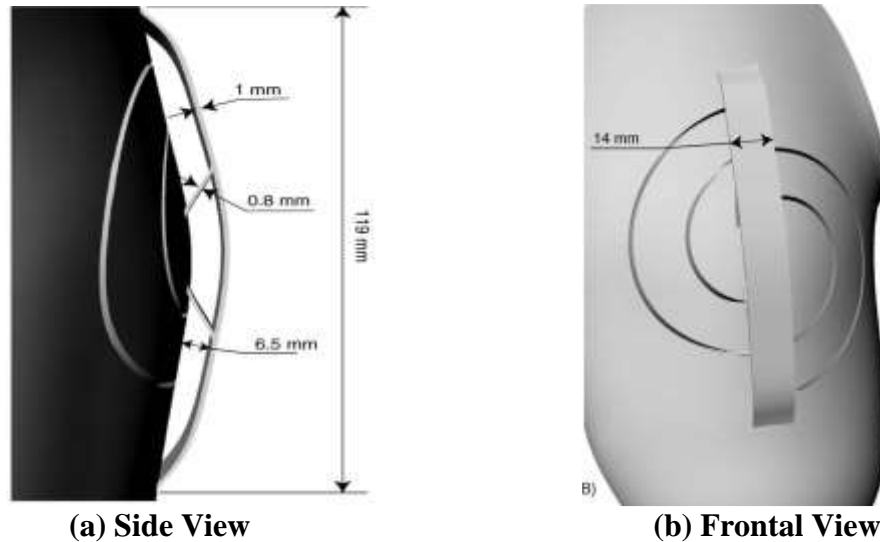
Fig. 2.6: Compliant support Prosthetic Sockets

</div>

One version of the spiral slots produced the largest pressure relief, with an average reduction in local interface pressure during single-leg stance (20–80% of the stance phase) from 172 to 66.4 kPa or 65.8% compared to a baseline socket with no compliant features. The integration of local compliant features is an effective method to reduce local contact pressure and improve the functional performance of prosthetic sockets (Mario *et al.,* 2006).

2.3.2.2 Biosensors

Micro cantilever beams have recently found applications in bio-medical research. Wu *et al.,* (2001) developed a cantilevered microscopic chip to detect prostate specific antigen (PSA) in human blood. As PSA sticks to the antibodies, the cantilevered chip

19

bends like a diving board as shown in Fig. 2.7(a), where the left cantilever bends as the protein PSA binds to the antibody. The other cantilevers, exposed to different proteins found in human blood serum (human plasminogen (HP) and human serum albumin (HSA)), do not bend because these molecules do not bind to the PSA antibody. The cantilevers themselves are about 50 microns wide (half the width of a human hair), 200 microns long (a fifth of a millimetre), and half a micron thick. The micro-cantilever technique has applications beyond prostate cancer. Any disease, from breast cancer to AIDS, with protein or DNA markers in blood or urine could conceivably be assayed by arrays of these micro-cantilevers.

(a) **Cantilever Sensors**   (b) **Molecular Motors**
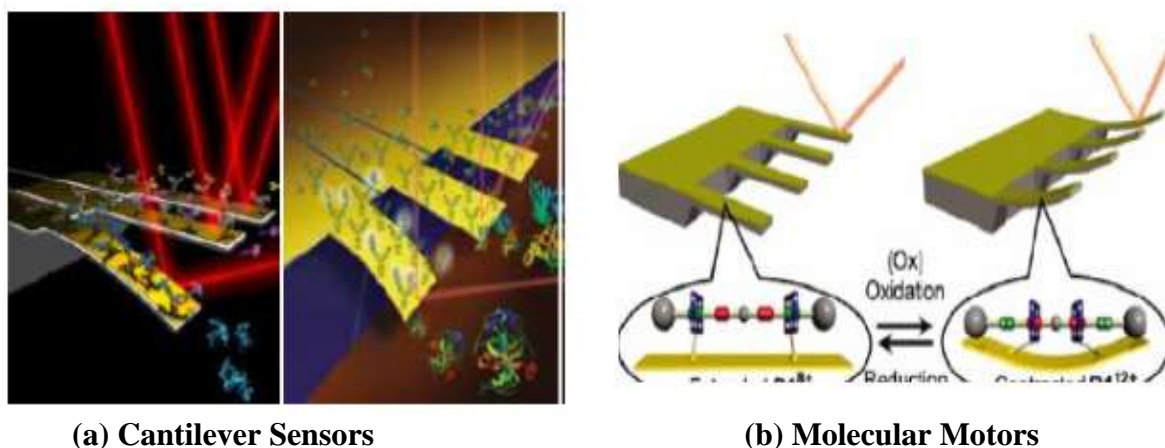
Fig. 2.7: Biosensors

Another application of micro cantilever beams is shown in Fig. 2.7(b). The array of micro cantilever beams, coated with a monolayer of edox-controllable (Huang *et al.,* 2004) rotaxane molecules, undergoes controllable and reversible bending when it is exposed to chemical oxidants and reductants. Conversely, beams that are coated with a redox-active but mechanically inert control compound do not display the same bending. The capability of transferring chemical energy to mechanical energy in this micro cantilever has potential of reduced scale operations compared with traditionally micro scale actuators.

2.3.3 Components in Transportations

An aircraft wing based on a compliant mechanism would bend and twist as a single piece to control flight, eliminating separate control surfaces such as ailerons, spoilers and flaps. This, in turn, simplifies construction and yields potentially much higher performance (Sanders, 2003). This design modification have the following benefits:

- Reduces radar cross-section thereby improving stealth characteristics; reduces weight and complexity; and increases aircraft maneuverability.
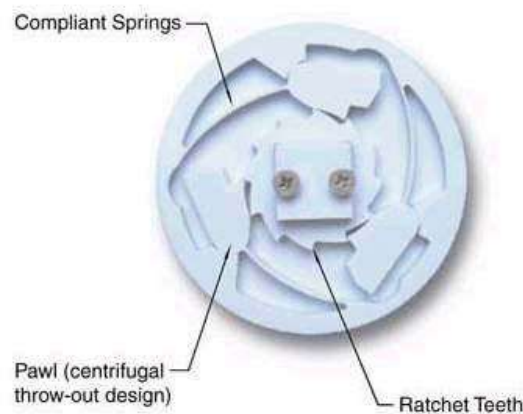
Fig. 2.8: Overrunning pawl clutches

Fig. 2.9: Bicycle brakes

- Over-running pawl clutches (Roach, 1998; Roach *et al.,* 1998; Roach and Howell, 1999), with or without centrifugal throw out, provide torque in one direction but freewheel in the other. They are used for one- and two-way rotation, as in pull-starts for small engines, bicycle and "Big Wheel®" free wheels, fishing reels, gear drives,

winches, conveyors, elevators, counters, collators, feed mechanisms and many other machines (Howell, 2003(a)) (Fig. 2.8).

- Centrifugal clutches made as compliant mechanisms eliminate numerous segments, springs, pins, rivets, etc. Flexible segments are designed into the single moving part so that when the hub (driven by a motor) spins the clutch up to speed, centrifugal force causes the heavy segments to engage the drum and drive the machinery. Small and medium horsepower applications include gokarts, mini-bikes, trimmers, tillers, chain saws, chippers, amusement rides, agriculture and industrial machine couplings (Howell, 2003(b)).

- Bicycle brakes of compliant design provide absolute parallel motion, have visual appeal and are preferred by experts for their strength, superior control, even wear and reduced noise (Mary, 2003). See example in Fig. 2.9.

2.3.4 Hand-Held Tools

Monolithic stapler helps in simplifying the design for assembly (DFA) and designs for manufacture (DFM) as shown in Fig. 2.10 (Ananthasuresh, 2003).

**Fig. 2.10: The number of separated parts in previous stapler (right)
Monolithic Stapler (left)**

Vibration damping for power tools: Reciprocating tools such as jackhammers, rivet guns and hammer drills can cause repetitive motion injuries such as nerve damage and

carpal tunnel syndrome. The vibration transmitted from the tool while it is operating causes the damage. Cable compliance technology can effectively reduce this vibration through shock isolation. Because it is small, this NASA technology can also be applied to hand tools (Barghout, 2003).

2.3.5 Electric and Electronic (EE) Systems

Microelectromechanical Systems (MEMS) are small, compliant devices for mechanical and electrical applications. MEMS are fabricated using techniques developed for the production of computer chips. Most MEMS devices are barely visible to the human eye with many features 1/50 the diameter of a human hair. However, they can perform micromanipulation tasks by converting thermal, electrostatic, mechanical, optical, electromagnetic or electrical energy to some form of controlled motion. Examples of MEMS application are medical instruments for in-body surgery, hearing aids, air-bag sensors, micro pumps and optics and tilting mirrors for projection devices (Sigmund, 1997).

Fig. 2.11: Bistable (2- position) mechanisms

Near-constant-force (NCF) electrical connectors use compliant technology to maintain constant connection between electrical connections over long periods of time. The majority of computer hardware and automotive electrical problems arise from faulty electrical contact integrity. The NCF electrical connector improves connections and

reliability (Howell, 2003(c)). Bistable (2-position) mechanisms move between two stable conditions (Open and Close positions, as in Fig. 2.11) and are useful as switches, circuit breakers, clamps, snap hinges, closures, positioning devices, etc. Though they require external force to move from position 1 to 2, no holding energy is required to remain in either position. Plastic prototypes have exceeded a million cycles in durability tests (Howell, 2003(c)).

2.3.6 Vibration Isolation Systems

Compliant mechanisms have been designed for various types of applications to transmit desired forces and motions. Tantanawat *et al.* (2004) explore an application of compliant mechanisms for active vibration isolation systems. For this type of application, an actuator and a compliant mechanism are used to cancel undesired disturbance, resulting in attenuated output amplitude. An actuator provides external energy to the system while a compliant mechanism functions as a transmission controlling the amount of displacement transmitted from the actuator to the payload to be isolated. They proposed compliant mechanisms as a means to provide efficient and low cost active vibration isolation. Fig. 2.12(i) shows the use of compliant mechanism as a substitute to the usual springs and dampers in Fig. 2.12(ii).

(a) Feed Forward Control   **(b) Feed Back Control**
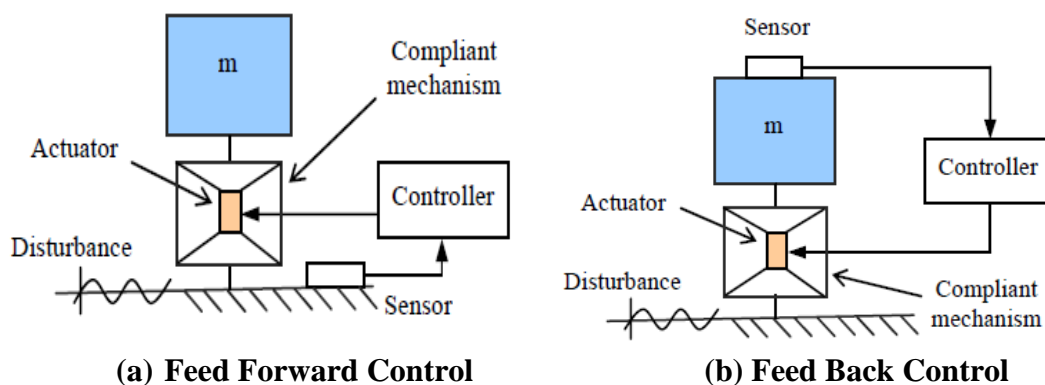
Fig. 2.12(i): Models illustrating the concept of using a compliant mechanism in an active vibration isolation system
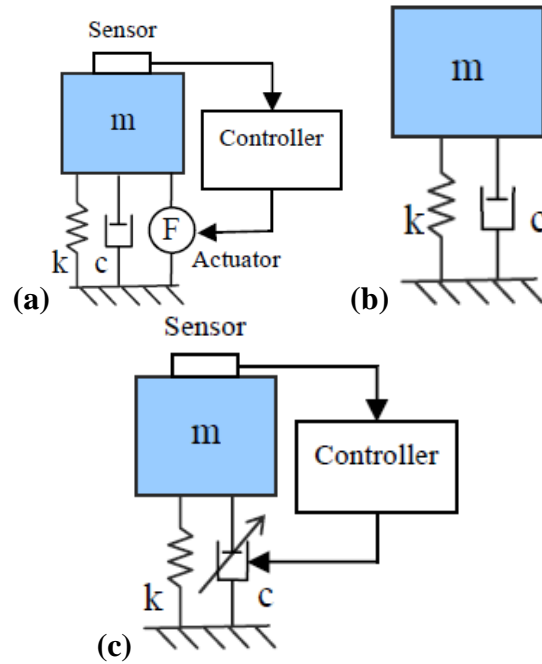
Fig. 2.12(ii): Simple models showing basic elements in different types of vibration isolation systems; (a) active, (b) passive, and (c) semiactive system

2.3.7   Automotive Seat Cushion

Jutte (2008) explored the use of nonlinear spring to replace the foam of the automotive seat cushion. The initial design was able to reduce the foam thickness to less than half of its original size without compromising the passenger's comfort and safety. Fig. 2.13 shows the automotive seat cushion and its compliant counterpart of equal strength.

Fig. 2.13: (a) Automotive Cushion   (b) Compliant Nonlinear Spring Seat

2.3.8   Live Bird Transfer System

Fig. 2.14 shows a live bird transfer system (Chao-Chieh, 2005). The system consists of ten compliant fingers, four compliant graspers, and two compliant indexers. The bird is supported between a pair of "compliant hands" that moves in the *y* direction.
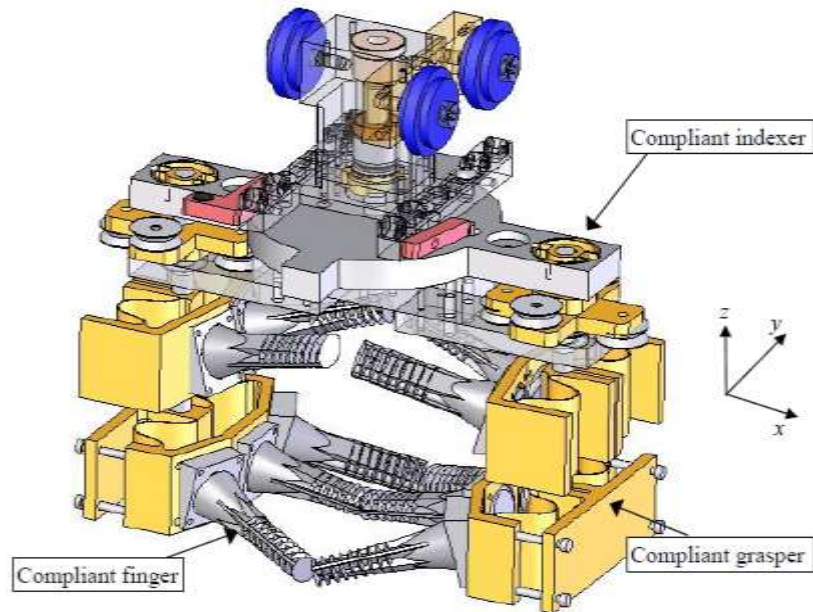
Fig. 2.14: Live Bird Transfer System

Each hand consists of lower fingers, upper fingers and two compliant graspers, whose functions are stated as follows:

- The three lower fingers support the weight of the bird while transferring.

- The two upper fingers prevent the bird from flapping and escaping the hands. Both the upper and lower fingers are designed to accommodate with a limit range of bird sizes in the *z* direction.

- Compliant graspers are designed to accommodate a limit range of bird sizes in the *x* direction.

In addition, the two compliant indexers are used to position a shaft that rotates the compliant grasper in the *z* direction every 90 degrees. They are compact in size and can replace traditional actuators. As will be shown, the proposed model can greatly simplify the design and analysis of these compliant mechanisms.

2.3.9   Medical

Physical therapy: A walker that uses NASA's cable compliance technology enables patients with limited use of their legs and lower backs to be supported for walking therapy (Mitchell, 2003).

Compliant end-effector (Frecker, and Dziedzic, 2001) **and piezoelectric actuator (**Edinger *et al.,* 2000): They are used for Minimally Invasive Surgery (MIS). A new compliant suture needle grasper has been designed for use in MIS procedures. This design eases the sterilization over current MIS tool designs.

Joint prosthesis: Prosthetic devices are typically expensive and short-lived and only the most expensive provide "human-like" response.

The compliant joint provides resistance similar to a human limb because of its nonlinear nature: as the cable in the joint bends the stiffness increases whereas standard mechanical devices have constant stiffness (Mitchell, 2003). Fig. 2.15 presents the compliant technology applied to a knee joint.

Fig. 2.15: 2-Knee-joint engineering prototype

2.3.10   Biomechanics

Biomechanics is the area that specializes in cardiovascular, orthopaedic, rehabilitation engineering and simulation. There are plenty of potential devices which can be simplified into single piece component such as joint at knee, hip, pelvic, etc. or to make the components to be more compliance with the natural flow of blood such as artificial heart valve.

2.3.11   Sports

2.3.11.1   Pole Vault

Compliant mechanisms find an important use in the sport of pole vaulting as shown in Fig. 2.16(a), which shows a sequence of movements by a world-class male pole vaulter.
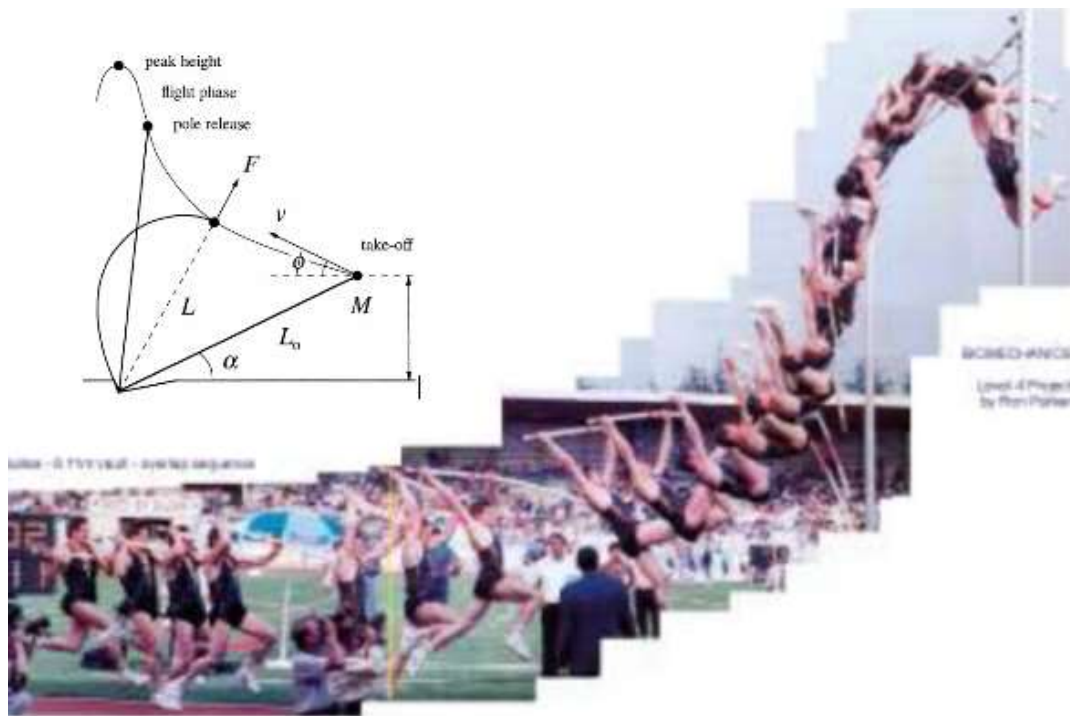
Fig. 2.16: Model of the vaulter with a flexible pole

Linthorne (2000) discussed the flexible pole's advantages in the pole vault by modelling the pole vaulting with flexible pole and predict the optimum take-off technique for a typical world-class pole vaulter. As illustrated in Fig. 2.16(b) which

28

shows the vaulter trajectory, the flexible pole acts as an energy transformer that transforms the kinetic energy of the vaulter into potential energy in the vaulting process.

2.3.11.2 Flex-Run

As shown in Fig. 2.17, Flex-Run was first introduced in 1984 by prosthetic user and research inventor Van Phillips. The advantages of Flex-Run over conventional prosthetic feet are its light weight and compliance.

(a) Side View   **(b) Vari-Flex**

(c) Flex-Run for Athletics

Fig. 2.17: Flex-Run Products

Two critical breakthroughs made this product unique and revolutionized the everyday aspirations of amputees. First, energy storage and release, is a function inherent in the patented carbon fibre design of Flex-Run. Second, vertical shock absorption enables a more natural gait and protects the sound limb and remaining joints of the amputated limb from excessive shock. Today different functions are available within the Flex-Run range to suit individual needs.

2.3.12   Robotics

NCF compression mechanism use compliant technology to achieve near-constant pressure with a deviation of only 2% in the compression forces. Several configurations have been designed to work over a range of travel patterns. No NCF compression mechanism is known on the market yet, so the opportunities are great. Uses of NCF compression mechanisms might include fitness products, robot end effectors, tool holder, motor brush holder, wear test apparatus and safety devices (Howell, 2003(c)).

2.4   Syntheses of Compliant Mechanisms

Typically, the two approaches known in the literature for the systematic syntheses of compliant mechanisms are the kinematics based approach (Howell and Midha, 1996) and the structural optimization based approach (Saxena and Ananthasuresh, 1998).

2.4.1   Kinematics-based approach

In kinematics approach, compliant segments are illustrated as several rigid links connected together by pin joints and torsional springs are added to resist torsion. The value of spring constants and where to place it in the model are calculated differently depending on types of segments. There are several familiar segments assigned by Howell and Midha (1996), i.e., small-length flexural pivots, cantilever beam with force at the free end (fixed pinned), fixed-guided flexible segment, initially curved cantilever beam and pinned-pinned segment. Different types of segments require different models; Howell discussed briefly how they might be applied to compliant mechanisms. Although this method is easier to analyse compared to its compliant counterpart, however, mechanism's force-deflection relationships are still difficult to be determined. Typically, there are two approaches introduced to determine existing relationship from

pseudo rigid-body models. The first method uses conventional Newtonian methods i.e., each links are analysed to obtain static equilibrium. Thus, the force system for the entire mechanism is established. On the other hand, principle of virtual work can also be selected to determine force-deflection relationship. The approach views the system entirely and does not include all the reaction forces (Howell, 2001). Typically, kinematics-based approach is well suited with mechanisms that undergo large, nonlinear deflections. Besides, this approach requires starting with a known rigid-links mechanism.

2.4.2 Structural Optimization Based Approach

In this approach it is not required to begin with a known rigid link mechanism. It focuses on the determination of the topology, shape and size of the mechanism (Saxena and Ananthasuresh, 2000). A numerical approach of topology optimization starts with a domain of material to which the external loads and supports are applied (Sigmund, 2000). The objective function is often the compliance, that is, the flexibility of the structure under the given loads, subject to a volume constraint. In general, there are two types of design domains i.e., ground structure (Ansola *et al.,* 2002) and continuum structures (Pedersen *et al.,* 2001). Ground structure uses an exhaustive set of truss or beam/frame elements in the design domain. The individual cross-section is defined as design variables. When the cross sectional area of an element goes to zero, that element will be removed. Thus after the optimization procedure converges, some elements will be removed from the original exhaustive set. The remaining elements will define the topology for the compliant mechanism (Saxena and Ananthasuresh, 2000).

In the continuum structures, design domain is typically divided into appropriate finite elements where every element has intrinsic structural properties (Funchs *et al.,* 2000). In solving topology optimization problems using this kind of domain (continuum), three major approaches are used. One is the homogenization method, which is based on the assumption of microstructure in which the properties are homogenized (Allaire and Castro, 2002). There are three design variables associated with each finite element. Two of them represent the dimensions of the rectangular hole in the element and the last one is for the orientation of the hole. The element is considered anisotropic due to the hole. Another approach is the density method in which the material density of each element is selected as the design variables. The density method assumes the material to be isotropic and each design variable varies between zero and one and the intermediate values should be penalized to obtain a "black and white" (zero-one) design (Borrvall and Petersson, 2001). Several penalization techniques have been suggested. In the SIMP approach (Solid Isotropic Microstructure with Penalization), a powerlaw model is used, where intermediate densities give very little stiffness in comparison to the amount of material used. Another approach is to add a concave penalty function that suppresses intermediate values to the objective function (Stolpe and Svanberg, 2001(a), (b)). The third approach is the evolutionary structural optimisation (ESO). The original idea of this method is to gradually remove lowly stressed elements to achieve the optimal design (Bulman *et al.,* 2001).

2.5   Fabrication of Compliant Mechanisms

2.5.1 Micro Fabrication

Fabrication of microstructures can be done using silicon surface micromachining in thin film materials. Currently, two-dimensional (2-D) fabrication procedures are well

developed, but effort is devoted to the development of fabrication methods for two-and-a-half and fully three-dimensional (3-D) micro mechanisms (Larsen *et al.,* 1997). However, there are relatively few of those machines existing in the world to fabricate MEMS in the quantities that are needed (Sorosiak, 2001).

2.5.2 Macro fabrication

Using traditional machining methods to fabricate flexible members of compliant mechanisms give a lot of challenges. But, since many new methods of fabrication have been developed recently, such as the use of 3-axis computer numeric controlled (CNC) milling, laser cutting, wire electrical discharge machining (EDM), abrasive water jet and rapid prototyping which make it possible to develop a prototype of compliant mechanisms (Mortensen *et al.,* 2000). However, in each of those methods, there is still limitation either from the machine itself or the material that will be used. Therefore, before proceeding into the drawing and machining phase, it is important to properly interact with the machine and material. For instance, care must be taken to ensure that there is enough space for the cutter to pass through the mechanisms or to design a mechanism with possible minimum radii and thickness that can be cut (Mortensen *et al.,* 2000).

2.6 Differences between Linear and Nonlinear Analysis

The differences between linear and nonlinear analysis are vital and one will realize there are optimum times to use one type of analysis versus the other. The term "stiffness" defines the fundamental difference between linear and nonlinear analysis. Stiffness is a property of a part or assembly that characterizes its response to the applied load. A number of factors affect stiffness:

1. **Shape**: An I-beam has different stiffness from a channel beam.

Fig. 2.18: An I-Beam and a Channel

2. **Material**: An aluminium beam is less stiff than the same size steel beam.

Fig. 2.19: An Aluminium Beam and a Steel Beam

3. **Part Support**: A beam with a simple support is less stiff and will deflect more than the same beam with built-in supports.
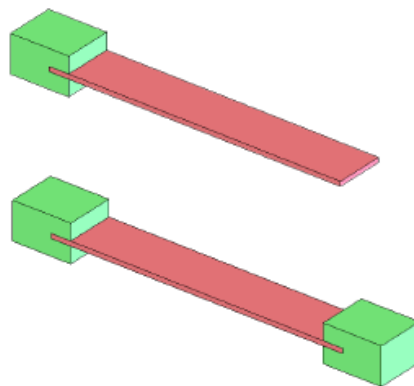
Fig. 2.20: A Cantilever and Two Fixed Supports

When a structure deforms under a load its stiffness changes, due to one or more of the factors listed above. If it deforms a great deal, its shape can change. If the material reaches its failure limit, the material properties will change. On the other hand, if the change in stiffness is small enough, it makes sense to assume that neither the shape nor material properties change at all during the deformation process. This assumption is the

fundamental principle of linear analysis. That means that throughout the entire process of deformation, the analysed model retained whatever stiffness it possesses in its undeformed shape prior to loading. Regardless of how much the model deforms, whether the load gets applied in one step or gradually, and no matter how high the stresses that develop in response to that load may be, the model retains its initial stiffness. This assumption greatly simplifies problem formulation and solution. Recall the fundamental Finite Element Analysis (FEA) equation:

$$[F] = [K]\{u\} \tag{2.1}$$

Where,

$[F]$ is the known vector of nodal loads

$[K]$ is the known stiffness matrix

$\{u\}$ is the unknown vector of nodal displacements

This matrix equation describes the behaviour of FEA models. It contains a very large number of linear algebraic equations, varying from several thousand to several million depending on the model size. The stiffness matrix $[K]$ depends on the geometry, material properties, and restraints. Under the linear analysis assumption that the model stiffness never changes, those equations are assembled and solved just once, with no need to update anything while the model is deforming. Thus linear analysis follows a straight path from problem formulation to completion. It produces results in a matter of seconds or minutes, even for very large models. Everything changes upon entering the world of nonlinear analysis, because nonlinear analysis requires engineers to abandon the assumption of constant stiffness. Instead, stiffness changes during the deformation process and the stiffness matrix $[K]$ must be updated as the nonlinear solver progresses through an iterative solution process. These iterations increase the amount of time it takes to obtain accurate results.

2.7   Understanding Different Types of Nonlinear Behaviour

Although the process of changing stiffness is common to all types of nonlinear analyses, the origin of nonlinear behaviour can be different, making it logical to classify nonlinear analyses based on the principal origin of nonlinearity. Because it isn't possible to point out a single cause of nonlinear behaviour in many problems, some analyses may have to account for more than one type of nonlinearity.

2.7.1   Geometric Nonlinearity

As already discussed, nonlinear analysis becomes necessary when the stiffness of the part changes under its operating conditions. If changes in stiffness come only from changes in shape, nonlinear behaviour is defined as geometric nonlinearity. Geometric nonlinearities refer to the nonlinearities in the structure or component due to the changing geometry as it deflects. Such shape-caused changes in stiffness can happen when a part has large deformations that are visible to the naked eye. That is, the stiffness $[K]$ is a function of the displacements $\{u\}$. The stiffness changes because the shape changes and/or the material rotates. The program can account for five types of geometric nonlinearities:

1. *Large strain* assumes that the strains are no longer infinitesimal (they are finite). Shape changes (e.g., area, thickness, etc.) are also taken into account. Deflections and rotations may be arbitrarily large.

2. *Large displacement and rotation* assumes that the displacement and rotations are large but the mechanical strains (those that cause stresses) are small and are evaluated using linearized expressions. The structure is assumed not to change shape except for rigid body motions. The elements of this class refer to the original configuration.

3. *Stress stiffening* assumes that both strains and rotations are small. A first order approximation to the rotations is used to capture some nonlinear rotation effects.

4. *Spin softening* also assumes that both strains and rotations are small. This option accounts for the radial motion of a body's structural mass as it is subjected to an angular velocity. Hence it is a type of large deflection but small rotation approximation.

5. *Pressure load stiffness* accounts for the change of stiffness caused by the follower load effect of a rotating pressure load. In a large deflection run, this can affect the convergence rate.

A generally accepted rule of thumb suggests conducting a nonlinear geometry analysis if the deformations are larger than 1/20th of the part's largest dimension. Another important factor to recognize is that in cases of large deformations, the load direction can change as the model deforms. Most FEA programs offer two choices to account for this direction change: following and non-following load. A following load retains its direction in relation to the deformed model. A non-following load retains its initial direction.

A pressure vessel subjected to very high pressure that undergoes a drastic change of shape provides another good example of the latter situation. The pressure load always acts normal to the walls of the pressure vessel. While linear analysis of this scenario assumes that the shape of the vessel does not change, realistic analysis of the pressure vessel requires analysing geometric nonlinearity with nonconservative loading (Fig. 2.21). Changes in stiffness due to shape can also occur when the deformations are small.

A typical example is an initially flat membrane deflecting under pressure. Initially, the membrane resists the pressure load only with bending stiffness. After the pressure load has caused some curvature, the deformed membrane exhibits stiffness additional to the original bending stiffness.
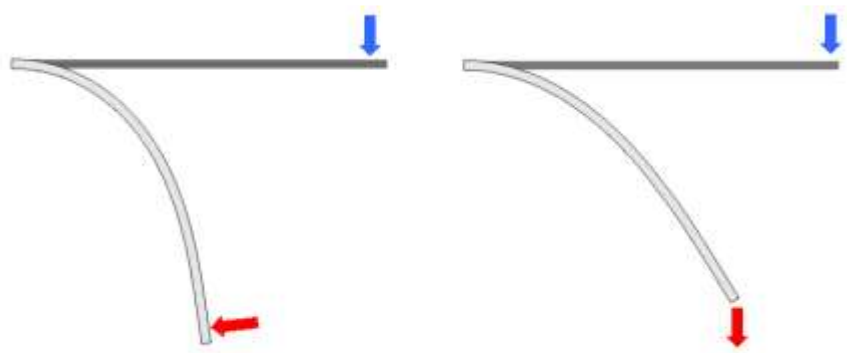
Fig. 2.21: Following (or nonconservative) load changes its directionduring the process of deformation and remains normal to the deformed beam (left). Nonfollowing, or conservative, load retains its original direction (right).

Deformation changes the membrane stiffness so that the deformed membrane is much stiffer than the flat membrane. Some FEA programs use confusing terminology, calling all analysis of geometric nonlinearities "large deformation analysis." This ignores the necessity to perform nonlinear analysis for smaller deformation.

2.7.2   Material Nonlinearity

If changes of stiffness occur due to changes in material properties under operating conditions, the problem is one of material nonlinearity. A linear material model assumes stress to be proportional to strain. That means it assumes that the higher the load applied, the higher the stresses and deformation will be, proportional to the changes in the load. It also assumes that no permanent deformations will result, and that once the load has been removed the model will always return to its original shape. Although this simplification is acceptable, if the loads are high enough to cause some

permanent deformations, as is the case with most plastics, or if the strains are very high (sometimes > 50 percent), as occurs with rubbers and elastomers, then a nonlinear material model must be used. Due to the vast differences in how various types of materials behave under their operating conditions, FEA programs have developed specialized techniques and material models to simulate these behaviours. Table 2.1 offers a short review of what material models work best for which problem.

Table 2.1: Classification of Nonlinear Material Models

Material Classification	Model	Comment
Elastoplastic	Von Mises or Tresca	These models work well for material for which a strain-stress curve shows a 'plateau' before reaching the ultimate stress. Most engineering metals and some plastics are well-characterized by this material model
	Drucker-Prage	This model works for soils and granular materials.
Hyperelastic	Mooney-Rivlin, Ogden and Neo Hookean	Work well for incompressible elastomers such as rubber
	Blatz-Ko	This model works for compressible polyure- than foam rubbers.
Viscoelastic	Several (optional with other models)	This model works for hard rubber or glass.
Creep	Several (optional with other models)	Creep is a time-dependent strain produced under a state of constant stress. Creep is observed in most engineering materials, especially metals at elevated temperatures, high

		polymer plastics, concrete, and solid propellant in rocket motors
Superelastic (Shape memory alloys)	Nitinol	Shape-memory-alloys (SMA) such as Nitinol present the superelastic effect. This material undergoes large deformations in loading-unloading cycles without showing permanent deformations

2.8 Impact of Nonlinear Analysis on Designed Products

The nature of frequently encountered analysis problems should be the yardstick by which to justify a decision to add nonlinear analysis capabilities to the engineer's analysis. If day-to-day work requires nonlinear analysis only occasionally, it may be better to ask for the help of a dedicated analyst or to hire a consultant. If, because of the nature of the designed products, design analysis problems routinely involve large deformations, membrane effects, nonlinear material, contact stresses, buckling, or nonlinear supports, then nonlinear analysis capabilities should be added to the analysis (SolidWorks, 2008).

Nature is nonlinear (Sugihara, 2010). That means linear analysis can only approximate the real nonlinear behaviour of parts and assemblies. Most of the time, such an approximation is acceptable, and linear analysis can provide valuable insight into product characteristics. In many cases, however, linear assumptions differ too much from reality and provide crude or misleading information (Trehan, 2011). Using the results of linear analysis to decide if a part will fail under its operating loads may lead to overdesign. For example, a bracket design analysed only with linear analysis requires the designer to stick with a requirement that stress must not exceed the yield. But

40

nonlinear analysis may show that some level of yielding is acceptable. In that event, it becomes possible to save on the amount of material used or to choose a less expensive material without compromising structural integrity. An engineer may be concerned about too large deflection of a flat panel tested with linear analysis. The panel might be overdesigned to compensate for that deflection without ever knowing that linear analysis exaggerated the deformations. Once an engineer gains enough experience to recognize nonlinear problems, it becomes obvious that application of this technology is not confined to exotic situations. Designs that require or may benefit from nonlinear analysis abound in every industry and in everyday design practice. To this end, compliant mechanisms fall into the category of engineering structures that exhibit nonlinear characteristics.

2.9   Nonlinear Analysis in Everyday Design Practice

Once an engineer gains enough experience to recognize nonlinear problems, it becomes obvious that application of this technology is not confined to exotic situations. Designs that require or may benefit from nonlinear analysis abound in every industry and in everyday design practice. Below are several examples of products where the correct design decision requires nonlinear analysis. Many of these problems involve more than one type of nonlinear behaviour.

2.9.1   Idler Pulley

This stamped steel pulley may buckle under belt load before it develops excessive stresses. Although a linear buckling analysis may be enough to determine the buckling load, nonlinear analysis is required to study its post buckling behaviour.
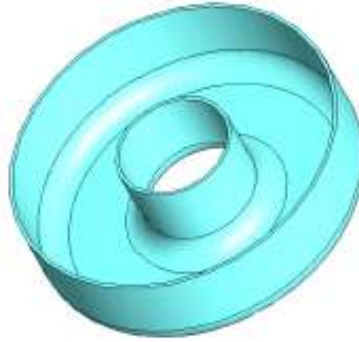
Fig. 2.22: Idler Pulley

2.9.2   Rollover Protective Structure

In the case of a rollover, the structure deforms past its yield, and absorbs rollover energy. During this process it experiences large deformation Understanding the effects of rollover requires combining nonlinear material and nonlinear geometry analysis.

Fig. 2.23: Rollover Protective Structure

2.9.3   Soft Obstetric Forceps

Soft obstetric forceps are designed to "mould" around a baby's head during forceps-assisted delivery. If too high traction and/or compression are applied, the forceps are designed to slip off the baby's head to prevent injuries. Analysis of such forceps must combine nonlinear material and nonlinear geometry to account for large deformations and nonlinear elastic material.

Fig. 2.24: Soft Obstetric Forceps

2.9.4   Fan Guard

This part requires nonlinear geometry analysis because of the membrane stresses that develop during the deformation process. A nonlinear material analysis may be required as well.
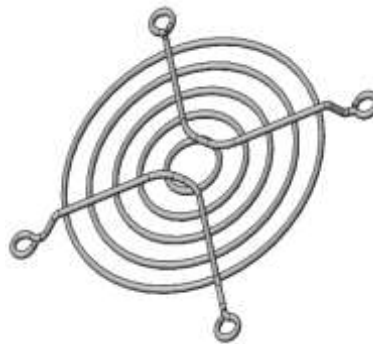
Fig. 2.25: Fan Guard

2.9.5   Diaphragm Spring

The nonlinear spring characteristic requires a nonlinear geometry analysis to account for membrane effects.

Fig. 2.26: Diaphragm Spring

2.9.6   Airline Luggage Container

This airline luggage container requires a nonlinear geometry analysis because of membrane effects in the blue Lexan® panels. In addition, the frame requires a buckling or post buckling analysis.
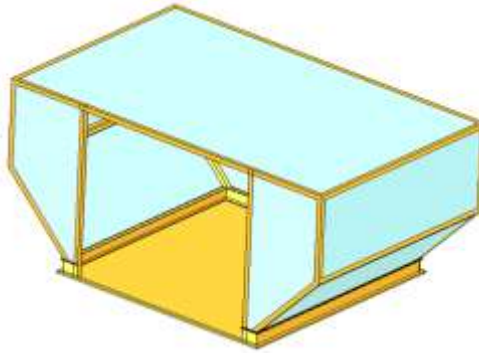
Fig. 2.27: Airline Luggage Container

2.9.7   Snap Ring

A nonlinear geometry analysis is required because of large deformations. This ring may also be a candidate for a nonlinear material analysis.

Fig. 2.28: Snap Ring

2.9.8   Allen Wrench

The contact between the wrench and the socket screw necessitates a contact stress analysis.
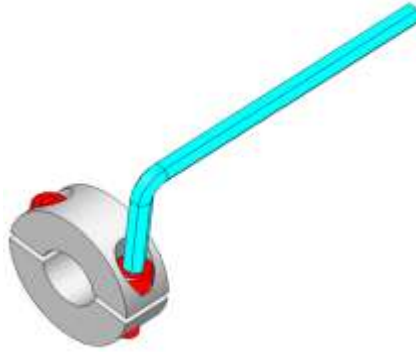
Fig. 2.29: Allen Wrench

2.9.9   Office Chair

In this example, large deformations of the frame may necessitate a nonlinear geometry analysis. The seat and backrest require nonlinear geometry and nonlinear material analysis.

Fig. 2.30: Office Chair

The nature of frequently encountered analysis problems should be the yardstick by which to justify a decision to add nonlinear analysis by the engineers. If day-to-day work requires nonlinear analysis only occasionally, it may be better to ask for the help of a dedicated analyst or to hire a consultant. If, because of the nature of the designed products, design analysis problems routinely involve large deformations, membrane effects, nonlinear material, contact stresses, buckling, or nonlinear supports, then nonlinear analysis should be added by the design engineers.

45

The past two decades have conditioned engineers to the use of FEA as a design tool. Now FEA software and computer hardware have matured enough so that nonlinear analysis can be added to their toolboxes.

2.10   Nonlinear Dynamic Analysis

Dynamic analysis accounts for inertial effects, damping, and time-dependent loads. A drop test, vibrations of an engine mount, airbag deployment, or crash simulation all require dynamic analysis. But is dynamic analysis linear or nonlinear? The qualifying rules are exactly the same as in static analysis. If model stiffness does not change significantly under the applied load, then linear dynamic analysis suffices. A vibrating engine mount or a tuning fork both experience small deformations about the point of equilibrium and so can be analysed with linear dynamic analysis. Problems such as crash simulation, analysis of airbag deployment, modelling a metal stamping process, or modelling of polymeric materials in structural design, all require nonlinear dynamic analysis because both large deformations and large strains occur.

2.11   Simulation Approach

2.11.1 Traditional FEM applications

During the last decades, important improvements have been achieved by using standard features of the currently available finite element (FE) package like *Abaqus, Feap, etc.* Numerical simulations are well established in several engineering fields, and all of them use several Mathematical models described by a system of differential equations. Most of existing numerical methods for solving partial differential equations could be divided into two main groups: *Finite Difference Method (*FDM*) and Finite Element Method (*FEM*).* Unfortunately, the definition of a new finite element method would be time

consuming, since a lot of time is spent to derive characteristic quantities like gradients, Jacobean, Hessian, etc. The use of commercial FEM environment represents a common practice to analyse a great variety of physical problems; however, the use of such large systems is not very awkward for developing and testing new numerical procedures. In fact, during the initial research phases, it's more efficient the use of the symbolic – numerical environments like *Mathematica* or *Maple*. Moreover, the identification of many design flow (such as poor convergence proprieties) could be easier through the use of symbolic environments. Despite these advantages, the symbolic level of analysis becomes very inefficiently if iterative procedures have to be performed, or if a large number of elements have to be considered. In order to assess element performances under real conditions the best way is to perform tests on sequential machines with good debugging procedures (programs written in FORTRAN or C/C++). By the classical approach, re-coding of the element in different languages would be extremely time consuming and for this reason it is never done.

2.11.2 Hybrid Symbolic-Numeric Computational Systems

The advances in reliability, generality and interdisciplinary nature of the new computational methods derived in recent years are primary result of a holistic approach to computational modelling. The use of advanced software technologies is playing a central role in the process that leads to the ultimate goal, i.e. a complete automation of computational modelling (Korelc, 2010). The problem of automation of computational methods has been explored by researches from the fields of mathematics, computer science and computational mechanics, resulting in a variety of approaches (e.g. a hybrid object-oriented approach (Eyheramendy and Zimmermann, 1999) and a hybrid symbolic-numeric approach (Korelc, 2002)) and available software tools (e.g. computer

algebra systems, automatic differentiation tools (Griewank, 2000), problem solving environments and numerical libraries). Automation can address all steps of the finite element solution procedure from the strong form of boundary-value problem to the presentation of results (Logg, 2007), but more often it is used only for the automation of the selected steps of the whole procedure. The paper presents a hybrid symbolic-numeric approach to automation of primal as well as sensitivity analysis (Korelc, 2009). The hybrid symbolic-numeric approach employs general-purpose automatic code generator (Korelc, 2012) to derive and code characteristic finite element quantities (e.g. residual vector and stiffness matrix) at the level of individual finite element and a general-purpose finite element environment to solve the global problem.

2.11.3   Automatic Code Generation

The automatic code generation approach presented combines a symbolic system Mathematica, an automatic differentiation technique with the simultaneous expression optimization and an automatic generation of program code in a selected compiled language. The automation of the finite element methods should not be restricted only to the repetition of the same procedures that are normally done manually on a sheet of paper. The true advantages of automation become apparent only if the description of the problem, the notation and the Mathematical apparatus used are changed as well. It is demonstrated in the paper that this can be achieved using the automatic differentiation technique.

The automatic differentiation technique is based on the fact that every computer program executes a sequence of elementary operations with known derivatives, thus allowing the evaluation of exact derivatives via the chain rule for an arbitrary complex

formulation (Griewank, 2000). Therefore, the automatic differentiation is a method to evaluate the derivative of a function specified by a computer program and represents an alternative to the classical manual derivation of derivatives. Recent advances in development of automatic differentiation technique, especially the backward mode implementation of the code-to-code approach to automatic differentiation, have rejected the traditional assumption that automatic differentiation is impracticable and that the automatic differentiation based numerical codes are intrinsically too slow for large-scale numerical computations. However, as powerful as automatic differentiation technique is, the results of the automatic differentiation procedure might not automatically correspond to the specific Mathematical formalism used to describe the mechanical problem. The essential feature of the proposed approach is that it extends the classical formulation of automatic differentiation technique by additional operators defining exceptions in automatic differentiation procedure. Based on these operators a new notation is introduced, representing a bridge between the classical Mathematical notation of computational models and the actual algorithmic implementation of finite elements. Thus, the basis for the proposed automation of computational modelling is an automatic differentiation based form of basic equations used to describe the problem. The introduced notation does not only simplify the derivation of the corresponding equations, but also reflects much more closely the actual algorithmic implementation. In this way, the Mathematical formulation and computer implementation become indistinguishable.

The automatically generated code is numerically efficient if the number of functions to differentiate and the number of calls to automatic differentiation procedure are kept to a minimum. One of the consequences of this rule is that, in general, formulations where

the element residual vector is derived as a gradient of scalar function, e.g. variational potential, lead to a more efficient numerical code than those based on weak form of the equilibrium equations where the variation of the kinematic quantities, e.g. strain tensor or tangential gap vector, requires differentiation of several scalar functions. Thus, the possibility of transforming the weak form into the "pseudo-potential" scalar function is worth exploring. The pseudo-potential has to be formed in a way that automatic differentiation of the pseudo-potential accompanied with the proper automatic differentiation exceptions leads to the correct equations of the problem.

2.11.4   AceGEN and AceFEM Overview

The AceFEM and AceGEN packages has been written and developed by Jože Korelc, professor at the University of Ljubljana's Faculty of Civil and Geodetic engineering. Each package combines use of Mathematica's facilities with external handling of intensive computation by compiled modules. The task of the Mathematica package AceGEN is the automatic and optimized derivation of formulae needed during numerical procedures. The great advantage of this tool, stands on his new and innovative approach which exploits all the symbolic and algebraic capabilities of Mathematica, avoiding all the typical troubles of such symbolic software during the analysis of complex mechanical models.

By using an innovative Symbolic-Numerical approach, AceGEN is able to combine different techniques, explained in the following chapters, in order to shorten the evolution route of any computing procedures. Besides the results could be exported as compiled FORTRAN or C code with automated interfacing, exploiting all the capabilities of such languages. AceGEN is set up to talk with other numerical

environments, including its sibling AceFEM. AceFEM is an innovative finite element environment designed to solve multi-physics and multi-field problems. The AceFEM package explores advantages of symbolic capabilities of Mathematica while maintaining numerical efficiency of commercial finite element environments.

AceFEM application could employ specific own elements or general codes previously created by AceGEN. The AceFEM package contains a large library of finite elements (solid, thermal, contact... 2D, 3D...) including full symbolic input for most of the elements. Additional elements can be accessed through the AceShare finite element file sharing system. The AceFEM package exploit an element oriented approach which enables easy creation of customized finite element based applications in Mathematica. The combination of the automatic code generation package AceGEN and the AceFEM package represent an ideal tool for a rapid development of new numerical models.

2.12   Review of Prior and Related Works on Compliant Mechanisms

This subsection comprises of three parts; the works that looked at geometric or both geometric and material nonlinearities; the works that formulated dynamic equation for dynamic performance of compliant mechanisms. Finally, the review of works on fatigue life prediction of compliant mechanisms was carried out.

2.12.1 Nonlinearity in the Design and Analysis of Compliant Mechanisms

Comparing with vast technical publications on design and analysis of compliant mechanisms with both linear geometry and material assumptions, very limited works can be cited on nonlinear geometry. Yixian and Liping (2008) presented a topology optimization approach using element-free Galerkin method (EFGM) for the optimal

design of compliant mechanisms with geometrically nonlinearity. EFGM was employed to discretize the governing equations and the bulk density field. Jutte (2008) presented a generalized nonlinear spring synthesis methodology for prescribed load-displacement functions. Four spring examples, J-curve, S-curve, constant-force, and linear, were used to demonstrate the effectiveness of the methodology in generating planar spring designs having distributed compliance and matching desired load-displacement functions. Jinqing and Xianmin (2011) presented a new methodology for geometrical nonlinear topology optimization of compliant mechanisms under displacement loading. Xian *et al.* (2009) integrated the element-free Galerkin (EFG) method, one of the important meshless methods, into topology optimization and a new topology optimization method for designing thermomechanical actuated compliant mechanisms with geometrical nonlinearities.

Aten *et al.* (2012) presented a performance-based comparison of quadratic shell elements with shear deformation and 3-D quadratic solid elements for modelling geometrically non-linear coupled in-plane and out- of-plane deflection of thin-film compliant microelectromechanical systems. Joo *et al.* (2001) presented a non-linear formulation for size and shape optimization of compliant mechanisms using tapered beam elements. They also investigated the scaling effect of the compliant mechanism. Borhan *et al.* (2006) developed a complete nonlinear finite element model for coupled-domain MEMS devices with electrostatic actuation and squeeze film effect. They employed a corotational finite element formulation for the dynamic analysis of planer Euler beams. Dinesh and Ananthasuresh (2007) presented a systematically obtained novel design of a compliant X-Y micro-stage with a large range of motion. They employed geometrically nonlinear finite element analysis to model the behaviour of the

compliant mechanism using a ground structure of frame elements. Cullinan *et al.* (2007) presented observations of the large displacement behaviour of a clamped-clamped carbon nanotube (CNT) flexure element and provided an overview of a new Pseudo Rigid Body (PRB) model that predicts its elastomechanic behaviour. Jorge (2010) addressed the force-displacement model of flexure-based planar compliant mechanisms considering large deflections under quasi-static conditions. A force-displacement model procedure consisting of three iterative steps, kinematic – force – large deflection analysis was developed. Attempts at geometric nonlinearity analysis have always neglected the influence of shear deformation. An investigation on the geometric nonlinearity analysis of compliant mechanisms where all flexible links are considered as two dimensional beams with shear deformation is presented. The energy equations were developed first; the discretization and the Lagrangian dynamics that produced the motion equation were thereafter established.

However, a few works took cognizance of material nonlinearity in the topology synthesis of compliant mechanisms. Swan and Rahmatalla (2004) proposed a methodology for continuum topology design of compliant mechanisms using finite elastic deformation within a continuum structural topology optimization framework. Rahmatalla and Swan (2005) designed formulation for design of continuous, hinge-free compliant mechanisms. It is developed and examined within a continuum structural topology optimization framework. The proposed formulation involves solving two nested optimization problems. Bruns and Tortorelli (2001) considered geometric nonlinearity to propose a well-posed topology optimization formulation that leads to convergent mesh-independent results. They accounted for large deformation of compliant mechanism by using nonlinear elastic analysis in the topology optimization.

Jung and Gea (2002; 2004) studied the topology optimization of both geometrically and materially nonlinear structure using a general displacement functional as the objective function. In order to consider large deformation, effective stress and strain are expressed in terms of 2nd Piolar–Kirchhoff stress tensor and Green–Lagrange strain tensor, and constitutive equation is derived from the relation between the effective stress and strain. Compliant mechanisms examples were used to validate the study. Material nonlinearity in these works were only introduced in the synthesis and topology optimizations of compliant mechanisms. No researcher has bordered to look at appropriate model to describe the large deformation behaviour of compliant mechanisms.

2.12.2 Dynamic Analysis of Compliant Mechanisms

Dynamic analyses of compliant mechanisms have been a subject of interest for simulation and control of flexible mechanical systems. Examples include space robot arms and high-speed robotic manipulators. Most of dynamic models are often based on the assumption of small deflection without considering geometric and material nonlinearities. This assumption is satisfactory provided that the link undergoes a small deflection such that the theory of linear elasticity holds. However, for mechanisms involving highly compliant links such as rubber fingers in (Lee, 1999), live bird transferring system (Chao-Chieh, 2005), light-weight arms, and high-precision elements, the effects of large deformation with geometric and material nonlinearities cannot be ignored. There are two main approaches used in literature in the dynamic analysis of compliant mechanisms – the pseudo rigid body model and the finite element method.

2.12.2.1   Pseudo Rigid Body Model

A number of works have been done on the dynamic analysis of compliant mechanisms using the Pseudo Rigid Body Model (PRBM). Ugwuoke (2008) presented simplified dynamic model and stability analysis for the constant-force compression spring (CFCS) based on the PRBM. Ugwuoke *et al.* (2009a) presented the frequency and modal analysis of constant-force mechanism based on the Pseudo Rigid Body Model. Ugwuoke (2009b) considered three useful plots in the evaluation of each of the dynamic models for their stability characteristics, which includes the polar plot based on the Routh-Hurwitz stability criterion, the Bode plot, and the Nyquist diagram which considers stability in the real frequency domain. Ugwuoke (2009c) presented the dynamic analysis of the compliant constant force mechanism using the PRBM. Yu *et al.* (2005) discussed the dynamic modelling of compliant mechanism based on Pseudo Rigid Body Model.

Lyon *et al.* (1997; 1999), discussed the dynamic response and prediction of the first natural frequency of a Compliant Mechanism using the Pseudo Rigid Body Model. Kimball and Tsai (2002) analysed the dynamic behaviour of the flexural beams in compliant mechanisms by means of PRBM. Boyle *et al.* (2003) presented the analytical and experimental study on the dynamic response of compliant constant - force compression mechanisms. Rezaei *et al.* (2006) explored a dynamic behaviour analysis of a compliant four-bar micromechanism. The Pseudo-Rigid-Body Model (PRBM) is used to model the compliant mechanism, and to analyse the large deflection of flexible segment. The model and Lagrange Equations are used to develop the dynamic equations.

2.12.2.2   Finite Element Method

Some other researchers have adopted the concept of finite element method in the dynamic analyses of compliant mechanisms. Li and Kota (2002) showed the dynamic performance of a compliant stroke multiplier. Their work covers the basic elements of dynamic analysis such as natural frequencies, natural modes, dynamic response, frequency spectrum analysis, and sensitivity analysis. Wang and Yu (2008; 2010) developed the dynamic equation of compliant mechanism based on the finite element method by using Lagrange equation. On this basis, they derived the natural frequencies and modes of the mechanism. A method for calculating the sensitivity of natural frequencies and modes to the design variables were also presented. Zhang and Hou (2010) developed the generalized Equations of motion based on the finite element method of the compliant mechanism considering the thermal effect. The right-circular flexure hinge was treated as a three nodes element, in which there are three degrees of freedom at each node. The closed-form solutions of the element stiffness and mass matrices for the flexure hinge were obtained. The model was validated with experimental studies. All the aforementioned dynamic analysis are based on linear assumptions.

The literature has revealed that adequate attention has not been paid to the combined effect of geometric and material nonlinearities in the determination of the deformation behaviour of compliant mechanisms.

2.13   Fatigue Failure of Compliant Mechanisms

Fatigue is one of the major failure mechanisms in engineering structures (Schutz, 1996). Time varying cyclic loads result in failure of components at stress values below the

yield or ultimate strength of the material. Fatigue failure of components takes place by the initiation and propagation of a crack until it becomes unstable and then propagates to sudden failure. The total fatigue life is the sum of crack initiation life and crack propagation life. Fatigue life prediction has become important because of complex nature of fatigue as it is influenced by several factors, statistical nature of fatigue phenomena and time consuming fatigue tests.

Though a lot of fatigue models have been developed and used to solve fatigue problems, the range of validity of these models is not well defined. No method would predict the fatigue life with the damage value by separating crack initiation and propagation phases. The methods used to predict crack initiation life are mainly empirical (Wang *et al.,* 1999) and they fail to define the damage caused to the material. Stress or strain based approaches followed do not specify the damage caused to the material, as they are mainly curve fitting methods. The limitation of this approach motivated the development of micromechanics models termed as local approaches based on Continuum Damage Mechanics (CDM). The local approaches are based on application of micromechanics models of fracture in which stress/strain and damage at the crack tip are related to the critical conditions required for fracture. These models are calibrated through material specific parameters. Once these parameters are derived for particular material, they can be assumed to be independent of geometry and loading mode and may be used to the assessment of a component fabricated from the same material. For some compliant structures, the desired motion may occur infrequently and the static theories may be enough for the analysis (Howell, 2001). However, by the definition of compliant mechanisms, deflection of flexible members is required for the motion. Usually, it is desired that the mechanism be capable of undergoing the motion

many times, and design requirements may be many millions of cycle of infinite life. This repeated loading cause fluctuating stresses in the members and can result in fatigue failure. Failure can occur at stresses that are significantly lower than those that cause static failure (Howell, 2001). A small crack is enough to initiate the fatigue failure. The crack progresses rapidly since the stress concentration effect becomes greater around it. If the stressed area decreases in size, the stress increases in magnitude and if the remaining area is small, the member can fail. A member failed because of fatigue shows two distinct regions. The first one is due to the progressive development of the crack, while the other one is due to the sudden fracture. Premature or unexpected failure of a device can result in unsafe design. The consumer confidence may be reduced in products that fail prematurely. For these and other reasons, it is critical that the fatigue life of compliant mechanism be analysed. Although fatigue failure is difficult to predict accurately, an understanding of fatigue failure prediction and prevention is very helpful in the design of compliant mechanisms. The theory can be used to design devices that will withstand these fluctuating stresses.

Several models are available for fatigue failure prediction. The stress-life and strain-life models are commonly used in the design of mechanical components (Howell, 2001). These theories are appropriate for parts that undergo consistent and predictable fluctuating stresses. Many machine components fit into this category because their motion and loads are defined by kinematics of the mechanism. There are three stress cycles with which loads may be applied to the component under consideration. The simplest being the reversed stress cycle (Fig. 2.31(a)). This is merely a sine wave where the maximum stress and minimum stress differ by a negative sign. An example of this

type of stress cycle would be in an axle, in which every half turn or half period as in the case of the sine wave, the stress on a point would be reversed.
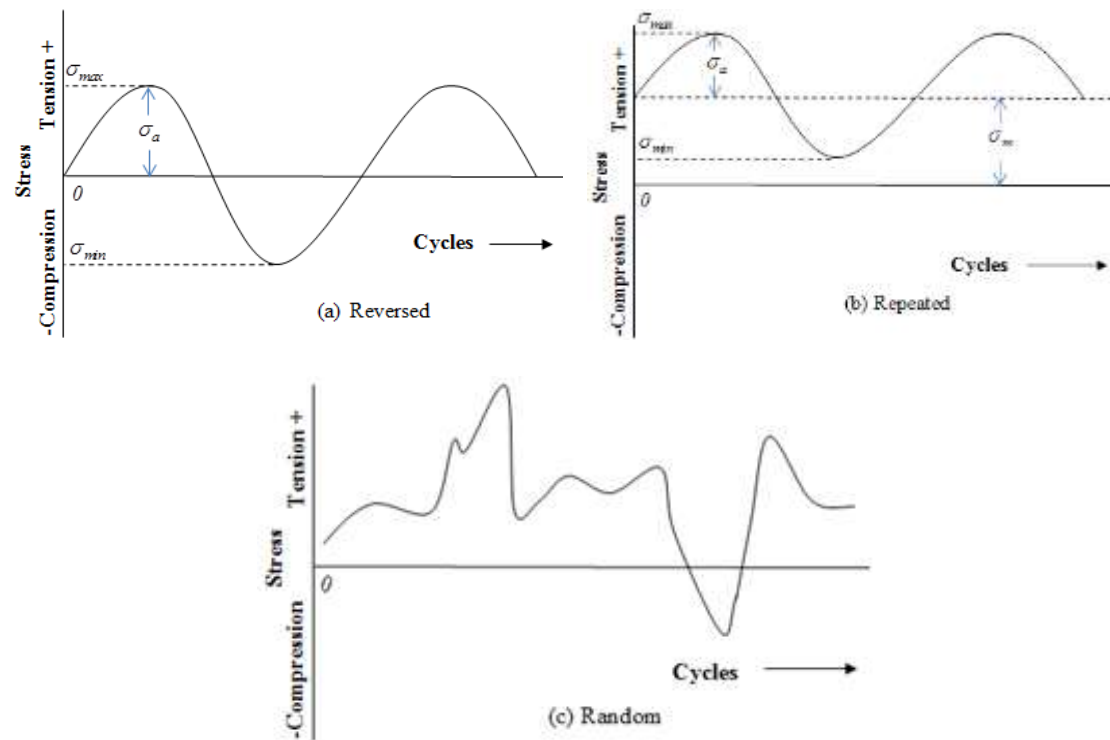
Fig. 2.31: Stress cycles showing (a) Reversed, (b) Repeated and (c) Random cycles

The most common type of cycle found in engineering applications is where the maximum stress and minimum stress are asymmetric (the curve is a sine wave) not equal and opposite (Fig. 2.31(b)). This type of stress cycle is called repeated stress cycle. A final type of cycle mode is where stress and frequency vary randomly (Fig. 2.31(c)). An example of this would be hull shocks, where the frequency magnitude of the waves will produce varying minimum and maximum stresses. Predicting the life of parts stressed above the endurance limit is at best a rough procedure. For the large percentage of mechanical and structural compliant systems subjected to randomly varying stress cycle intensity (for example, compliant automotive suspension and compliant aircraft structural components etc.), the prediction of fatigue life is further complicated. The normal stress-life and strain-life models cannot be adopted in the

fatigue prediction. Models such as continuum damage mechanics can be used in dealing with this situation.

The fatigue failure of thermoplastics polymers generally develops in two phases (Li *et al.,* 1995). First, the material accumulates fatigue damage (i.e. in the initiation phase), which ultimately leads to the formation of visible crazes. The crazes further grow, form cracks and propagate (i.e. in the propagation phase) until final failure occurs. In general, the damage process in polymers is regarded as the formation and development of micro defects and crazes within an initially perfect material. The material remains the same but its macroscopic properties change with its microscopic geometry (Tang *et al.,* 1996). In polymers, craze formation is generally believed to be one of the main causes of material damage, which is both a localized yielding process and the first stage of fracture. Crazes are usually initiated either at surface flaws and scratches or at internal voids and inclusions, and affect significantly the subsequent deformation and bulk mechanical behaviours of polymers (Passaglia, 1987). The Continuum Damage Mechanics first introduced by Kachanov and developed within the framework of thermodynamics discusses systematically the effects of micro-defects on the subsequent development of micro-defects, and the states of stress and strain in materials. It has been applied to fatigue and fracture of different materials.

An isotropic damage evolution equation for finite viscoelasticity characteristic of polymeric CMs is proposed, which is based on the Continuum Damage Mechanics (CDM). A new damage model is developed to establish the fatigue life formula for such compliant systems. The compliant material is idealized as a continuous isotropic hyperelastic material. Commonly used polymeric material, Low Density Polypropylene

(LDPP) and Low Density Polyethylene (LDPE) were tested to obtain the fatigue life as a function of the strain amplitude.

2.13.1 Previous Works on Fatigue Failure of Compliant Mechanisms

A few researchers have looked into the fatigue failure of compliant systems. Li *et al.* (2011) used the modified Basquin equation to determine the life cycle till failure for compliant fast tool servo. The fatigue life according to the equation is a function of the equivalent reverse stress, fatigue stress concentration factor, the range stress, the ultimate strength, the average stress, and the endurance limit. Demirel *et al.* (2010) and Subaşi (2005) used the factor of safety expressed in terms of the fluctuating stresses, endurance limit, mean stress component and an alternating stress component for fatigue failure prediction of compliant mechanism. If the stress condition is below the two lines described in modified Goodman diagram for fatigue failure, the compliant member is expected to have an infinite life. Howell *et al.* (1994) proposed a method for the probabilistic design of a bistable compliant slider-crank mechanism which its objective function is the maximization of the mechanism reliability in fatigue. Cannon *et al.* (2005) used the modified fatigue strength at cycles which is expressed in terms of Marin correction factors and the theoretical fatigue strength to predict the failure behaviour of a compliant end-effector for microsribing. This gives the S-N diagram for the mechanism where the maximum stress is compared with the modified fatigue strength.

2.13.2   Previous Works on Fatigue Failure by Continuum Damage Mechanics

Quite a number of researchers have employed the concept of damage evolution in the prediction of fatigue failure of engineering structures and components. Jiang, (1995)

derived a damaged evolution model for strain fatigue of ductile metals based on Lemaitre's potential of dissipation. Then the equation of fatigue-life prediction and the criterion of cumulative fatigue damage were deduced. The model was validated with experiment. Shi *et al.* (2011) proposed a new damage mechanics model to predict the fatigue life of fibre reinforced polymer lamina and adopted the singularity of stiffness matrix as the failure criterion of lamina in this article, which inventively transformed the complex anisotropic issue of composite lamina fatigue into the analysis of single-variable isotropic damages for fibre and matrix. Akshantala and Talreja (2000) proposed a methodology for fatigue life prediction that utilizes a micromechanics based evaluation of damage evolution in conjunction with a semi-empirical fatigue failure criterion. The specific case treated was that of cross ply laminates under cyclic tension. The predicted results were compared with experimental data for several glass, epoxy and carbon epoxy laminates. Ping *et al.* (2003) proposed a nonlinear Continuum Damage Mechanics model to assess the creep–fatigue life of a steam turbine rotor, in which the effects of complex multiaxial stress and the coupling of fatigue and creep are taken into account. The results were compared with those from the linear accumulation theory that had been dominant in life assessment of steam turbine rotors. The comparison shows that the nonlinear continuum damage mechanics model describes the accumulation and development of damage better than the linear accumulation theory. Ali *et al.* (2010) investigated the fatigue behaviour of rubber using dumb-bell test specimens under uniaxial loading. In modelling fatigue damage behaviour, a continuum damage model was presented based on the function of the strain range under cyclic loading. Upadhyaya and Sridhara (2012) predicted strain controlled fatigue life of EN 19 steel and 6082- T6 aluminium alloy considering both crack initiation and crack propagation phases. The theory of Continuum Damage Mechanics was used in

the study of fatigue damage phenomena such as the nucleation and initial defect growth (microvoids and micocracks) in elastomers by Wang *et al.* (2002) and Mahmoud *et al.* (2007).

2.14   Previous Works that adopted Symbolic Computation

Computer algebra systems like MACSYMA, REDUCE, Maple, Mathematica, and to a certain extent other types of systems as Matlab and Mathcad, give possibility to carry out not only numerical but also symbolical computations. Symbolic computations have found broad applications in many areas of science and engineering. It has led to new approaches for problems solving and provide tools that enable an automatic and computerized solution of problems in ways that are not possible with conventional computing systems. The symbolic-numeric approach to FEM was extensively studied in the last few years. Various studies of symbolic computation in structural mechanics and mathematics have been done. Mattern and Schweizerhof, (2010) used the symbolic programming tool AceGEN, a plug-in for the computer algebra software Mathematica to implement a formulated "Solid-shell"- element. The formulation of the element was done with linear and quadratic interpolation of the in-plane geometry and displacement in the thickness as well as in shell surface direction, with "assumed natural strain" and "enhanced assumed strain" in order to reduce artificial stiffness effect on the element. They showed some numerical examples to prove the superiority of AceGEN generated element routines over the manually performed implementation and concluded that symbolic computation is clearly advantageous in many applications in structural mechanics. Pomeranz (2000) described how the computer algebra system, Mathematica, can be used to introduce students to the finite element method. Typical students are juniors, seniors, and beginning graduate students in mathematics, computer

science, and various engineering disciplines. Students were given template code. They were instructed to modify the code in order to solve two-dimensional elliptic boundary-value problems and to verify the correctness of their numerical solutions. Paláncz and Popper (2000) applied Symbolic computation to Runge-Kutta technique in order to solve a two-point boundary value problem. Their procedure was illustrated by solving the boundary value problem of the mechanical analysis of a liquid storage tank. Computations were carried out by the Mathematica symbolic system. Huet (2003) presented two design issues concerning fundamental representation structures for symbolic and logic computations. The first one concerns structured editing, or more generally the possibly destructive update of tree-like data-structures of inductive types. Instead of the standard implementation of mutable data structures containing references. The second method is a uniform sharing function, which is a variation on the traditional technique of hashing. They advocate the zipper technology, fully applicative. Alur *et al.* (2005) formulated and compared various symbolic computational techniques for deciding the existence of winning strategies. The game structure is given implicitly, and the winning condition is either a reachability game of the form "p *until* q" (for state predicates p and q) or a safety game of the form "*Always* p". Korelc and kristanič (2005) presented design sensitivity analysis and optimization based on symbolic-numeric approach to evaluation of design velocity field by direct differentiation of symbolically parameterized mesh. Korelc (2004) developed a hybrid system in which Mathematica was used for the automatic derivation of material model and the generation of symbolic nonlinear finite element codes.

Alnæs *et al* (2007), addressed the use of high level languages, symbolic Mathematical tools and code generation in an implementation of the finite element method, using a

nonlinear hyperelasticity equation as example. The application we have in mind for the equations they presented is the simulation of the passive elastic properties of heart and blood vessel tissue. Wei *et al.* (2007) proposed the use of symbolic computation for the evaluation of measurement uncertainty. The general method and procedure were discussed, and its great potential and powerful features for measurement uncertainty evaluation were demonstrated through examples. Although the symbolic computation was performed using Maple's powerful Mathematical computing engine, it is possible to use other technologies for this same symbolic computation. Gurung and Freere (2007) presented the use of Matlab symbolic computation technique to model and simulate self-excited induction generator. In this technique, the computer itself carries out both the tedious job of deriving the complex coefficients of the polynomial equations and solving them. Hence the modelling and programming becomes very simple yet versatile. Good agreement between the results they obtained from the conventional method and that obtained using symbolic computation validates the effectiveness of their new technique. Jiang and Wang (2008) developed a FEM program by using Mathematica, a symbolic algebra system to help students to understand how finite element methods (FEM) deal with the plasticity. The program is compact and of very good readability and would positive results in the teaching the theory of plasticity. Lee (2009) offered contemporary look at how the historical elements in symbolic computation has led to a renewed interest symbolic in engineering modelling and simulation today. Symbolic techniques are showing promise for the modernization of model development and coding techniques in hardware in the loop (HiL) simulation applications. Emerging methodologies are indicating significant reduction in effort in model development and an acceleration of the actual computation coded in HiL and embedded code applications.

Papusha *et al.* (2009) proposed a new symbolic technique for offshore design technology. Illustrations were given for a drill stem and a riser. Both symbolic and numerical solutions derived with *Mathematica* are applied to solve problems in offshore design technology. All symbolic approaches are based on solutions of the linear boundary problems that arise. Additionally, a new symbolic solution for the generic boundary problem was also discussed. Adeleye and Fakinlede (2010) also developed a symbolic finite element solution for the problem of heat transfer in radial fin of triangular profile. The result of their symbolic computation was used for optimization of fin material usage. Alnæs and Mardal (2010) showed that employing a symbolic engine inside a finite element form compiler can lead to speed-up of several orders of magnitude in addition to a user-friendly and time saving problem solving environment. Their efforts resulted in the open source package SyFi which generates unified form-assembly (UFC) code that is directly importable in DOLFIN and other libraries implementing this thin interface. Ari *et al.* (2005) presented a paper that deals with Maple as a symbolic computation techniques. After introducing some capabilities of Maple, some examples were discussed to illustrate the Maple.

3
CHAPTER 3: METHODOLOGY

3.1 Large Deformation Model of Compliant Mechanisms

3.1.1 Continuum Mechanics Formulation

The basic continuum compliant mechanism problem is sketched in Fig. 3 1. It shows the general domain Ω for the design of a mechanism that transforms force applied at the input port to a desired displacement at the output port in an efficient way. The position vector $\boldsymbol{X}$ in the reference position is transformed to $\boldsymbol{x}$ in its current position. u_{in} is the displacement at the input boundary Γ_{in} as a result of the applied force F_{in} at the boundary while F_{out} is a virtual force at the output boundary Γ_{out} specifying the direction of the desired boundary displacement u_{out}. Γ_g is the support boundary.
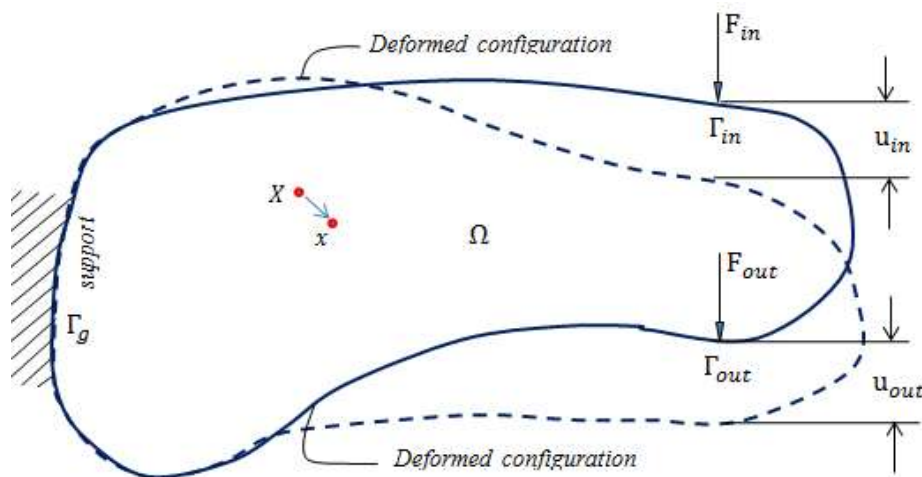
Fig. 3.1: Deformed continuum compliant mechanism

The boundary conditions of imposed displacement on Γ_{in} are called the Dirichlet, whereas the conditions of imposed traction on Γ_σ are referred to as the Neumann boundary conditions. In any well-posed boundary value problem, the complete

boundary is split between the Dirichlet and von Neumann boundary $\Gamma_{in} \cup \Gamma_\sigma = \Gamma$, such that the two never intersect $\Gamma_{in} \cap \Gamma_\sigma = \emptyset$. In other words, if we want to ensure that a boundary value problem is well posed, we must not impose both displacement and traction at the same boundary. The main goal of the solution procedure for a boundary value problem is to find the displacement field $u(x)$ resulting from applied volume $b(x)$, imposed traction t and imposed displacement $\bar{u}$. The resulting displacement field can be computed starting either from strong or weak form of the boundary value problem. It is important to note that not only the displacement field is of interest, but also the strain and stress field. In fact, the latter are often more important than the displacement for verifying the risk of damage or fracture

A bare minimum of fundamental concepts in continuum mechanics are provided here, as theoretical background for large deformations and hyperelastic constitutive material relations. Most, if not all of the information provided in this section have been extensively discussed in numerous publicly available sources of literature. As a proposed starting point, the interested reader is referred to Holzapfel (2000) and Mase and Mase (1999) for a quite comprehensive review of continuum mechanics, to Criscione (2002) and Freed (1995) for a thorough synopsis of natural strain and strain rate, and finally to Bonet and Wood (1997) for a similar review of the basic concepts of continuum mechanics used in constitutive laws for hyperelasticity.

3.1.0.1   Kinematics

A compliant mechanism has material points whose positions are given by the vector X in a fixed reference configuration Ω_r in 2-D space. After the body is loaded each material point is described by its position vector x, in the current configuration Ω_c. The

position vector in the current configuration is given in terms of its Cartesian components as,

$$\boldsymbol{X} = X_i \boldsymbol{E}_i \tag{3.1}$$

$$\boldsymbol{x} = x_i \boldsymbol{e}_i \tag{3.2}$$

$\boldsymbol{E}_i$ and $\boldsymbol{e}_i$ are the unit vectors and summations are implied.

3.1.1.2 Cauchy-Green Deformation Tensors

There are two Cauchy-Green Deformation Tensors in the analysis of deformable continuum. We have the right and left Cauchy-Green Deformation Tensors. Right Cauchy-Green tensor is given as,

$$\boldsymbol{C} = \dot{\boldsymbol{F}}^T \cdot \boldsymbol{F} \tag{3.3}$$

In the same way, the Left Cauchy-Green Deformation (also known as Finger) tensors is given as,

$$\boldsymbol{b} = \boldsymbol{F} \cdot \dot{\boldsymbol{F}}^T \tag{3.4}$$

The Deformation Gradient $\boldsymbol{F}$ is given as,

$$\boldsymbol{F} = \frac{\partial \boldsymbol{x}}{\partial \boldsymbol{X}} \tag{3.5}$$

The determinant of the deformation gradient is usually denoted by J and is a measure of the change in volume, i.e.

$$J = \dot{det} \, \boldsymbol{F} \tag{3.6a}$$

$$J^2 = \dot{det} \, \boldsymbol{C} \tag{3.6b}$$

3.1.1.3 Strain Measures

The change in scalar product can be found in terms of the material vectors dX_1 and

dX_2

$$\frac{1}{2}(dx_1 \cdot dx_2 - dX_1 \cdot dX_2) = \frac{1}{2}dX_1 \cdot (\boldsymbol{C} - \boldsymbol{1}) \cdot dX_2 = (dX_1 \cdot \boldsymbol{E} \cdot dX_2) \tag{3.7}$$

Green (Lagrangian) strain $\boldsymbol{E}$ is then given as,

$$\begin{aligned} \boldsymbol{E} &= \frac{1}{2}(\boldsymbol{C} - \boldsymbol{1}) = \frac{1}{2}(\boldsymbol{F}^T \cdot \boldsymbol{F} - \boldsymbol{I}) \\ &= \frac{1}{2}(\nabla \boldsymbol{u} + (\nabla \boldsymbol{u})^T + \nabla \boldsymbol{u} \cdot (\nabla \boldsymbol{u})^T) \end{aligned} \tag{3.8}$$

Index notation:

$$E_{ij} = \frac{1}{2}(F_{kl} - \delta_{ij}) = \frac{1}{2}\left(\frac{\partial u_i}{\partial X_j} + \frac{\partial u_j}{\partial X_i} + \frac{\partial u_k}{\partial X_J} + \frac{\partial u_k}{\partial X_i}\right) \tag{3.9}$$

Alternatively, the same change in scalar product can be expressed with reference to the spatial elemental vectors dx_1 and dx_2,

$$\begin{aligned} \frac{1}{2}(dx_1 \cdot dx_2 - dX_1 \cdot dX_2) &= \frac{1}{2}(dx_1 \cdot (\boldsymbol{I} - \boldsymbol{b}^{-1}) \cdot dx_2 \\ &= dX_1 \cdot \boldsymbol{e} \cdot dX_2 \end{aligned} \tag{3.10}$$

Almansi (Eulerian) strain is then given as,

$$\boldsymbol{e} = \frac{1}{2}(\boldsymbol{I} - \boldsymbol{b}^{-1}) = \frac{1}{2}(\boldsymbol{I} - \boldsymbol{F}^{-T} \cdot \boldsymbol{F}^{-1}) \tag{3.11}$$

3.1.1.4 Isotropic Hyperelasticity

Large strain elasticity, or hyperelasticity, is defined in terms of a strain energy function. In order to facilitate the extension of the above equations to the hyperelastic case, the standard theory of isotropic hyperelasticity is briefly reviewed first in this section. Hyperelasticity implies the existence of a strain energy density function Ψ dependent upon the Lagrangian or right Cauchy-Green tensors as

$$\Psi = \Psi(\boldsymbol{C}, \boldsymbol{X}) = (\boldsymbol{E}, \boldsymbol{X}) \tag{3.12}$$

The second Piola-Kirchhoff stress tensor $\boldsymbol{S}$ can now be expressed as

70

$$S = 2\frac{\partial \Psi}{\partial C} = \frac{\partial \Psi}{\partial E} \tag{3.13}$$

The stress-strain relation could be written in terms of the Lagrangian elasticity tensor

C as

$$\mathbb{C} = \frac{\partial S}{\partial E} = 2\frac{\partial S}{\partial C} = 4\frac{\partial^2 \Psi}{\partial C \partial C} \tag{3.14}$$

3.1.2 Development of Large deformation Model for Compliant Mechanisms

Finite element implementations of nearly incompressible material models often employ decoupled numerical treatments. The strain energy density function for such a material is decoupled into the dilatation, U (J) and deviotoric, Ψ (C) parts (Sun *et al.,* 2008) as.

$$\Psi(C) = \Psi(\overline{C}) + U(J) \tag{3.15}$$

Where

$$\Psi(\overline{C}) = \frac{1}{2}\mu(trC - 3) \tag{3.16}$$

$$U(J) = \frac{1}{2}k(J - 1)^2 \tag{3.17}$$

k and μ are the material properties known as bulk and shear modulus respectively.

$$C = F^T F \tag{3.18}$$

Mixed elements are often used to accommodate the volume constraint in incompressible material problem. They are designed to model fully or nearly incompressible hyperelastic materials. For a hyperelastic model that can have multiple deformations state for the same stress level, the penalty factor and the use of Lagrangian multipliers might not be most adequate. It is convenient to use a three-field mixed Hu-Washizu variation form to overcome volumetric locking (Wriggers, 2010). Assuming an independent approximation of the displacement u, the hydrostatic pressure p and the

volumetric change parameter θ, a variational form for the finite deformation hyperelastic problem is given by (Mathisen *et al.*, 2011)

$$\delta\Pi(u, p, \theta) = \int_\Omega [\Psi(\overline{C}) + p(J - \theta)]dV + \delta\Pi_{ext} \tag{3.19}$$

Where Π_{ext} is the functional for effects of body forces and surface tractions and p is the mixed pressure in the deformed configuration. It is convenient to make a multiplication split of the deformation gradient into a dilatation part F^{vol} and isochoric part F^{iso}.

$$F = F^{vol}F^{iso} \tag{3.20}$$

Mathisen *et al.* (2011) defined the two parts as,

$$F^{vol=}J \tag{3.21}$$

$$F^{iso=}1 \tag{3.22}$$

Equation (3.22) is required for constant volume state. The mixed right Green deformation tensor is expressed as,

$$\overline{C} = \overline{F}^T \overline{F} \tag{3.23}$$

Where

$$\overline{F} = \left(\frac{\theta}{J}\right)F \tag{3.24}$$

$\overline{C}$ is the mixed right Cauchy-Green deformation tensor. The variation of Eq. (3.19) gives,

$$\delta\Pi = \int_\Omega \left[\frac{\partial\Psi}{\partial\overline{C}} : \delta\overline{C} + \delta p(J - \theta) + p(\delta J - \delta\theta)\right]dV + \delta\Pi_{ext} \tag{3.25}$$

A second Piola-Kirchhoff stress is related to the derivative of the stored energy function through Eq. (3.26).

$$S = 2\frac{\partial\Psi}{\partial\overline{C}} \tag{3.26}$$

Substituting Eq. (3.26) into Eq. (3.19) we have,

$$\delta\Pi = \int_{\Omega} \left[\frac{1}{2} \delta\bar{C} : \bar{S} + \delta p(J - \theta) + p(\delta J - \delta\theta) \right] dV + \delta\Pi_{ext} \tag{3.27}$$

The first term in Eq. (3.27) is the inner virtual work $\delta\Pi_{inner}$ given as,

$$\delta\Pi_{inner} = \int_{\Omega} \left[\frac{1}{2} \bar{S} : \delta\bar{C} \right] dV \tag{3.28}$$

The variation of the mixed right deformation tensor $\bar{C}$ is given as,

$$\delta\bar{C} = \left(\frac{\theta}{J} \right) \delta C + \left(\frac{\delta\theta}{\theta} - \frac{\delta J}{J} \right) \bar{C} \tag{3.29}$$

But

$$\delta J = J C^{-1} : \delta C \tag{3.30}$$

Substituting Eq. (3.30) into Eq. (3.29), gives

$$\delta\bar{C} = \left(\frac{\theta}{J} \right) \left[I - \frac{1}{3} C \otimes C^{-1} \right] : \delta C \tag{3.31}$$

The integrand in Eq. (3.28) could now be expanded as

$$\begin{aligned} \delta\bar{C}_{rs}\bar{S}_{rs} &= \delta\bar{F}_{ir}\bar{F}_{is}\bar{S}_{rs} \\ &= \frac{1}{3}\frac{\delta\theta}{\theta}\bar{F}_{ir}\bar{F}_{is}\bar{S}_{rs} + \left(\frac{\theta}{J} \right) [\delta F_{ir} - \frac{1}{3}\delta F_{js}F_{js}^{-1}F_{ir}]\bar{F}_{is}\bar{S}_{rs} \end{aligned} \tag{3.32}$$

The Kirchhoff and Cauchy stresses based on the mixed deformation gradient are related as (Zienkiewicz and Taylor, 2000)

$$\bar{\tau}_{ij} = \bar{F}_{ir}\bar{F}_{is}\bar{S}_{rs} = \theta\bar{\sigma}_{ij} \quad ; \qquad \bar{\tau} = \frac{1}{\theta}\bar{F}S\bar{F}^T = \bar{\sigma} \tag{3.33}$$

If we also note that

$$\delta F_{js}F_{js}^{-1} = \delta u_{j,k}F_{ks}F_{ks}^{-1} = \delta u_{j,k}\delta_{kj} = \delta u_{j,j} \tag{3.34}$$

Substituting Eqs. (3.33) and (3.34) into Eq. (3.32), gives

$$\begin{aligned} \delta\bar{C}_{IJ}\bar{S}_{IJ} &= \frac{1}{3}\left(\frac{\delta\theta}{\theta} - \delta u_{jj} \right)\bar{\tau}_{rr} + \delta u_{ij}\bar{\tau}_{ij} \\ &= \left(\frac{1}{3}\frac{\delta\theta}{\theta}\bar{\tau}_{rr} + \frac{\partial u_i}{\partial x_j} \right) + \left(\bar{\tau}_{ij} - \frac{1}{3}\delta_{ij}\bar{\tau}_{rr} \right) \end{aligned} \tag{3.35}$$

Equation (3.35) could be expressed in terms of Cauchy stress using Eq. (3.33) as

$$\delta \bar{C}_{ij} \bar{S}_{ij} = \frac{1}{3} \delta\theta \bar{\sigma}_{kk} + \delta u_{ij} \left(\bar{\sigma}_{ij} - \frac{1}{3} \delta_{ij} \bar{\sigma}_{kk} \right) \theta \tag{3.36}$$

Substituting Eq. (3.36) into Eq. (3.27) gives

$$\delta\Pi = \int_{\Omega} [\delta\theta(\bar{p} - p) + \delta p(J - \theta)]dV + \int_{\Omega} \delta u_{i,j}(\bar{\sigma}_{ij} + \delta_{ij}\bar{p})\,\theta + p\delta J \tag{3.37}$$
$$+ \delta\Pi_{ext}$$

Where

$$\bar{p} = \frac{\bar{\sigma}_{ii}}{3} = tr\bar{\boldsymbol{\sigma}} \tag{3.38}$$

The variation of the deformation tensor is also given as (Bonet and Wood, 1997)

$$\delta J = J \, div\delta\boldsymbol{u} \tag{3.39}$$

Equation (3.39) simplifies Eq. (3.37) to

$$\delta\Pi = \int_{\Omega} [\delta\theta(\bar{p} - p)]dV + \int_{\Omega} \delta\varepsilon_{ij} \left[\bar{\sigma}_{ij} + \delta_{ij} \left(\frac{J}{\theta} p - \bar{p} \right) \right] \theta dV$$
$$+ \int_{\Omega} [\delta p(J - \theta)]dV + \delta\Pi_{ext} \tag{3.40}$$

3.1.3   Finite Element Discretization

The current configuration $\boldsymbol{x}$ may be expressed in terms of a displacement $\boldsymbol{u}$ from the reference configuration coordinates $\boldsymbol{X}$ as

$$\boldsymbol{x} = \boldsymbol{X} + \boldsymbol{u} \tag{3.41}$$

The reference coordinate and displacement field are approximated by isoparametric interpolations given in Eqs. (3.42) and (3.43) respectively.

$$X_i = N_r(\xi)\hat{X}_i^r \tag{3.42}$$

$$u_i = N_r(\xi)\hat{u}_i^r \tag{3.43}$$

The approximation of the displacement tensor becomes

$$u_{i,j} = N_{r,j}\hat{u}_i^r \tag{3.44}$$

The pressure and volume are interpolated as

$$p = N_p\hat{\boldsymbol{p}} \tag{3.45}$$

$$\theta = N_p \widehat{\boldsymbol{\theta}} \tag{3.46}$$

Using the approximations of Eqs. (3.42) and (3.43) the matrix form of Eq. (3.40) becomes

$$\delta \Pi = \delta \widehat{\boldsymbol{u}}^T \int_\Omega \boldsymbol{B}_u^T \breve{\sigma} \theta dV + \delta \widehat{\boldsymbol{p}}^T \int_\Omega N_p^T (J - \theta) dV$$
$$+ \delta \widehat{\theta}^T \int_\Omega N_\theta^T (\bar{p} - p) dV + \delta \Pi_{ext} \tag{3.47}$$

Where $\boldsymbol{B}_u$ is the strain displacement matrix given by

$$\boldsymbol{B}_u = \begin{bmatrix} \dfrac{\partial N_r}{\partial x_1} & \dfrac{\partial N_r}{\partial x_2} & 0 \\[2mm] 0 & \dfrac{\partial N_r}{\partial x_2} & 0 \\[2mm] \dfrac{\partial N_r}{\partial x_2} & \dfrac{\partial N_r}{\partial x_1} & 0 \end{bmatrix} \tag{3.48}$$

$$\breve{\sigma} = \bar{\sigma} + \left(\frac{J}{\theta} p - \bar{p} \right) \boldsymbol{m} \tag{3.49}$$

$\bar{p}$ and $\boldsymbol{m}$ are the mean stress and the mean matrix operator respectively, given as

$$\bar{\boldsymbol{p}} = \frac{1}{3} \boldsymbol{m}^T \bar{\boldsymbol{\sigma}} \tag{3.50}$$

$$\boldsymbol{m} = [1,1,1,0,0,0]^T \tag{3.51}$$

3.1.4   Linearization of inner Virtual Work

Linearization of Eq. (3.25) using the Gâteaux derivative may be assembled as

$$\Delta(\delta \Pi) = \int_\Omega \left[\delta \bar{\boldsymbol{C}} : \mathbb{C} : \Delta \bar{\boldsymbol{C}} + \Delta(\delta \bar{\boldsymbol{C}}) : \frac{\partial \Psi}{\partial \bar{\boldsymbol{C}}} \right] dV + \int_\Omega p \Delta(\delta J) dV$$
$$+ \int_\Omega \delta p (\Delta J - \Delta \theta) dV + \int_\Omega \Delta p (\delta J - \delta \theta) dV + \Delta(\delta \Pi_{ext}) \tag{3.52}$$

Where $\Delta \theta$, Δp, $\Delta \bar{\boldsymbol{C}}$, ΔJ etc. represent incremental quantities and $\mathbb{C}$ is the material tangent moduli given as

$$\mathbb{C} = 4 \frac{\partial^2 \Psi}{\partial \bar{\boldsymbol{C}} \partial \bar{\boldsymbol{C}}} = 2 \frac{\partial \bar{\boldsymbol{S}}}{\partial \bar{\boldsymbol{C}}} \tag{3.53}$$

Eq. (3.52) could be written in indicial form as

$$\Delta(\delta\Pi) = \int\limits_{\bar{\Omega}} \left[\delta\bar{C}_{ij}\bar{\mathbb{C}}_{ijkl}\Delta\bar{C}_{ij} + \frac{1}{2}\Delta(\delta\bar{C}_{ij})\bar{S}_{ij} \right] dV + \int\limits_{\Omega} p\,\Delta\,(\delta J)dV$$
$$+ \int\limits_{\Omega} \delta p\,(\Delta J - \Delta\theta)dV + \int\limits_{\Omega} \Delta p\,(\delta J - \delta\theta)dV + \Delta(\delta\Pi_{ext}$$

(3.54)

The spatial tangent of a constitutive model of Eq. (3.53) is denoted by the transformation given as (Zienkiewicz and Taylor, 2000)

$$\hat{\mathbb{C}} = \frac{1}{\theta}\,\bar{F}\,\bar{F}\mathbb{C}\,\bar{F}^T\bar{F}^T$$

(3.55)

The inner virtual work of Eq. (3.54) could be written in matrix form as

$$\Delta(\delta\Pi_{inner}) = \begin{bmatrix} \delta\boldsymbol{u}^T, \delta\boldsymbol{u}_p^T, \delta\widehat{\boldsymbol{\theta}}^T \end{bmatrix} \begin{bmatrix} \boldsymbol{K}_{uu} & \boldsymbol{K}_{u\theta} & \boldsymbol{K}_{up} \\ \boldsymbol{K}_{\theta u} & \boldsymbol{K}_{\theta\theta} & -\boldsymbol{K}_{\theta p} \\ \boldsymbol{K}_{pu} & -\boldsymbol{K}_{p\theta} & 0 \end{bmatrix} \begin{bmatrix} \Delta\widehat{\boldsymbol{u}} \\ \Delta\widehat{\boldsymbol{\theta}} \\ \Delta\widehat{\boldsymbol{p}} \end{bmatrix}$$

(3.56)

Eq. (3.56) may be split into the constitutive $\boldsymbol{K}_{ij}^m$ and geometric $\boldsymbol{K}_{ij}^g$ parts

$$\boldsymbol{K}_{ij} = \boldsymbol{K}_{ij}^m + \boldsymbol{K}_{ij}^g$$

(3.57)

The constitutive tangent terms for symmetric moduli are expressed as

$$\boldsymbol{K}_{uu}^m = \int\limits_{\Omega} \boldsymbol{B}_u^T\,\bar{\boldsymbol{D}}_{11}\boldsymbol{B}_u\theta dV$$

(3.58a)

$$\boldsymbol{K}_{u\theta}^m = \int\limits_{\Omega} \boldsymbol{B}_u^T\,\bar{\boldsymbol{D}}_{12}\boldsymbol{B}_u N_\theta dV = \boldsymbol{K}_{u\theta}^m{}^T$$

(3.58b)

$$\boldsymbol{K}_{up}^m = \int\limits_{\Omega} \boldsymbol{B}_u^T\,\boldsymbol{m}\,N_p\,JdV = \boldsymbol{K}_{pu}^m{}^T$$

(3.58c)

$$\boldsymbol{K}_{\theta\theta}^m = \int\limits_{\Omega} N_u^T\,\bar{\boldsymbol{D}}_{22}\,N_\theta\theta\,dV$$

(3.58d)

Where

$$N_\theta = \frac{1}{\theta}N$$

(3.59)

and in matrix notation

$$\bar{\boldsymbol{D}}_{11} = \boldsymbol{I}_{dev}\bar{\boldsymbol{D}}\boldsymbol{I}_{dev} - \frac{2}{3}\left(\boldsymbol{m}\,\bar{\boldsymbol{\sigma}}_{dev}^T + \bar{\boldsymbol{\sigma}}_{dev}\boldsymbol{m}^T\right) + 2(\bar{p} - \hat{p}\,)\hat{I}$$
$$- \left(\frac{2}{3}\,\bar{p} - \hat{p}\right)\boldsymbol{m}\,\boldsymbol{m}^T$$

(3.60a)

$$\overline{\boldsymbol{D}}_{12} = \frac{1}{3}\boldsymbol{I}_{dev}\overline{\boldsymbol{D}}\,\boldsymbol{m} + \frac{2}{3}\,\overline{\sigma}_{dev} = \overline{\boldsymbol{D}}_{21}^T \tag{3.60b}$$

$$\overline{\boldsymbol{D}}_{22} = \frac{1}{9}\boldsymbol{m}^T\,\overline{\boldsymbol{D}}\,\boldsymbol{m} - \frac{1}{3}\,\bar{p} \tag{3.60c}$$

$\overline{\boldsymbol{D}}$ is the transformation of $\hat{\mathbb{C}}$ given as

$$\overline{\boldsymbol{D}} \rightarrow \hat{\mathbb{C}} = \begin{bmatrix} D_{11} & D_{12} & D_{13} & D_{14} & D_{15} & D_{16} \\ D_{21} & D_{22} & D_{23} & D_{24} & D_{25} & D_{26} \\ D_{31} & D_{32} & D_{33} & D_{34} & D_{35} & D_{36} \\ D_{41} & D_{42} & D_{43} & D_{44} & D_{45} & D_{46} \\ D_{51} & D_{52} & D_{53} & D_{54} & D_{55} & D_{56} \\ D_{61} & D_{62} & D_{63} & D_{64} & D_{65} & D_{66} \end{bmatrix} \tag{3.61}$$

and the deviatoric matrix operator $\boldsymbol{I}_{dev}$ and stress $\overline{\boldsymbol{\sigma}}_{dev}$ are given as

$$\boldsymbol{I}_{dev} = \boldsymbol{I} - \frac{1}{3}\boldsymbol{m} \otimes \boldsymbol{m} \tag{3.62a}$$

$$\overline{\boldsymbol{\sigma}}_{dev} = \boldsymbol{I}_{dev} : \overline{\boldsymbol{\sigma}} \tag{3.62b}$$

$\boldsymbol{I}$ is the fourth rank unit tensor. $\hat{\boldsymbol{I}}$ is the matrix form of the fourth rank identity tensor

$$\hat{\boldsymbol{I}} = \frac{1}{2}\begin{bmatrix} 2 & 0 & 0 & 0 & 0 & 0 \\ 0 & 2 & 0 & 0 & 0 & 0 \\ 0 & 0 & 2 & 0 & 0 & 0 \\ 0 & 0 & 0 & 1 & 0 & 0 \\ 0 & 0 & 0 & 0 & 1 & 0 \\ 0 & 0 & 0 & 0 & 0 & 1 \end{bmatrix} \tag{3.63}$$

The geometric tangent term of Eq. (3.57) is given as

$$\boldsymbol{K}_{uu}^g = \int_{\Omega} (\nabla \boldsymbol{N} : \overline{\boldsymbol{\sigma}}\,\nabla \boldsymbol{N})dV \; ; \qquad \boldsymbol{K}_{uu}^g = \int_{\Omega} N_{r,i}\overline{\sigma}_{ij}N_{s,j}dV \tag{3.64}$$

Where $\nabla \boldsymbol{N}$ is the spatial gradient of the shape function

The compact form of linearized inner virtual work of Eq. (3.57) could be written in the form of the geometric element stiffness matrix $\boldsymbol{k}_g^e(\boldsymbol{u}^e)$ and the deformation-dependent material element stiffness matrix $\boldsymbol{k}_m^e(\boldsymbol{u}^e)$.

$$\Delta\delta\Pi_{inner}^e \approx \delta\boldsymbol{u}^e \cdot \left[\boldsymbol{k}_g^e(\boldsymbol{u}^e) + \boldsymbol{k}_m^e(\boldsymbol{u}^e)\right]\Delta\boldsymbol{u}^e \tag{3.65}$$

77

$$= \delta \boldsymbol{u}^e . \boldsymbol{k}_t^e(\boldsymbol{u}^e) \Delta \boldsymbol{u}^e$$

with the sum yielding the tangential element stiffness matrix $\boldsymbol{k}_t^e(\boldsymbol{u}^e)$ and $\delta \boldsymbol{u}^e$ is the variation of the displacement vector.

3.1.5 Principle of Virtual Work

The principle of virtual work postulates that the external and the internal virtual work are the same.

$$\delta \Pi_{internal} = \delta \Pi_{inertial} + \delta \Pi_{inner} = \delta \Pi_{ext} \qquad (3.66)$$

This means that the internal virtual work stored in the material is equal to the external virtual work done on the material by external forces. If we consider contact force $\boldsymbol{t}$ and body force $\boldsymbol{b}$ as external forces the following relation holds:

$$\delta \Pi_{ext} = \int_{\Omega} \delta \boldsymbol{u} \cdot \boldsymbol{b} \, \rho \, dV + \int_{\Omega} \delta \boldsymbol{u} \cdot \boldsymbol{t} \, dS \qquad (3.67)$$

The virtual inertial work resulting from the kinetic energy is given as

$$\delta \Pi_{iinertia} = \int_{\Omega} \delta \boldsymbol{u} \cdot \ddot{\boldsymbol{u}} \, \rho \, dV \qquad (3.68)$$

3.1.6   Approximation of Inertial Virtual Work

Besides discretization of inner virtual work, transient mechanical problems also demand discretization of dynamic virtual work. If we approximate the variation of displacements as well as continuous accelerations with the assistance of shape functions according to Eqs. (3.42) and (3.43), we get the approximation of virtual work of inertial forces.

$$\delta \Pi_{inertial}^e = \delta \boldsymbol{u}^e \cdot \int_{\Omega} \boldsymbol{N}^T \boldsymbol{N} \, \rho \, dV \, \ddot{\boldsymbol{u}}^e = \delta \boldsymbol{u}^e \cdot \boldsymbol{m}^e \cdot \ddot{\boldsymbol{u}}^e \qquad (3.69)$$

Where

$$\boldsymbol{m}^e = \int\limits_{\Omega} \boldsymbol{N}^T \, \boldsymbol{N} \, \rho \, dV \qquad (3.70)$$

Then the system mass matrix $\boldsymbol{M}$ is given as

$$\boldsymbol{M} = \bigcup_{e=1}^{NE} \boldsymbol{m}^e \qquad (3.71)$$

NE is the number of elements

3.1.7 Approximation of Virtual Work of External Loads

The loads acting on a plane element can be divided into loads acting in the field and those acting at the boundaries of the field. Typical loads in the field are gravitational loads whereas actual structural loads are dominated by boundary loads such as pressure. With the help of displacement variation approximation as in Eqs. (3.42) and (3.43), a consistent element load vector of volume loads $\boldsymbol{b}$ can be obtained based on external virtual work.

3.1.7.1 Volume loads

$$\delta \Pi_{ext}^{\Omega} = \delta \boldsymbol{u}^e \cdot \int\limits_{\Omega} \boldsymbol{N}^T \, \boldsymbol{b} \, \rho \, dV = \delta \boldsymbol{u}^e \cdot \boldsymbol{r}_p^e \qquad (3.72)$$

Where the element vector of volume forces $\boldsymbol{r}_p^e$ is then given as

$$\boldsymbol{r}_p^e = \int\limits_{\Omega} \boldsymbol{N}^T \, b \, \rho \, dV \qquad (3.73)$$

3.1.7.2 Boundary loads

The element load vector of element boundary loads $\boldsymbol{t}$ is derived by observation of external virtual work. Here, the boundary Γ can be divided into four boundaries Γ_i of the element.

$$\delta \Pi_{ext}^{\Gamma} = \int_{\Omega} \delta \boldsymbol{u} \, \boldsymbol{t} \, d\Gamma = \sum_{i=1}^{4} \int_{\Gamma_i} \delta \boldsymbol{u} \, \boldsymbol{t} \, d\Gamma_i = \sum_{i=1}^{4} \delta \Pi_{ext}^{\Gamma_{ie}} \tag{3.74}$$

The approximation of displacement variation of each boundary Γ_{ie} after the Jacobi transformation is given as

$$\delta \Pi_{ext}^{\Gamma_i} = \delta \boldsymbol{u}^e \cdot \boldsymbol{r}_{ni}^e \tag{3.75}$$

The summation of all correspondingly calculated equivalent loads $\boldsymbol{r}_{ni}^e$ for $\boldsymbol{r} = 1, 2, 3, 4$ yields the consistent equivalent loads of an element.

$$\delta \Pi_{ext}^{\Gamma} = \sum_{i=1}^{4} \delta \Pi_{ext}^{\Gamma_i} = \sum_{i=1}^{4} \delta \boldsymbol{u}^e \cdot \boldsymbol{r}_{ni}^e = \delta \boldsymbol{u}^e \cdot \sum_{i=1}^{4} \boldsymbol{r}_{ni}^e = \delta \boldsymbol{u}^e \cdot \boldsymbol{r}_n^e \tag{3.76}$$

Where the element vector of boundary forces $\boldsymbol{r}_n^e$ is then given as

$$\boldsymbol{r}_n^e = \int_{\Omega} \boldsymbol{N}^T \boldsymbol{t} \, d\Gamma \tag{3.77}$$

3.1.8 Nonlinear Elastomechanics Equations of the Continuum Compliant Mechanism

The principle of virtual work can now be approximated in the element plane as

$$\delta \mathbf{u}^e \cdot \mathbf{m}^e \ddot{\mathbf{u}}^e + \delta \mathbf{u}^e \cdot \mathbf{r}_i^e(\mathbf{u}^e) = \delta \mathbf{u}^e \cdot (\mathbf{r}_p^e + \mathbf{r}_n^e) \tag{3.78}$$

By summing Eq. (3.78) or explicitly, the vector of inner loads,

$$\boldsymbol{r}_i(\boldsymbol{u}) = \bigcup_{e=1}^{NE} \boldsymbol{r}_i^e(\boldsymbol{u}^e) \tag{3.79}$$

with the vector of external loads $(\mathbf{r}_p^e + \mathbf{r}_n^e)$ and the mass matrix $\mathbf{m}^e$, we obtain the system-related spatially discrete formulation of the principle of virtual work,

$$\delta \boldsymbol{u} \cdot \boldsymbol{M} \ddot{\boldsymbol{u}} + \delta \boldsymbol{u} \cdot \boldsymbol{r}_i(\boldsymbol{u}) = \delta \boldsymbol{u} \cdot \boldsymbol{r} \tag{3.80}$$

which can be transferred to an initial value problem of non-linear elastodynamics by application of lemma of variation calculus. The problem is defined by the semi-discrete differential equation of motion of the second order.

$$M\ddot{u} + r_i(u) = r \tag{3.81}$$

For elastostatic or quasi-static problems of the continuum compliant mechanism, we can formulate the discrete equation of nonlinear static equilibrium by neglecting the inertial forces $M\ddot{u} = 0$.

$$r_i(u) = r \tag{3.82}$$

In the scope of the iterative solution of nonlinear dynamic differential vector Eq. (3.81) or the nonlinear static vector Eq. (3.82), the linearization of inner forces is of great importance. In the element plane, the linearization of inner forces $r_i(u)$ is defined by linearization of the inner virtual work in Eq. (3.79). By summing the linearized inner forces and parts of the tangential stiffness matrix

$$\Delta r_i(u) = \bigcup_{e=1}^{NE} \Delta r_i^e(u^e) \tag{3.83}$$

$$k_m(u) = \bigcup_{e=1}^{NE} k_m^e(u^e) \tag{3.84}$$

$$k_g(u) = \bigcup_{e=1}^{NE} k_g^e(u^e) \tag{3.85}$$

$$k_t(u) = \bigcup_{e=1}^{NE} k_t^e(u^e) \tag{3.86}$$

The linearization of the system vector of internal forces is eventually gotten as function of the material system stiffness matrix $K_m(u)$, the geometric system stiffness matrix $K_g(u)$, the tangential system stiffness matrix $K_t(u)$ and the increment of the system displacement vector Δu

$$\Delta r_i(u) = \left(K_g(u) + K_m(u)\right)\Delta u = K_t(u)\Delta u \tag{3.87}$$

3.2 Effect of Shear Deformation in the Analysis of Compliant Mechanism

The model is based on the selection of the geometry, material properties, the loading and boundary conditions, and any other specific assumptions made. The purpose of the analysis is to answer certain questions regarding the stiffness, stresses developed and strength of the structure. Hence, when studying the behaviour of the structure, we would like to predict the future not only when the structure is operating in normal conditions, which mostly only requires a linear analysis, but also when the structure is subjected to severe loading conditions, which usually requires a highly nonlinear analysis. When considering nonlinear analysis, it is necessary to include the shear deformation terms.
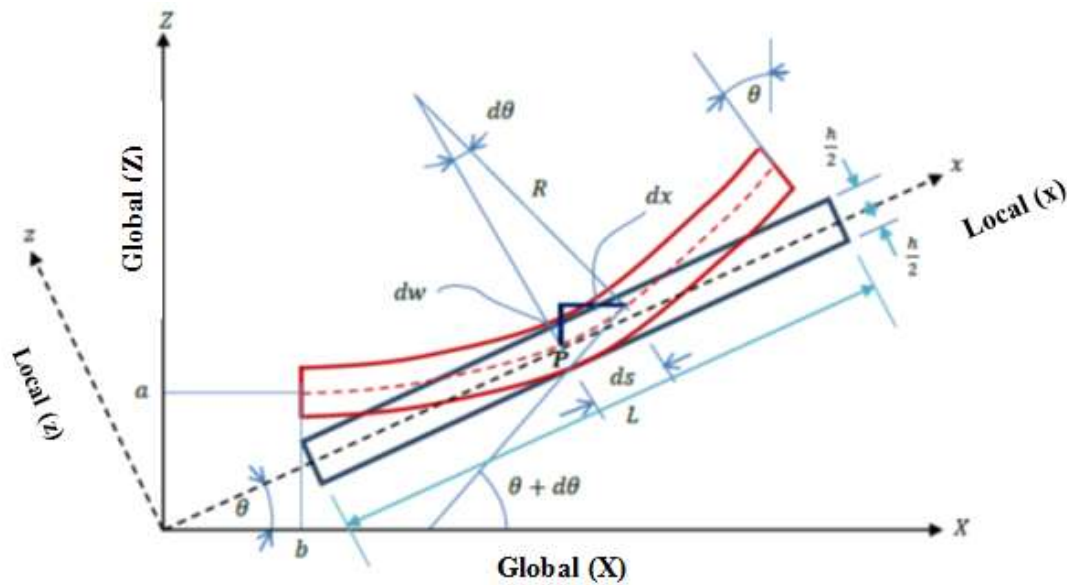
Fig. 3.2: Deformed and Underformed Beam Element
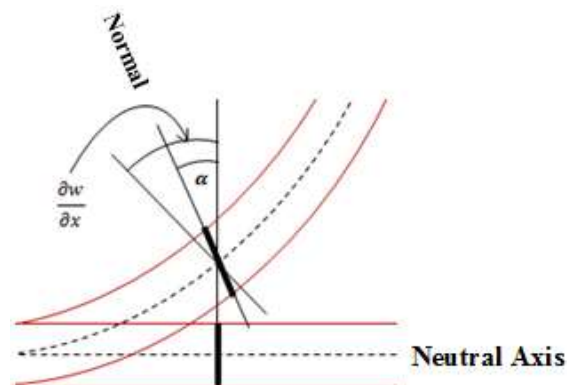
Fig. 3.3: Detail of the Beam Element with Shear Deformation

Fig.3. 2 shows the deformed and underformed beam element in the $x - z$ plane while Fig. 3.3. shows the detail of the beam element with shear deformation. R is the radius of curvature of the beam. dx, dw and ds form a right angled triangle. ds is a very small portion on the centroid of the beam. The curvature k of the beam element is given as

$$k = \frac{cd^2w}{dx^2} \tag{3.88}$$

Where

$$c = 1/\left(\sqrt{1 + \left(\frac{dw}{dx}\right)^2}\right)^3 \tag{3.89}$$
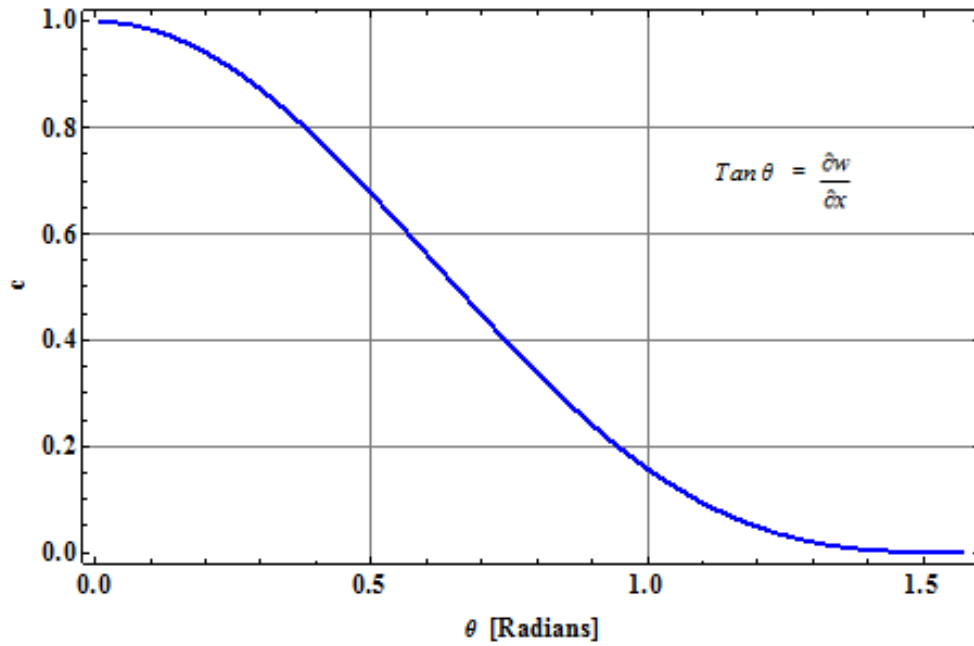
Fig. 3.4: c plotted against θ for $0 \leq \theta \leq \pi/2$

Fig. 3.4 is the graph of c against θ. The deviation of the value of c from unity represents the factor by which the compliant system undergoes large deflection. Compliant members undergo large deflections which introduce geometric nonlinearity. For small deflection, the slope of the deflected middle surface are small compared to unity so that the curvature is approximated as

$$k \approx \frac{d^2w}{dx^2} \tag{3.90}$$

3.2.1 Kinetic Energy

In Fig. 2. the displacement vector along the neutral axis in axial direction is given as

$$s_x = aCos\theta + bSin\theta + x + u \tag{3.91a}$$

$$s_z = bCos\theta + aSin\theta + w \tag{3.91b}$$

Eqs. (3.91a) and (3.91b) could be combined in the form

$$S = (aCos\theta + bSin\theta + x + u)i + (bCos\theta + aSin\theta + w)k \tag{3.92}$$

Where a and b are the coordinates of end 1 of the beam element. x is the coordinate measured along the element's neutral axis from 1 to 2. θ is the angle between the body motion and the x-axis. u and w are the axial and transverse displacements of point P from the rigid body position. For small value of θ, $Cos\ \theta \approx 1$ and $Sin\ \theta \approx 0$. Substituting these values into Eq. (3.92), gives

$$S = (a + b\theta + u)i + (b - a\theta + w)k \tag{3.93}$$

Differentiating Eq. (3.93), the velocity of a particle at point, P is given as

$$V = \frac{ds}{dt} = \left(b\frac{d\theta}{dt} + \frac{dx}{dt} + \frac{du}{dt}\right)i + \left(a\frac{d\theta}{dt} + \frac{dw}{dt}\right)k \tag{3.94}$$

The kinetic energy T_p of beam particles can be expressed as

$$T_p = \frac{1}{2}\iint \rho A_x V^2 dx dz \tag{3.95}$$

Where ρ is the mass density of the beam material and A_{xz} is the cross sectional area of the beam element. The kinetic energy T_s associated with transverse shear is also given as

$$T_s = \frac{1}{2}\iint \rho I_z \left(\frac{\partial \alpha}{dt}\right)^2 dx dz \tag{3.96}$$

α is the measure of transverse shear angle. The angular velocity V_α of any differential line segment on the neutral axis of the element is given by

$$V_\alpha = \frac{\partial \theta}{\partial t} + \frac{\partial^2 w}{\partial x \partial t} \tag{3.97}$$

The kinetic energy T_R due to rotatory inertia of the beam element is given as

$$T_R = \frac{1}{2} \iint \rho I_z \left(\frac{d\theta}{dt} + \frac{d^2 w}{dxdt} \right)^2 dxdz$$

(3.98)

The total kinetic energy T of the beam element becomes

$$T = T_p + T_s + T_R$$

(3.99)

It should be noted that the limits of the double integration in Eqs. (3.95), (3.96) and

(3.98) are from $-\frac{h}{2}$ to $\frac{h}{2}$ and 0 to L. Eq. (3.99) becomes

$$T = \frac{1}{2} \int_{-\frac{h}{2}}^{\frac{h}{2}} \int_0^L \left[\rho A_{xx} \left(\left(b\frac{d\theta}{dt} + \frac{dx}{dt} + \frac{du}{dt} \right)^2 + \left(a\frac{d\theta}{dt} + \frac{dw}{dt} \right)^2 \right) \right.$$
$$\left. + \rho I_z \left(\left(\frac{d\alpha}{dt} \right)^2 + \left(\frac{d\theta}{dt} + \frac{d^2 w}{dxdt} \right)^2 \right) \right] dxdz$$

(3.100)

3.2.2 Strain – Displacement Relation

u_x, u_y and u_z are displacements of the member at any point in the x, y and z directions

respectively. u, v and w are displacements of the middle surface in the x, y and z

directions respectively. The Green strain is given as

$$\varepsilon_{xx} = \frac{\partial u_x}{\partial x} + \frac{1}{2} \left[\left(\frac{\partial u_x}{dx} \right)^2 + \left(\frac{\partial u_y}{dx} \right)^2 + \left(\frac{\partial u_z}{dx} \right)^2 \right]$$

(3.101)

The von Karman strains are related to the displacement by

$$\varepsilon_{xx} = \varepsilon_{xx}^0 + z\varepsilon_{xx}^1$$

(3.102a)

$$\varepsilon_{xx}^0 = \frac{\partial u_x}{\partial x} + \frac{1}{2} \left(\frac{\partial u_z}{dx} \right)^2 = \frac{\partial u_x}{\partial x} + \frac{1}{2} \left(\frac{\partial w}{dx} \right)^2$$

(3.102b)

Eq. (3.102b) stands for the strain equation for geometric nonlinearity due to stretching

of the neutral axis. Eq. (3.102c) is equivalent to the curvature displacement relation for

small deflection in Eq. (3.90). Therefore, for large deflection analysis which results in

geometric nonlinearity due to curvature, Eq. (3.102a) becomes

$$\varepsilon_{xx} = \varepsilon_{xx}^0 + zk$$

(3.103a)

$$\varepsilon_{xx} = \frac{\partial u_x}{\partial x} + \frac{1}{2}\left(\frac{\partial w}{dx}\right)^2 + zc\frac{\partial^2 w}{\partial x^2} \tag{3.103b}$$

In order to present realistic proportional links, the links are assumed to be of the same cross section. Each link is divided into elements of the same length with constant areas. The integrations involved in the element equations are carried out in a piecewise fashion with areas in each section taken as a constant.

3.2.3 Strain Energy

The virtual strain energy Ψ for the element may be written as

$$\Psi = \iint \sigma\delta\varepsilon\,dxdz + \frac{1}{2}\iint \tau_{xz}\gamma_{xz}\,dxdz \tag{3.104}$$

Where σ is the normal stress, ε is the normal strain, τ_{xz} and γ_{xz} are the shear stress and shear strain respectively.

But,

$$\tau_{xz} = G_{xz}\gamma_{xz} \tag{3.105a}$$

$$\gamma_{xz} = \left(\alpha + \frac{\partial w}{\partial x}\right)^2 \tag{3.105b}$$

Where G_{xz} is the shear modulus. Substituting Eq. (3.105) into Eq. (3.104), we have

$$\Psi = \iint \sigma\delta\varepsilon\,dxdz + \frac{1}{2}\iint G_{xz}\left(\alpha + \frac{\partial w}{\partial x}\right)^2 dxdz \tag{3.106}$$

Taking the variation of Eq. (3.103b), gives

$$\delta\varepsilon_{xx} = \frac{\partial\delta u}{\partial x} + \frac{\partial w}{\partial x}\frac{\partial\delta w}{\partial x} + zc\frac{\partial^2\delta w}{\partial x^2} \tag{3.107}$$

Substituting Eq. (3.105) into Eq. (3.106) gives

$$\Psi = \iint \sigma_{xx}\left(\frac{\partial\delta u}{\partial x} + \frac{\partial w}{\partial x}\frac{\partial\delta w}{\partial x} + zc\frac{\partial^2\delta w}{\partial x^2}\right)dxdz$$
$$+ \frac{1}{2}\iint G_{xz}\left(\alpha + \frac{\partial w}{\partial x}\right)^2 dxdz \tag{3.108}$$

But,

$$\iint G_{xz} dx dz = G_{xz} A_{xz} = q G_{xz} A_z \tag{3.109}$$

Here, q is a constant (for a rectangular section, $q = {}^6/_5$; for a circular section, $q = {}^{37}/_{32}$), A_{xz} is the $x - z$ plane area, A_s is the shear area and $G_{xz} A_s$ is the shear stiffness.

$$\Psi = \iint \sigma_{xx} \left(\frac{\partial \delta u}{\partial x} + \frac{\partial w}{\partial x} \frac{\partial \delta w}{\partial x} + zc \frac{\partial^2 \delta w}{\partial x^2} \right) dx dz \tag{3.110}$$
$$+ \frac{1}{2} q G_{xz} A_s \iint \left(\alpha + \frac{\partial w}{\partial x} \right)^2 dx dz$$

Integrating Eq. (3.110) within the depth of z leads to

$$\Psi = \int_0^L \left[N_{xx} \left(\frac{\partial \delta u}{\partial x} + \frac{\partial w}{\partial x} \frac{\partial \delta w}{\partial x} \right) \right.$$
$$+ \left(M_{xx} \frac{\partial^2 \delta w}{\partial x^2} \left(1 / \left(1 + \left(\frac{\partial w}{\partial w} \right)^2 \right)^{3/2} \right) \right) \tag{3.111}$$
$$\left. + \frac{1}{2} q G_{xz} A_s \int_{-\frac{h}{2}}^{\frac{h}{2}} \left(\alpha + \frac{\partial w}{\partial x} \right)^2 dz \right] dx$$

Where

$$\int \sigma_{xx} dz = N_{xx} \tag{3.112a}$$

$$\int \sigma_{xx} z = M_{xx} \tag{3.112b}$$

N_{xx} is the axial force and M_{xx} is the bending moment in the beam. The Lagrangian function L_f is defined as

$$L_f = \sum_{r=1}^{k} \sum_{s=1}^{n} (T - \Psi)_{rs} \tag{3.113}$$

The limits of the summation is from the first element $s = 1$ of each link to the last element n of the same link and $r = 1$ of each link of the mechanism to the last link k of the mechanism. Substituting the value for the total kinetic energy, T from Eq. (3.100) and that of the strain energy density Ψ from Eq. (3.111), the Lagrangian can be expressed in terms of u, v, w, α and θ.

3.2.4   Finite Element Formulation

The Rayleigh-Ritz method is used to approximate both transverse and axial deformation variables. Hermite polynomials are used to approximate the transverse displacement w, transverse shear α and beam angle θ, while the Lagrange linear interpolation functions are used to approximate the axial displacement u in order to satisfy the boundary conditions of various types of compliant mechanisms easily and to ensure interelement compatibility. It should be noted that nodes 1 and 2 are the end nodes. The axial deformation u with its variation δu are approximated by a shape function given by

$$u_{(x,t)} = g_u U = \sum_{i=1}^{2} U_i(x,t) N_i(x) \tag{3.114}$$

$$N_1 = (1 - \bar{x}) \tag{3.115a}$$

$$N_1 = \bar{x} \tag{3.115b}$$

Where N_i (i.e g_u) is the Lagrange interpolation function, $\bar{x}$ is the element coordinate with the origin at node 1. Let ϑ_i be the first derivative of the shape function N_i so that the approximation of Eq. (3.114) becomes

$$\dot{u}_{(x,t)} = \dot{g}_u U = \sum_{i=1}^{2} U_i(x,t) \vartheta_i(x) \tag{3.116}$$

Similarly, the transverse deformation w with its variation δw are approximated by fifth degree Hermite polynomials given by

$$w_{(x,t)} = g_w W = \sum_{i=1}^{6} W_i(x,t) \phi_i(x) \tag{3.117}$$

Where

$$\phi_1 = 1 - 10\left(\frac{\bar{x}}{L}\right)^3 + 15\left(\frac{\bar{x}}{L}\right)^4 - 6\left(\frac{\bar{x}}{L}\right)^5 \tag{3.118a}$$

$$\phi_2 = \bar{x}\left[1 - 6\left(\frac{\bar{x}}{L}\right)^2 + 8\left(\frac{\bar{x}}{L}\right)^3 - 3\left(\frac{\bar{x}}{L}\right)^4\right] \tag{3.118b}$$

$$\phi_3 = \frac{\bar{x}^2}{2}\left[1 - 3\frac{\bar{x}}{L} + 3\left(\frac{\bar{x}}{L}\right)^2 - \left(\frac{\bar{x}}{L}\right)^3\right] \tag{3.118c}$$

$$\phi_4 = 10\left[\left(\frac{\bar{x}}{L}\right)^3 - 15\left(\frac{\bar{x}}{L}\right)^4 + 6\left(\frac{\bar{x}}{L}\right)^5\right] \tag{3.118d}$$

$$\phi_5 = -\bar{x}\left[4\left(\frac{\bar{x}}{L}\right)^2 - 7\left(\frac{\bar{x}}{L}\right)^3 + 3\left(\frac{\bar{x}}{L}\right)^4\right] \tag{3.118e}$$

$$\phi_4 = \frac{\bar{x}^2}{2}\left[\frac{\bar{x}}{L} - 2\left(\frac{\bar{x}}{L}\right)^2 + \left(\frac{\bar{x}}{L}\right)^3\right] \tag{3.118f}$$

The initial transverse displacement is approximated as

$$w_{(x,t)} = g_w W = \sum_{j=i.4} W_j(x,t)\Delta_j(x) \tag{3.119}$$

While the first and second derivatives of the transverse displacement are approximated

as

$$\dot{w}_{(x,t)} = \dot{g}_w W = \sum_{j=2,5} W_j(x,t)\Phi_j(x) \tag{3.120}$$

$$\ddot{w}_{(x,t)} = \ddot{g}_w W = \sum_{j=3,6} W_j(x,t)\Theta_j(x) \tag{3.121}$$

Φ_j (i.e $\dot{g}_w$) are the first derivatives of the second and fifth Hermite polynomials; Θ_j (i.e

$\ddot{g}_w$) are the second derivatives of the third and sixth Hermite polynomials. For the

purpose of compatibility, θ is also approximated by the fifth order polynomial.

$$\theta_{(x,t)} = g_\theta \theta = \sum_{j=i.4} \theta_j(x,t)\Delta_j(x) \tag{3.121a}$$

$$\dot{\theta}_{(x,t)} = \dot{g}_\theta \theta = \sum_{j=2,5} \theta_j(x,t)\Phi_j(x) \tag{3.121b}$$

And α is approximated by

$$\alpha_{(x,t)} = g_\alpha \alpha = \sum_{j=i.4} \alpha_j(x,t)\Delta_j(x) \tag{3.122a}$$

$$\dot{\alpha}_{(x,t)} = \dot{g}_\alpha \alpha = \sum_{j=2,5} \alpha_j(x,t)\Phi_j(x) \tag{3.122b}$$

Substituting the approximations from Eqs. (3.114-3.122) into Eq. (3.100), the kinetic energy can now be rewritten as

$$T = \frac{1}{2}\int_{-\frac{h}{2}}^{\frac{h}{2}}\int_0^L [(\rho A_{xx}((b\,\dot{g}_\theta\theta + \dot{x} + \dot{g}_u U)^2 + (a\,\dot{g}_\theta\theta + \dot{g}_w W)^2) + \rho I_z((\dot{g}_\alpha\alpha)^2 + (\dot{g}_\theta\theta + \ddot{g}_w W)^2)]\,dxdz \tag{3.123}$$

Equally, the strain energy density of Eq. (3.111) can be rewritten as

$$\Psi = \int_0^L \left[N_{xx}(\dot{g}_u U + (\dot{g}_w W)^2) + \left(M_{xx}\ddot{g}_w W\left(1/(1 + (\dot{g}_w W)^2)^{3/2}\right)\right)\right.$$
$$\left. + \frac{1}{2}qG_{xz}A_s \int_{-\frac{h}{2}}^{\frac{h}{2}}(g_\alpha\alpha + \dot{g}_w W)^2 dz \right] dx \tag{3.124}$$

The transformation of coordinates is now introduced to change from moving coordinates system associated with the element to global coordinates. Only the nodal displacements U_i and W_i need to be transformed. The other coordinates are angles or derivative of angles which are not directional on the $_{xz}$ coordinate system used. The corresponding transformation is given as

$$\begin{bmatrix} U_1 \\ W_1 \\ W_2 \\ W_3 \\ U_2 \\ W_4 \\ W_5 \\ W_6 \end{bmatrix} = \begin{bmatrix} Cos\,\theta & Sin\,\theta & 0 & 0 & 0 & 0 & 0 & 0 \\ -Sin\,\theta & Cos\,\theta & 0 & 0 & 0 & 0 & 0 & 0 \\ 0 & 0 & Cos\,\theta & Sin\,\theta & 0 & 0 & 0 & 0 \\ 0 & 0 & -Sin\,\theta & Cos\,\theta & 0 & 0 & 0 & 0 \\ 0 & 0 & 0 & 0 & Cos\,\theta & Sin\,\theta & 0 & 0 \\ 0 & 0 & 0 & 0 & -Sin\,\theta & Cos\,\theta & 0 & 0 \\ 0 & 0 & 0 & 0 & 0 & 0 & Cos\,\theta & Sin\,\theta \\ 0 & 0 & 0 & 0 & 0 & 0 & -Sin\,\theta & Cos\,\theta \end{bmatrix} \begin{bmatrix} \bar{U}_1 \\ \bar{W}_1 \\ \bar{W}_2 \\ \bar{W}_3 \\ \bar{U}_2 \\ \bar{W}_4 \\ \bar{W}_5 \\ \bar{W}_6 \end{bmatrix} \tag{3.125}$$

$$[U_1, W_1, W_2, W_3, U_2, W_4, W_5, W_6]^T = [T_f][\bar{U}_1, \bar{W}_1, \bar{W}_2, \bar{W}_3, \bar{U}_2, \bar{W}_4, \bar{W}_5, \bar{W}_6]^T \tag{3.126}$$

T_f is the transformation matrix. $\bar{U}_1, \bar{W}_1, \bar{W}_2, \bar{W}_3, \bar{U}_2, \bar{W}_4, \bar{W}_5, \bar{W}_6$ are the nodal displacements in global coordinate. Substituting the expression from Eqs. (3.123) and

(3.124) into the Eq. (2.113), the equation for the global displacement vectors for the system is given as

$$
\begin{aligned}
L_f = \sum_{r=1}^{k} \sum_{s=1}^{n} \Bigg[\frac{1}{2} \int_{-\frac{h}{2}}^{\frac{h}{2}} \int_{0}^{L} & [(\rho A_{xx}((b\,\dot{g}_\theta \theta + \dot{x} + \dot{g}_u U)^2 \\
& + (a\,\dot{g}_\theta \theta + \dot{g}_w W)^2) \\
& + \rho I_z((\dot{g}_\alpha \alpha)^2 + (\dot{g}_\theta \theta + \ddot{g}_w W)^2)]\, dxdz \\
& - \int_0^L \Bigg[N_{xx}(\dot{g}_u U + (\dot{g}_w W)^2) \\
& + \left(M_{xx}\ddot{g}_w W \left(1/(1 + (\dot{g}_w W)^2)^{3/2} \right) \right) \\
& + \frac{1}{2} q G_{xz} A_s \int_{-\frac{h}{2}}^{\frac{h}{2}} (g_\alpha \alpha + \dot{g}_w W)^2 dz \Bigg] dx \Bigg]_{rs}
\end{aligned}
\tag{3.127}
$$

The global coordinates for the system are given by

$$
q = [\bar{U}_1,\ \bar{W}_1,\ \bar{W}_2, \bar{W}_3\,,\theta_1,\alpha_1, \bar{U}_2\,,\bar{W}_4\,,\bar{W}_5\,,\bar{W}_6\,,\theta_2,\alpha_2]
\tag{3.128}
$$

Differentiating the Lagrangian with respect to the element coordinates gives the Lagrange equation of motion.

$$
\frac{d}{dt}\left(\frac{\partial L_f}{\partial \dot{q}} \right) - \frac{\partial L_f}{\partial q} = 0
\tag{3.129}
$$

The operation carried out in Eq. (3.129) results in a system of nonlinear element differential equations. Assembling the element matrices for particular compliant mechanism being solved results in the global system of equations given as

$$
[M]\{Q_{,tt}\} + [C]\{Q_{,t}\} + [K]\{Q\} = \{F\}
\tag{3.130}
$$

Where

$$
[K] = [K_l] + [K_{nl}]
\tag{3.131}
$$

Q and F are the displacement and force vectors respectively. The M, C, K_l and K_{nl}, matrices are all functions of time t. The C matrix results from the kinetic energy of the system. The matrix K_l is the linear portion of the stiffness matrix. The matrix K_{nl} is the nonlinear portion of the stiffness matrix. Eq. (3.130) give a system of nonlinear

equations that will be solved iteratively for a given compliant mechanism problem. The

Newton - Raphson iteration method will be employed for the iteration process.

3.3   Fatigue Failure Prediction Model

The strain energy density of nearly incompressible material models (Eq. 3.15) could be

expressed in terms of the principal stretches, λ_j as

$$\Psi(\lambda_1, \lambda_2, \lambda_3) = \sum_{p=1}^{n} \frac{\mu_p}{\alpha_p} \left(\bar{\lambda}_1^{\alpha_p} + \bar{\lambda}_2^{\alpha_p} + \bar{\lambda}_3^{\alpha_p} \right) + \sum_{p=1}^{n} \beta (J-1)^2 \tag{3.132}$$

Where

$$\mu_p = \frac{1}{2} \sum_{i=1}^{n} \mu_i \tag{3.133a}$$

$$\beta = \frac{k_i}{2} \tag{3.133b}$$

The principal components of the Cauchy stress are given by (Ogden, 1997)

$$\sigma_i = \frac{\lambda_i}{\lambda_1 \lambda_2 \lambda_3} \frac{\partial \Psi}{\partial \lambda_i} \qquad\qquad i = 1,2,3 \tag{3.134}$$

The strain energy potential can be written as either function of the principal stretch

ratios or as a function of the invariants of the strain tensor $\boldsymbol{C}, I_1, I_2, I_3$. The invariants of

$\boldsymbol{C}$ are defined as

$$I_1 = tr\boldsymbol{C} = \boldsymbol{C} : \boldsymbol{I} \tag{3.135a}$$

$$I_2 = tr\boldsymbol{C}\boldsymbol{C} \tag{3.135b}$$

$$I_3 = det\, C = J^2 \tag{3.135c}$$

In terms of the principal stretch ratio, the invariants are written as

$$I_1 = \lambda_1^2 + \lambda_2^2 + \lambda_3^2 \tag{3.136a}$$

$$I_2 = \lambda_1^2 \lambda_2^2 + \lambda_2^2 \lambda_3^2 + \lambda_3^2 \lambda_1^2 \tag{3.136b}$$

$$I_3 = \lambda_1^2 \lambda_2^2 \lambda_3^2 \tag{3.136c}$$

The invariants could be expressed in terms of the deviatoric principal stretches as

$$\bar{I}_1 = J^{-\frac{2}{3}} I_1 \tag{3.137a}$$

$$\bar{I}_2 = J^{-\frac{4}{3}} I_2 \tag{3.137b}$$

$$\bar{I}_3 = J^2 \tag{3.137c}$$

Substituting Eq. (3.136a) and Eq. (3.137a) into Eq. (3.132) gives

$$\Psi = \sum_{p=1}^{n} \frac{\mu_p}{\alpha_p} \left(J^{-2/3} \left(\lambda_1^{\alpha_p} + \lambda_2^{\alpha_p} + \lambda_3^{\alpha_p} \right) - 3 \right) + \sum_{p=1}^{n} \beta (J-1)^2 \tag{3.138}$$

Using Eq. (3.134), Eq. (3.138) becomes

$$\lambda_i \frac{\partial J}{\partial \lambda_i} = \sum_{p=1}^{n} \frac{\mu_p}{\alpha_p} \left(-\frac{2}{3} J^{-5/3} \lambda_i \frac{\partial J}{\partial \lambda_i} \left(\lambda_1^{\alpha_p} + \lambda_2^{\alpha_p} + \lambda_3^{\alpha_p} \right) + J^{-2/3} \alpha_p \lambda_i^{\alpha_p} \right)$$
$$+ \sum_{p=1}^{n} 2\beta (J-1) \lambda_i \frac{\partial J}{\partial \lambda_i} \tag{3.139}$$

Since

$$J = \lambda_1^2 \lambda_2^2 \lambda_3^2 \tag{3.140b}$$

we have

$$\lambda_i \frac{\partial J}{\partial \lambda_i} = \lambda_1^2 \lambda_2^2 \lambda_3^2 = J \tag{3.140b}$$

Hence

$$\lambda_i \frac{\partial \Psi}{\partial \lambda_i} = \sum_{p=1}^{n} \frac{\mu_p}{\alpha_p} J^{-2/3} \left(\alpha_p \lambda_i^{\alpha_p} - \frac{2}{3} \left(\lambda_1^{\alpha_p} + \lambda_2^{\alpha_p} + \lambda_3^{\alpha_p} \right) \right)$$
$$+ \sum_{p=1}^{n} 2\beta J (J-1) \tag{3.141}$$

Therefore the principal Cauchy stresses are given as

$$\sigma_i = \sum_{p=1}^{n} \frac{\mu_p}{\alpha_p} J^{-5/3} \left(\alpha_p \lambda_i^{\alpha_p} - \frac{2}{3} \left(\lambda_1^{\alpha_p} + \lambda_2^{\alpha_p} + \lambda_3^{\alpha_p} \right) \right) + \sum_{p=1}^{n} 2\beta J (J-1) \tag{3.140b}$$

Then, the difference between the principal stresses become

$$\sigma_1 - \sigma_3 = \sum_{p=1}^{n} \mu_p J^{-5/3} \left(\lambda_1^{\alpha_p} - \lambda_3^{\alpha_p} \right) \tag{3.143a}$$

$$\sigma_2 - \sigma_3 = \sum_{p=1}^{n} \mu_p J^{-5/3} \left(\lambda_2^{\alpha_p} - \lambda_3^{\alpha_p} \right) \tag{3.143b}$$

$$\sigma_1 - \sigma_2 = \sum_{p=1}^{n} \mu_p J^{-5/3} \left(\lambda_1^{\alpha_p} - \lambda_2^{\alpha_p} \right) \tag{3.143c}$$

Since force is applied in one direction in most compliant mechanisms, we will consider a mechanism undergoing uniaxial stress state. The principal stretches become

$$\lambda_1 = \lambda \tag{3.144a}$$

$$\lambda_2 = \lambda_3 = \sqrt{J/\lambda} \tag{3.144b}$$

λ s the stretch in the loading direction ; λ_2 and λ_3 are the principal stretches on plane perpendicular to loading direction. Substitution Eq. (3.144) into Eqs. (3.143a,b,c) gives

$$\sigma_1 - \sigma_3 = \sigma_1 - \sigma_2 = \sum_{p=1}^{n} \mu_p J^{-5/3} \left(\lambda^{\alpha_p} - \left(\frac{J}{\lambda} \right)^{\alpha_p/2} \right) \tag{3.145a}$$

$$\sigma_2 - \sigma_3 = 0 \tag{3.145b}$$

The effective stress is given by the equation tensor

$$\begin{aligned}
\sigma_e &= \left(\frac{1}{2} (\sigma_1 - \sigma_2)^2 + (\sigma_2 - \sigma_3)^2 + (\sigma_1 - \sigma_3)^2 \right)^{1/2} \\
&= \left(\frac{3}{2} S_{ij} S_{ij} \right)^{1/2}
\end{aligned} \tag{3.146}$$

Where S_{ij} are the components of the deviatoric tensor $\boldsymbol{\sigma}_{dev}$

$$\boldsymbol{\sigma}_{dev} = \boldsymbol{\sigma} - \frac{1}{3} (tr\boldsymbol{\sigma}) \boldsymbol{I} \tag{3.147}$$

Substituting Eqs. (3.145a,b) into Eq. (3.146) gives

$$\sigma_e = \sum_{p=1}^{n} \mu_p J^{-5/3} \left(\lambda^{\alpha_p} - \left(\frac{J}{\lambda} \right)^{\alpha_p/2} \right) \tag{3.148}$$

The stretch ratio in the loading direction is given by (Haslach and Armstrong, 2004)

$$\lambda = 1 + \varepsilon \tag{3.149}$$

ε is the nominal strain. Substituting Eq. (3.149) into Eq. (3.148) gives

$$\sigma_e = \sum_{p=1}^{n} \mu_p J^{-5/3} \left((1+\varepsilon)^{\alpha_p} - \left(\frac{J}{(1+\varepsilon)} \right)^{\alpha_p/2} \right) \tag{3.150}$$

Equally, substituting Eq. (3.144) into Eq. (3.138), the strain energy density can be rewritten in the forms

$$\begin{aligned} \Psi &= \sum_{p=1}^{n} \frac{\mu_p}{\alpha_p} \left(J^{-2/3} \left((\lambda)^{\alpha_p} - \left(\frac{J}{\lambda} \right)^{\alpha_p/2} \right) - 3 \right) + \sum_{p=1}^{n} \beta (J-1)^2 \\ &= \sum_{p=1}^{n} \frac{\mu_p}{\alpha_p} \left(J^{-2/3} \left((1+\varepsilon)^{\alpha_p} - \left(\frac{J}{(1+\varepsilon)} \right)^{\alpha_p/2} \right) - 3 \right) \\ &\quad + \sum_{p=1}^{n} \beta (J-1)^2 \end{aligned} \tag{3.151a}$$

3.3.1 Continuum Damage Mechanics Model

Material damage usually induces the stiffness change of the material. Therefore, the damage state can be characterized by the change of elastic constants. Consider a representative volume element (RVE) of an anisotropic material with stiffness $[E]$ is damaged under a system of loading $\{\sigma_e\}$. The stiffness matrix of the damaged material is $[E_d]$. The damage matrix $[D]$ is defined as (Tang and Lee, 1995)

$$[D] = [I] - [E_d][E]^{-1} \tag{3.152}$$

Where $[I]$ is the identity matrix. The strain $\{\varepsilon\}$ is given as

$$\begin{aligned} \{\varepsilon\} &= [I] - [E_d]^1 \{\sigma_e\} \\ &= [E]^{-1} [[I] - [D]]^{-1} \{\sigma_e\} \\ &= [E]^{-1} \{\bar{\sigma}_e\} \end{aligned} \tag{3.153}$$

Where

$$\{\bar{\sigma}_e\} = [[I] - [D]]^{-1} \{\sigma_e\} \tag{3.154}$$

The matrix $\{\bar{\sigma}_e\}$ is defined as the effective stress matrix after material damage. Hence, the damage effect matrix $[M]$ is

95

$$[M] = \left[[I] - [D]\right]^{-1} \qquad\qquad (3.155)$$

3.3.2 Isotropic Model

Consider a damaged body as shown in Fig. 3.5, in which a representative volume element is isolated. Damaged variable is physically defined by the surface density of microcracks and intersections of micro-voids lying on a plane cutting RVE of cross section δA (Lemaitre and Desmorat, 2005).
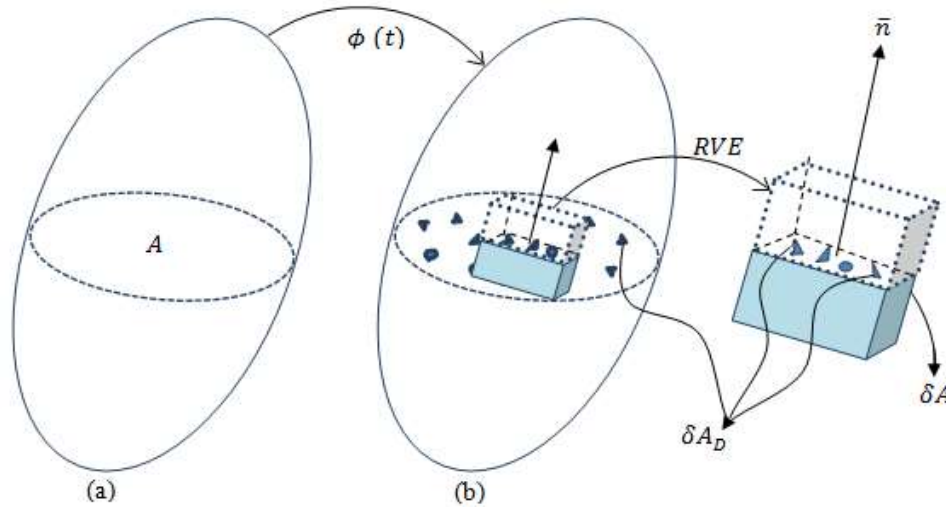

Fig. 3.5: Transformation $\phi(t)$ from the (a) initial undamaged configuration to (b) the damaged configuration

Damaged variable $D_{(\bar{n})}$, for the plane defined by normal $\bar{n}$ is

$$D_{(\bar{n})} = \frac{\delta A_D}{\delta A} \quad , \qquad 0 \leq D_{(\bar{n})} \leq 1 \qquad\qquad (3.156)$$

Where δA_D is the effective area of the intersection of all micro-cavities or microcracks that lie in the initial area δA at time t. An isotropic damage variable is equally distributed in all directions defined as

$$D = \frac{\delta A_D}{\delta A} \qquad\qquad (3.157)$$

Eq. (3.157) is the percentage of the damaged area to initial area. D is a scalar. Isotropic damage is assumed in this concept of continuum damage mechanics. The damage

parameter can be obtained by reducing the rank of matrix to zero. This reduces Eq. (3.152) to

$$D = 1 - E_d \cdot E^{-1} \tag{3.157}$$

The effective stress after material damage, $\bar{\sigma}_e$ and damage strain energy release rate are related by (Lemaitre, 1985)

$$\bar{\sigma}_e = M \cdot \sigma_e = \frac{\sigma_e}{1 - D} \tag{3.159}$$

The nominal stress – strain relation of a damage material is the same in form as that of an undamaged material (Sidoroff, 1981). This means that

$$\bar{\sigma}_e = \sigma_e \tag{3.160}$$

so that

$$\frac{\sigma_e}{1 - D} = \sum_{p=1}^{n} \mu_p J^{-\frac{5}{3}} \left(\lambda^{\alpha_p} - J^{\alpha_p/2} \lambda^{-\alpha_p/2} \right) \tag{3.161}$$

The constitutive equation for damage evolution is given by (Lemaitre and Desmorat, 2005)

$$\dot{D} = -\frac{\partial \alpha_0}{\partial Y} \tag{3.162}$$

α_0 is the dissipation potential; Y is the damage strain energy release rate; $\dot{D}$ is the damage growth rate. The dissipation potential is assumed as (Jiang, 1995)

$$\alpha_0 = \frac{s_0}{q_0 + 1} \left(-\frac{Y}{s_0} \right)^{q_0+1} \tag{3.163}$$

q_0 and s_0 are material parameters determined by the experimental fatigue life as a function of the strain range. But the strain energy of a damaged and undamaged material is the same (Tang and Lee, 1995). From the CDM theory, the damaged strain energy should be a function of the effective nominal normal stress of the damaged configuration. Hence, in the uniaxial stress state, the damaged strain energy released rate Y is defined as

$$-Y = \frac{\partial \Psi}{\partial D} = \frac{\partial \Psi(\bar{\sigma}_e)}{\partial D} \tag{3.164}$$

Substitution Eq. (3.151) into Eq. (3.164), we have

$$
\begin{aligned}
-Y &= \frac{\partial \Psi(\bar{\sigma}_e)}{\partial D} = \frac{\partial \Psi}{\partial \lambda}\frac{\partial \lambda(\bar{\sigma}_e)}{\partial D} \\
&= \sum_{p=1}^{n} \mu_p J^{-2/3}\left(\alpha_p\lambda^{\alpha_p-1} - \alpha_p J^{\alpha_p/2}\lambda^{-(\alpha_p/2-1)}\right)\frac{\partial \lambda(\bar{\sigma}_e)}{\partial D}
\end{aligned}
\tag{3.165}
$$

Taking the partial derivative of Eq. (3.161) with respect to D, gives

$$\frac{\partial \lambda(\bar{\sigma}_e)}{\partial D} = \sum_{p=1}^{n} \frac{1}{\mu_p}\frac{\sigma_e}{(1-D)^2}\left[J^{-5/3}\left(\alpha_p\lambda^{\alpha_p-1} + \frac{\alpha_p}{2}J^{\alpha_p/2}\lambda^{-\left(\alpha_p/2-1\right)}\right)\right]^{-1} \tag{3.166}$$

Substitution Eq. (3.166) into Eq. (3.165), we have

$$
\begin{aligned}
-Y = \sum_{p=1}^{n} \frac{1}{\alpha_p}\frac{\sigma_e}{(1-D)^2}J\Bigg[&\left(\alpha_p\lambda^{\alpha_p-1}\right.\\
&\left. - \alpha_p J^{\alpha_p/2}\lambda^{-\left(\alpha_p/2+1\right)}\right)\left(\alpha_p\lambda^{\alpha_p-1}\right.\\
&\left. + \frac{\alpha_p}{2}J^{\alpha_p/2}\lambda^{-\left(\alpha_p/2+1\right)}\right)^{-1}\Bigg]
\end{aligned}
\tag{3.167}
$$

Substitution Eq. (3.161) into Eq. (3.167) gives

$$
\begin{aligned}
-Y = \sum_{p=1}^{n} \frac{\mu_p}{\alpha_p}\Bigg[&\frac{\left(\lambda^{\alpha_p} - J^{\alpha_p/2}\lambda^{-\alpha_p/2}\right)}{1-D}J^{-2/3}\left(\alpha_p\lambda^{\alpha_p-1}\right.\\
&\left. - \alpha_p J^{\alpha_p/2}\lambda^{-\left(\alpha_p/2+1\right)}\right)\left(\alpha_p\lambda^{\alpha_p-1}\right.\\
&\left. + \frac{\alpha_p}{2}J^{\alpha_p/2}\lambda^{-\left(\alpha_p/2+1\right)}\right)^{-1}\Bigg]
\end{aligned}
\tag{3.168}
$$

Using Eqs. (3.162), (3.163), and (3.168) we have

$$
\begin{aligned}
\dot{D} = \sum_{p=1}^{n} \frac{\mu_p}{\alpha_p}\left(s_0^{-1}\right)\Bigg[&\frac{\left(\lambda^{\alpha_p} - J^{\alpha_p/2}\lambda^{-\alpha_p/2}\right)}{1-D}J^{-2/3}\left(\alpha_p\lambda^{\alpha_p-1}\right.\\
&\left. - \alpha_p J^{\alpha_p/2}\lambda^{-\left(\alpha_p/2+1\right)}\right)\left(\alpha_p\lambda^{\alpha_p-1}\right.\\
&\left. + \frac{\alpha_p}{2}J^{\alpha_p/2}\lambda^{-\left(\alpha_p/2+1\right)}\right)^{-1}\Bigg]^{q_0}
\end{aligned}
\tag{3.169}
$$

Under a cyclic loading condition, the damage will accumulate with the number of cycles and the damage evolution will depend on the strain amplitude. The time rate change of damage variable $\dot{D}$ can be represented in terms of the evolution of D with respect to the number of cycles. Based on this consideration, the principal stretch amplitude $\Delta\lambda$ is used to replace λ, the fatigue damage evolution per cycle is then expressed as

$$
\frac{dN}{dN} = \sum_{p=1}^{n} \frac{\mu_p}{\alpha_p} (s_0^{-1}) \left[\frac{\left(\Delta\lambda^{\alpha_p} - J^{\alpha_p/2} \Delta\lambda^{-\alpha_p/2} \right)}{1 - D} J^{-2/3} \left(\alpha_p \Delta\lambda^{\alpha_p - 1} \right. \right.
$$
$$
- \alpha_p J^{\alpha_p/2} \Delta\lambda^{-\left(\alpha_p/2 + 1 \right)} \Big) \left(\alpha_p \Delta\lambda^{\alpha_p - 1} \right.
$$
$$
\left. \left. + \frac{\alpha_p}{2} J^{\alpha_p/2} \Delta\lambda^{-\left(\alpha_p/2 + 1 \right)} \right)^{-1} \right]^{q_0} \tag{3.170}
$$

where $\Delta\lambda$ is the principal stretch amplitude and N is the number of cycles. Assuming that the damage variable D is zero at the beginning of the cyclic loading, that is, $D = 0$ when $N = 0$, then the damage value at any cycle can be determined by integrating Eq. (3.170), which gives

$$
\int_0^D (1 - D)^{q_0} \, dN
$$
$$
= \int_0^N \sum_{p=1}^{n} \frac{\mu_p}{\alpha_p} (s_0^{-1}) J^{-2/3} \left[\left[\left(\Delta\lambda^{\alpha_p} \right. \right. \right.
$$
$$
- J^{\alpha_p/2} \Delta\lambda^{-\alpha_p/2} \Big) \left(\alpha_p \Delta\lambda^{\alpha_p - 1} \right.
$$
$$
- \alpha_p J^{\alpha_p/2} \Delta\lambda^{-\left(\alpha_p/2 + 1 \right)} \Big) \left(\alpha_p \Delta\lambda^{\alpha_p - 1} \right.
$$
$$
\left. \left. \left. + \frac{\alpha_p}{2} J^{\alpha_p/2} \Delta\lambda^{-\left(\alpha_p/2 + 1 \right)} \right)^{-1} \right]^{q_0} \right] dN \tag{3.171}
$$

The relation between the damage variable D and number of cycles N could be deduced as

$$
\begin{aligned}
[1 - (1-D)^{q_0+1} \\
= (q_0 \\
+ 1)\left[\sum_{p=1}^{n}\frac{\mu_p}{\alpha_p}(s_0^{-1})J^{-2/3}\left[\left(\Delta\lambda^{\alpha_p}\right.\right.\right. \\
\left. - J^{\alpha_p/2}\Delta\lambda^{-\alpha_p/2}\right)\left(\alpha_p\Delta\lambda^{\alpha_p-1}\right. \\
\left. - \alpha_p J^{\alpha_p/2}\Delta\lambda^{-\left(\alpha_p/2+1\right)}\right)\left(\alpha_p\Delta\lambda^{\alpha_p-1}\right. \\
\left.\left.\left. + \frac{\alpha_p}{2}J^{\alpha_p/2}\Delta\lambda^{-\left(\alpha_p/2+1\right)}\right)^{-1}\right]^{q_0}\right]N
\end{aligned}
\tag{3.172}
$$

The damage variable is expressed as the ratio of the number of cycles N to the fatigue life N_f as (Jiang, 1995)

$$
D = \frac{N}{N_f}
\tag{3.173}
$$

Eq. (3.173) indicates that the damage is linearly distributed to each cycle during the loading. Therefore, if a material has been subjected to cyclic loading, the damage is

$$
D = \frac{N}{\left(N_f\right)_i}
\tag{3.174}
$$

and when the fatigue rupture occurs, we have

$$
D = D_c = 1
\tag{3.175}
$$

D_c is the critical value of the damage variable. Eqs. (3.173) - (3.175) show that at the moment of failure,

$$
N = N_f
\tag{3.176}
$$

and the fatigue life N_f is expressed as

$$
\begin{aligned}
N_f \\
= (q_0 \\
+ 1)^{-1}\left[\sum_{p=1}^{n}\frac{\mu_p}{\alpha_p}(s_0^{-1})J^{-2/3}\left[\frac{\left(\Delta\lambda^{\alpha_p} - J^{\alpha_p/2}\Delta\lambda^{-\alpha_p/2}\right)}{1-D}\left(\alpha_p\Delta\lambda^{\alpha_p-1}\right.\right.\right. \\
\left.\left.\left. - \alpha_p J^{\alpha_p/2}\Delta\lambda^{-\left(\alpha_p/2+1\right)}\right)\left(\alpha_p\Delta\lambda^{\alpha_p-1} + \frac{\alpha_p}{2}J^{\alpha_p/2}\Delta\lambda^{-\left(\alpha_p/2+1\right)}\right)^{-1}\right]\right]^{-q_0}
\end{aligned}
\tag{3.177}
$$

Using Eq. (3.149), the principal stretch amplitude, $\Delta\lambda$ and the nominal strain amplitude, $\Delta\varepsilon$ are related as

$$\Delta\lambda = 1 + \Delta\varepsilon \qquad (3.178)$$

Substitution Eq. (3.178) into Eq. (3.177), the formula for the fatigue life is expressed as a function of the nominal strain amplitude for a compliant mechanism under large deformation and cyclic loading.

$$
\begin{aligned}
N_f &= (q_0 \\
&+ 1)^{-1}\left[\sum_{p=1}^{n}\frac{\mu_p}{\alpha_p}(s_0^{-1})J^{-2/3}\left[\frac{\left((1+\Delta\varepsilon)^{\alpha_p} - J^{\alpha_p/2}(1+\Delta\varepsilon)^{-\alpha_p/2}\right)}{1-D}\left(\alpha_p(1\right.\right.\right. \\
&+ \Delta\varepsilon)^{\alpha_p-1} \\
&- \alpha_p J^{\alpha_p/2}(1+\Delta\varepsilon)^{-\left(\alpha_p/2+1\right)}\right)\left(\alpha_p(1+\Delta\varepsilon)^{\alpha_p-1}\right. \\
&+ \left.\left.\left.\frac{\alpha_p}{2}J^{\alpha_p/2}(1+\Delta\varepsilon)^{-\left(\alpha_p/2+1\right)}\right)^{-1}\right]\right]^{-q_0}
\end{aligned}
\qquad (3.179)
$$

If $n = 1$; $\alpha = 2$ and $J = 1$, Eq. (3.179) reduces to the fatigue life N_f for a Neo-Hookean incompressible model

$$
\begin{aligned}
N_f = (q_0 + 1)^{-1}&\left[\frac{\mu_p}{\alpha_p}(s_0^{-1})[[[(1+\Delta\varepsilon)^2 - (1+\Delta\varepsilon)^{-1}]2[(1+\Delta\varepsilon)\right. \\
&- \left.(1+\Delta\varepsilon)^{-2}][2(1+\Delta\varepsilon)+(1+\Delta\varepsilon)^{-2}]^{-1}]\right]^{-q_0}
\end{aligned}
\qquad (3.180)
$$

Based on the experimental results and curve fitting, q_0 and s_0 are obtained as 5.54 and 6.83 MPa respectively for LDPP and 7.33 and 7.29 MPa for LDPE.

3.4   Impact – Contact Analysis of Compliant Mechanisms

Impact is defined as the process involved in the collision of two or more objects. Common terminology limits the phrase 'impact' to collisions in which the mass effect of both impacting bodies must be taken into account, excluding case of 'impulsive loading' where one of striking objects does not possess the characteristics of a solid

(Flores *et al.,* 2008). Compared to usual analysis problems, impact-contact problems are extremely difficult to solve because of strong nonlinearities. Impact-contact can occur in static or dynamic conditions. In static analysis the inertia effect is negligible. Dynamic contact occurs when the inertia effect is important and all solution variables are time-dependent which are determined only when both boundary conditions and initial conditions are specified. Dynamic contact when the duration time of contact is very small is called impact-contact. An example of impact-contact is the case of a Flex-Run being struck onto the ground surface by an athlete. In the design of such mechanisms where strength, durability, precision and reliability are required, it is important to predict whether these products will break, or partially break, when they are struck.

Systems subjected to several impact loadings are vulnerable to failure due to damage. Such failure could be catastrophic if it is a mission critical system like the Flex-Run use by amputated athletes. This section investigates the dynamic response characteristics of a compliant system impacting on a surface. The dynamic impact-contact governing equations for both the target and impactor are derived based on the updated Lagrangian approach.

3.4.1   Formulation of impact-contact model

In studying the impact dynamics, a complete model is one that fully accounts for the dynamic behaviour of the structure, the contact behaviour, and the dynamics of the projectile. The general formulation is illustrated with reference to contact between two bodies as shown in Fig. 3.6
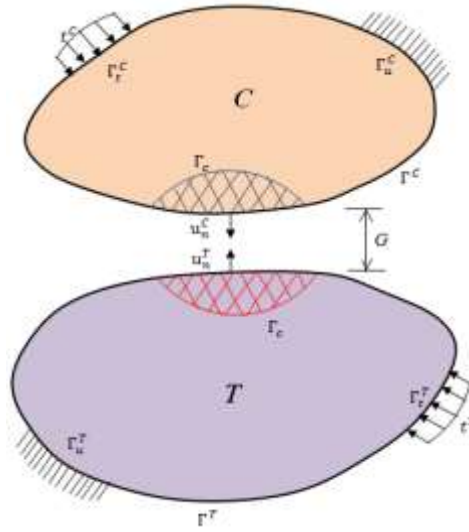
Fig. 3.6: Continuum Model of Contact and Target Bodies

The fixed body is the target T, and the other a contactor C with current domains Ω_0^C and Ω_0^T and boundaries Γ^T and Γ^C, respectively, and common contact zone Γ_c. U_n^C and U_n^T are the displacement of each body along their common opposite normal n^C and n^T.

At each point,

$$n^T = -n^C \tag{3.181}$$

Before the contact,

$$\Gamma_u^C \cup \Gamma_t^C = \Gamma^C \; ; \quad \Gamma_u^C \cap \Gamma_t^C = \{\} \tag{3.182}$$

$$\Gamma_u^T \cup \Gamma_t^T = \Gamma^T \; ; \quad \Gamma_u^T \cap \Gamma_t^T = \{\} \tag{3.183}$$

Subscripts u and t stand for boundaries with prescribed displacements and tractions respectively while superscripts C and T represents the contactor and target respectively. After contact and as long as their normal reaction is compression, we have

$$\Gamma^C \cap \Gamma^T = \Gamma_c \; ; \quad \Omega_0^C \cap \Omega_0^T = \{\} \tag{3.184}$$

The boundary condition compatibility or impenetration equation is give as

$$U_u^C(x, y, z) = U_u^T(x, y, z) \quad , \qquad (x, y, z) \in \Gamma_c \tag{3.185}$$

(x, y, z) is a space point on contact zone Γ_c which satisfy the constrain

$$U_u^T - U_u^T \leq 0 \qquad on \qquad \Gamma_c \tag{3.186}$$

The momentum equation and the natural boundary condition are given respectively as Eqs. (3.187) and (3.188)

$$\sigma_{ij,j} + \rho b_i = \rho \ddot{U}_i \qquad in \qquad \Omega_0^C \ \ and \ \ \Omega_0^T \tag{3.187}$$

$$\sigma_{ij} n_i = t_j \qquad in \qquad \Gamma_t^C \ \ and \ \ \Gamma_t^T \tag{3.188}$$

σ_{ij}, ρ, b_i, t_j, u_i and n_i are Cauchy stress tensor, body force, traction, displacement vector, and normal vector components respectively. Ω_0^C and Ω_0^T are the current domain of the contactor C and the target T. The physical constraint of contact – impact with no penetration is given as

$$g \leq 0 \ , \quad g = U_u^C - U_u^T + G \qquad in \qquad \Gamma_c \tag{3.189}$$

G and g are the initial and current gap dimension functions respectively.

3.4.2 Forces on the Contact Surface

The normal forces on both the target and the contactor surface are defined using the unit normal of the target surface,

$$F_n^T = (t^T) n^T \qquad ; \qquad F_n^C = (t^C) n^C \tag{3.190}$$

For equilibrium, the sum of the normal forces must be zero. Thus,

$$F_n^T + F_n^C = 0 \tag{3.191}$$

$$F_n \equiv F_n^T = -F_n^C \leq 0 \tag{3.192}$$

3.4.3 Principle of Virtual Work

Applying the principle of virtual work for the bodies in Fig. 3.6, Eqs. (3.187), (3.188) and (3.189) could be coupled as

$$\int_{\Omega_0} S_{ij} \delta E_{ij} d\Omega_0 + \int_{\Omega_0} \rho \ddot{U}_i \delta U_i d\Omega_0 + \int_{\Gamma_c} \tau_n \delta(U_n^C - U_n^C + G) d\Gamma$$
$$= \int_{\Omega_0} \rho b_i \delta U_i d\Omega_0 + \int_{\Gamma_t} t_i \delta U_i d\Gamma \tag{3.193}$$

Where

$$\Gamma_t = \Gamma_t^C \cup \Gamma_t^T = \Gamma_c \quad ; \quad \Omega_0^C \cup \Omega_0^T \qquad (3.194)$$

τ_n is the Lagrangian multipliers; $\boldsymbol{S}$ and $\boldsymbol{E}$ are conjugate stress and strain with reference to the derivative of displacement vector U_i; δ is any infinitesimal variation which is consistent with displacement boundary conditions. Using a penalty proportion parameter α_n, we have

$$\tau_n = \alpha_n g \quad ; \quad \tau_n = \alpha_n (U_n^C - U_n^T + G) \qquad (3.195)$$

Eq. (3.195) violates the impenetration condition. Also large value of α_n will lead to numerical errors. Farahani *et al.* (2000) proposed a method where the contactor and target are considered as a united body. The contact interaction bodies are now as internal forces of the whole body, and the work of traction forces is unnecessary. Therefore, Eq. (3.193) reduces to the form

$$\int_{\Omega_0} S_{ij} \delta E_{ij} d\Omega_0 + \int_{\Omega_0} \rho \ddot{U}_i \delta U_i d\Omega_0 = \int_{\Omega_0} \rho b_i \delta U_i d\Omega_0 + \int_{\Gamma_t} t_i \delta U_i d\Gamma \qquad (3.196)$$

3.4.4 Finite Element Formulation

For the purpose of studying the dynamic impact-contact problem with hyperelastic model, the nonlinear relationship between strain and displacement cannot be ignored. The Lagrange strain tensor of Eq. (3.8) could be decoupled into the well-known linear part $\boldsymbol{D}_E \boldsymbol{u}$ and the nonlinear part $\boldsymbol{E}^{nl}(\boldsymbol{u})$.

$$\boldsymbol{E} = [\boldsymbol{D}_E + \boldsymbol{E}^{nl}(\boldsymbol{u})]\boldsymbol{u} = \boldsymbol{E}_l + \boldsymbol{E}_{nl} \qquad (3.197)$$

$\boldsymbol{D}_E \boldsymbol{u}$ and $\boldsymbol{E}^{nl}(\boldsymbol{u})$ are defined as follows (summation over $k = 1, 2, 3$).

$$D_E u = E_l = \begin{bmatrix} u_{1,1} \\ u_{2,2} \\ u_{3,3} \\ u_{1,2} + u_{2,1} \\ u_{2,3} + u_{3,2} \\ u_{1,3} + u_{3,1} \end{bmatrix} \tag{3.198a}$$

$$E^{nl}(u) = E_{nl} = \begin{bmatrix} \frac{1}{2} u_{k,1} u_{k,1} \\ \frac{1}{2} u_{k,2} u_{k,2} \\ \frac{1}{2} u_{k,3} u_{k,3} \\ u_{k,1} + u_{k,2} \\ u_{k,2} + u_{k,3} \\ u_{k,1} + u_{k,3} \end{bmatrix} \tag{3.198b}$$

The subscript l and nl stand for linear and nonlinear. From Eq. (3.197), the incremental form of the strain – displacement relationship is

$$\delta E = \left(D_E + E^{nl}(u) \right) \delta u \tag{3.199}$$

From the principle of virtual displacement, the virtual work, δW is

$$\delta W = \delta u^T M \ddot{u} + \delta u^T A \dot{u} + \int_{\Omega_0} \delta E^T S \, d\Omega_0 - \delta u^T F_{ext} - \delta u^T R = 0 \tag{3.200}$$

Where Ω_0 is the domain of the initial configuration; F_{ext} is the vector external loads; R is the contact reaction vector; A is the damping matrix; M is the mass matrix; $\dot{u}$ is the velocity vector and $\ddot{u}$ is the acceleration vector. The Lagrangian elasticity tensor of Eq. (3.14) can be split into deviotoric and pressure components, respectively as

$$\mathbb{C} = \frac{\partial S}{\partial E} = \mathbb{C}_d + \mathbb{C}_p \tag{3.201}$$

These two components can be evaluated to a Neo Hookean case as (Bonet and Wood, 1997)

$$\mathbb{C}_d = 2 \frac{\mu}{J^{2/3}} \left[\frac{1}{3} tr C \, J^2 - \frac{1}{3} I \otimes C^{-1} - \frac{1}{3} C^{-1} \otimes I + \frac{1}{9} tr C C^{-1} \otimes C^{-1} \right] \tag{3.202a}$$

$$\mathbb{C}_p = k(J - 1) J \left[C^{-1} \otimes C^{-1} - 2\mathbb{I} \right] \tag{3.202b}$$

k is the bulk modulus, $\boldsymbol{C}$ is the right Cauchy - Green Tensor, J is the measures of change in volume, and the fourth order tensor $\mathbb{I}$ is defined as,

$$\mathbb{I} = \frac{\partial \boldsymbol{C}^{-1}}{\partial \boldsymbol{C}} \tag{3.203a}$$

$$\mathbb{I}_{ijkl} = \frac{\partial (C^{-1})_{ij}}{\partial C_{kl}} = (C^{-1})_{ik}(C^{-1})_{jl} \tag{3.203b}$$

Using Eq. (3.199), Eq. (3.201) becomes

$$\delta \boldsymbol{S} = \mathbb{C}\delta \boldsymbol{E} = \mathbb{C}\left(\boldsymbol{D}_E + \boldsymbol{E}^{nl}(\boldsymbol{u}) \right)\delta \boldsymbol{u} \tag{3.204}$$

Substituting Eq. (3.199) into Eq. (3.200) gives

$$\delta W = \delta \boldsymbol{u}^T \boldsymbol{M}\ddot{\boldsymbol{u}} + \delta \boldsymbol{u}^T \boldsymbol{A}\dot{\boldsymbol{u}} + \delta \boldsymbol{u}^T \int_{\Omega_0} \left(\boldsymbol{D}_E + \boldsymbol{E}^{nl}(\boldsymbol{u}) \right)^T \boldsymbol{S} \, d\Omega_0 - \delta \boldsymbol{u}^T \boldsymbol{F}_{ext}$$
$$- \delta \boldsymbol{u}^T \boldsymbol{R} = 0 \tag{3.205}$$

The vector of internal forces is defined by

$$\boldsymbol{F}_{int} = \int_{\Omega_0} \left(\boldsymbol{D}_E + \boldsymbol{E}^{nl}(\boldsymbol{u}) \right)^T \boldsymbol{S} \, d\Omega_0 \tag{3.206}$$

Eq. (3.205) reduces to a set of nonlinear equations given as

$$\boldsymbol{M}\ddot{\boldsymbol{u}} + \boldsymbol{A}\dot{\boldsymbol{u}} + \boldsymbol{F}_{int} - \boldsymbol{F}_{ext} - \boldsymbol{R} = 0 \tag{3.207}$$

Eq. (3.207) could be rewritten as

$$\boldsymbol{M}\ddot{\boldsymbol{u}} = \boldsymbol{F} + \boldsymbol{R} \tag{3.208}$$

Where

$$\boldsymbol{F} = \boldsymbol{F}_{ext} - \boldsymbol{F}_{int} - \boldsymbol{A}\dot{\boldsymbol{u}} \tag{3.209}$$

Eq. (3.208) is to be solved with initial conditions at $t = 0$,

$$\dot{\boldsymbol{u}} = \dot{\boldsymbol{u}}_0 \quad and \quad \boldsymbol{u} = \boldsymbol{u}_0 \tag{3.210}$$

3.4.5 Tangent Stiffness Matrix

Differentiating $\boldsymbol{F}_{int}$ with respect to the nodal displacement $\boldsymbol{u}$ gives the tangent stiffness matrix

$$K = \frac{\partial F_{int}}{\partial u} = K_e + K_g + K_u \tag{3.211}$$

where K_e, K_g and K_u are the elastic, geometric and initial displacement stiffness matrices respectively given as

$$K_e = \int_{\Omega_0} D_E^T \mathbb{C} D_E \, d\Omega_0 \tag{3.212a}$$

$$K_g = \int_{\Omega_0} \frac{\partial E_{nl}^T}{\partial u} S \, d\Omega_0 \tag{3.212b}$$

$$K_u = \int_{\Omega_0} \left(D_E^T \mathbb{C} E_{nl} + E_{nl}^T \mathbb{C} D_E + E_{nl}^T \mathbb{C} E_{nl} \right) d\Omega_0 \tag{3.212c}$$

3.5 Pseudo-Rigid-Body-Model of Compliant Athletics Systems

3.5.1 Flex-Run

Based on the pseudo-rigid-body-model, a 2R pseudo-rigid-body-model that consist of three rigid links joined by two revolute joints and two torsion springs has been proposed by Yu *et al* (2012).
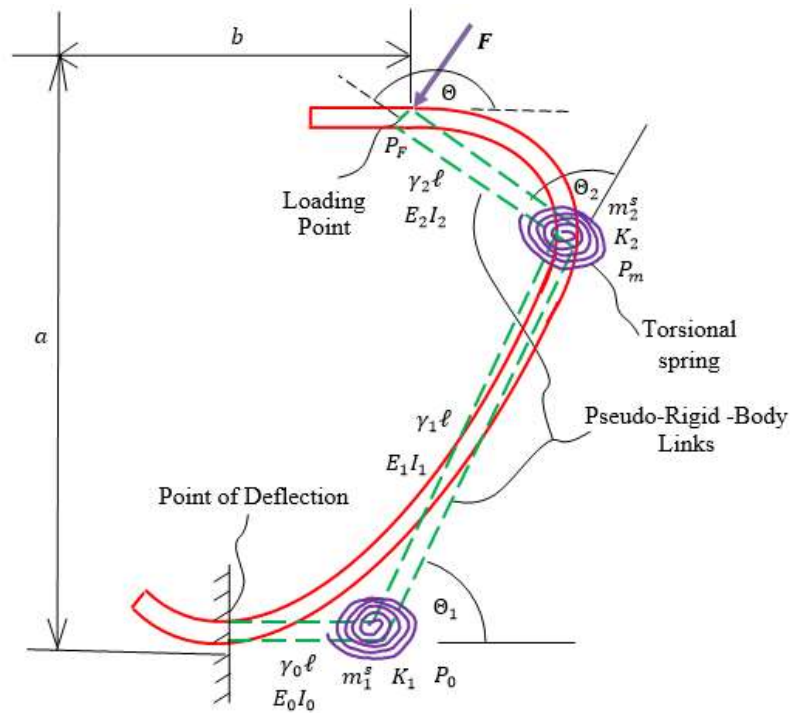

Fig. 3.7: PRBM of a Flex-Run

The 2R pseudo-rigid-body-model is significant to expand the application of pseudo-rigid-body-model in analysis and design of CMS particularly in the further study on the dynamics of CMS. For a 2R pseudo-rigid-body-model with end force, the path of the beam end may be accurately modelled by three rigid links joined at two pivots. Torsion springs represent the resistance of the beam deflection. The length of each link in the pseudo-rigid-body-model is γ_i ($i = 0,1,2$) and γ_i is called the characteristics radius factor. The product $\gamma_i l$ is the characteristic radius. The pseudo-rigid-body approximation will be used to parameterize the deflection path, angular deflection of the beam end and the pseudo-rigid-body angle represented by the load-deflection relation in Θ_i ($i = 1, 2$) the slope angle of the 2R pseudo-rigid-body-model is the angle between the pseudo-rigid-body link $\gamma_i l$ ($i = 1, 2$) and its undeflected position $\Theta = \Theta_1 + \Theta_2$ as shown in Fig. 3.7. a and b are the y and x coordinate of the beam deflection. The deflection angles of two torsion springs are Θ_1 and Θ_2. The characteristic radius factor of the three pseudo-rigid links are γ_0, γ_1 and γ_2 satisfying

$$\gamma_0 + \gamma_1 + \gamma_2 = 1 \tag{3.213}$$

The part of the applied force $\boldsymbol{P}_F = \begin{bmatrix} P_{Fx} \\ P_{Fy} \end{bmatrix} = \begin{bmatrix} b/l \\ a/l \end{bmatrix}$ are

$$P_{Fx} = \gamma_0 + \gamma_1 \cos \Theta_1 + \gamma_2 \cos \Theta \tag{3.214a}$$

$$P_{Fy} = \gamma_1 \sin \Theta_1 + \gamma_2 \sin \Theta \tag{3.214b}$$

The vector from part of the first torsion spring P_0 to P_F is $\boldsymbol{P}_{0F} = \begin{bmatrix} P_x \\ P_y \end{bmatrix}$; where

$$P_x = P_{Fx} - \gamma_0 \tag{3.215a}$$

$$P_y = P_{Fy} \tag{3.215b}$$

$$\Theta_2 = \cos^{-1}\left(\frac{P_x^2 + P_y^2 - \gamma_1^2 - \gamma_2^2}{2\gamma_1\gamma_2}\right) \tag{3.215c}$$

$$\Theta_1 = cos^{-1} \frac{P_x\left(P_x^2 + P_y^2 - \gamma_1^2 - \gamma_2^2\right) \pm P_y\sqrt{4\gamma_1^2\left(P_x^2 + P_y^2\right) - \left(P_x^2 + P_y^2 - \gamma_1^2 - \gamma_2^2\right)^{\cdot}}}{2\gamma_1(P_x^2 + P_y^2)} \quad \text{(3.215d)}$$

Yu *et al* (2012) found the optimal characteristic radius factors as $\gamma_0 = 0.1$; $\gamma_1 = 0.54$ and $\gamma_2 = 0.36$. The spring constant K_1 and K_2 depend on the stiffness coefficient $K_{\Theta 1}$ and $K_{\Theta 2}$; geometry I/l ; charactereristic radius factor γ_1 and γ_2 and material properties E, i.e

$$K_1 = \gamma_1 K_{\Theta 1} \frac{EI}{l} \quad \text{(3.216a)}$$

$$K_2 = \gamma_2 K_{\Theta 2} \frac{EI}{l} \quad \text{(3.216b)}$$

Yu *et al.* (2012) defined the stiffness coefficient as $K_{\Theta 1} = 3.4042$ and $K_{\Theta 2} = 1.5813$ The pseudo-rigid-body-dynamic-model for CMs can be developed according to the principle of dynamic equivalence. The kinetic parameters and characteristics of the dynamic model is

$$r_1 = \gamma_0 l \; ; \quad r_2 = \gamma_1 l \; ; \quad r_3 = \gamma_2 l \quad \text{(3.217)}$$

r_1 ; r_2 and r_3 are the characteristic radii of the three links. The dynamic springs are not the same as the springs with constant K in the pseudo-rigid-body-model because the menses are not considered in the static and kinematic analysis of CMs. Generally, are lumped mass and two torsion springs are needed for the dynamic equivalence of one link. The dynamic equivalence of kinetic energy, T_1 for link 1 can be expressed as

$$T_1 = \frac{1}{2} m_1^s V_1^2 = \frac{1}{2} m_1 V_{m1}^2 + \frac{1}{2} J_1 \omega_1^2 \quad \text{(3.218)}$$

Where

$$V_1 = r_1 \omega_1 \; ; \quad V_{m1} = \frac{1}{2} r_1 \omega_1 \quad \text{(3.219)}$$

$$m_1^s = \frac{1}{4} m_1 + \frac{J_1}{r_1^2} \quad \text{(3.220)}$$

m_1; J_1 and $\omega_1$are the mass, mass moment of inertia and the angular velocity of link 1.

Equally, for the link 2, the dynamic equivalence if kinetic energy, T_2 can be expressed

as

$$T_2 = \frac{1}{2}\left(m_1^{s'} + m_2^{s'}\right)V_2^2 \tag{3.221}$$

Where

$$V_2 = r_2\omega_2 \tag{3.222}$$

$$m_1^{s'} = \frac{1}{4}(m_1 - m_2) + \frac{J_1 - J_2}{r_1^2 - r_2^2} \tag{3.223}$$

$$m_2^{s'} = \frac{1}{4}(m_2 - m_3) + \frac{J_2 - J_3}{r_2^2 - r_3^2} \tag{3.224}$$

m_2; J_2 and ω_2 are the mass, mass moment of inertia and angular velocity of link 2. m_3

and J_3 are the mass and angular velocity of inertia of link 3

Also, for the link 3, the dynamic equivalence of kinetic energy, T_3 can be expressed as

$$T_3 = \frac{1}{2}m_2^s V_3^2 = \frac{1}{2}m_3 V_{m3}^2 + \frac{1}{2}J_3\omega_3^2 \tag{3.225}$$

Where

$$V_3 = r_3\omega_3 \; ; \;\; V_{m3} = \frac{1}{2}r_3\omega_3 \tag{3.226}$$

$$m_2^s = \frac{1}{4}m_3 + \frac{J_3}{r_3^2} \tag{3.227}$$

ω_3 is the angular velocity of link 3.

Therefore, the kinetic energy, T of the dynamic system is

$$T = \frac{1}{2}m_1^s V_1^2 + \frac{1}{2}m_2^s V_2^2 + \frac{1}{2}\left(m_1^{s'} + m_2^{s'}\right)V_2^2 \tag{3.228}$$

Which could be rewritten as;

$$T = \frac{1}{2}m_1^s r_1^2\left(\dot{\Theta}_1\right)^2 + \frac{1}{2}\left(m_1^{s'} + m_2^{s'}\right)r_2^2\left(\dot{\Theta}_2\right)^2 + \frac{1}{2}m_2^s r_3^2\left(\dot{\Theta}\right)^2 \tag{3.229}$$

Eq, (3.229) can be expressed in the form

$$T = \frac{1}{2} M_d (\dot{\Theta})^2 \tag{3.230}$$

Where M_d is the generalised mass of the system.

The elastic deformation energy, W of the flexible beam is given as

$$W = \int_0^\delta \boldsymbol{F}.d\delta \tag{3.231}$$

Where $\boldsymbol{F}$ is the applied force and δ is the resulting deflection. The deflection, δ can be obtained as

$$d\delta = \gamma_T l d\Theta \tag{3.232}$$

Where

$$\gamma_T = \gamma_0 l + \gamma_1 l + \gamma_2 l \tag{3.233}$$

Therefore, Eq. () becomes

$$W = \int_0^\Theta F \gamma_T l \, d\Theta \tag{3.234}$$

The torque, T_{qP} on the pin joints is given as

$$T_{qp} = K_1 \Theta_1 + K_2 \Theta_2 \tag{3.235}$$

Expressing the, T_{qP} as a product of the transverse force F and the moment arm gives

$$T_{qp} = F \left[cl + (\gamma_1 l + \gamma_0 l \, cos\Theta_1) cos\Theta_2 \right] \tag{3.236}$$

Combining Eqs. (3.235) and (3.236) results in

$$F = \frac{K_1 \Theta_1 + K_2 \Theta_2}{\gamma_2 l + (\gamma_1 l + \gamma_0 l \, cos\Theta_1) cos\Theta_2} \tag{3.237}$$

Substituting Eq. (3.237) into Eq. (2.234) yields

$$W = f(K_1, K_2, \Theta, \gamma_0, \gamma_1, \gamma_2) \tag{3.238}$$

This implies that the potential energy, U of the dynamic torsion spring, is

$$U = f(K_1, K_2, \Theta, \gamma_0, \gamma_1, \gamma_2) \tag{3.239}$$

Substituting the kinetic energy T of Eq. (3.230) and potential energy U of Eq. (3.239) unto the Lagrangian equation.

$$\frac{d}{dt}\left(\frac{\partial T}{\partial \dot{\Theta}}\right) - \frac{\partial T}{\partial \Theta} + \frac{\partial U}{\partial \Theta} = Q \tag{3.240}$$

This gives the generalized dynamic equation of the dynamic system for the compliant mechanism in the following form.

$$M_d \ddot{\Theta} + K_d \dot{\Theta} = P \tag{3.241}$$

Where K_d is the potential energy of the dynamic torsion spring for the Flex-Run.

3.5.2 Pole Vault
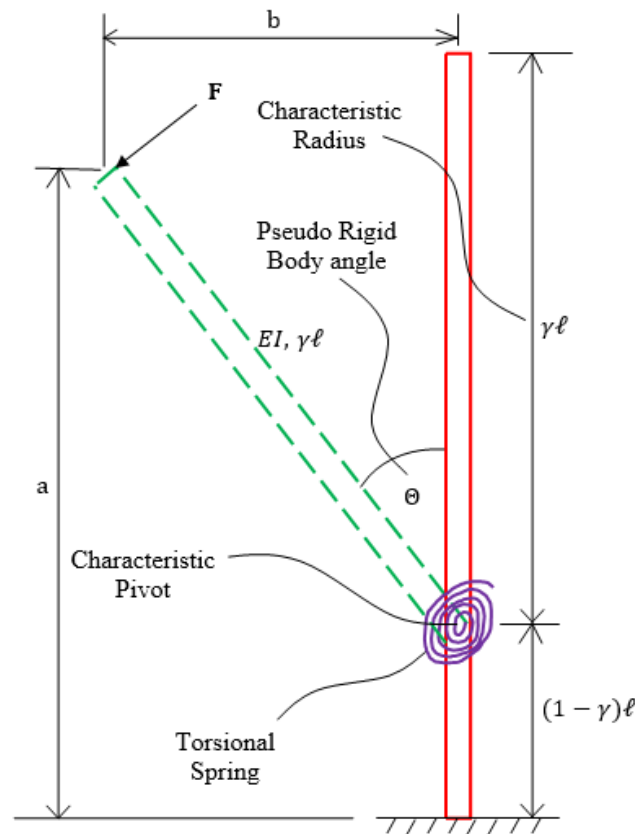
Fig. 3.8: PRBM of the pole vault

The pseudo-rigid-body approximation shown in Fig. 3.8 will be used to parameterize the deflection path, the angular deflection of the pole vault and load-deflection relationships in Θ, the pseudo-rigid-body angle which is the angle between the pseudo-

rigid-body and its undeflected position. The coordinate of the end the deflected pole

vault may be given by equations parameterized in terms of the pseudo-rigid-body angle,

Θ written as

$$\frac{a}{l} = 1 - \gamma(1 - cos\Theta) \tag{3.242}$$

$$\frac{b}{l} = \gamma sin\Theta \tag{3.243}$$

γ is the characteristic radius factor. The spring constant K', may be written as

$$K' = \gamma K'_\theta \frac{EI}{l} \tag{3.244}$$

The kinetic parameters and characteristics of the dynamic model is

$$r'_1 = \gamma_0 l \; ; \quad r'_2 = \gamma_1 l \tag{3.245}$$

For the dynamic model of the pole vault, the dynamic equivalence of kinetic energy,

T'_1 of link 1 can be expressed as

$$T'_1 = \frac{1}{2} m_1^{s'} V_1'^2 = \frac{1}{2} m'_1 V_{m1}'^2 + \frac{1}{2} J'_1 \omega_1'^2 \tag{3.246}$$

Where

$$V'_1 = r'_1 \omega'_1; \quad V'_{m1} = \frac{1}{2} r'_1 \omega'_1 \tag{3.247}$$

$$m_1^{s'} = \frac{1}{4} m'_1 + \frac{J'_1}{r_1'^2} \tag{3.248}$$

Also, for the link 2, the dynamic equivalence of kinetic energy, T'_2 can be expressed as

$$T'_2 = \frac{1}{2} m_2^{s'} V_2'^2 = \frac{1}{2} m'_2 V_{m2}'^2 + \frac{1}{2} J'_2 \omega_2'^2 \tag{3.249}$$

Where

$$V'_2 = r'_2 \omega'_2; \quad V'_{m2} = \frac{1}{2} r'_2 \omega'_2 \tag{3.250}$$

$$m_2^{s'} = \frac{1}{4} m'_2 + \frac{J'_2}{r_2'^2} \tag{3.251}$$

Therefore the kinetic energy, T'

$$T' = \frac{1}{2} m_1^{s'} V_1'^2 + \frac{1}{2} m_2^{s'} V_2'^2 \tag{3.252}$$

Which could be rewritten as;

$$T' = \frac{1}{2} m_1^{s'} r_1'(\dot{\Theta})^2 + \frac{1}{2} m_2^{s'} r_2'(\dot{\Theta})^2 \tag{3.253}$$

Eq (h) can be expressed in the form

$$T' = \frac{1}{2} M_d'(\dot{\Theta})^2 \tag{3.254}$$

Where M_d' is the generalised mass of the system.

The potential energy, U' of a dynamic torsion spring, is

$$U' = \frac{1}{2} K_d' \Theta^2 \tag{3.255}$$

Where K_d' is the potential energy of the dynamic torsion spring for the pole vault. It implies that

$$K' = K_d' \tag{3.256}$$

This means that the stiffness constant of the dynamic torsional spring in the dynamic system is approximately the same as that of the spring in pseudo-rigid-body-model. Substituting the kinetic energy T' of Eq () and potential energy U of Eq () unto the Lagrangian equation.

$$\frac{d}{dt}\left(\frac{\partial T'}{\partial \dot{\Theta}}\right) - \frac{\partial T'}{\partial \Theta} + \frac{\partial U'}{\partial \Theta} = Q' \tag{3.257}$$

This gives the generalized dynamic equation if the dynamic system for the pole vault in the following form.

$$M_d' \ddot{\Theta} + K_d' \dot{\Theta} = P' \tag{3.258}$$

3.6   Solution Procedure

AceGEN is used for the automatic derivation of formulae needed in the numerical procedures. Symbolic derivation of the characteristic quantities (e.g. gradients, tangent operators, sensitivity vectors etc.) leads to exponential behavior of derived expressions,

both in time and space. AceGEN offers multi-language code generation (Fortran, C, Mathematica etc.) and automatic interface to general numerical environments (MathLink connection to Mathematica) and specialized finite element environments (AceFEM, FEAP, ELFEN, ABAQUS etc.). Fig. 5.55 shows the system for generating a finite element code and its further analysis through the end compiler AceFEM.
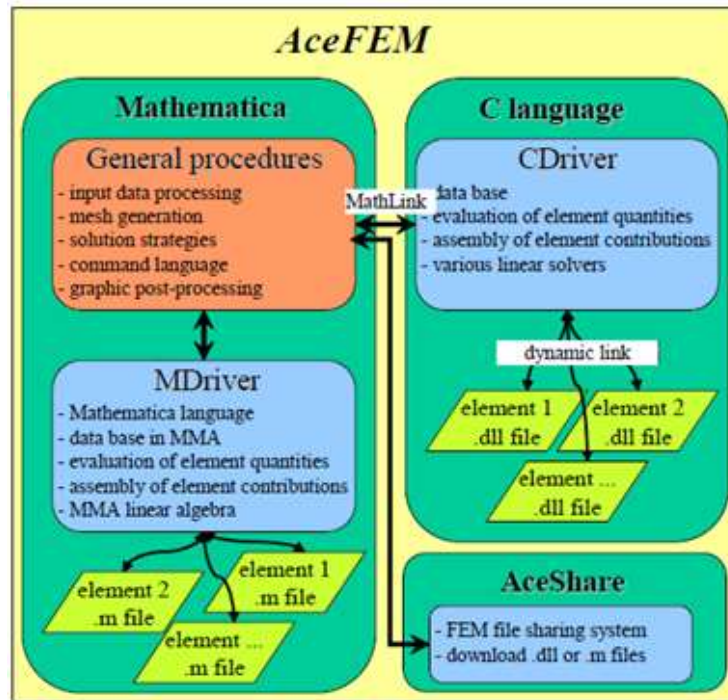

Fig. 3.9: System for generating a finite element code and its further analysis

CHAPTER 4: EXPERIMENTAL TEST VALIDATION

The BOSE® ElectroForce (ELF) 3200 testing machine (Fig. 4.1) in conjunction with the WinTest® control software was used to conduct the mechanical experiments in uniaxial cyclic loading and uniaxial tension. The test instrument incorporate proprietary Bose linear motion technologies and WinTest controls to provide a revolutionary approach to mechanical fatigue and dynamic characterization. Fig 4.2 is the WinTest control overview.

Test specimen
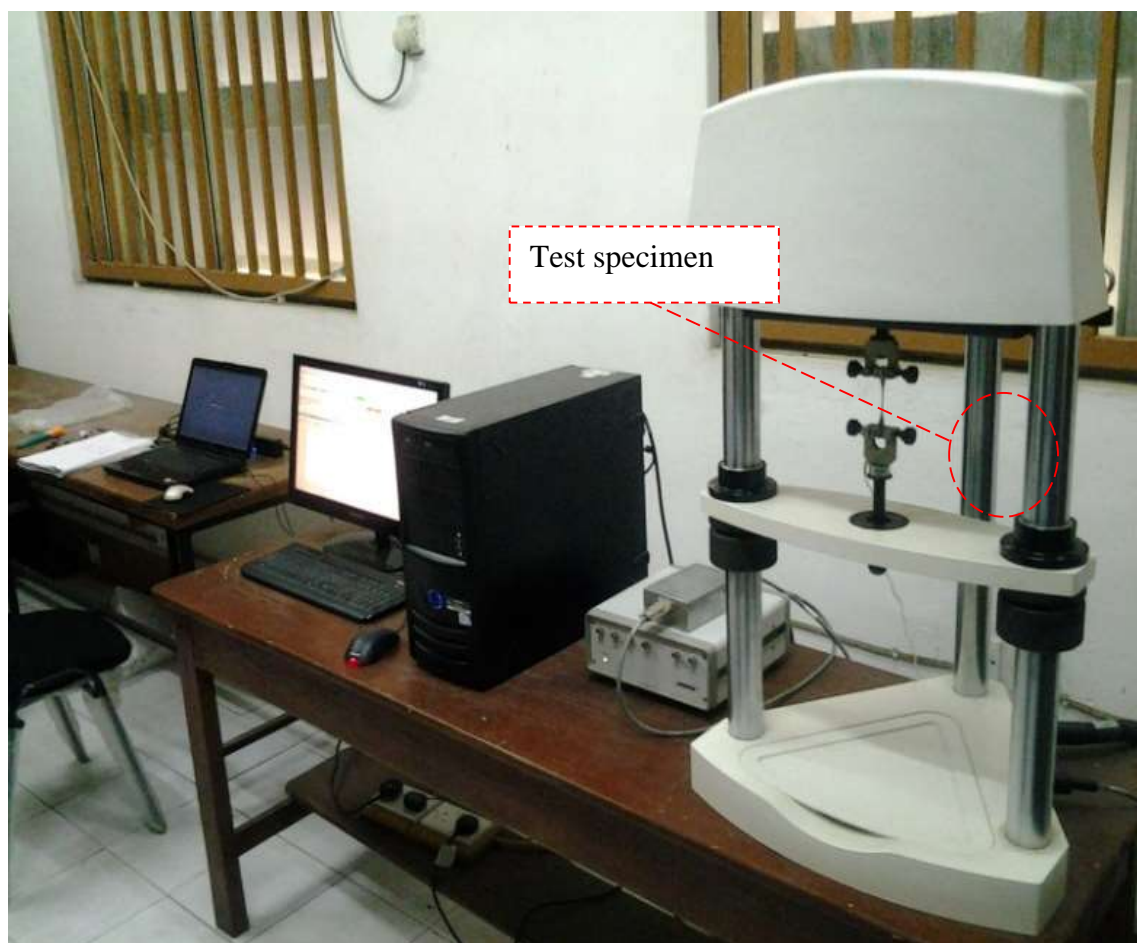
Fig. 4.1: Test Equipment Setup
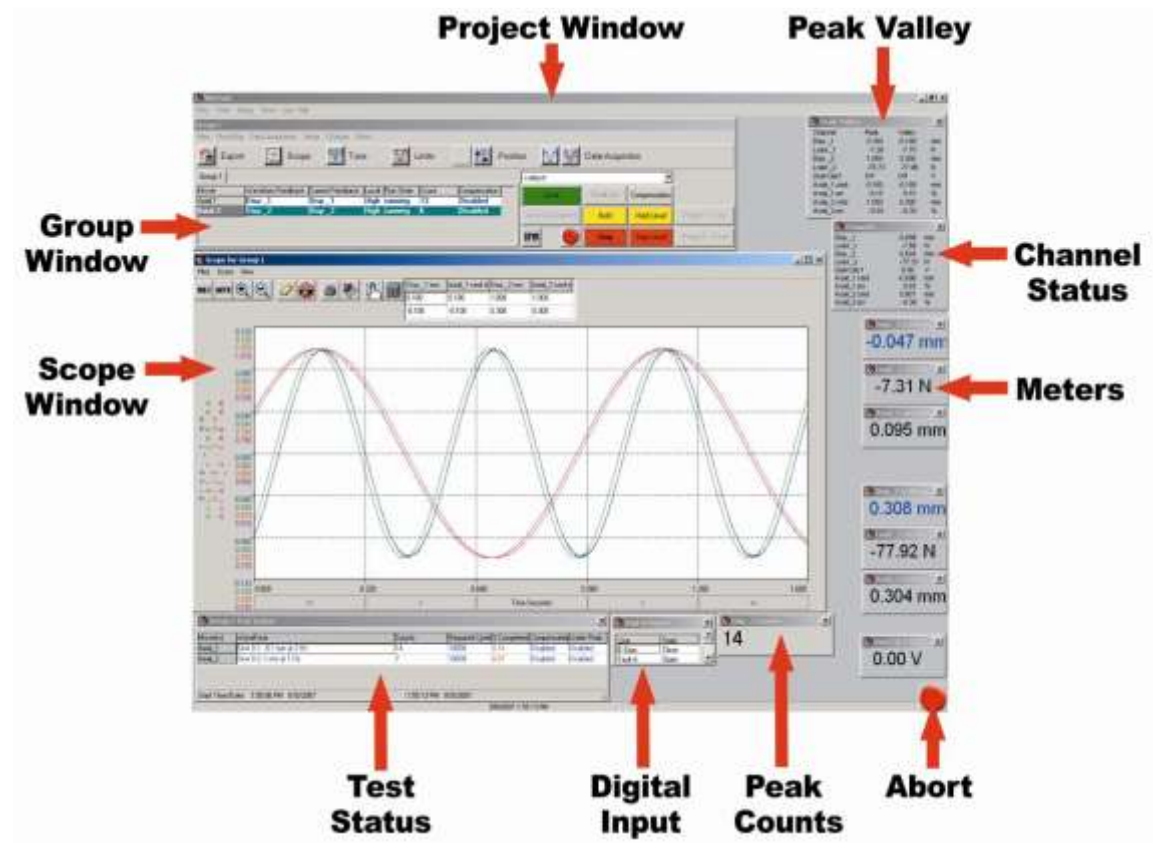
Fig. 4.2: WinTest Overview

The ELF has a maximum load of 225 N and a maximum frequency of 400 Hz. A set of low mass grips, Model GRP-TCDMA450N from BOSE ElectroForce (Eden Prairie, MN, USA), were used. The load cell had a maximum load rating of 2.5 N (250 g) and resolution of ±10 mg. The ELF 3200 measures displacements via a Capacitec 100 μm displacement transducer (Model HPC-40/ 4101) used as a feedback for the control loop. Knowing the width and thickness of the specimen, cross-sectional area of the specimen could be calculated using the formula:

$$Area = Width \times Thickness \tag{4.1}$$

The stress on the sample could be calculated by using the formula:

$$Stress = {Force}/{Area} \tag{4.2}$$

Now, engineering strain is given by the formula:

$$\varepsilon = {\Delta l}/{L_0} \tag{4.3}$$

118

The displacement obtained from the testing data is Δl. L_0 is the gauge length (22mm). So strain, ε could be calculated. Knowing stress and strain, stress versus strain curves could be plotted.

4.1 Sample preparation

Low Density Polypropylene (LDPP) and Low Density Polyethylene (LDPE) were selected as the test materials. The geometry and test length of the specimens are as shown in Fig. 4 3. It has a gauge length of 22mm. The specimen's dimensions were obtained with the use of the micrometre screw gauge and the vernier calliper.
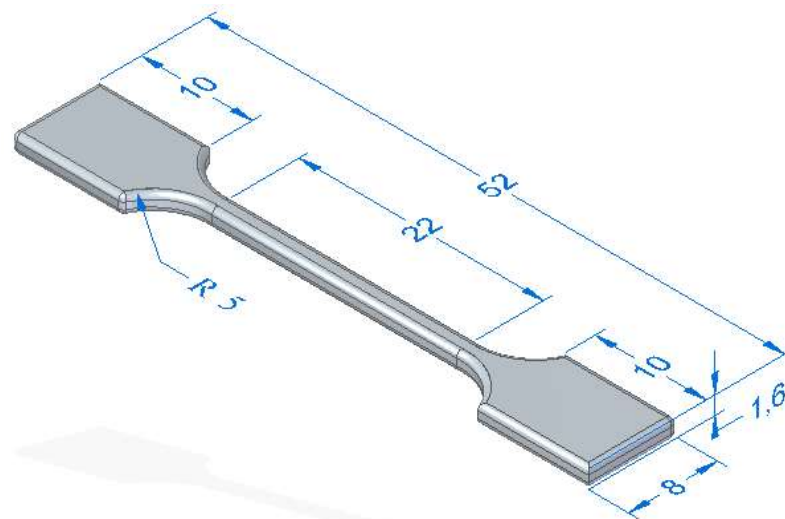
Fig. 4.3: Geometry of Test Specimens

4.2 Uniaxial Tensile Tests

The aim of tensile testing was to evaluate the mechanical response of the materials to a known strain or deformation rate. This gives a plot of stress versus strain from which a wealth of information may be obtained such as the brittle or ductile behaviour, tensile modulus or an indication of stiffness of the material, tensile strength etc. The tensile testing data was obtained as a text file in force versus displacement form. The testing procedure can be described in steps as follows:

- The machine and the software were turned on.

- The specimen for tensile testing was a dumbbell-shaped strip, which was cut from the compression-moulded sheet using a penknife. Its width and thickness were measured using a micrometre.

- The specimen was placed between the grips and the grips were tightened. Over-tightening of the grips was avoided, in order to avoid failure at grips.

- The linear motor was turned on using the "locals" button in the software.

- Load and displacement associated with the grips were tarred.

- The system was first tuned for a square wave of certain amplitude. The purpose of tuning was to make the command given to the machine by the software and the output generated by the machine match as closely as possible. Adjusting the (Proportional-Integral-Derivative) PID control parameters during the time when the square wave was acting on the system did the required tuning.

- The tuning was double checked by re-tuning the system with a sinusoidal waveform.

- The waveform was set to "ramp". This was the waveform used for tensile testing. Strain rate could be set according to requirements, by typing the value in the appropriate box.

- File names for saving the test data were specified using the data acquisition menu. This menu also allowed deciding the rate of scanning, number of scans and time between the scans for acquiring data.

- The machine stopped automatically after the specimen failed. In case the specimen did not fail, the machine stopped acquiring data beyond a critical extension of the specimen. This value was 6.5mm. 2-3 specimens were tested for each material (LDPP and LDPE).
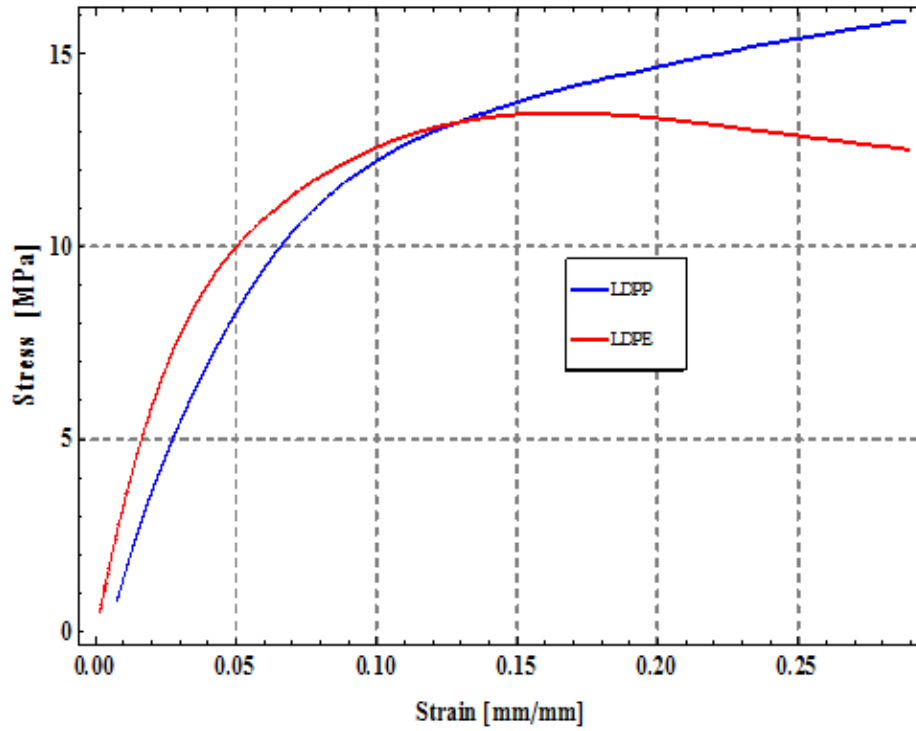
Fig. 4.4: Stress – strain curve of some polymers

The specimens were placed under tension at a controlled rate of displacement (0.02 mm/s). The clamping length was about 40 mm. The mechanical properties, i.e. Young's modulus, shear modulus, ultimate strain and stress were assessed for the specimens. The average of the results was taken as the resultant value. The local data (stress and strain) is determined from the global data (force and displacement). The gradients of the straight line section of the resulting stress–strain curves shown in Fig. 4.4 give their elastic moduli. The material parameter μ_p, is obtained by fitting the experimental stress–strain curve into Eq. (3.150). This yield $\mu_p = 43.04\ MPa$ for LDPP and $\mu_p = 71.19\ MPa$ for LDPE.

4.3 Fatigue Tests

The fatigue experiments were conducted between a minimum and maximum load in tension for a prescribed number of cycles using a set frequency. All fatigue tests were

conducted at 10 Hz. The residual strain was determined by considering the displacement reading on the oscilloscope at the initiation of the test and at the conclusion of the dwell phase. The residual strain was measured by subtracting the oscilloscope displacement value at the initiation of the test from the displacement at the conclusion of the constant-stress amplitude fatigue phase. Once the specimen was unloaded to zero stress and allowed to dwell for a short time. It should be noted that the test was displacement controlled, i.e., the specimen was pulled by a pre-determined amount with each step of testing. The corresponding load exerted on the sample for pulling was recorded. The same method of data acquisition employed in the tensile test is adopted in the fatigue test.

Ten samples for each of the test materials (LDPP and LDPE) were tested in this investigation. Approximately six samples broke at the grip interface at the conclusion of the fatigue loading phase, which indicated premature failure due to a stress concentration near the grip interface. For this reason, these experimental results were omitted from the results in this study.

Fig. 4.5 is the oscilloscope output of load and displacement verses time response of the LDPP samples while Figs. 4.6 and 4.7 display their 1s interval of the strain verses time and stress verses time response under sinusoidal cyclic loading conditions after equilibrium stress and strain values were reached. These samples were subjected to uniaxial fatigue loading conditions. The graphs show the behaviour of the samples under different displacement inputs. The strain range increases with an increase in the input displacement
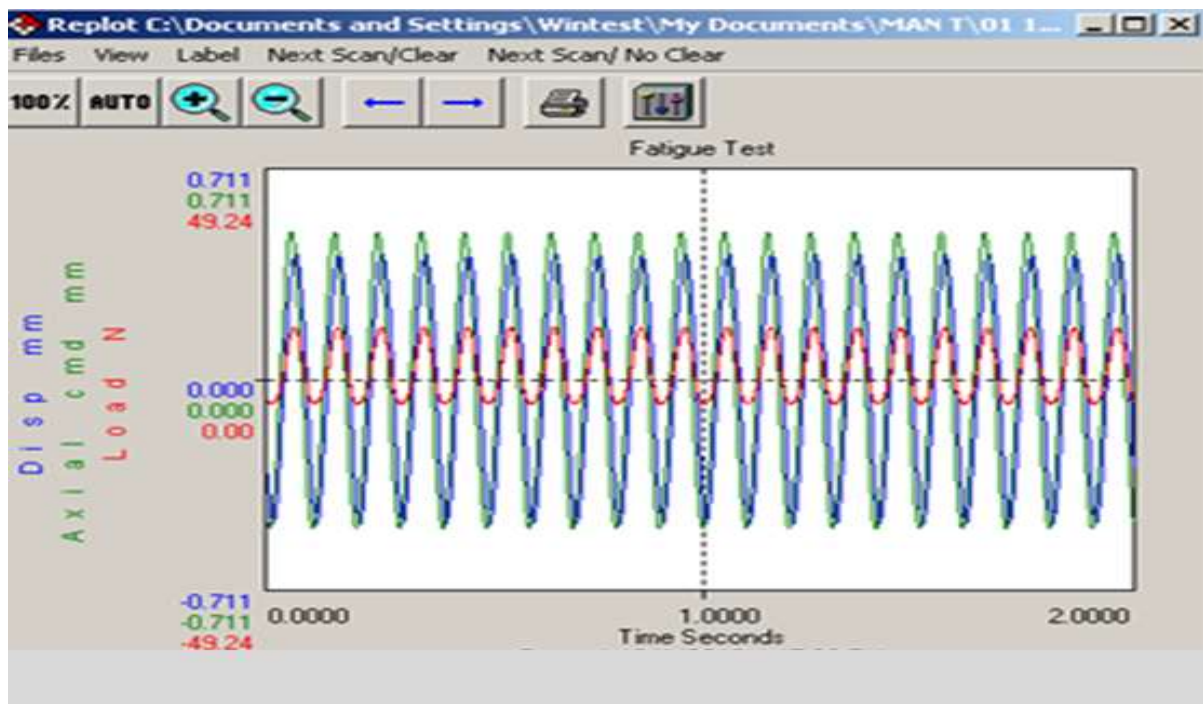
Fig. 4.5: Oscilloscope output of load and displacement versus time response of a sample undergoing uniaxial sinusoidal loading
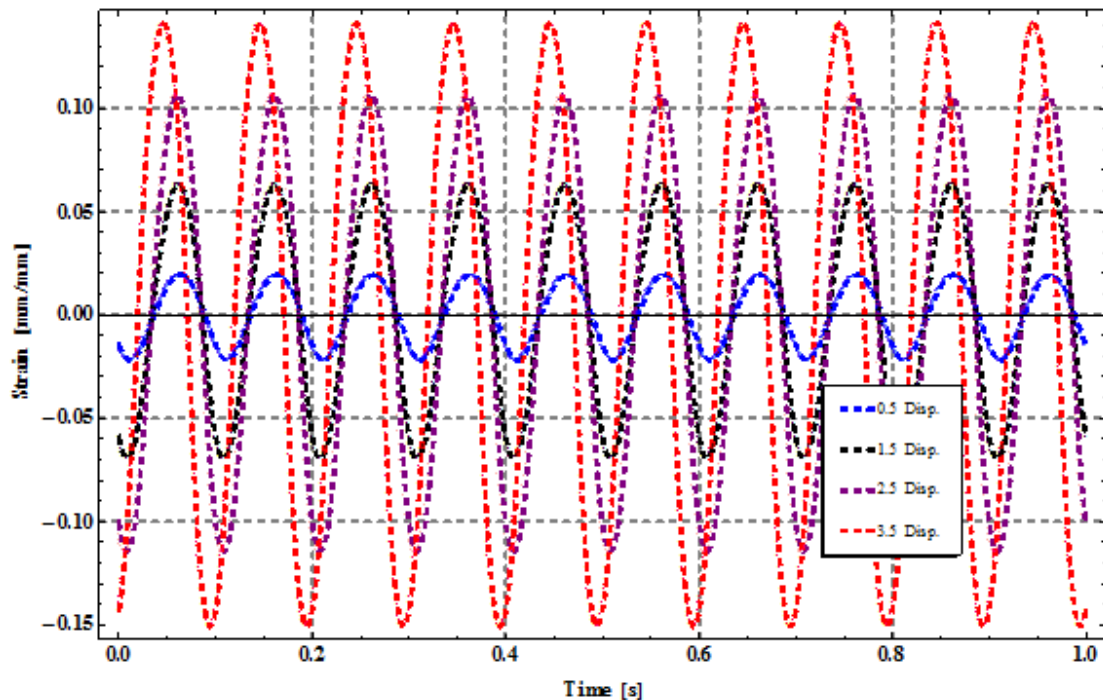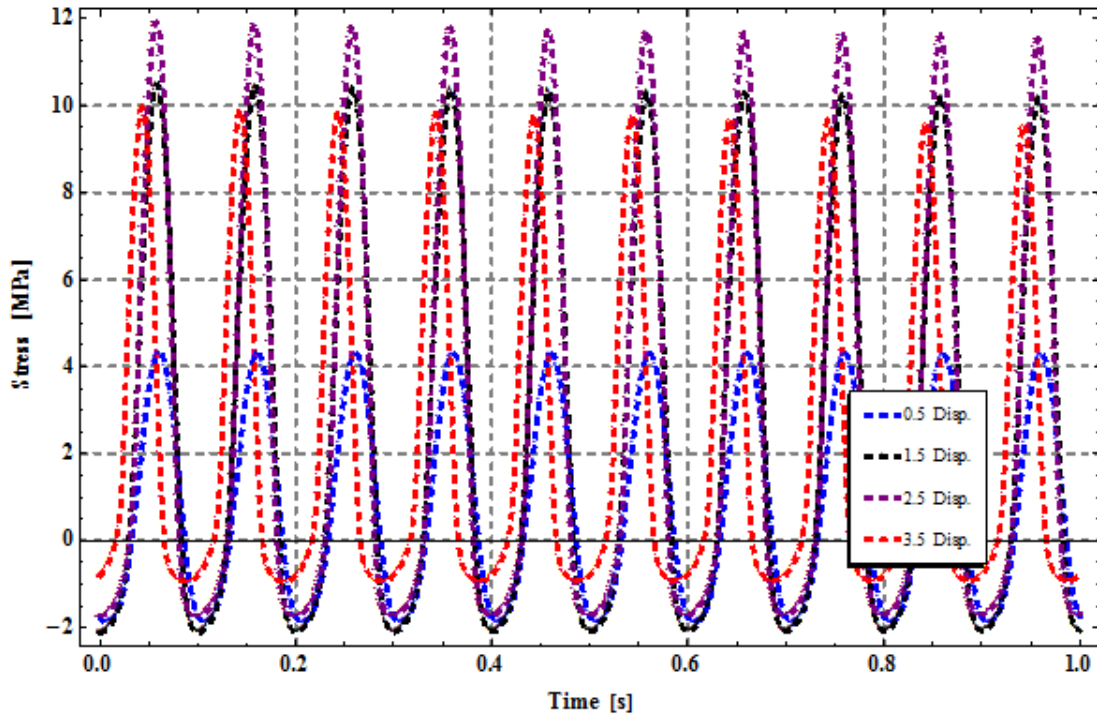

Fig. 4.6: A second strain cycles

Fig. 4.7: A second stress cycles

4.4   Hysteresis Loop

In fatigue, the area of a stress–strain hysteresis loop is a measure of mechanical energy lost due to viscoelastic damping during each cycle of extension and compression. For a viscoelastic material subject to the cyclic loading, the hysteresis of the material can be defined by plotting the input stress $\sigma(t)$ versus the responding strain $\varepsilon(t)$ for one cycle of motion. Polymeric material hysteresis loops are difficult to analyse but can reveal interesting insight into the behaviour of the material during fatigue testing (Fern *et al.,* 2012). Fig. 4.8 shows hysteresis loops of the low density polypropylene for 10 complete cycles. From the figure, the hysteresis curves for LDPP are generally asymmetrical. The graph shows an early increase in maximum stress with increase in the input displacement load before it got to the maximum value and started decreasing. The loops had immediate stability for all range of displacement load input.
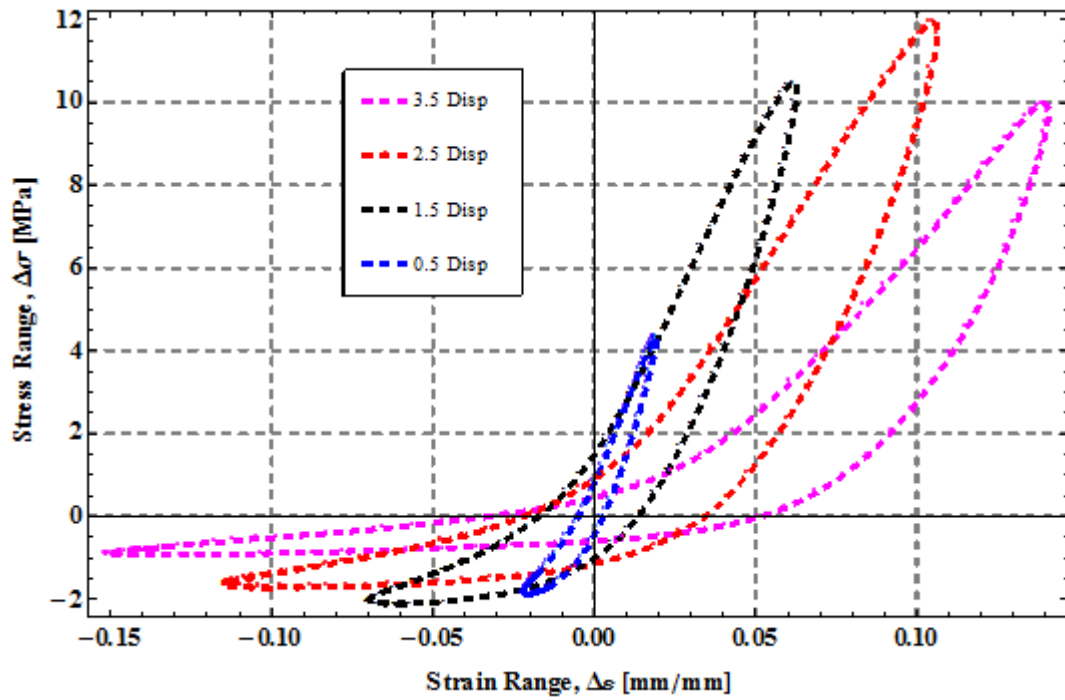
Fig. 4.8: Hysteresis loop for the LDPP material

The area captured within the hysteresis loop is equal to the dissipation energy per cycle of harmonic motion by the material. Within the tensile portion of the loop considerable plastic strain and crack propagation energy is lost as the intersection through the zero stress line is at a positive strain value. During compression the intersection of the zero stress line is very close to zero, implying little plastic strain. This behaviour of the material in compression reduces the amount of energy lost per cycle.

5

CHAPTER 5: DISCUSSION OF RESULTS

Results were obtained for a number of CMs. Simulation results were compared with published laboratory investigated CMs. Four cases were looked into for this analysis. The entire mechanisms geometries were built as adequate with the essential and natural boundary conditions stated.

5.1 Simulation Examples with Published Laboratory Investigated Compliant Mechanisms

5.1.1 Compliant Bistable Micromechanism (CBMM)

The experimental setup by Tsay *et al.,* (2005) composes of vibration isolation platform to separate external vibrations; a micrograph system to capture images to be recorded by computer; a workbench where the chip is laid; scanning electronic microscope (SEM) for observation and measurement; power supply system to drive the actuators. The purpose of their experiment was to observe if the micromechanism was bistable and to measure the deflection of the bistable mechanism.
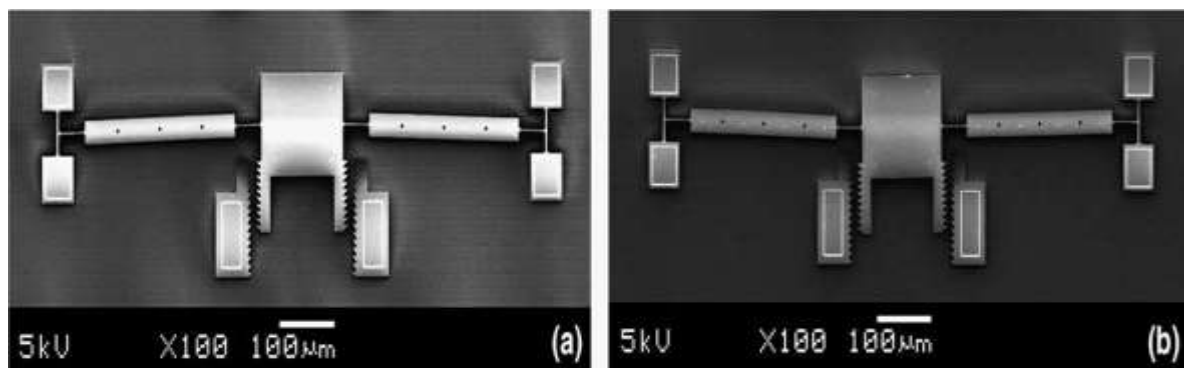

Fig. 5.1: SEM images of the Compliant Bistable Mechanism switched by a probe.
(a) Before switched;   (b) After switched

Fig. 5.1(a) and (b) show the images of the compliant bistable micromechanism before and after being switched. After stirred by the probe, the compliant bistable micromechanism switched from the first stable position to the second one and held still. It indicates that the compliant bistable micromechanism functioned as expected. The displacement of central mass was measured by the attached function of SEM. Fig. 5.2 is the deformed and undeformed Compliant Bistable Micromechanism simulated from AceFEM.
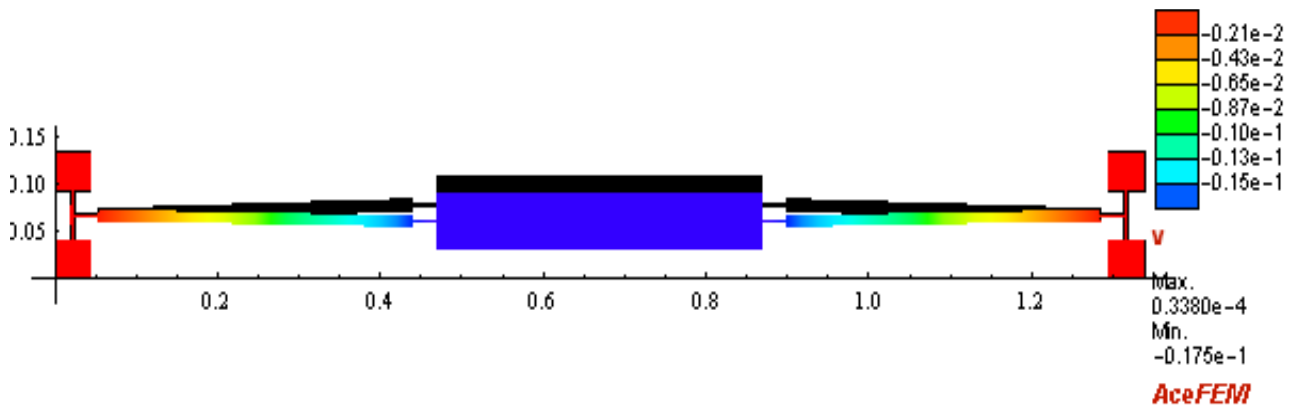

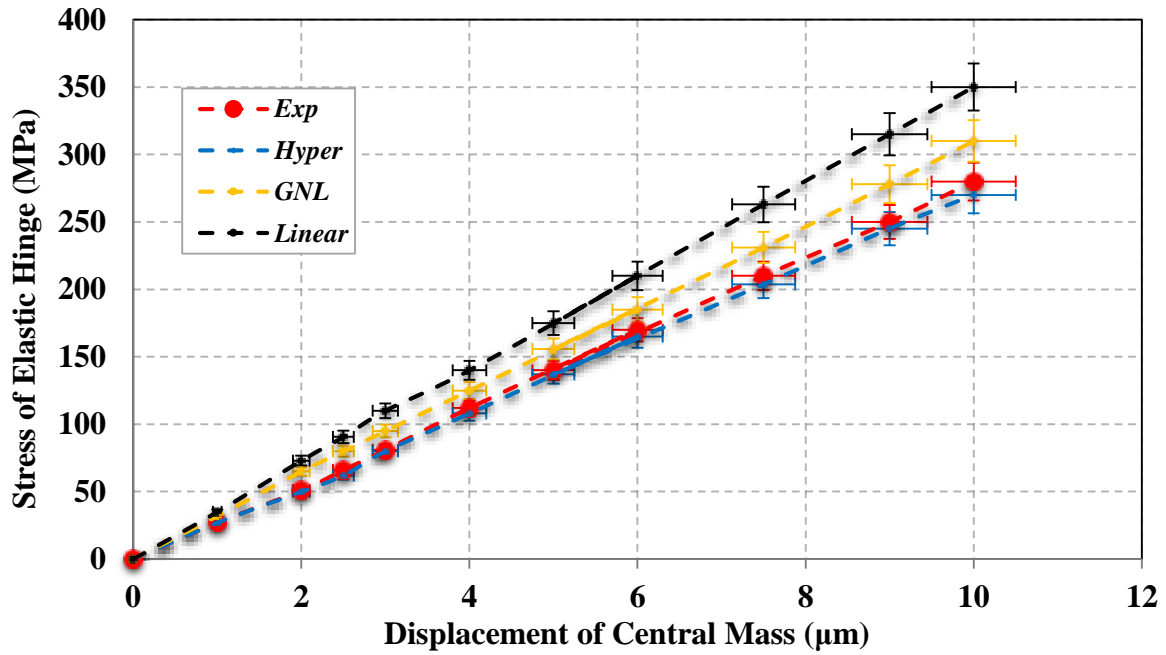**Fig. 5.2: Deformed and undeformed Complaint Bistable Micromechanism**

Fig. 5.3: Stresses of elastic members of Complaint Bistable Micromechanism

Fig. 5.3 shows the load - stress history of the CBMM. Error bars at 5% deviation show that the linear and geometric nonlinear results did not show any form of convergence with the experimental results unlike the hyperelasticity results.

There is a wider range of deviation between the linear model and the experimental results while the results obtained from the geometric nonlinear model displayed a deviation from the experimental results. The results of the hyperelasticity model however are in agreement with that from experiment. We attribute the little discrepancy between the experimental and the hyperelasticity results to the differences in the device geometry, mainly in the thickness of the compliant mechanism which is highly uncertain due to low fabrication tolerances of micromachining.

5.1.2 Compliant Mechanical Amplifier (CMA)

Ouyang *et al.* (2008) conducted an experiment using the prototype Compliant Mechanical Amplifier (CMA) as shown in Fig. 5.4. The strokes of PZT actuators generated the required input while the output displacement of the CMA was captured using an eddy current sensor and recorded by a voltmeter. Fig. 5.5 is the deformed and undeformed Complaint Mechanical Amplifier simulated from AceFEM.
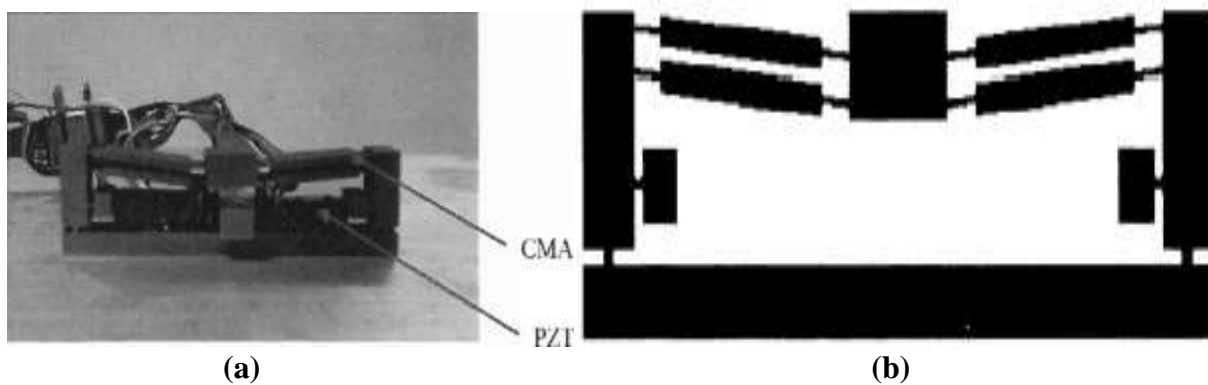

(a) (b)

Fig. 5.4: (a) Prototype of CMA (b) Compliant Mechanical Amplifier

The linear and geometric analysis in Fig. 5.6 give a different result pattern from the results obtained in the experiment and finite deformation in the input - output displacement graph. Error bars at 5% deviation show that the linear and geometric nonlinear analyses did not display any form of convergence with the experimental results unlike the hyperelasticity analysis.
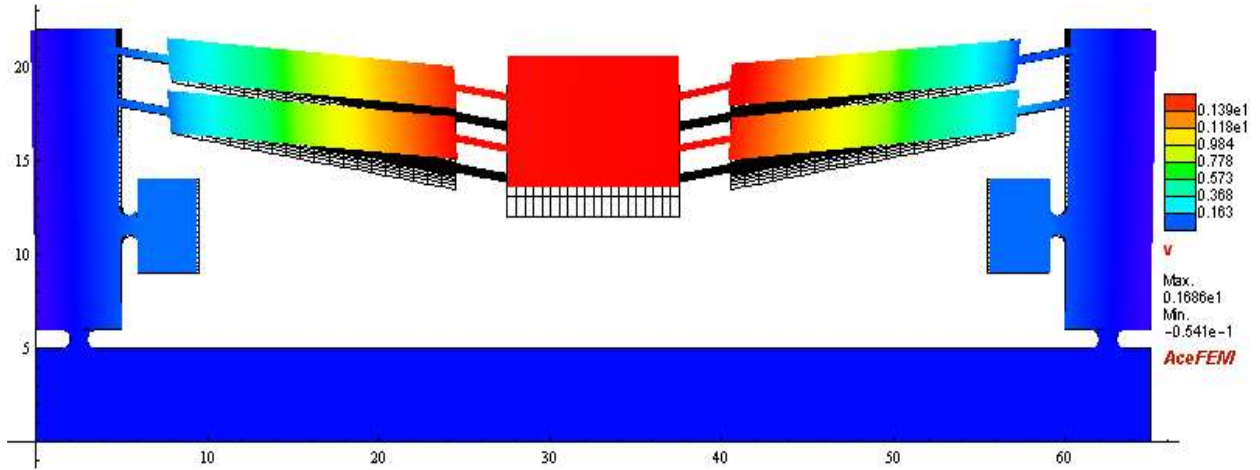

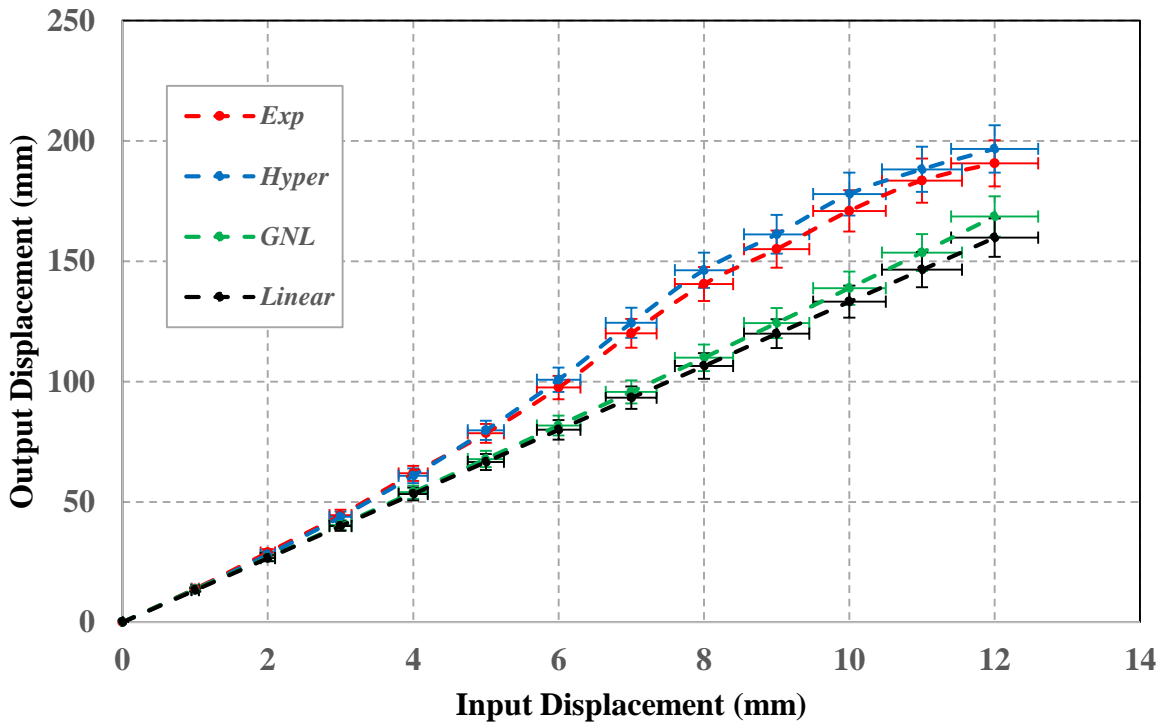**Fig. 5.5: Deformed and undeformed Complaint Mechanical Amplifier**

Fig. 5.6: Output - Input displacement history of the Compliant Mechanical Amplifier

However, the three categories of analysis results show an initial agreement before parting ways at the 3 mm input displacement. It means that before this deviation, ordinary linear or only geometric nonlinear analysis could capture the deformation behaviour in the compliant mechanism. Any result obtained after this would not be reliable for any engineering inference.

5.1.3   Compliant Forceps

Shuib *et al.* (2007) used the pseudo rigid body method as a methodology to perform the stress analysis of a compliant forceps. They used finite element analysis by I – DEAS (Integrated Design Engineering Analysis Software) to validate this compliant mechanism. Fig. 5.7 shows the compliant forceps and its finite element analysis meshing.

Fig, 5.7: Compliant forceps and its finite element analysis

The load – maximum stress history of the compliant forceps is shown in Fig. 5.8. The I-DEAS result, linear and geometric nonlinear assumptions results are all in the same line graph. The inclusion of material nonlinearity, gave a different graph pattern from previous three graphs. However, the PRBM result shows a wide range of deviation at 5% error bars deviation. The results show that using the PRBM, linear finite analysis, linear or geometric nonlinear models cannot effectively interpret the large deformation behaviour of CMs.
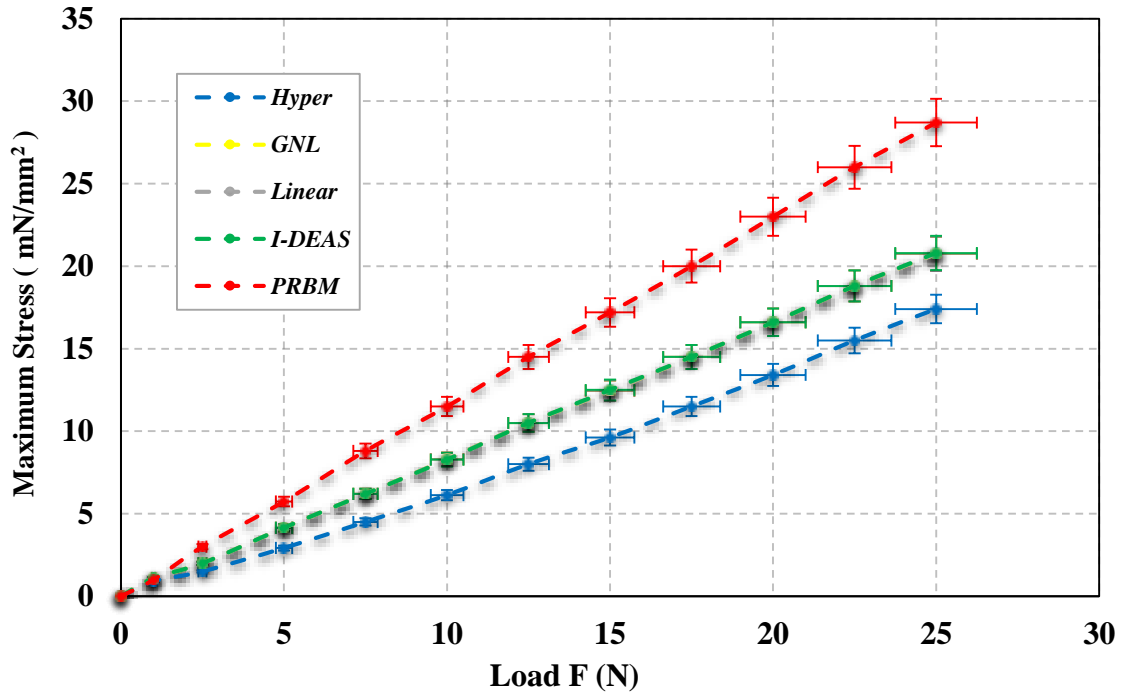
Fig. 5.8: Load verses Maximum stress history of Compliant Forceps

5.1.4 Compliant Stroke Amplifier (CSA)

A planar compliant stroke amplifier is described with initial topology, size, shape and boundary conditions as shown in Fig. 5.9.
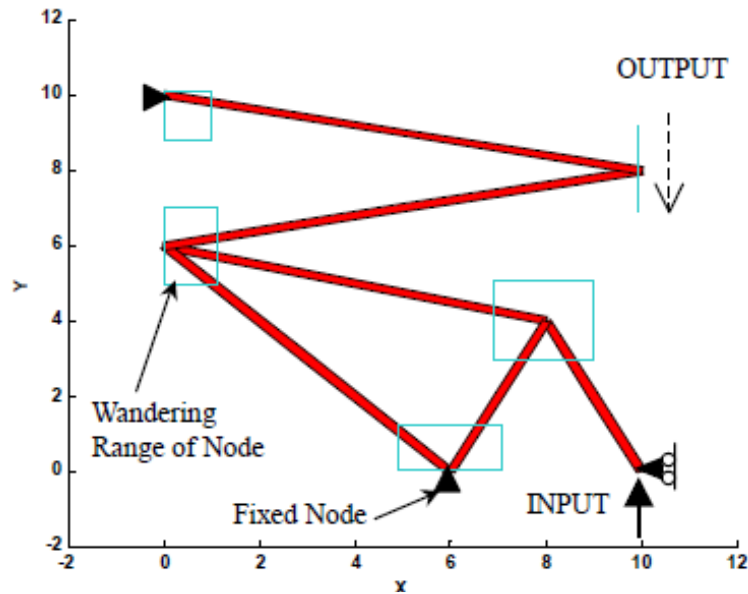

Fig, 5.9: Problem specification for stroke amplifier design

The direction of the desired output motion is out of phase (opposite to input direction) with the input displacement Joo *et al.* (2001). The CM was analysed using linear, geometric nonlinear and hyperelasticity assumptions. The deformed and undeformed mechanisms with the respective assumptions are shown in Figs. 5.10 - 5.12
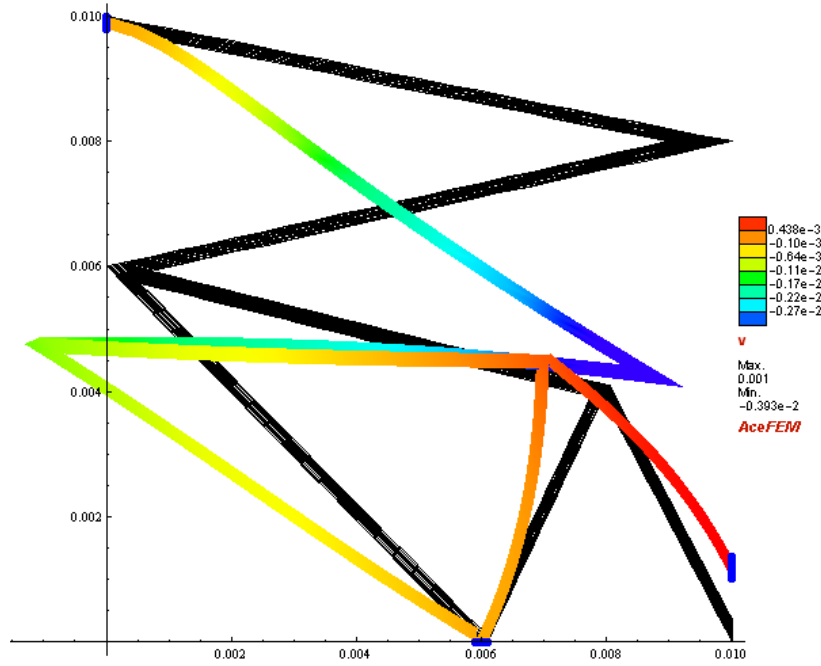

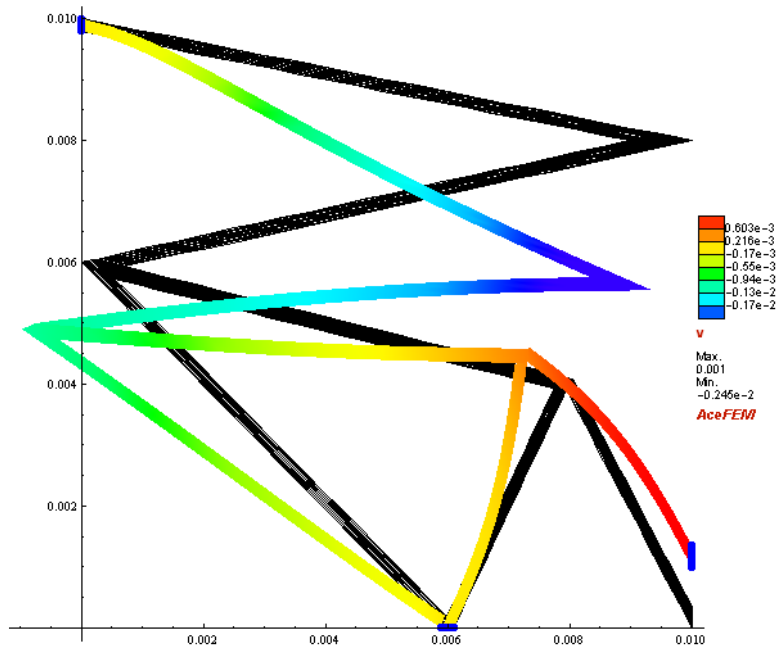**Fig. 5.10: Deformed complaint stroke amplifier mechanism modelled with all linearity**

Fig. 5.11: Deformed complaint stroke amplifier mechanism modeled with geometric nonlinearity (GNL)
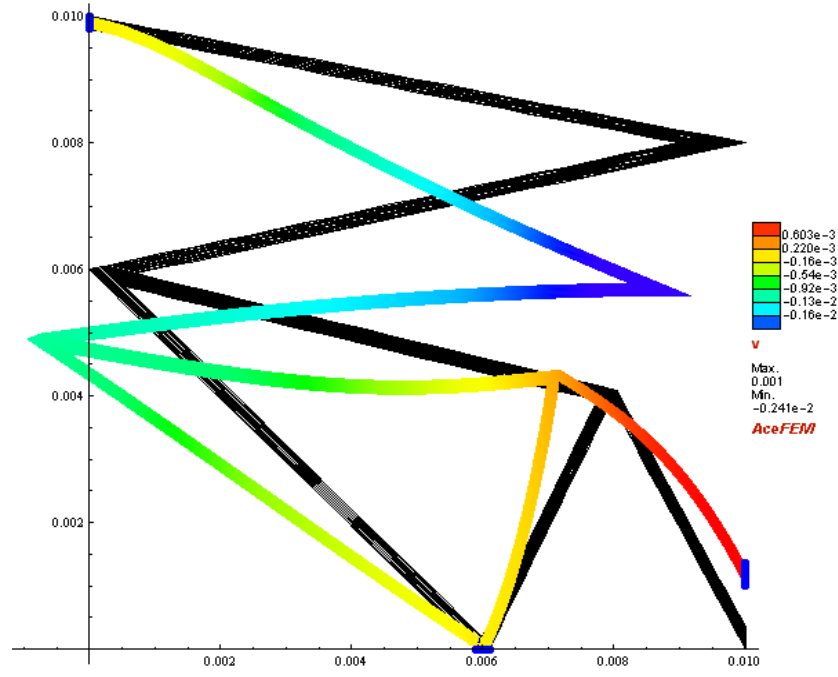
Fig. 5.12: Deformed complaint stroke amplifier mechanism modeled with hyperelasticity
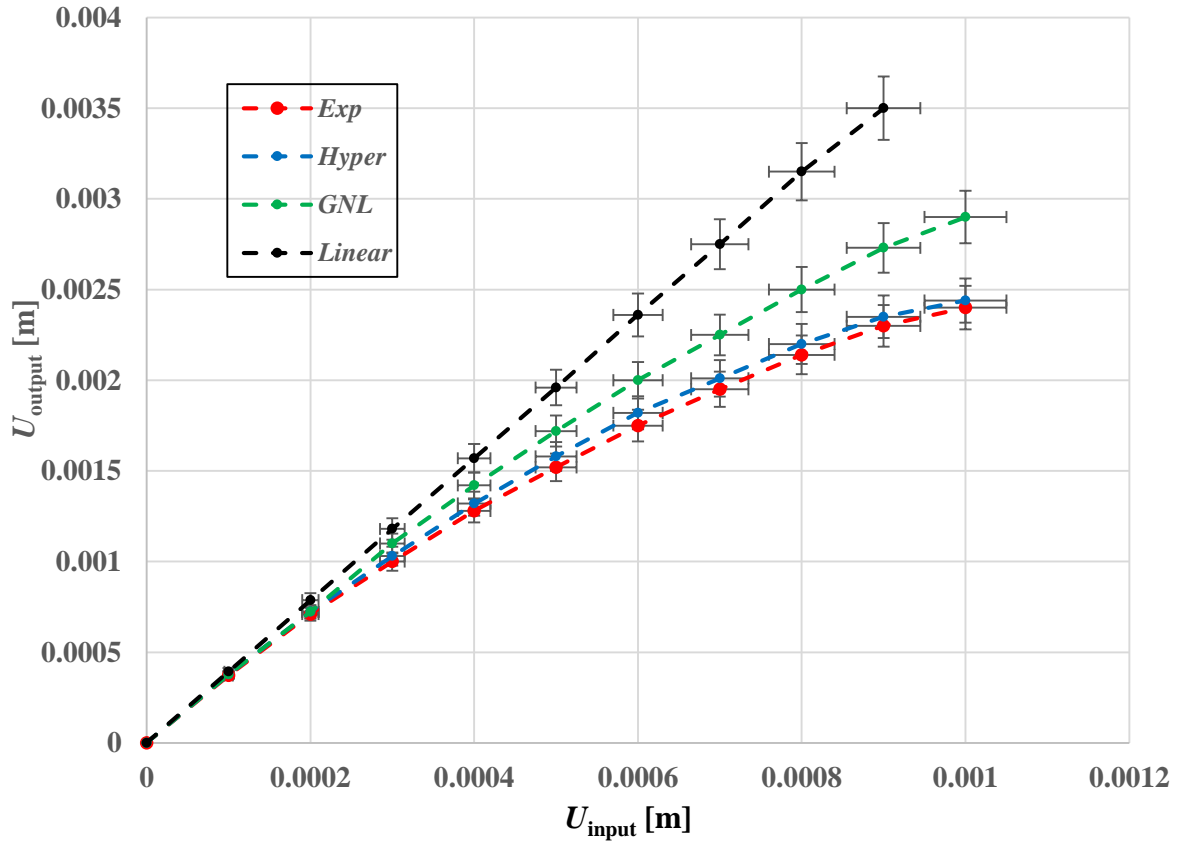

Fig. 5.13: Output - Input displacement history of Complaint Stroke Amplifier Mechanism

Fig. 5.13 is the input - output displacement graph for the CSA. Error bars at 5% deviation show that the linear and geometric nonlinear analyses did not display any form of convergence with the experimental results unlike the hyperelasticity analysis. Nevertheless, there is an initial agreement of the three categories of analysis before deviating noticeably from the 0.2 mm input displacement. It means that before this deviation, usual linear or only geometric nonlinear analysis could capture the deformation behaviour in the compliant mechanism. Any result obtained after this would not be reliable for any engineering inference.

Fig. 5.14 shows the dynamic response of compliant links of the CSA. Unsteady conditions are observed between 0 and 20 milliseconds for the three graphs. The geometric nonlinear and linear signals show that there are respectively, less than 75% and 50% probabilities that any deviation from the hyperelasticity result is due to chance.
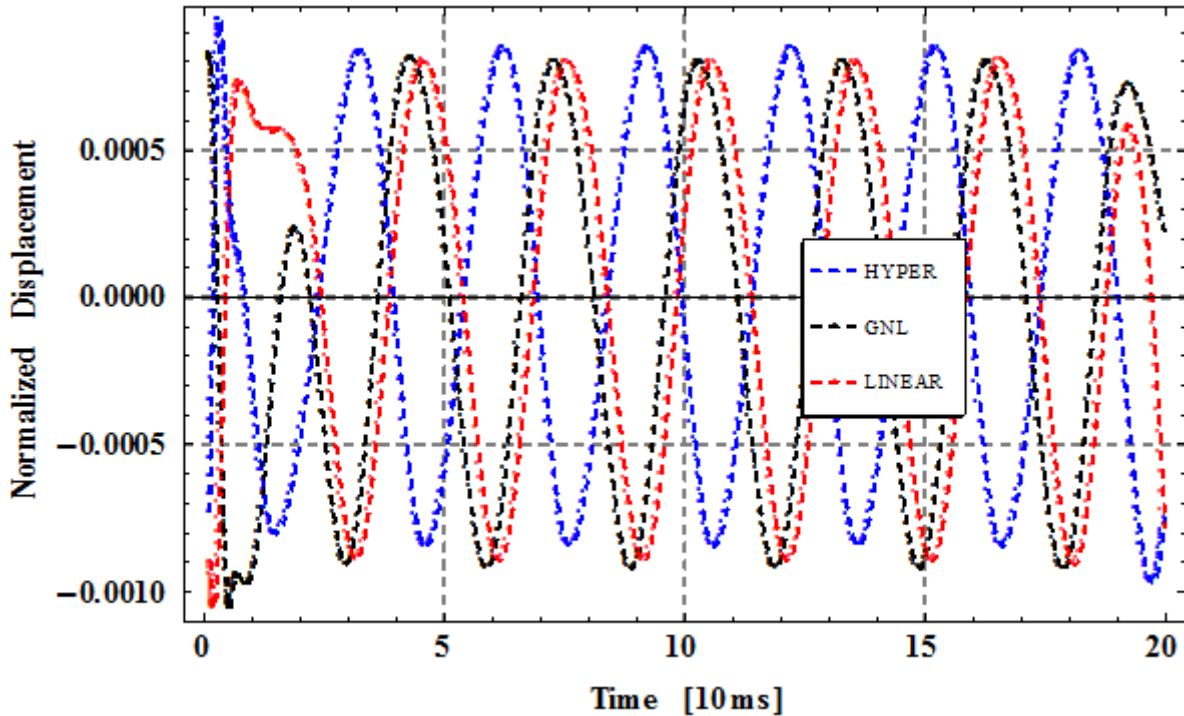

Fig. 5.14: Dynamic response of a compliant link

Based on the standard probability *p>0.95*, these probabilities are not within the accepted deviation. In all, the combined effect of geometric and material nonlinearities show a wide

deviation from the linear and geometric nonlinear assumptions. Initially, the displacement amplitude changes with each motion, stabilizes at the middle of the motion and varies towards the end of the motion cycle. Hyperelasticity effects become critically important at the end points. Failure may result from these end points. This further show why compliant systems that are subjected to large deformations cannot be modelled accurately using linear or only geometrical nonlinear models.

5.2   Simulation Examples with compliant athletics systems

5.2.1   Flex-Run

Fig. 5.15 shows the deformation of the Flex-Run simulated from AceFEM .

Fig. 5.15: Deformed Flex-Run

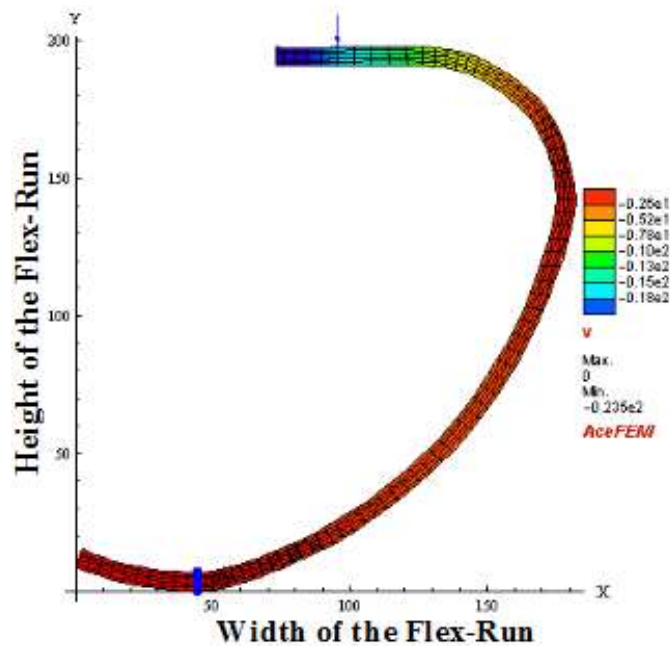The dynamic response of the Flex-Run is shown in Fig. 5.16. Unsteady conditions are observed between 0 and 15 milliseconds. The produced harmonics of hyperelasticity, GNL and linear results exhibit a wide deviation from one another between 15 and 92.5 milliseconds with the linear result being the farthest.
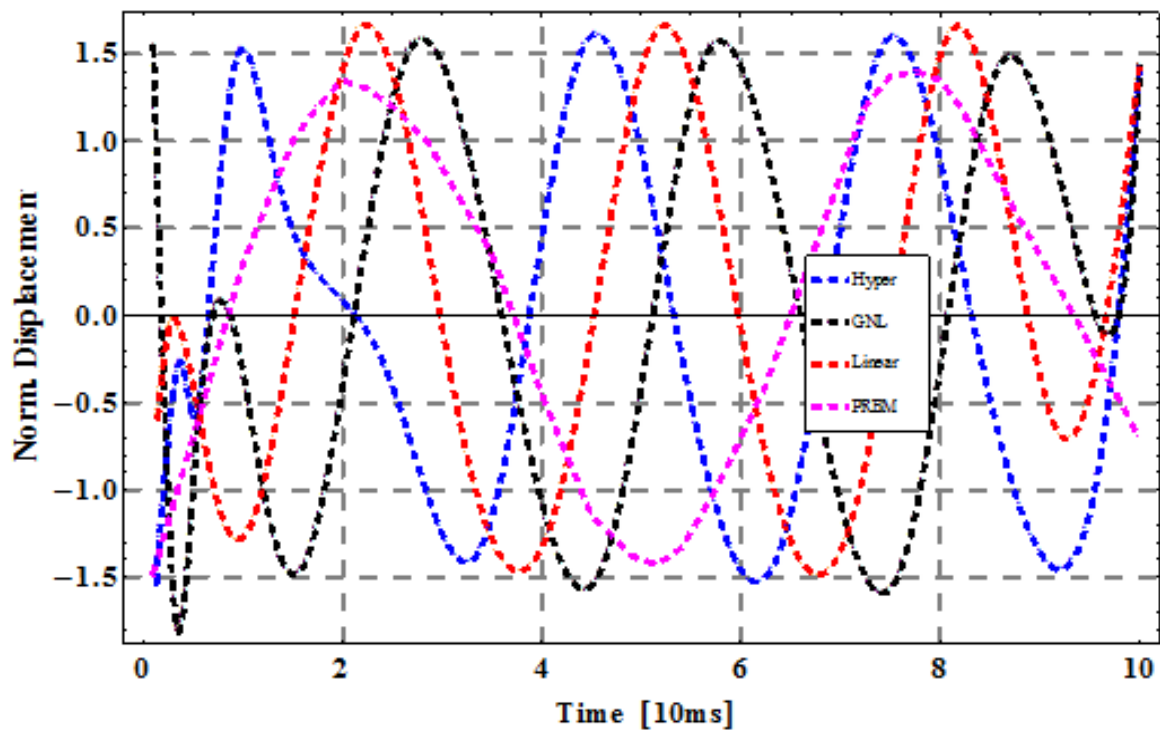
Fig. 5.16: Dynamic Response of Flex-Run
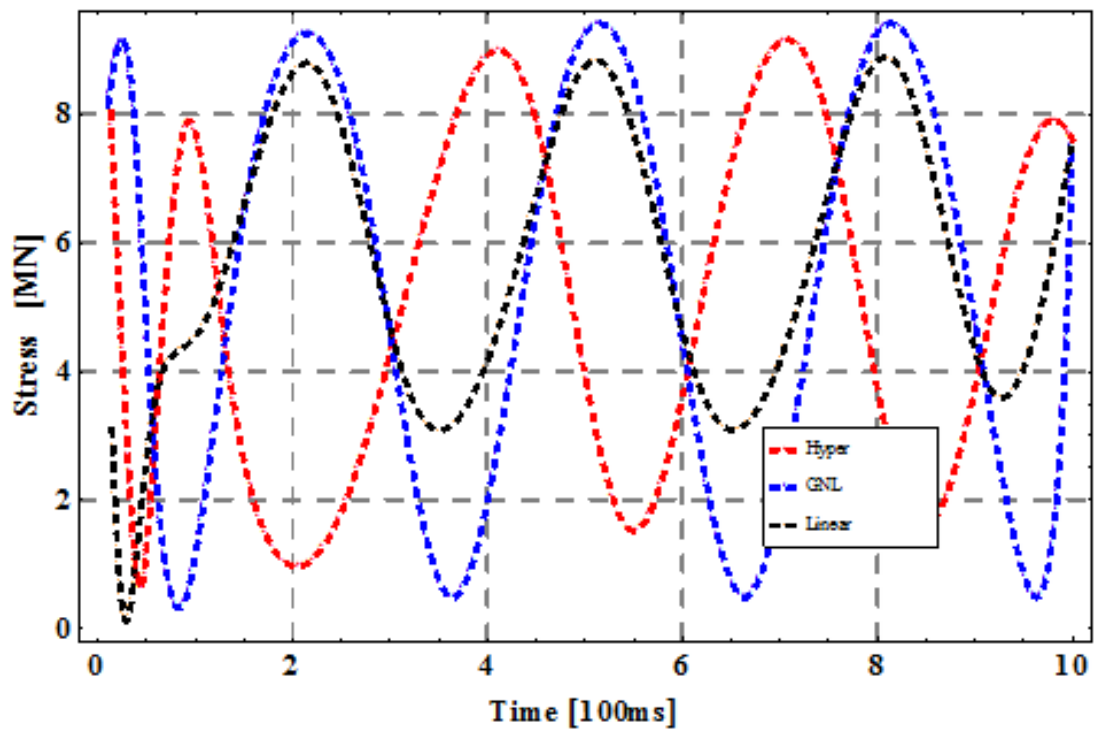
Fig. 5.17: Stress vs Time for Flex-Run
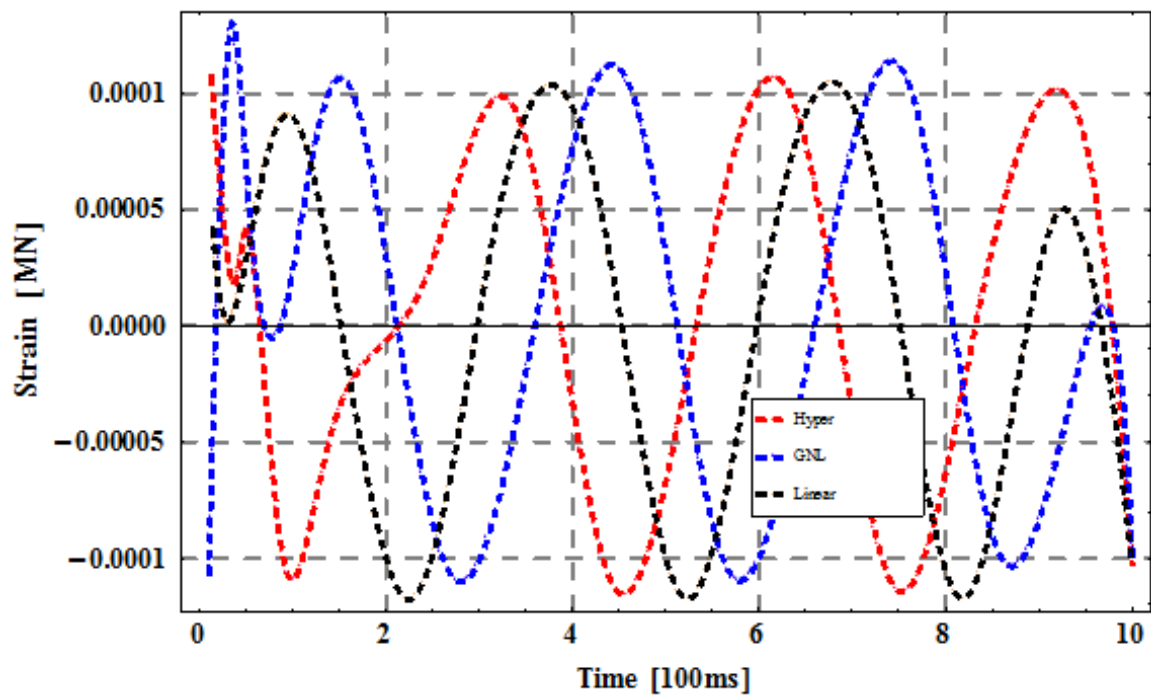
Fig. 5.18: Strain vs Time for Flex-Run

Figs. 5.17 and 5.18 are the stress and strain of the Flex-Run plotted in time domain. The produced harmonics in Fig. 5.17 shows that the hyperelasticity has the shortest amplitude within the middle range.

Fig. 5.19: Norm. Displacement vs Frequency for Flex-Run

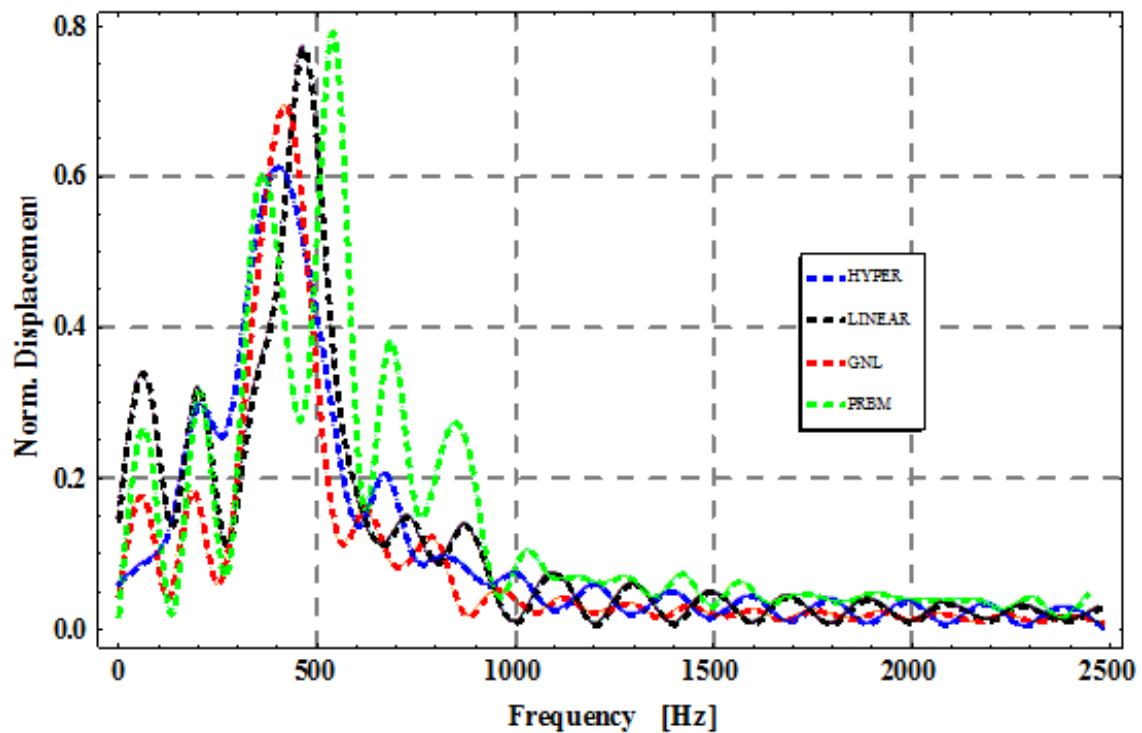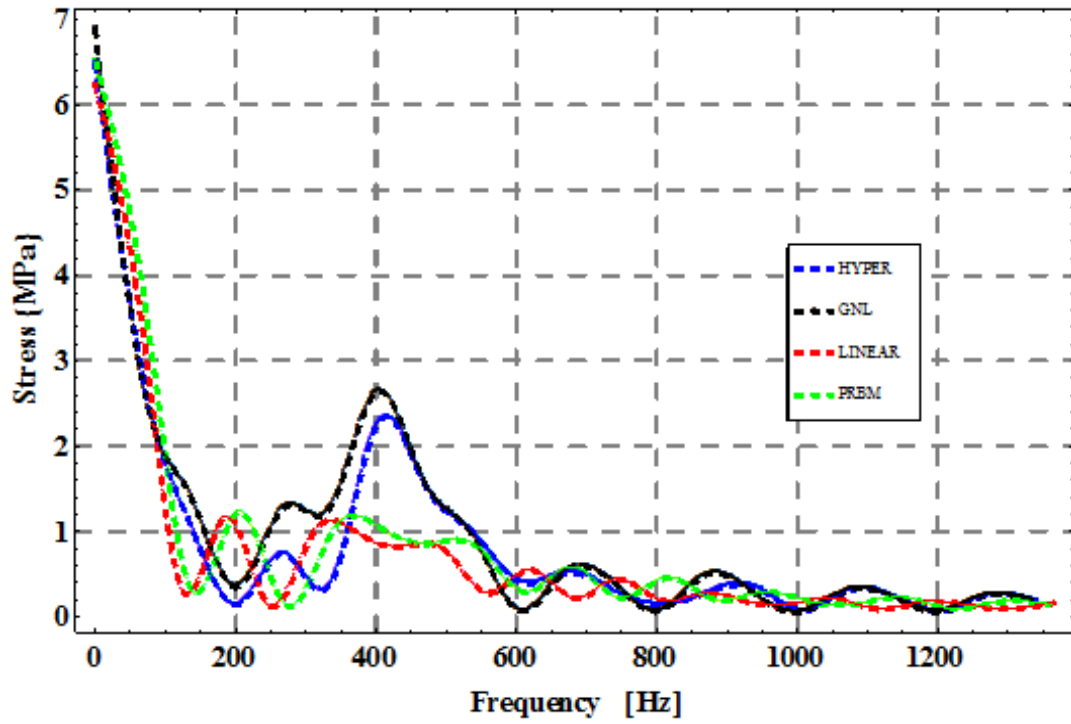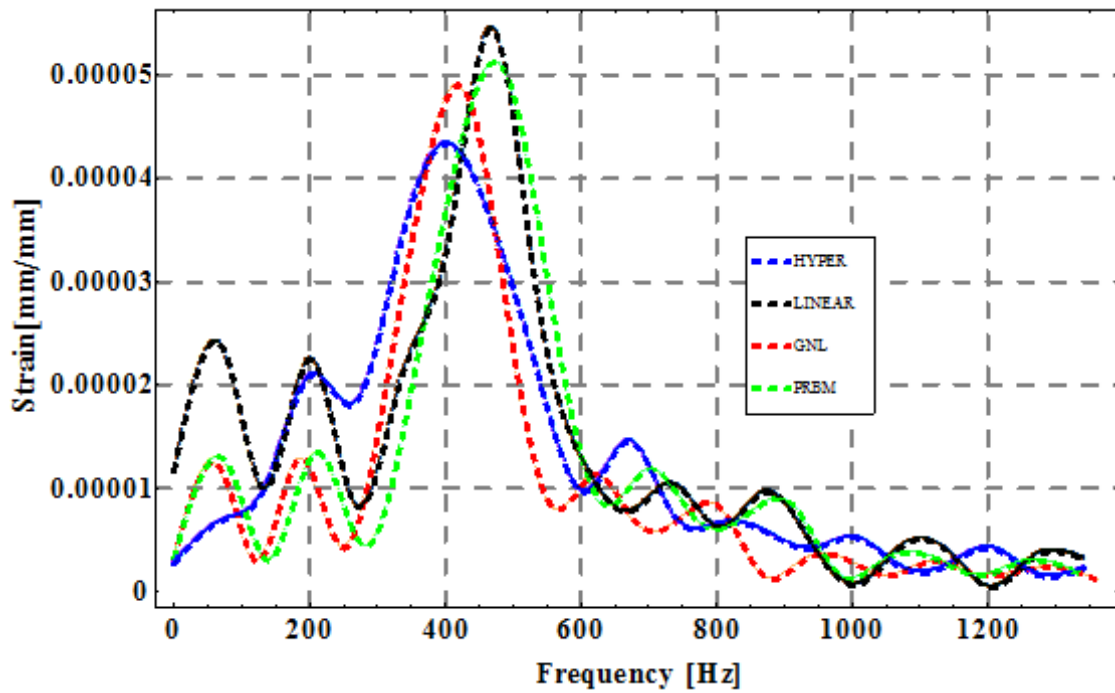**Fig. 5.20: Stress vs Frequency for Flex-Run**

Fig. 5.21: Strain vs Frequency for Flex-Run

Figs. 5.19, 5.20 and 5.21 are the displacement, stress and strain of the Flex-Run plotted in frequency domain. The graphs have shown the disparities that exist when hyperelasticity is considered compared to other assumptions. The maximum frequencies with their

corresponding displacement, stress and strain occur at different points on the graphs for each analysis assumption.

In all, from the dynamic response, GNL signal shows there is less 75% probability that any deviation from the hyperelasticity result is due to chance; while the linear and PRBM signals show that there are less 50% probabilities that any deviation from the hyperelasticity result is due to chance. Based on the standard probability *p>0.95*, these probabilities are not within the accepted deviation. In all, the combined effect of geometric and material nonlinearities show a wide deviation from the linear and geometric nonlinear assumptions. Initially, the displacement amplitude changes with each motion, stabilizes at the middle of the motion and varies towards the end of the motion cycle. Hyperelasticity effects become critically important at the end points.

5.2.2 Pole Vault

Fig. 5.22 shows deformation of the pole vault simulated from AceFEM used for the displacement - stress history. Fig. 5.23 is the displacement - stress history of the curve edge of the pole vault. The PRBM and the linear assumption show a straight line graph which is not ideal for such large deformation. However, the four results show an agreement up to 0.012 normalized input displacement beyond which only geometric nonlinear and hyperelasticity results show some agreement before parting ways at 0.040 normalized input displacement.

Figs. 5.24, 5.25 and 5.26 are the stress and strain of the pole vault plotted in time domain. The produced harmonics a wide deviation that exist without material nonlinearity inclusion. Figs. 5.27, 5.28 and 5.29 are the displacement, stress and strain of the pole vault plotted in frequency domain. The maximum frequencies with their corresponding displacement, stress and strain

occur at different points on the graphs for each analysis assumption revealing the deviation that

exist when material nonlinearity is considered compared to other assumptions.

Fig. 5.22: Deformed pole vault

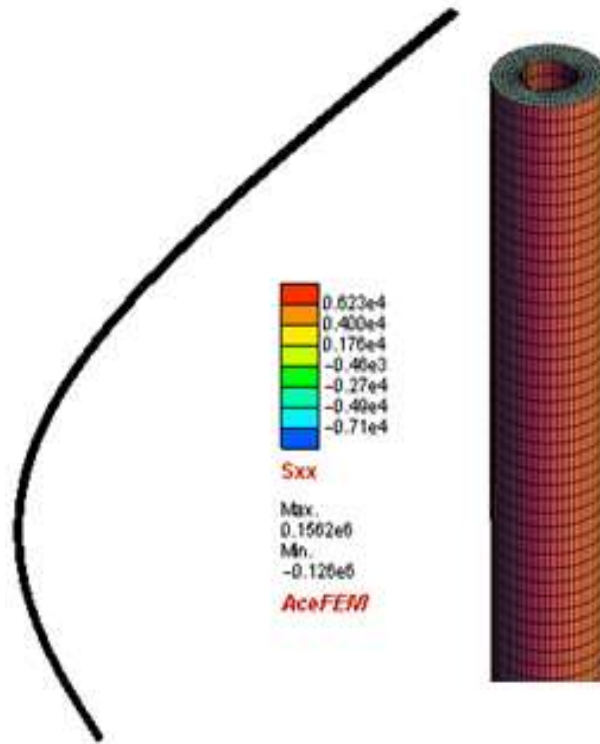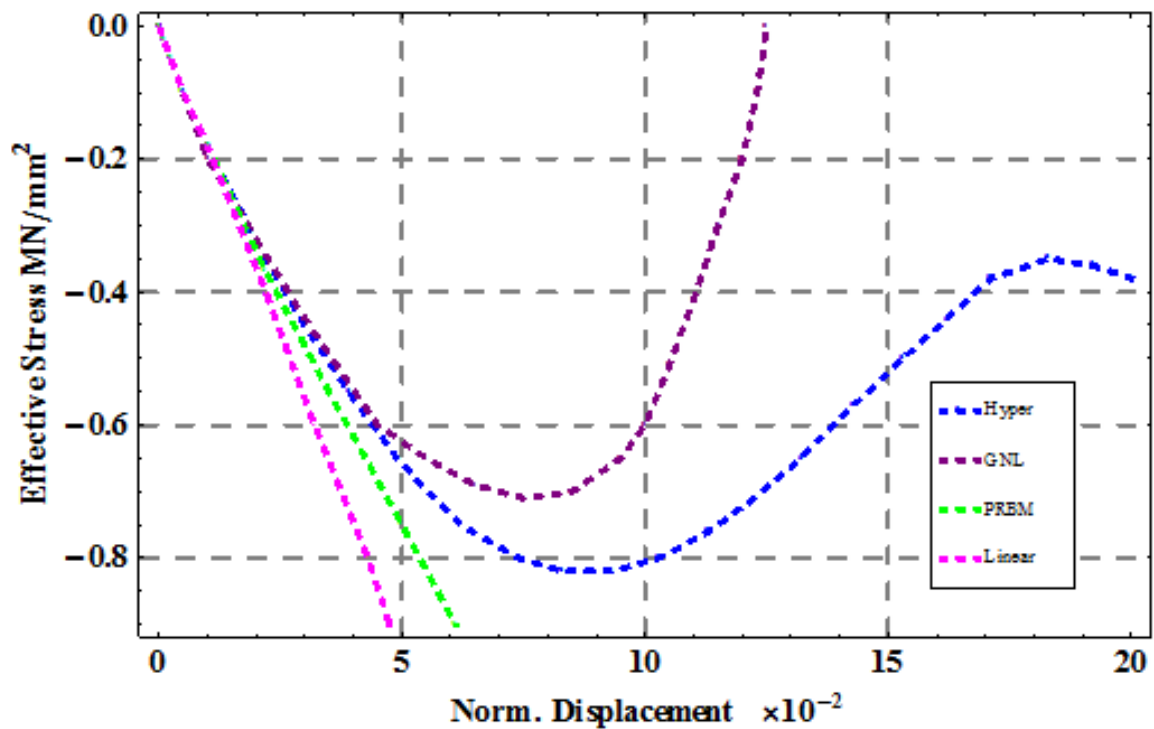**Fig. 5.23: Stress – Displacement history of the curved edge of a pole vault**
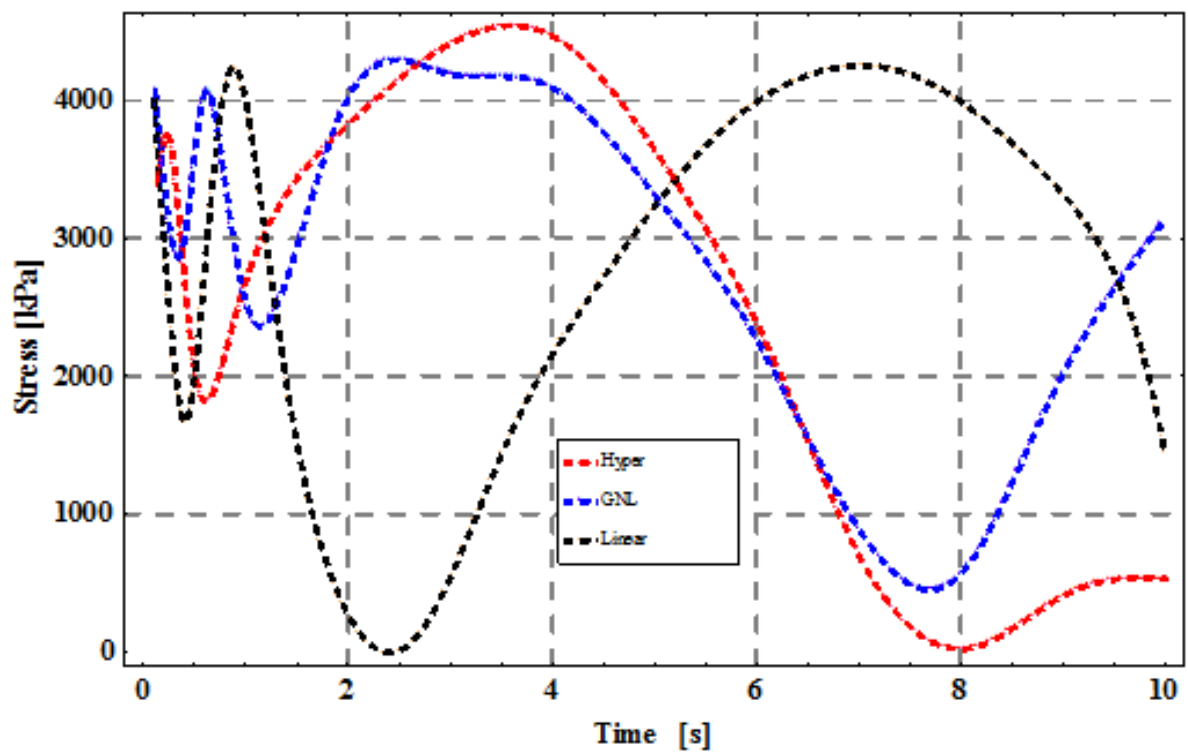
Fig. 5.24: Stress vs Time for Pole Vault
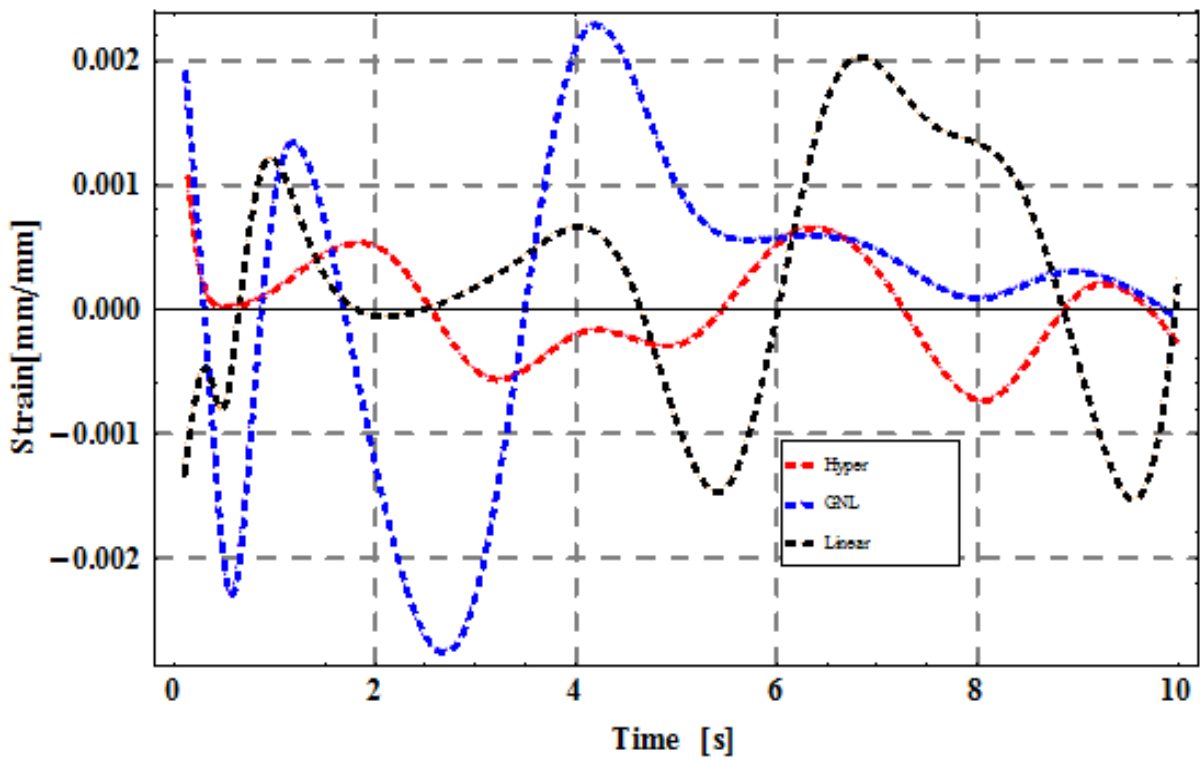
Fig. 5.25: Strain vs Time for Pole Vault
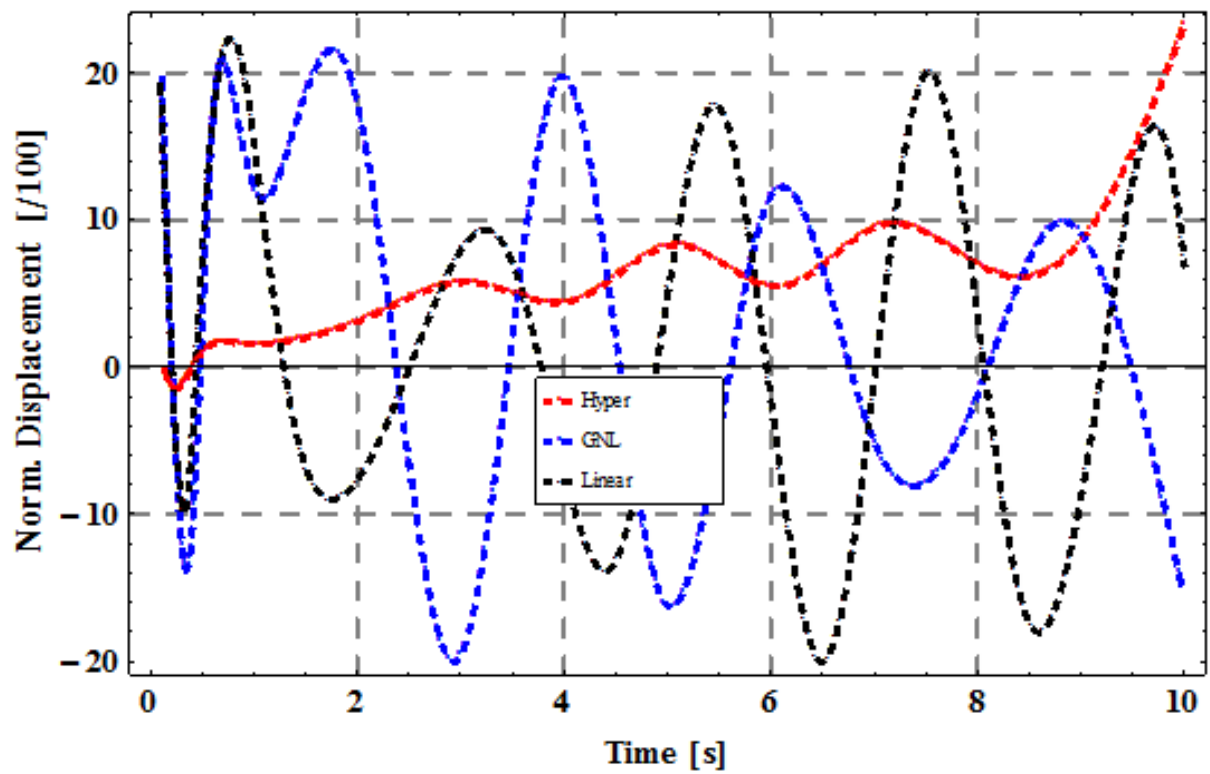
Fig. 5.26: Displacement vs Time for Pole Vault
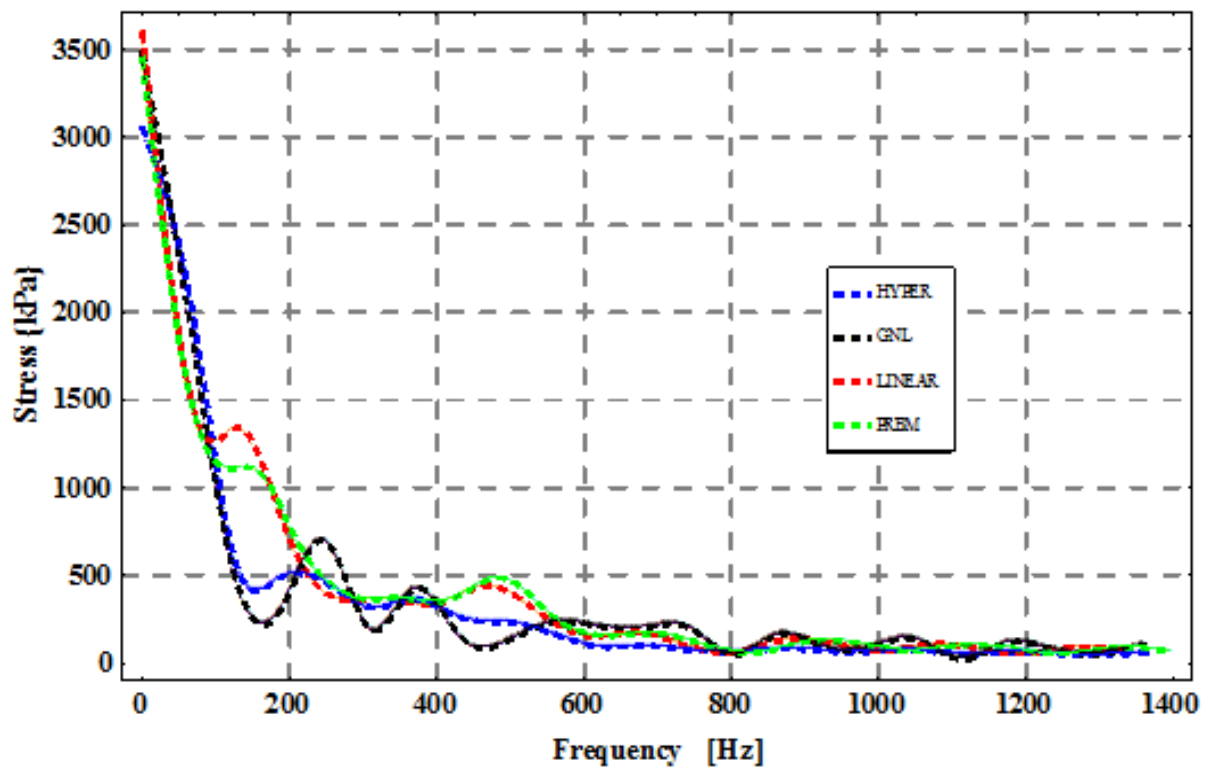
Fig. 5.27: Stress vs Frequency for Pole Vault
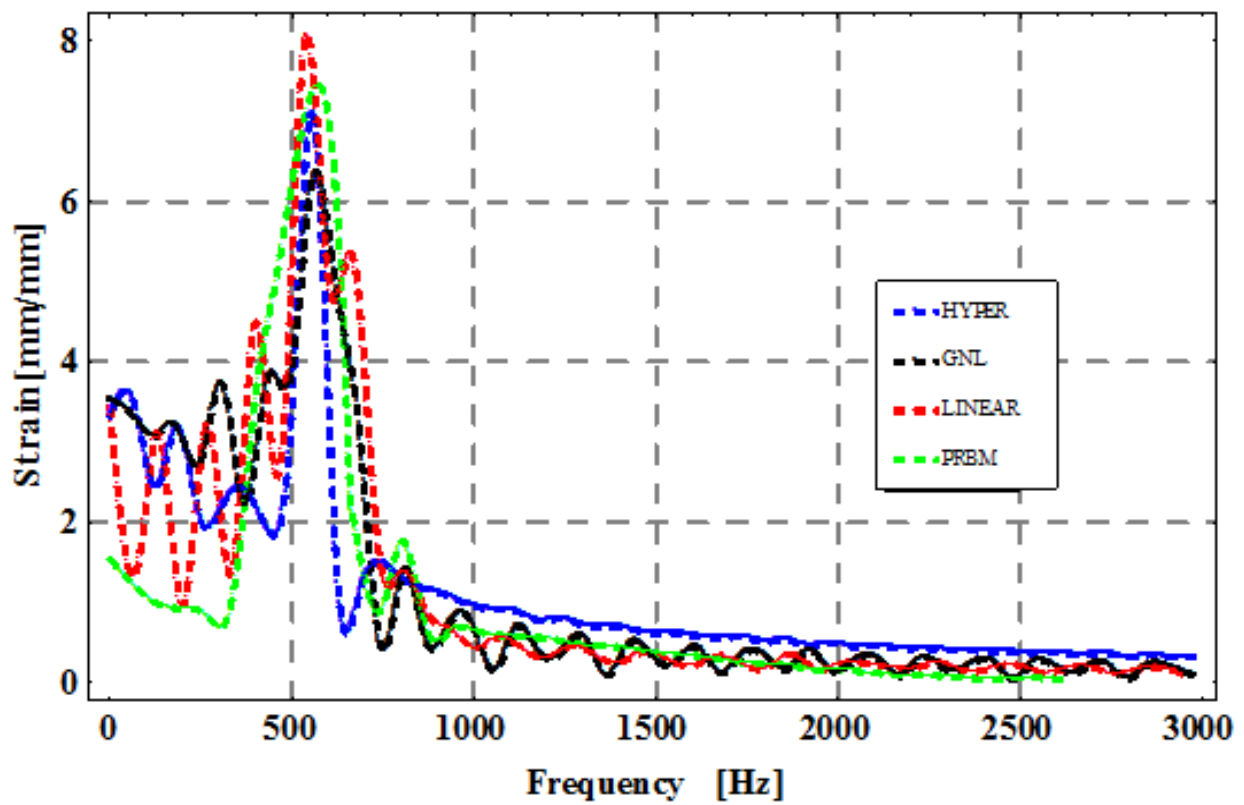
Fig. 5.28: Strain vs Frequency for Pole Vault
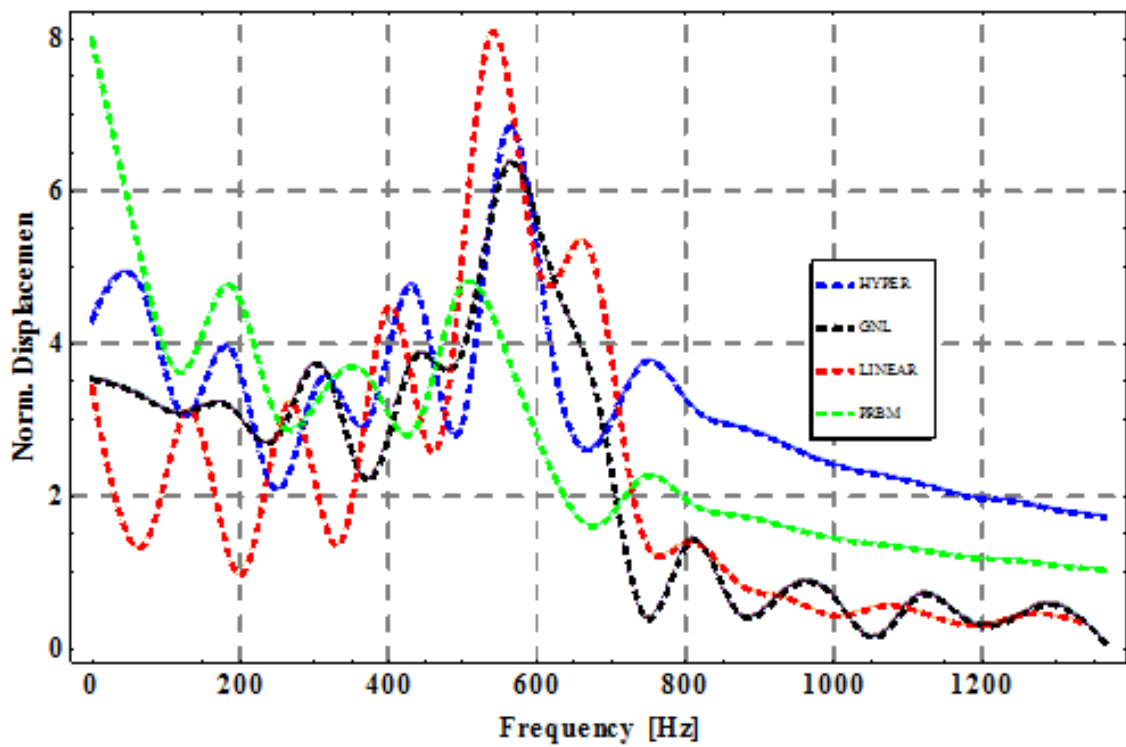
Fig. 5.29: Norm. Displacement vs Frequency for Pole Vault

5.3 Effect of Shear Deformation using Compliant Cantilever and Four Bar Mechanism

Compliant cantilever and four bar mechanisms are analysed and presented. Figs. 5.30 and 5.32 are the deformed and undeformed mechanisms. For the finite element implementation of the governing equation, AceFEM was used. The entire mechanisms geometry were built as adequate. The essential boundary and natural boundary conditions were stated with the base of the mechanism clamped. Table 5.1 are the parameters used for simulation of the results.

Table 5.1: Parameters for Simulation of Results

Definition	Symbol	Value
Lengths of the mechanism links	$l_1 = l_3$	*0.7 m*
	l_2	*0.4 m*
Young's Modulus	$E_1 = E_2 = E_3$	*1103.61 MPa*
Density of material	$\rho_1 = \rho_2 = \rho_3$	*913 kg/m^3*
Poisson ratio	$v_1 = v_2 = v_3$	*0.35*
Breadth of the compliant links	$b_1 = b_3$	*0.00318 m*
	b_2	*0.00239 m*
Heights of the compliant links	$h_1 = h_3$	*0.00863 m*
	h_2	*0.00863 m*
Areas of the compliant links	$A_1 = A_3$	*27.4434 µm^2*
	A_2	*20.6257 µm^2*
Second moments of areas of the compliant links	$I_1 = I_3$	*0.170325 nm^4*
	I_2	*0.128012 nm4*
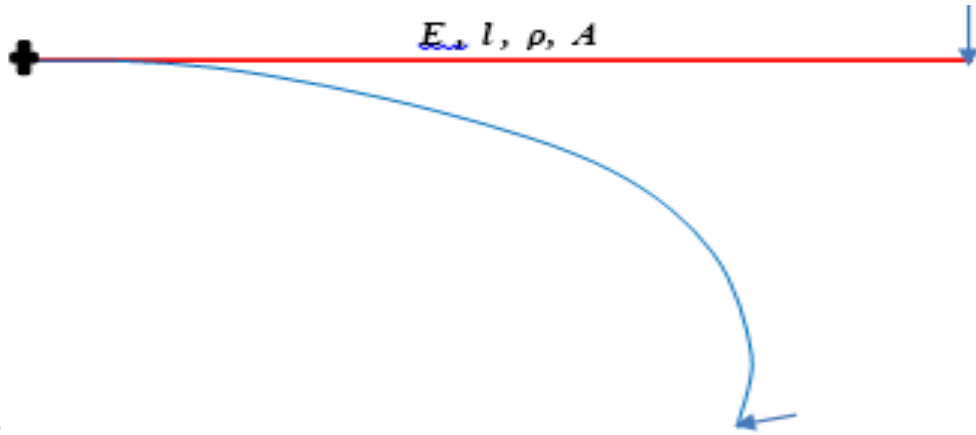
Fig. 5.30: Deformation of the compliant cantilever mechanism endpoint
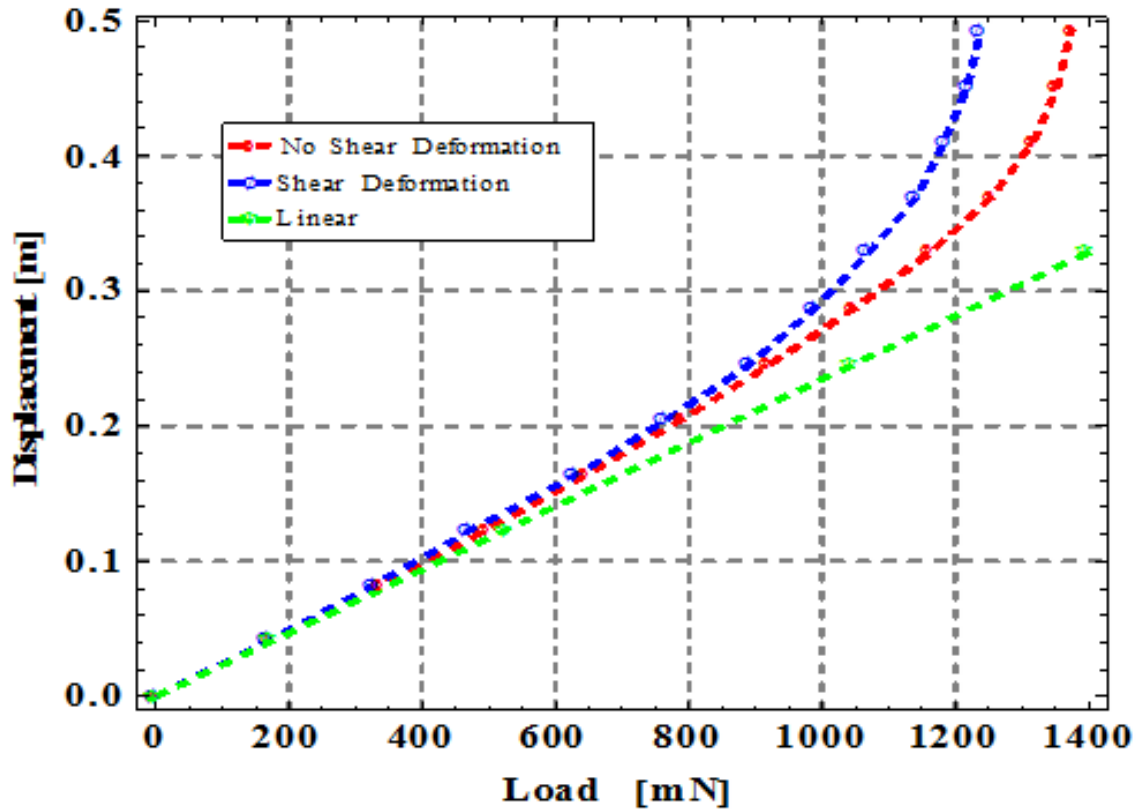
Fig. 5.31: Load–displacement of the compliant cantilever mechanism endpoint

The simulated results in Figs. 5.31 and 5.36 show a deviation from straight line graph from linear assumptions to normal curves considering the effect of geometric nonlinearity. However, there is also a deviation between the geometric nonlinear consideration when the effect of shear deformation is captured and when it is not. Initially, the two nonlinear graphs show the same behaviour until 100 mN and 220 mN input forces for the compliant cantilever and four bar mechanisms respectively when the effect of the shear deformation is much that the deviation

145

starts becoming noticeable. Figs. 5.33 - 5.35 are the bending moment, axial and shear forces distributions of the deformed compliant four bar mechanism.
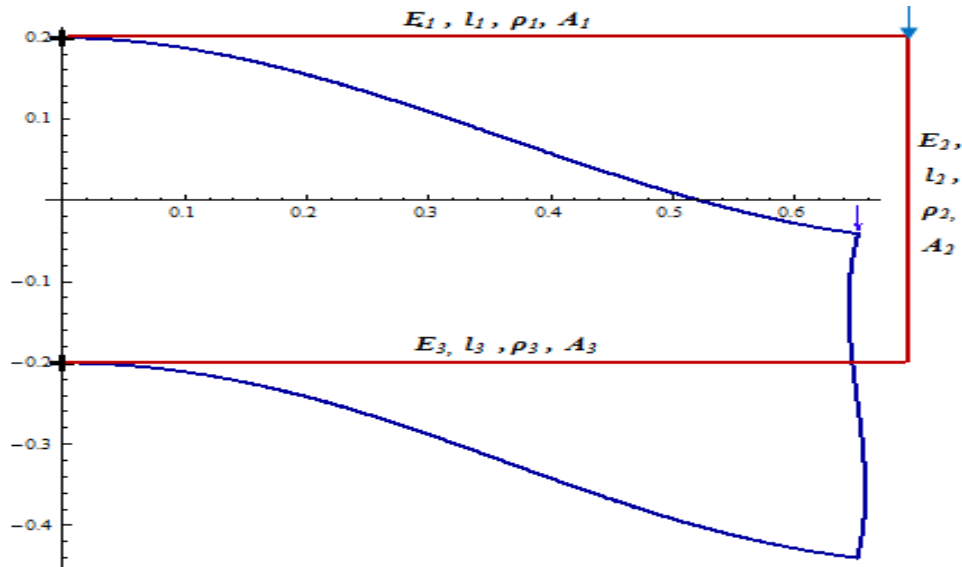
Fig. 5.32: Deformation of the deformed mechanism
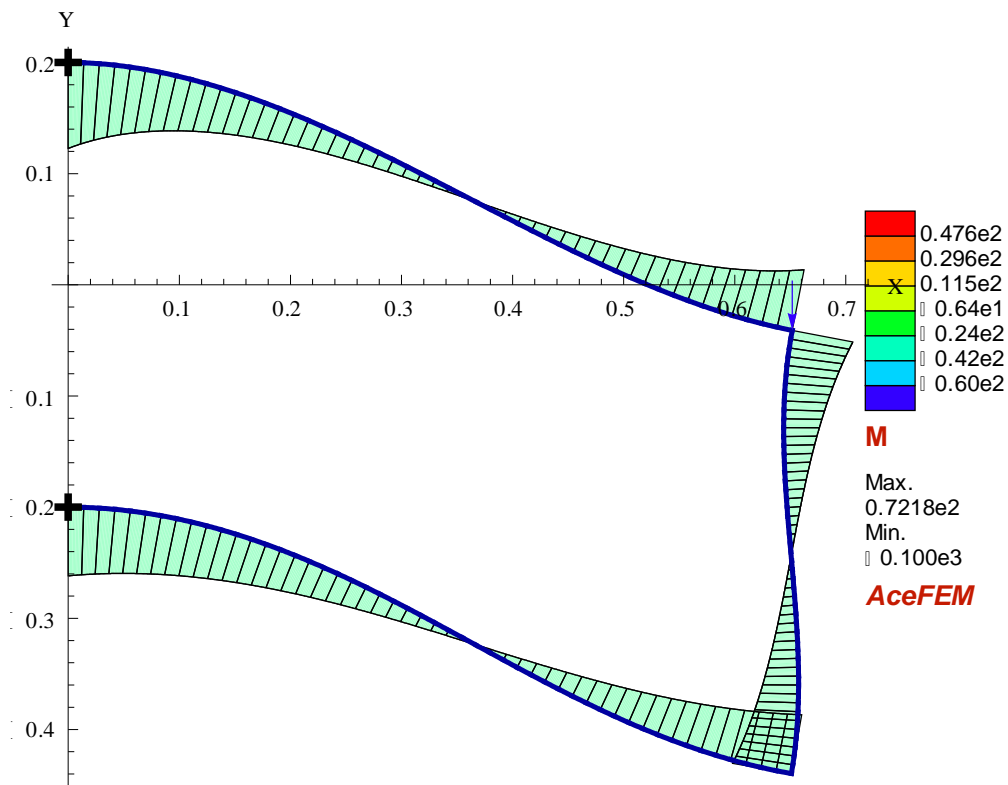
Fig. 5.33: Bending Moment of the deformed mechanism
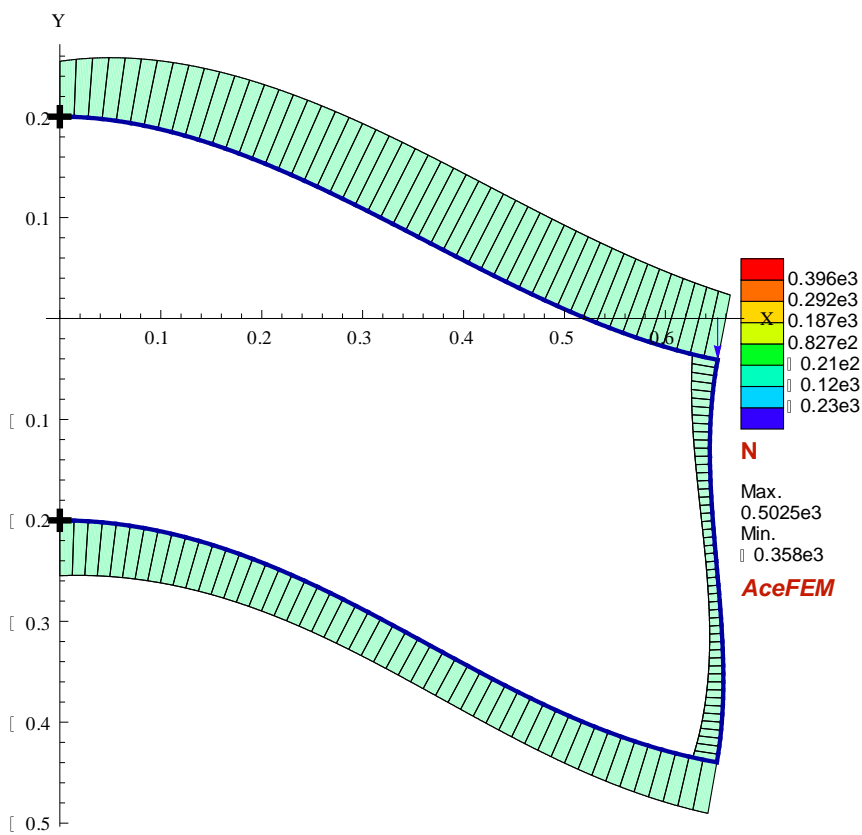
Fig. 5.34: Axial Force of the deformed mechanism
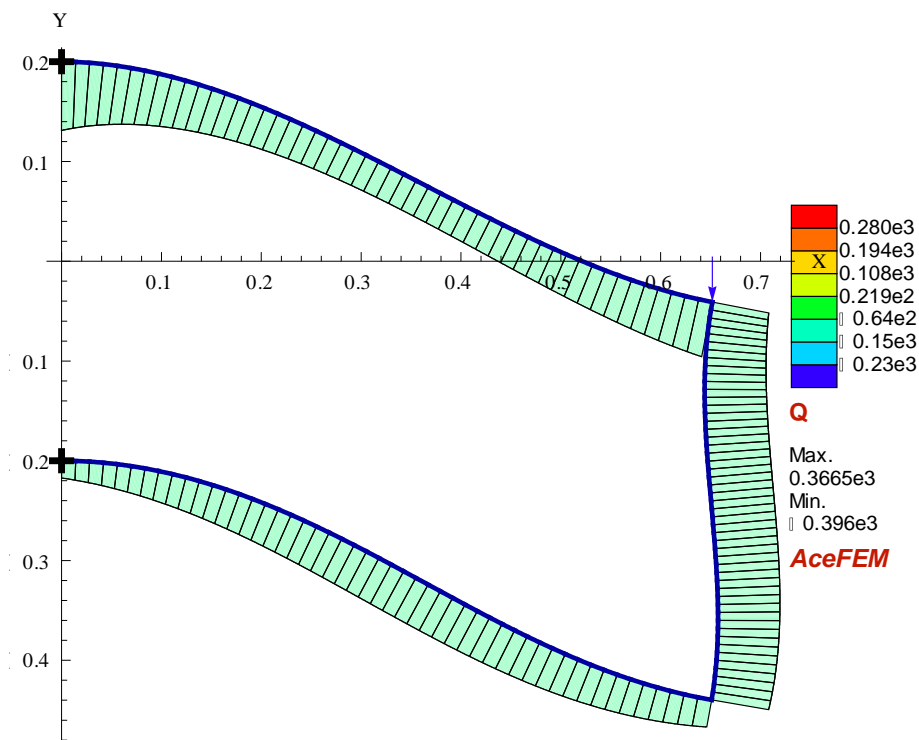
Fig. 5.35: Shear Force of the deformed mechanism
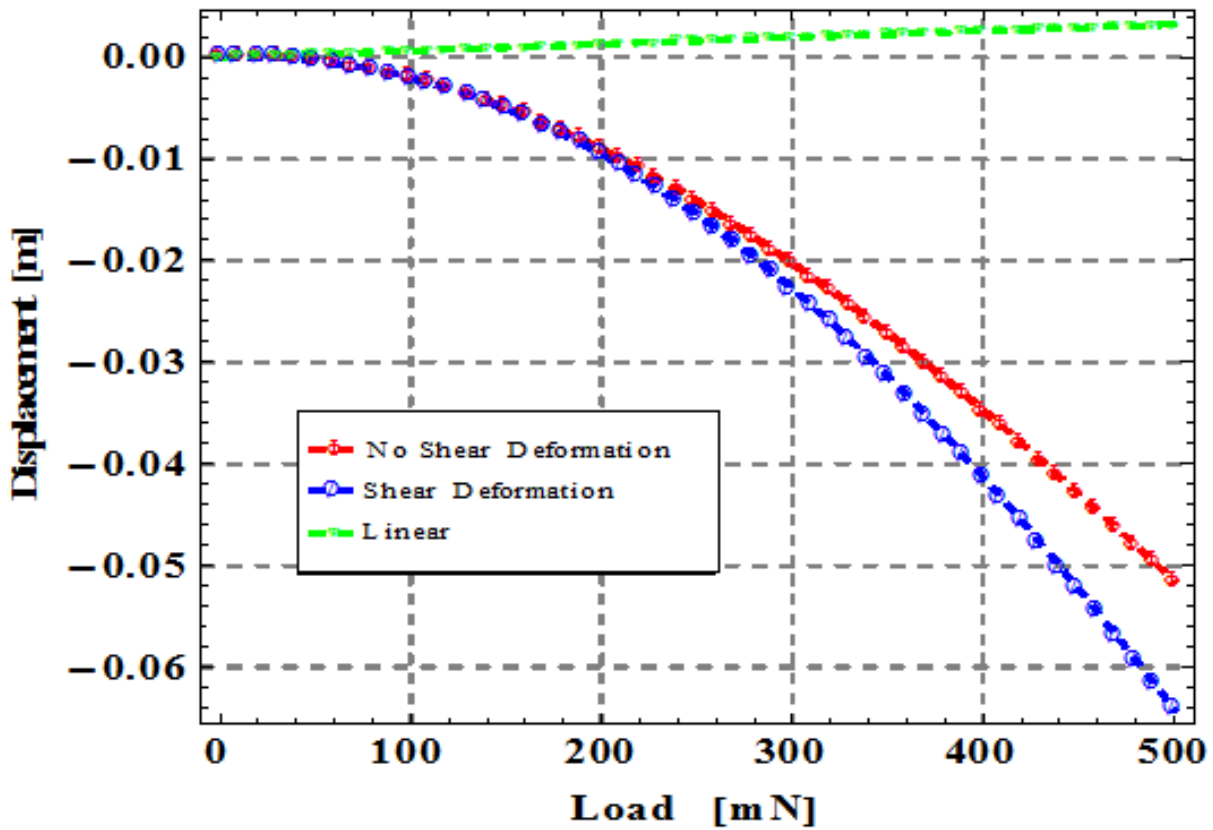
Fig. 5.36: Load – displacement of the coupler midpoint

5.4   Stress-Strain and Fatigue Life Results

The stress – strain curve shown in Fig. 4.4 is for low density polypropylene (LDPP) and low density polyethylene (LDPE). It has shown that the constitutive law of a typical polymer exhibits a nonlinear relation. Hence, a linear material assumption will definitely not be appropriate for compliant mechanisms made of polymers.

The fatigue life versus strain amplitude in a logarithmic scale are shown in Figs. 5.37 and 5.38 for LDPP and LDPE respectively. The scattered points represent experimental results. The developed model result is compared with models used by earlier researchers. The comparative analysis of the theoretical prediction formula with the experimental data results show a strong agreement. However, the two models from literature show a level of agreement at high strain

amplitude but deviate noticeably from 0.10 mm/mm strain amplitude. The least square analysis of the results show that the result from the developed model has the least deviation from the experimental test results. It means that the developed model is more appropriate to study fatigue life of continuum polymeric compliant systems.

Figs. 5.39 and 5.40 show the fitting of the experimental data with a curve and plotting this on the same axis with the prediction model for LDPP and LDPE at different damage variable values. It was found that the value of the damage variable, *D* that produces the curve that compared well with the experimental fitted curve is *0.0751*.
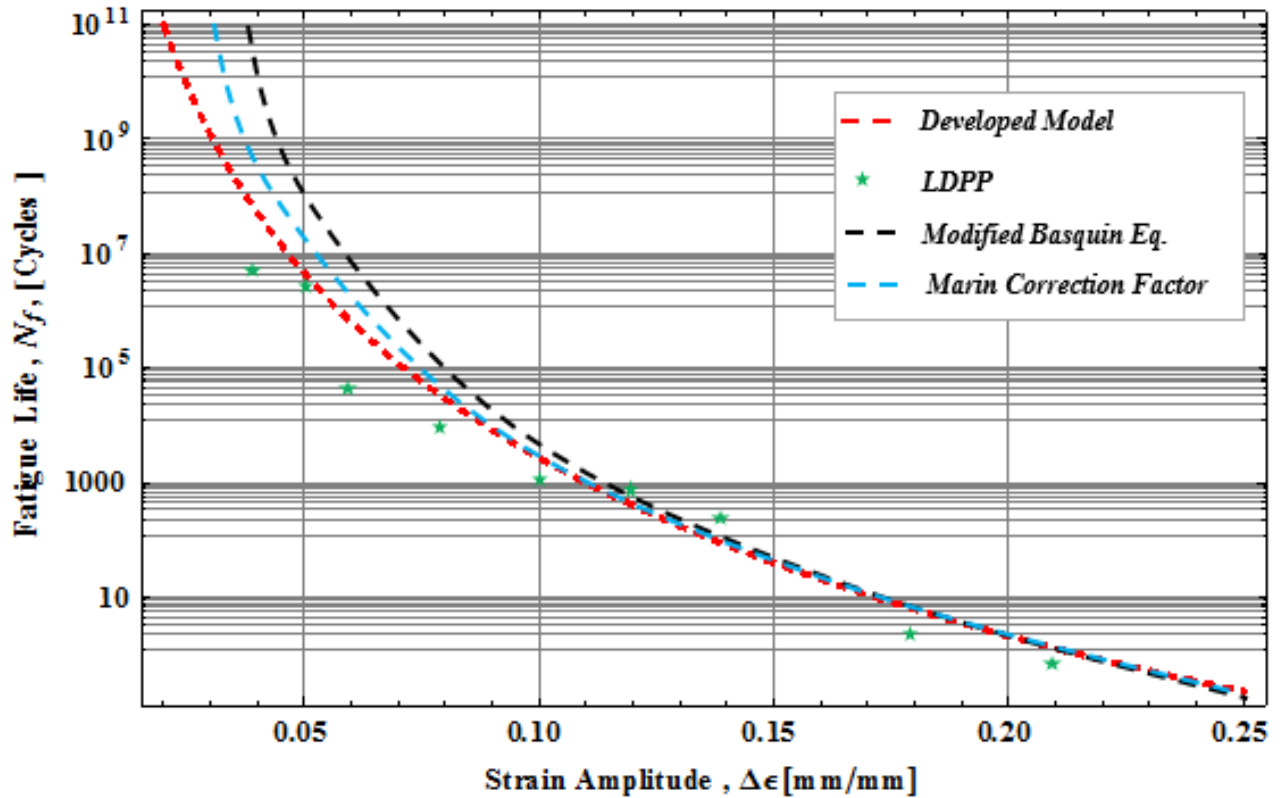
Fig. 5.37: Fatigue Life, N_f versus strain amplitude for LDPP
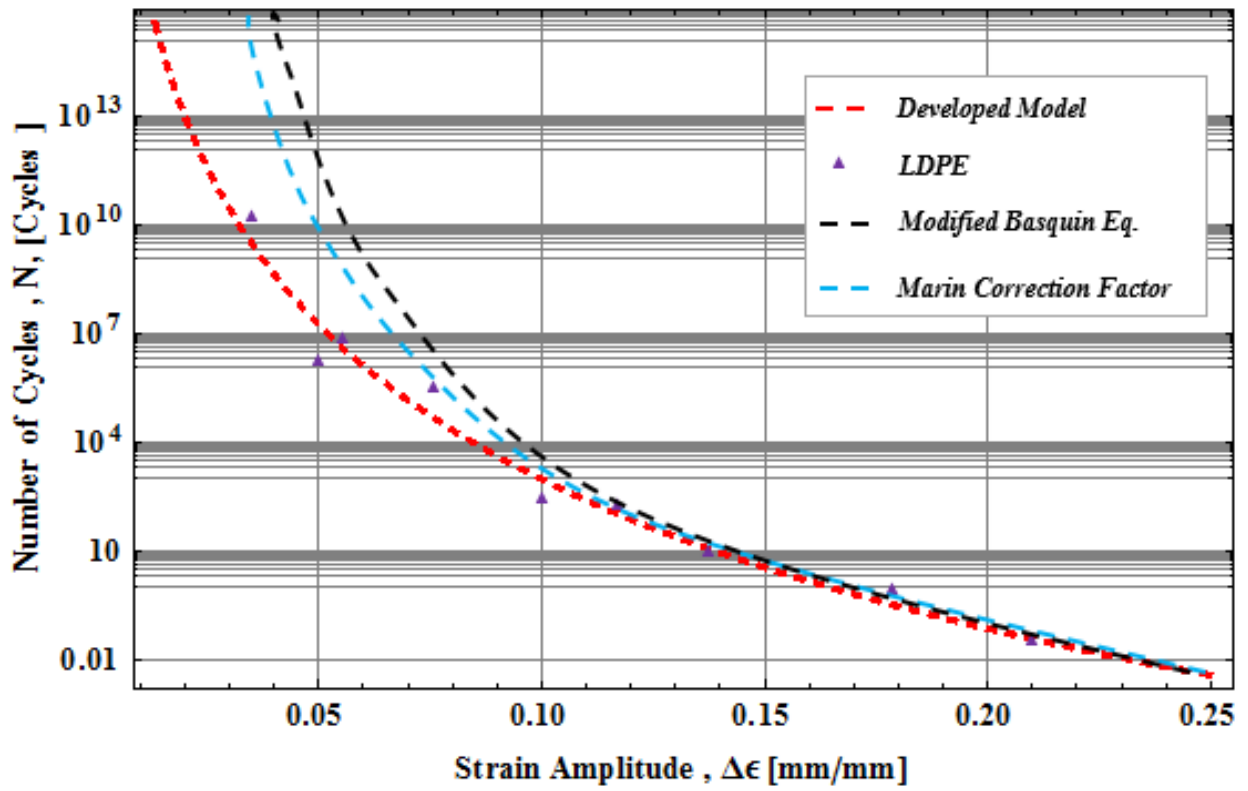
Fig. 5.38: Fatigue Life, N_f versus strain amplitude for LDPE
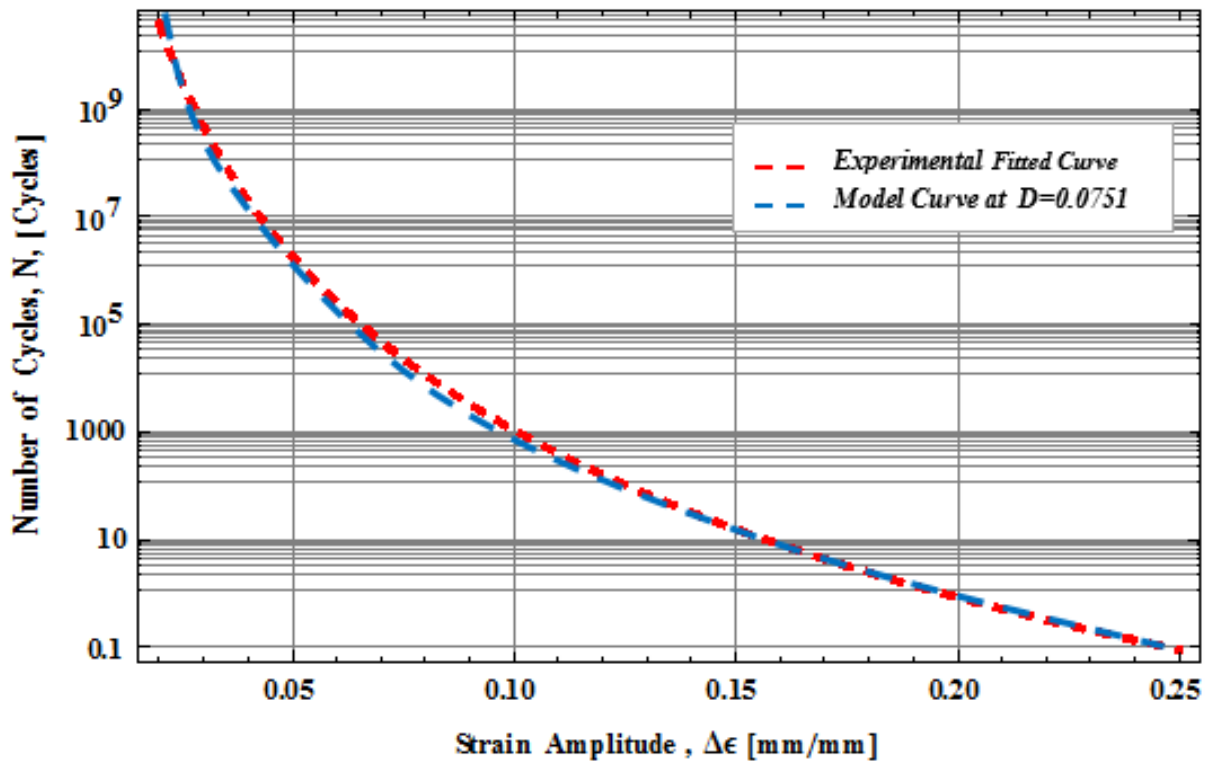
Fig. 5.39: Number of Cycles, N versus strain amplitude for Critical Damage Parameter and Experimental Fitted Curve for LDPP
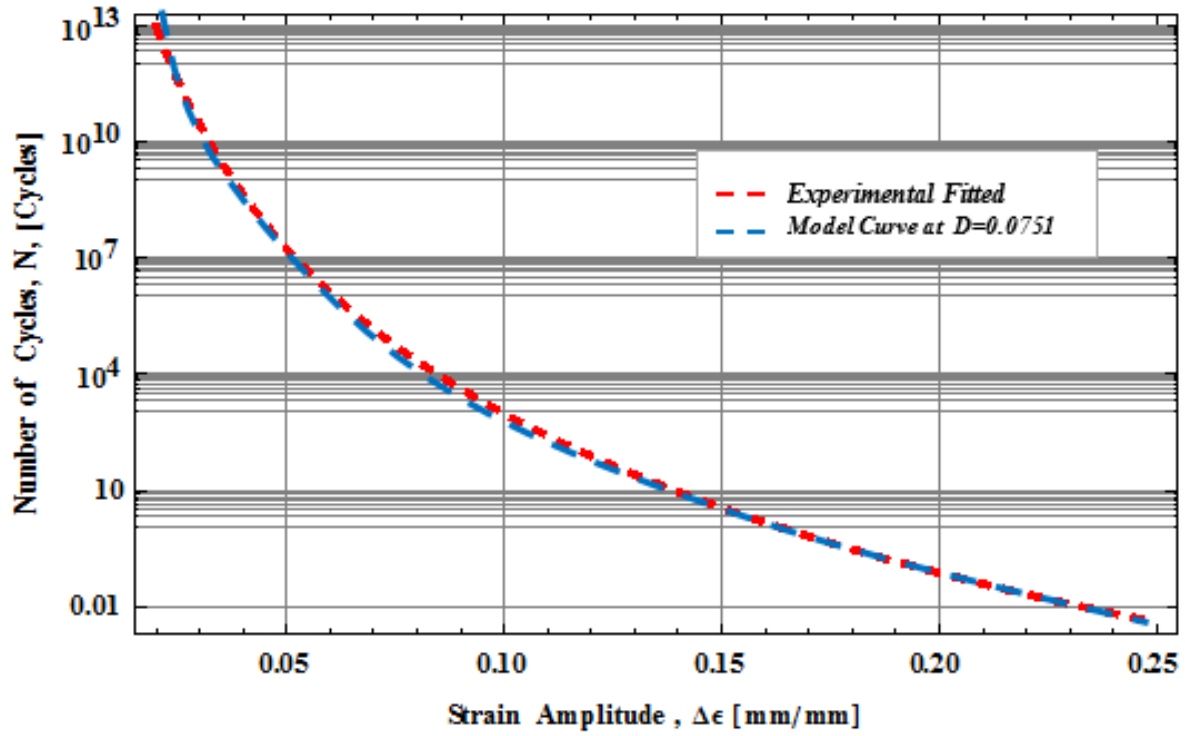
Fig. 5.40: Number of Cycles, N versus strain amplitude for Critical Damage Parameter and Experimental Fitted Curve for LDPE

5.5   Impact – Contact Analysis Results

The impact-contact analysis of the Flex-Run is illustrated with an example problem where the goal is to determine the effects of impact force and contact time on the responses of an impacting Flex-Run. For the finite element approximation of the above formulations we used 4-node isoperimetric elements. The entire mechanism geometry and the target surface were built as adequate. The essential and natural boundary conditions were stated for both the target and the contactor. The target is fixed while the contactor is impacting on the fixed target. The impact force and the contact time is varied in order to determine their influences on the responses of the Flex-Run. Fig. 5.41 is the deformed Flex-Run on impact with the target surface. The Flex-Run material is carbon-fibre-reinforced polymer with average density of 1740 kg/m^3 and Young's modulus of 72 GPa while the target surface is idealized as turf made from medium density polypropylene with average density of 980 kg/m^3 and Young's modulus of 1.8 GPa. The thickness of the turf is 10 mm.
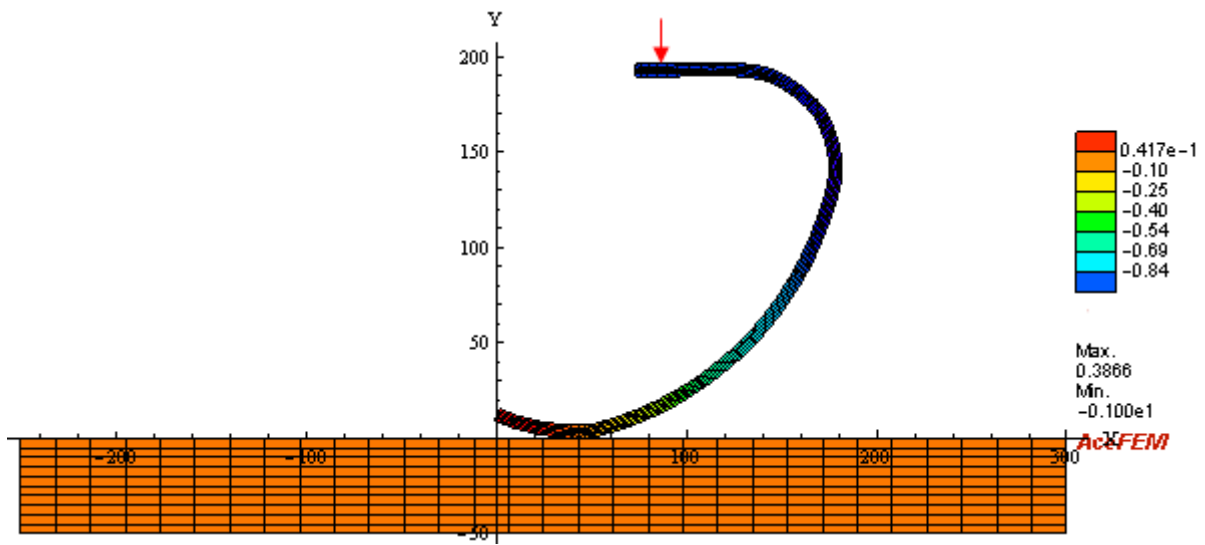
Fig. 5.41: Deformed Flex-Run on impact

5.5.1 Dynamic Response Characteristics

Figs. 5.42, 5.43 and 5.44 illustrate the time histories of the effective stress, the impact force and the effective strain of the Flex-Run, respectively. Results reveal that Fig. 5.42 exhibits linear stress variation between 0.20 s and 0.30s contact time before stabilizing to a constant stress value of 148 MPa after 0.40s.
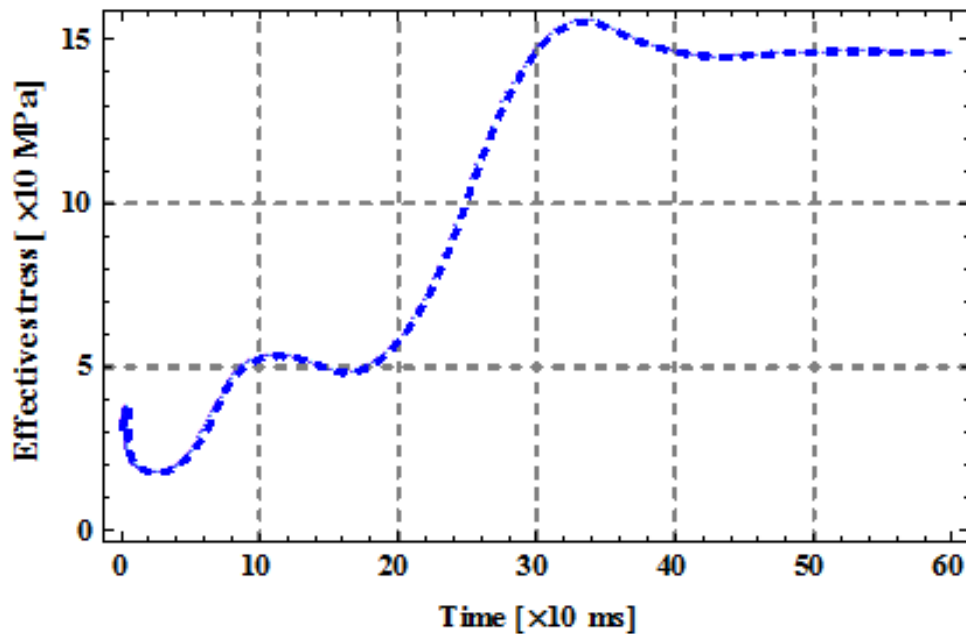
Fig. 5.42: Effective stress of the flex-run against the contact time

In Fig. 5.43, there is an impulsive effect of about 0.1s at the initial time, after which force increases linearly with time in stages. Fig. 5.44 shows linear strain variation between 0.025s and 0.14s contact time after which there is a constant strain value of 0.202mm/mm, forming a shifted signal.
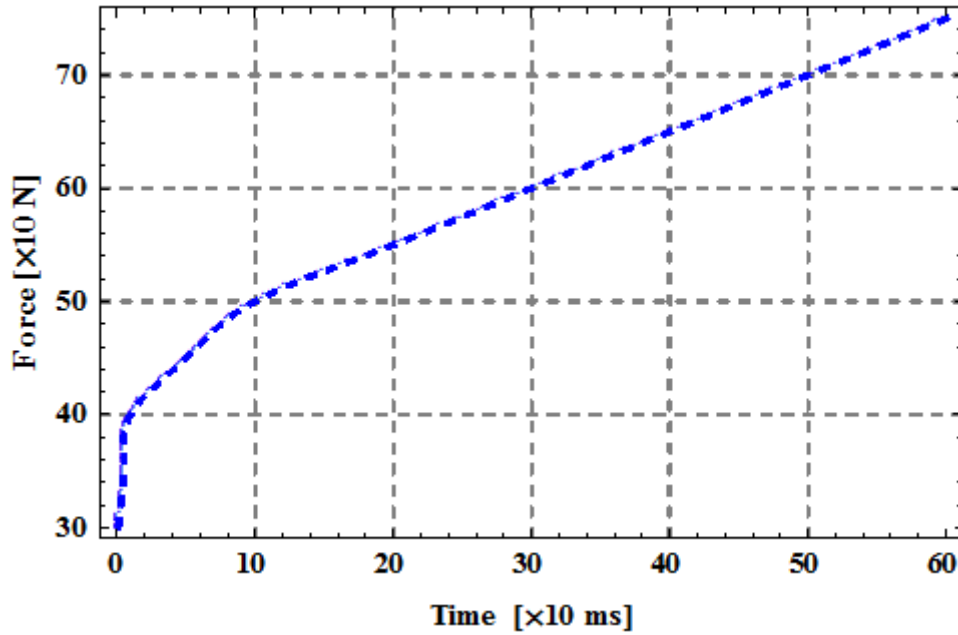
Fig. 5.43: Impacting force of the flex-run against the contact time
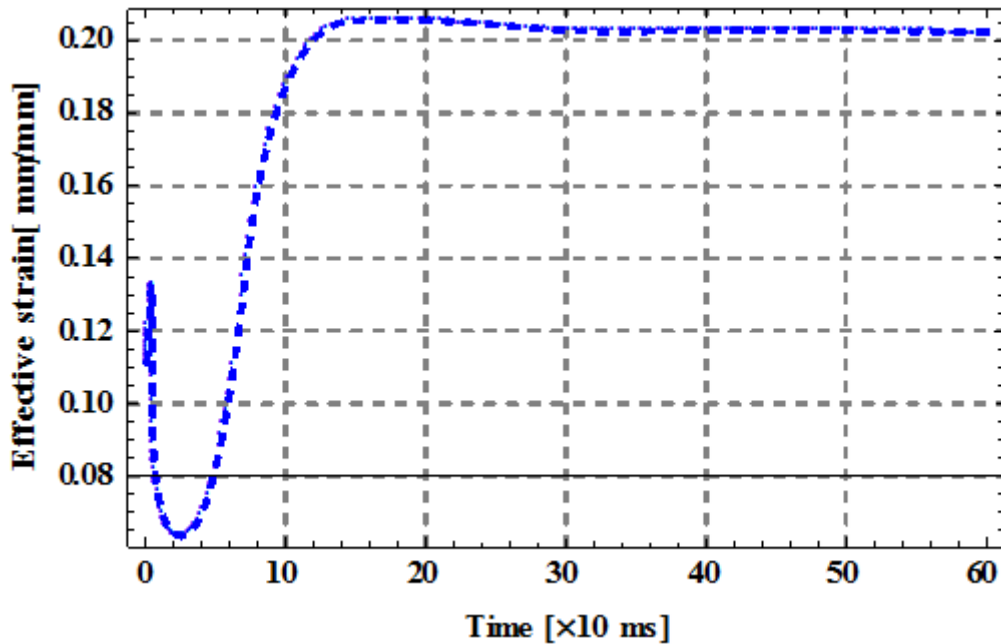
Fig. 5.44: Effective strain of the flex-run against the contact time

Figs. 5.45, 5.46 and 5.47 illustrate the effect of impact force on the effective stress, the impact force and the effective strain of the Flex-Run respectively. Fig. 5.45, shows that the effective stress has an irregular increase before stabilizing to a constant stress value of 145MPa after 0.62 impact force. In Fig. 5.46, the normalized displacement showed a Sigmund formation before stabilizing to a constant displacement value of 0.386 after 0.62kN impact force. Fig. 5.47 reveals that there is a Sigmund formation that adjusted to step signal after 0.52kN impact force.
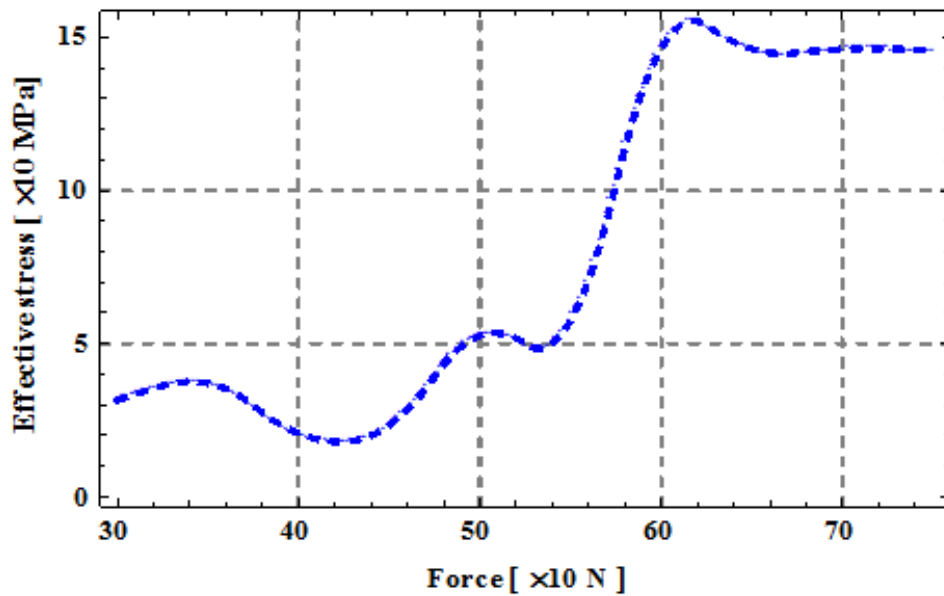
Fig. 5.45: Effective stress of the flex-run against the impacting force
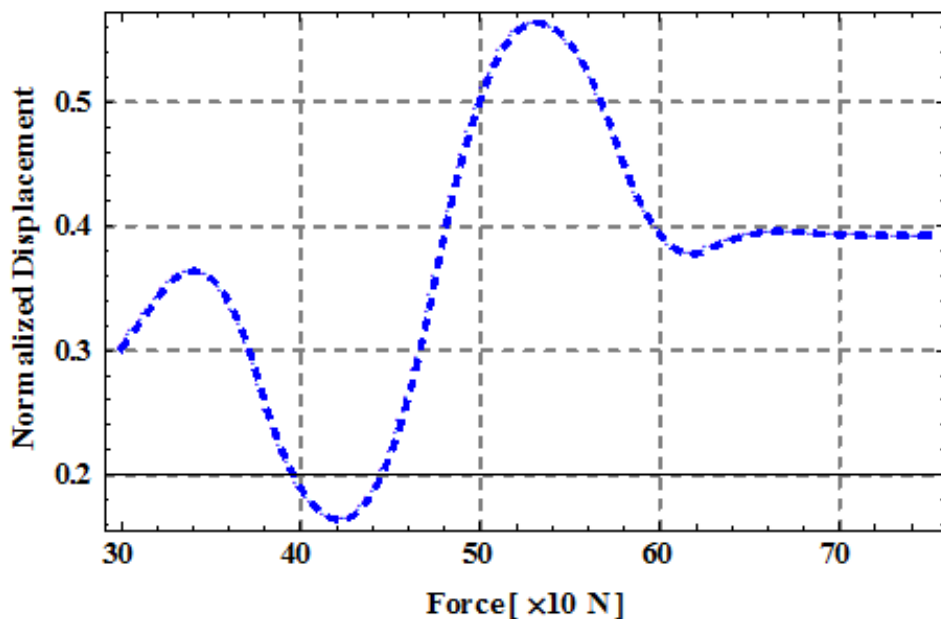
Fig. 5.46: Normalized displacement of the flex-run against the impacting force
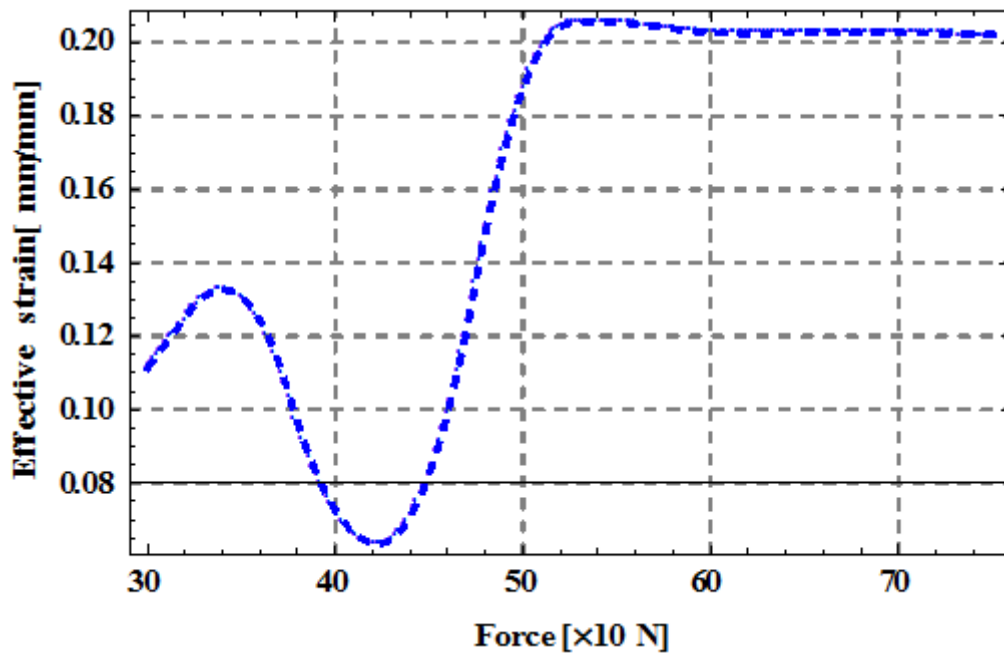
Fig. 5.47: Effective strain of the flex-run against the impacting force

5.5.2 Combined effect of impact force and contact time

Fig. 5.48, 5.49 and 5.50 illustrate the combined effect of impact force and contact time on the displacement characteristics, the strain and stress behaviour of the impacting Flex-Run.
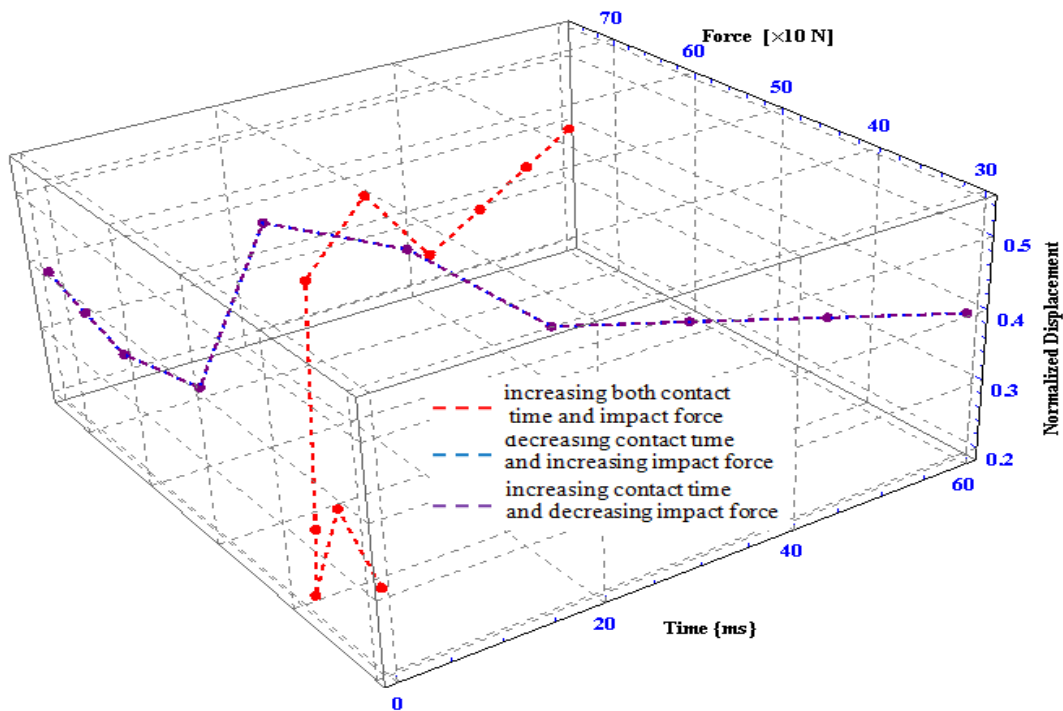
Fig. 5.48: Displacement behaviour with contact time and force

155
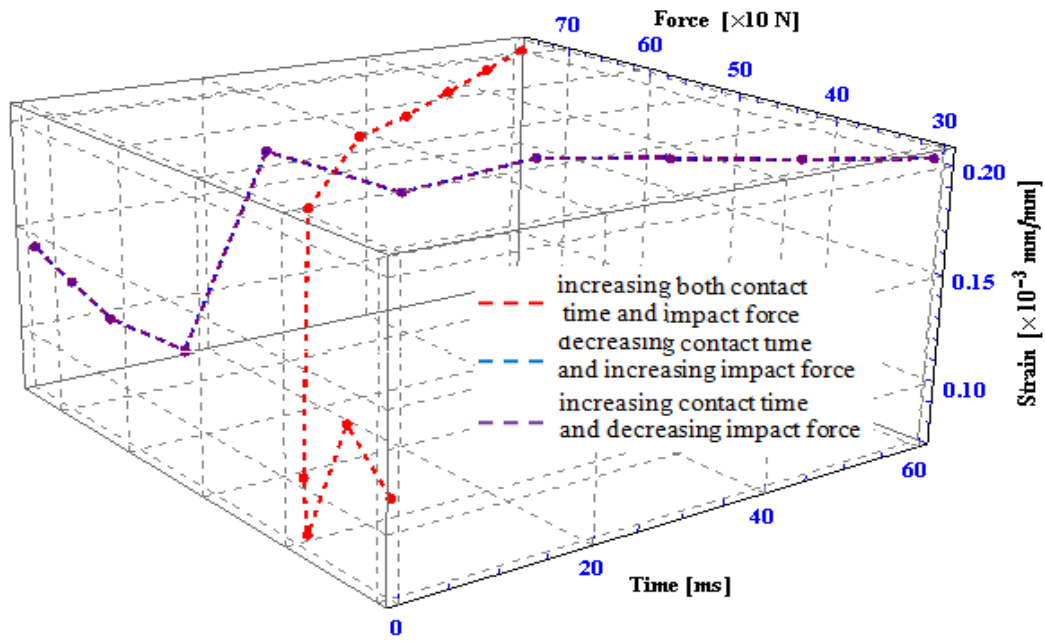
Fig. 5.49: Strain behaviour with contact time and force
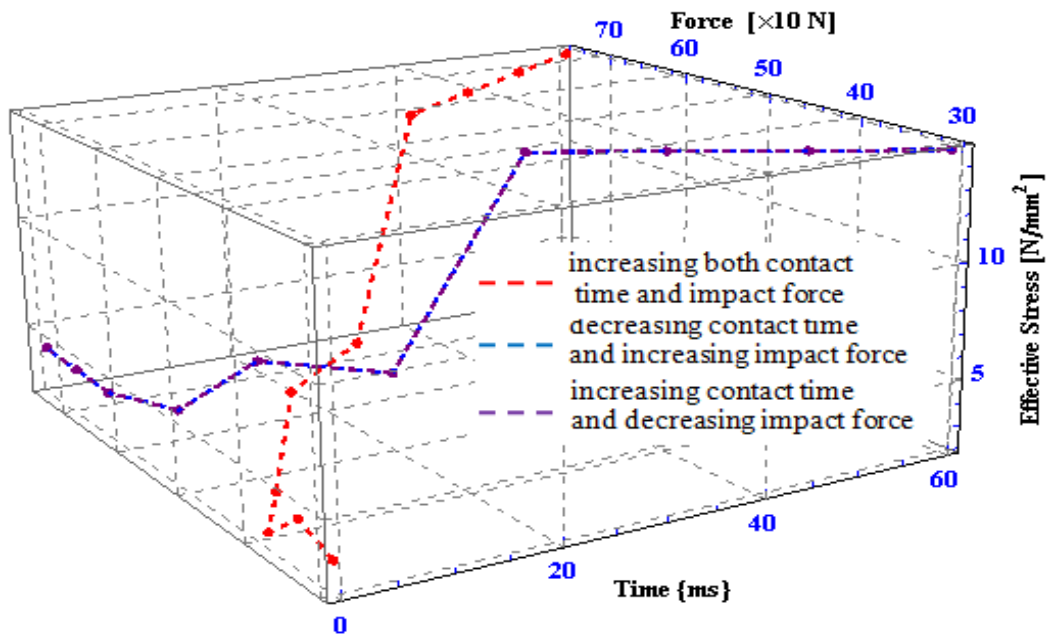
Fig. 5.50: Stress behaviour with contact time and force

Results reveal that increasing both the impact force and contact time showed an initial waveform and then increases to a peak value before decreasing to a constant value of the displacement. Increasing contact time and decreasing impact force showed the same response pattern as the former except that there is an initial decrease in displacement. Decreasing contact

time and increasing impact force showed the reverse behaviour of increasing impact time and decreasing force.

Results also reveal that increasing both the impact force and contact time initially increased the strain and effective stress, and decreased thereafter before steeply increasing up to a constant peak values. Increasing contact time and decreasing impact force showed a waveform pattern before finally increasing up to a constant peak value of the effective strain and effective stress. The reverse of the graph behaviour is seen when decreasing impact time and increasing force.

5.6   Impact Analysis with LS DYNA

The modelling of the Flex-Run was carried out in Solid Edge ST 5, imported into LS PrePost and automatically meshed while LS DYNA performed the solution. The Flex-Run material is carbon-fibre-reinforced polymer with average density of $1740\ kg/m^3$ and Young's modulus of $72\ GPa$ while the target surface is idealized as turf made from medium density polypropylene with average density of 980 kg/m^3 and Young's modulus of $1.8\ GPa$. In the implementation of the material properties, the Ogden model was used. Poisson ratio v and Ogden exponents α_p values of 0.4995 and 2 were used which reduces the Ogden model to the nearly incompressible hyperelastic model when the summation limit $n = 1$. The entire finite element model was built with the necessary boundary conditions. The kinetic energy, strain, stress and displacement histories as well as the resultant velocity response characteristics of the Flex-Run were shown at different impacting velocities.

From the simulation results in Fig. 5.51, it was found that the effective strain shows a shifted step response, stabilizing to different constant strain values at different impacting velocities.
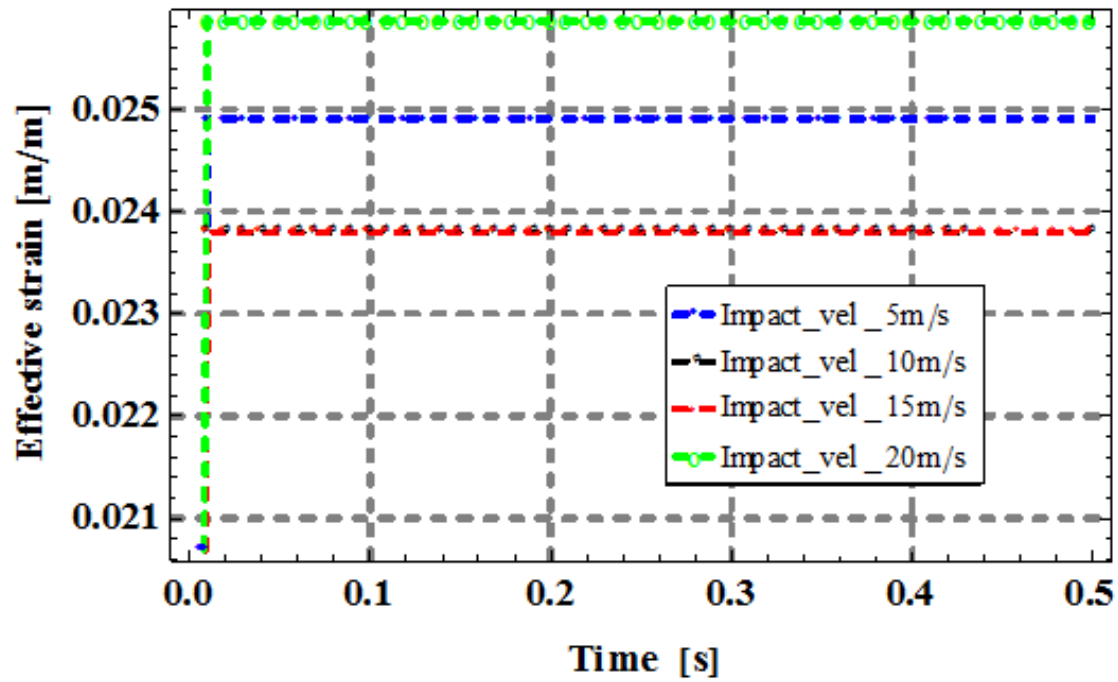
Fig. 5.51: Effective strain response of the Flex-Run at different impacting velocities

The minimum stability point is at 10 m/s and 15 m/s impacting velocities while the maximum point is at 20 m/s impacting velocity. The middle value lies when the impacting velocity is 5 m/s. This displays a non-proportionality relation of the impacting velocity with effective strain.
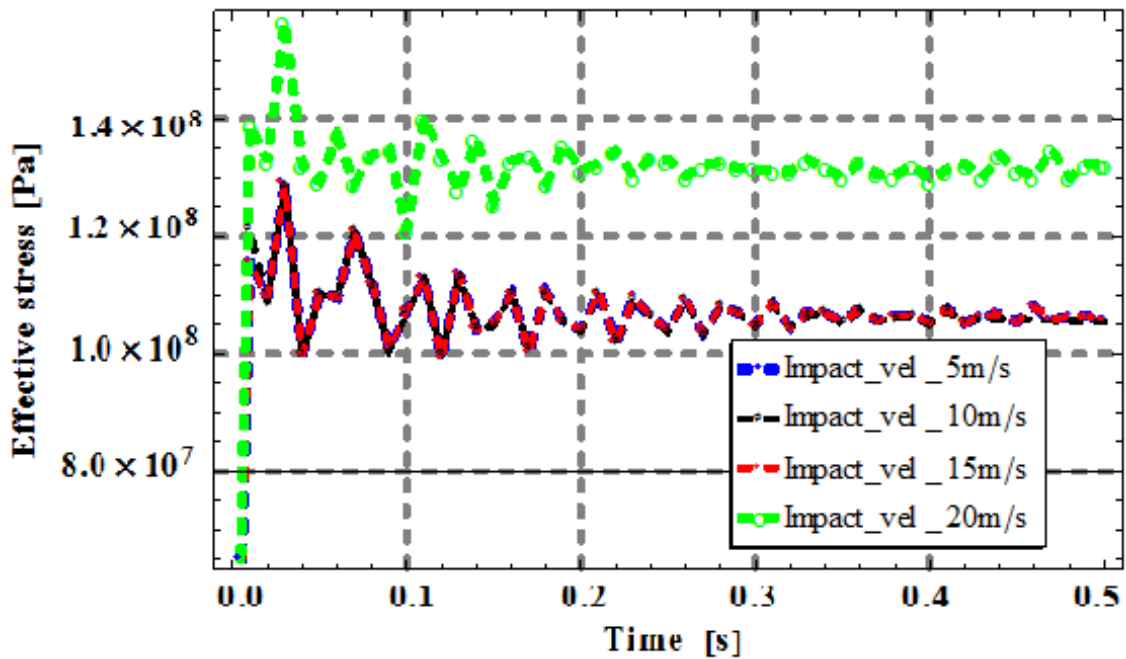
Fig. 5.52: Effective stress responses of the Flex-Run at different impacting velocities

The responses of the effective stress in Fig. 5.52 show an exponentially increasing triangular waveform observable within a time range. The same behaviour is observable for 5 m/s, 10 m/s and 15 m/s impacting velocities while the 20 m/s impacting velocity shows a higher stress level.

The kinetic energy responses in Fig. 5.53 for the different impacting velocities show a step function. The same behaviour is observable for all impacting velocities except for 10 m/s where the kinetic energy has a lower constant value.
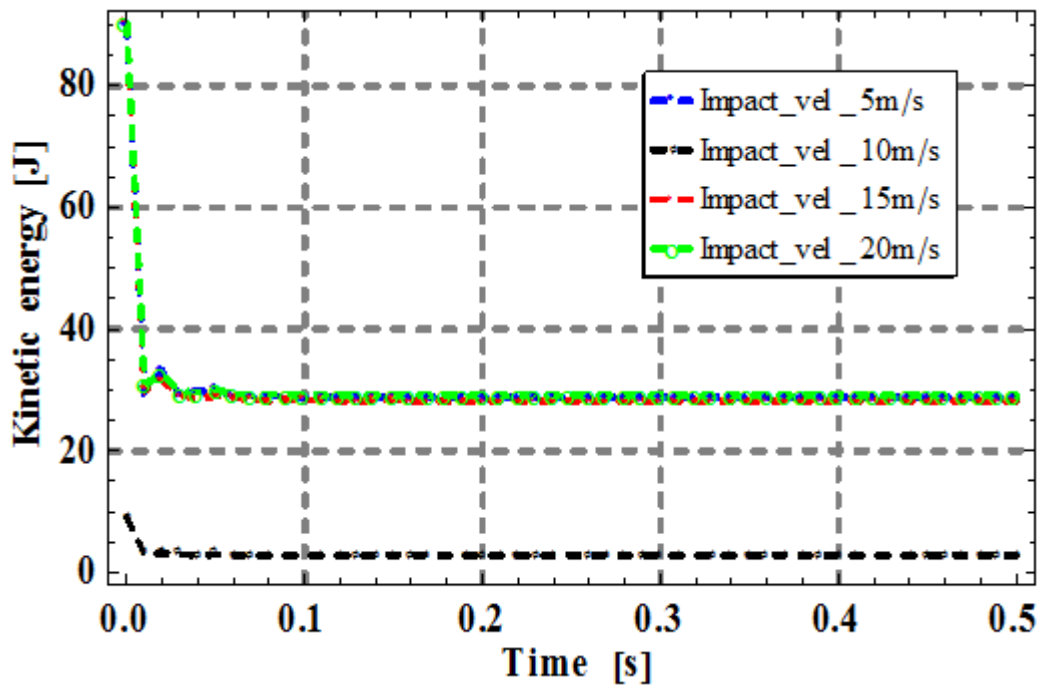
Fig. 5.53: Kinetic Energy responses of the Flex-Run at different impacting velocities

By comparing the displacement time histories between the transient analysis results using the different impacting velocities in Fig. 5.54, an exponentially increasing triangular waveform was found.
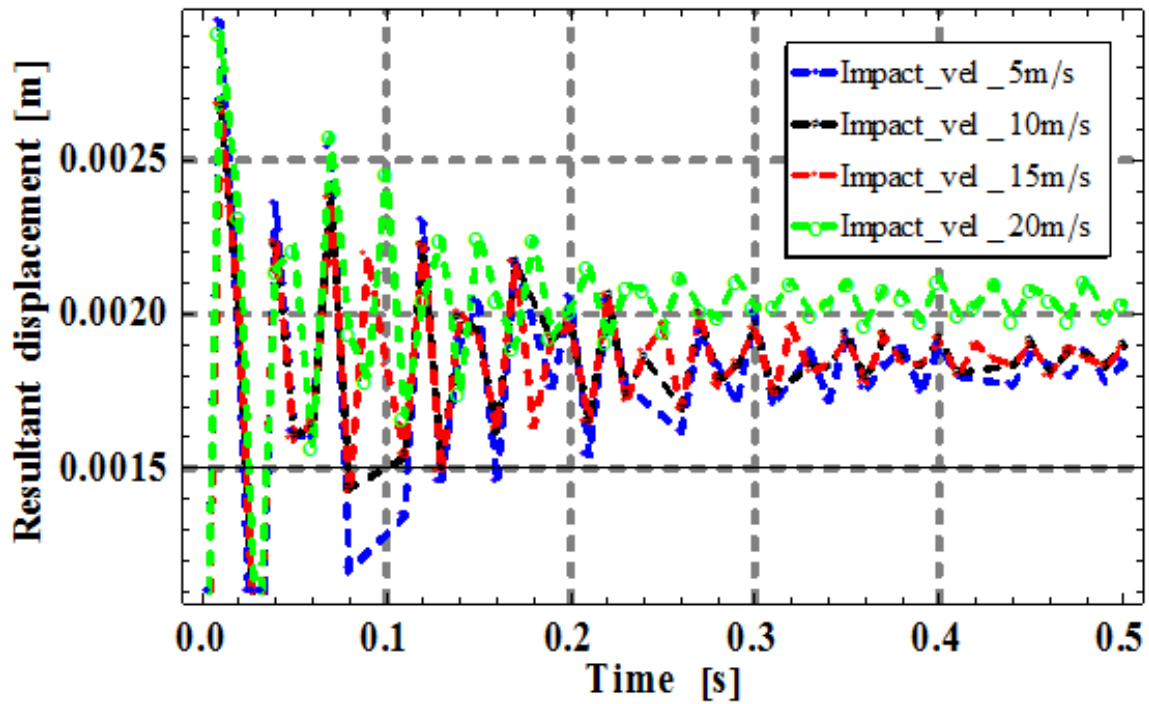
Fig. 5.54: Resultant displacement responses of the Flex-Run at different impacting velocities

5.7 Computational Algorithm

5.7.1 AceGEN Procedure

AceGen procedure for generating code to work in finite element environment consists of several steps:

Step 1 – Initialization

▪ Read of AceGEN code generator

   $<<$*"AceGEN";*

▪ Select the working environment

SMSInitialize ["CompliantMechanism",
"Environment" → "AceFEM"]

▪ Select the type of finite element (Q1- 2D four node finite element)

   SMSTemplate["SMSTopology" →"Q1",
   "SMSSymmetricTangent" → True]

160

Step 2 – Definition of user subroutine

SMSStandardModule["Tangent and residual"];

- Definition of input-output variables

- Kinematics of the selected type of finite element

- Definition of test function

- Definition of governing equations

- Definition of Jacobian matrix

- Definition of stiffness matrix

Step 3 – Definition of output variables using subroutine for postprocessing

SMSStandardModule["Postprocessing"];

Step 4 – Generation of code

SMSWrite[];

5.7.2   AceFEM Procedure

Standard AceFEM procedure consists two basic phase.

1. Phase Data Entry

- phase starts with *SMTInputData[]*

- description of the material model of finite element (*SMTAddDomain*) defined by code

  which must be generated before analysis

- mesh generating

  InputData,SMTAddElement

- setting boundary conditions

  SMTAddEssentialBoundary

- setting loads

  SMTAddNaturalBoundary

2. Phase analysis

- phase starts with *SMT Analysis*

- solution procedures are executed by the user enters inputs (*SMTConvergence*)

- solving problem by standard Newton-Raphson iterative method

- postprocessing of results as part of analysis

SMTShowMesh or later independently of the analysis *SMTPut*

6

CHAPTER 6: SUMMARY OF FINDINGS, CONCLUSION, CONTRIBUTION TO KNOWLEDGE AND FUTURE WORK

6.1   Summary of Findings

The deformation analysis of a continuum compliant mechanisms has been presented.

The summary of findings is hereby presented.

Table 6.1:   Summary of Findings

Objectives	Findings
1) To develop a model that can adequately capture the effect of geometric and material nonlinearities to the analysis of CMs.	The model that can be used to analyze the finite deformation behaviour and characteristics of CMs has been developed.
2) To investigate the combined effect of geometric and material nonlinearities in the analysis of CM.	i) It was established that the hyperelasticity model is correct more than 95% confidence level with the experimental results. ii) It was established that geometric nonlinear or even linear assumptions could capture the

	output displacement of CM when the input load or displacement is 20% of the total input. iii) It was established that the stress history did not give tolerance for either linear or geometric nonlinear assumptions. iv) End point effect in the dynamic analysis of CM show that neglecting material nonlinearity could lead to failure.
3) To investigate the influence of shear deformation in the nonlinear analysis of CMs	It was established that after 50% of the maximum input force, neglecting the effect of shear stress will lead to incorrect and misleading results when the deflection of CM is large.
4) To develop a mathematical model for the fatigue failure prediction of polymeric CMs at any strain cycle.	i) It was established that linear constitutive assumption is inappropriate for polymeric CMs. ii) It was established that for strain amplitude lower than 0.100mm/mm, the developed model is more appropriate to predict the fatigue life of polymeric CMs than other models. iii) It was established that the critical value of the micorcracks and microvoids of a polymeric compliant material start at 7.51% of the initial cross sectional area.

6.2   Conclusion

New methodologies for the analysis and fatigue failure prediction of compliant mechanisms has been presented. The study has shown that the choice of either linear or geometric nonlinear analysis is reliable to a certain extent in the deformation behaviour of compliant mechanisms. While geometric nonlinear or even linear model could capture the CM deformation behaviour when input load or displacement is relatively small, results obtained have shown that for large input load or displacement, the only reliable result is that from hyperelasticity. To avoid catastrophic failure of CMs, especially in mission critical systems, a proper understanding of the deformation behaviour is necessary. The results of this work will help the developers of CMs to incorporate appropriate sensor based indicators capable of predicting the accurate deformation limits and fatigue life which can guide the users of such systems to understand the deformation and fatigue behaviour of the compliant mechanism.

6.3   Contributions to Knowledge

The research work has made some significant contributions in computational mechanics and compliant systems.

i)   This study developed a model that can be used for both dynamic and static analyses of CMs with geometric and material nonlinear behaviour.

ii) This work established the threshold input displacement for geometric nonlinear and linear deformation assumptions for CMs undergoing finite deformation and the onset of shear deformation for CMs undergoing large deflection.

iii) This study developed an improved model for fatigue life prediction of polymeric continuum CMs.

iv) This study established the critical value of the damage variable for polymeric continuum compliant material.

6.4   Recommendation

Some recommendations for further improving the computational models are summarized as follows:

- The fatigue and deformation behaviour of compliant materials with changes in weather and environmental conditions need to be investigated.

- The model should be extended to compliant polymeric materials that undergo viscous response using viscoelastic models.

- There is need to model compliant mechanisms that undergo plastic deformation using elastoplastic models.

REFERENCES

Adeleye, O. A. and Fakinlede, O. A. (2010). "Symbolic Analysis of Heat Transfer in Radial Fin". *Journal of Engineering Research, University of Lagos.* **15(2):** 1-10.

Akshantala, N. V. and Talreja, R. (2000). "A Micromechanics Based Model for Predicting Fatigue Life of Composite Laminates". *Materials Science and Engineering.* **285:** 303–313.

Ali, A., Hosseini, M., and Sahari, B. (2010). "Continuum Damage Mechanics Modeling for Fatigue Life of Elastomeric Materials". *International Journal of Structural Integrity.* **1(1):** 63 – 72.

Allaire, G. and Castro, C. (2002). "Optimisation of nuclear fuel reloading by the homogenization". *Struct. Multidisc. Optim.* **24:** 11-22.

Alnæs, M. S. and Mardal, K. A. (2010). "On the Efficiency of Symbolic Computations Combined with Code Generation for Finite Element Methods". *ACM Transactions on Mathematical Software.* **37 (8):** 1-26.

Alnæs, M. S., Mardal, K. A. and Sundnes, J. (2007). "Application of symbolic finite element tools to nonlinear hyperelasticity", Fourth national conference on Computational Mechanics (MekIT'07), ed. by B. Skallerud and H.I. Andersson. NO-7005 Trondheim, Tapir Academic Press (ISBN: 978-82-519-2235-7). 87-101.

Alur, R., Madhusudan, P. and Nam, W. (2005). "Symbolic computational techniques for solving games". *International Journal on Software Tools for Technology Transfer (STTT).* DOI: 10.1007/s10009-004-0179-0. **7(2):** 118-128.

Ananthasuresh, G. K. (2003). "Single piece compliant stapler". *http://www-mtl.mit.edu/~suresh/ stapler*

Ananthasuresh, G. K. and Frecker, M. (2001). ''Optimal synthesis with continuum models'',Compliant Mechanisms. *John Wiley, New York.* 301-335.

Ananthasuresh, G. K., Kota, S. and Gianchandani, Y. (1994). "A methodical approach to the synthesis of micro-compliant mechanisms". *Tech. Digest, Solid-State Sensor and Actuator Workshop (held on Hilton Head Island, SC).* 189-192.

Ansola, R., Canales, J., Tarrago, J. A. and Rasmussen, J. (2002). "On simultaneous shape and material layout optimisation of shell structures". *Struct. Multidisc. Optim.* **24:** 175-184.

ANSYS Release Documentation. (2012).

http://www.kxcad.net/ansys/ANSYS/ansyshelp/thy_mat5.html.

Ari, N., Ashirov, T., Usonbek, J. (2005). **"**Symbolic Computation Techniques Using Maple". University of Applied Sciences Zurich Switzerland Technoparkstr. 1, CH-8005 Zurich, Switzerland.

Aten, Q. T., Jensen, B. D., and Howell, L. L. (2012). "Geometrically non-linear analysis of thin-film compliant MEMS via shell and solid elements" *Finite Elements in Analysis and Design* **49:** 70–77.

Barghout, J., (2003). "Description of compliant cable technology". *http://nasa.rti.org/nasa/gsfc/*

Bonet, J., Wood R. D. (1997). "Nonlinear Continuum Mechanics for Finite Element Analysis". *Cambridge University Press.*

Borhan, H. and Ahmadian, M. T. (2006). "Dynamic modeling of geometrically nonlinear electrostatically actuated microbeams (Corotational finite element formulation and analysis)" *Journal of Physics: International MEMS Conference.* DOI:10.1088/1742-6596/34/1/100. **34:** 606–613..

Borrvall, T. and Petersson, J. (2001). "Topology optimisation using relularized intermediate density control". *Comput.. Methods Appl. Mech. Engrg*., **190:** 4911-4928.

Bower A. F. (2010). "Applied Mechanics of Solids". *CRC Press*.

Boyle, C., Howell, L. L. and Magleby S. P. (2003). "Dynamic modeling of compliant constant-force compression mechanisms". *Mechanism and Machine Theory*. **38:** 1469-1487.

Bruns, T. E. and Tortorelli, D. A. (2001). "Topology optimization of nonlinear elastic structures and compliant mechanisms". *Computer Methods and Application in Mechanical Engineering*. **190:** 3443-3459.

Bulman, S., Sienz, J. and Hinton, E. (2001). "Comparisons between algorithms for structural topology optimisation using a series of benchmark studies". *Computers & Structures*. **79:** 1203-1218.

Canfield, S. and Frecker, M. (2000). "Topology optimisation of compliant mechanical amplifiers for piezoelectric actuators". *Struct. Multidisc. Optimum.* **20:** 269-279.

Cannon, B. R., Lillian, T. D., Magleby, S. P., Howell, L. L. and Linford, M. R. (2005). "A Compliant End-Effector for Microscribing", *Precision Engineering*. **29:** 86–94.

Chao-Chieh L. (2005). "Computational Models for Design and Analysis of Compliant Mechanisms". *Ph D Thesis 2005. Georgia Institute of Technology.*

Chen, L. (2001). "Microfabrication of heterogeneous, optimized compliant mechanisms". *NSF Summer Undergraduate Fellowship in Sensor Technologies (SUNFEST 2001), University of Rochester, Advisor, G.K. Ananthasuresh.*

Criscione, J. C. (2002). "Direct tensor expression for natural strain and fast, accurate approximation". *Computer ans Strctures*. **80(25):** 1895 – 1905.

Cullinan, M., DiBiasio C., Howell, L. L., Culpepper, M. and Panas, R. (2007). "Modeling of a clamped-clamped carbon nanotube flexural element for use in nanoelectromechanical systems," *13th National Conference on Mechanisms and Machines (NaCoMM07), IISc, Bangalore, India*. NaCoMM-2007-103.

Demirel, B., Emirler, M. T., Sönmez, Ü. and Yörükoğlu, A. (2010). "Semicompliant Force Generator Mechanism Design for a Required Impact and Contact Forces". *Journal of Mechanisms and Robotics, ASME. 2:*

Dinesh, M. and Ananthasuresh, G. K. (2007). "A Topology-Optimized Large-Range Compliant X-Y Micro Stage". *13th National Conference on Mechanisms and Machines (NaCoMM07), IISc, Bangalore, India*. NaCoMM-2007-109.

Edinger, B., Frecker, M. and Gardner, J. (2000). "Dynamic modeling of an innovative piezoelectric actuator for minimally invasive surgery". *J. Intelligent Material Systems and Structures.* **11:** 765-770.

Erdman, A.G. and Sandor, G.N. (1991). "Mechanisms Design: Analysis and Synthesis". *Prentice Hall, Englewood Cliffs, New Delhi.*

Eyheramendy, D. and Zimmermann, T. (1999). "Object-oriented symbolic derivation and automatic programming of finite elements in mechanics'. *Engineering with Computers*, **15(1):** 12-36.

Farahani, K., Mofid, M. and Vafai, A. (2000). "A solution method for general contact-impact problems, Comput". *Methods Appl. Mech. Engrg.* **187:** 69-77

Fern, N., Alam , P., Touaiti, F. and Toivakka, M. (2012) "Fatigue life predictions of porous composite paper coatings", *International Journal of Fatigue*. **38:** 181–187.

Flores, P., Ambrósio, J., Claro, J. C. P. and Lankarani, H.M. (2008). "Contact-Impact Force Models for   Mechanical Systems": in Kinematics and Dynamics of Multibody Systems with Imperfect Joints, *Lecture Notes in Applied and Computational Mechanics*. **34:** 47-66.

Frecker, M. I., (1997). "Optimal design of compliant mechanisms". *Ph. D. Thesis, Mechanical Engineering in the University of Michigan.*

Frecker M. I., Ananthasuresh G. K., Nishiwaki S., Kikuchi N., and Kota S., (1997). "Topological synthesis of compliant mechanisms using multi-criteria optimization," *Journal of Mechanical Design*. **19(2):** 238–245.

Frecker, M. and Canfield, S. (2000). "Optimal design and experimental validation of compliant mechanical amplifiers for piezoceramic stack actuators". *Journal of Intelligent Material Systems and Structures.* **11:** 360-369.

Frecker, M. I. and Dziedzic, R. (2001). "Design of multifunctional compliant mechanisms for minimally invasive surgery". *In: Proc. ASME DETC: Design automation conference symposium on mechanisms and devices for medical applications.* DETC01/DAC-21055

Frecker, M. I., Kota, S. and Kikuchi, N. (1999). "Topology optimisation of compliant mechanisms with multiple outputs." *Struct. Optim.* **17:** 269-278.

Freed, A. D., (1995). "Natural Strain". *J. Eng. Mater. Technol.* **117:** 379-385.

Funchs, M.B. and Moses, E. (2000). "Optimal structural topologies with transmissible loads". *Struct. Multidisc. Optim.* **19:** 263-273.

Gong, X. Y. and Moe, R. (2002). "On stress analysis for a hyperelastic material". *ANSYS Conference.*

Griewank, A. (2000). "Evaluating Derivatives: Principles and Techniques of Algorithmic Differentiation". *Philadelphia, PA: SIAM*.

Gurung K., Freere P. (2007). "Matlab symbolic computation for the steady state modeling of symmetrically loaded self excited induction generator". *Kathmandu University Journal of Science, Engineering and Technology*. **1(3):**

Haslach, H. W. and Armstrong, R. W. (2004). *"*Deformable Bodies and Their Material Behavior". *Wiley, New York*.

Holzapfel, G. A. (2000). "Nonlinear Solid Mechanics - A Continuum Approach for Engineering". *John Wiley & Son, Chichester*.

Howell, L.L. (2001). "Compliant Mechanisms". *John Wiley & Sons, Inc. United States of America.*

Howell, L.L., (2003). "Pseudo-rigid-body models and compliant mechanisms". *http://research.et. byu.edu/llhwww*

Howell, L.L., (2003). "Over-running clutch". *http://research.et.byu.edu/llhwww/*

Howell, L.L. (2003). "Introduction to bistable compliant mechanisms". *http://research.et.byu.edu/ llhwww/*

Howell, L.L. and Midha, A., (1996). "A Loop-Closure Theory for the Analysis and Synthesis of Compliant Mechanisms". *Journal of Mechanical Design*, **118(1):** 121-125.

Howell, L. L., Rao, S. S. and Midha, A. (1994). "Reliability-Based Optimal Design of a Bistable Compliant Mechanism*". Journal of Mechine Design.* **116 (4):** 1115-1122.

Huang, T. J., Brough, B., Ho, C. M., Liu, Y., Flood, A. H., Bonvallet, P. A., Tseng, H.-R., Stoddart, J. F., Baller, M., and Magonov, S., (2004), *"*A Nanomechanical

Device Based on Linear Molecular Motors," *Applied Physics Letters*. **85(22):** 5391-5393.

Huet G. (2003). "Linear contexts and the sharing functor: Techniques for symbolic computation". *In Workshop on Thirty Five Years of Automath.*

Jiang, M. (1995). "A Damaged Evolution Model for Strain Fatigue of Ductile Metals". *Engineering Fracture Mechanics.* **52(6):** 971-975.

Jiang Y. and Wang C. (2008). "On Teaching Finite Element Method in Plasticity with Mathematica". *Computer Applications in Engineering Education.* **16(3):** 233–242.

Jinqing, Z. and Xianmin, Z. (2011) "Topology optimization of compliant mechanisms with geometrical nonlinearities using the ground structure approach". *Chinese Journal of Mechanical Engineering*. **24:**

Joo, J., Kota, S. K. and Kikuchi, N. (2001). "Large deformation behavior of compliant mechanisms". *Proceedings of DETC'01 ASME 2001 Design Engineering Technical Conference and Computers and Information in Engineering Conference Pittsburgh, PA, September 9-12.*

Jorge, E. C. P. (2010). "Force-Displacement Model of Planar Compliant Mechanisms Based On Assur Groups Decomposition" *Project. Eafit University, School of Engineering Mechanical Engineering Department, Medellin.*

Jung, D. and Gea, H. C. (2002). "Compliant mechanism design with non-linear materials using topology optimization," *Proceedings of the 2002 ASME Design Engineering Technical Conferences, Montreal, Canada.* DETC2002/DAC-34150.

Jung, D. and Gea, H. C. (2004). "Topology optimization of nonlinear structures," *Finite Elements in Analysis and Design.* **40:** 1417–1427.

Jutte, C. V. (2008). "Generalized Synthesis Methodology Of Nonlinear Springs For Prescribed Load-Displacement Functions". *Ph D Thesis. The University of Michigan.*

Kimball, C. and Tsai, L.W. (2002). "Modeling of flexural beams subjected to arbitrary end loads". *Transaction of ASME: Journal of Mechine Design.* **124:** 223-235.

Korelc, J. (2002). "Multi-language and multi-environment generation of nonlinear finite element codes". *Engineering Computers.* **18:** 312-327.

Korelc, J. (2004). "Symbolic Formulation and Automatic Derivation of Complex Material Model". *Proceedings of Multi-Physics and Multi-Scale Computer Models in Non-Linear Analysis and Optimal Design of Engineering Structures under Extreme Condition. Bled, Slovenia.*

Korelc, J. (2009). "Automation of primal and sensitivity analysis of transient coupled problems". *Computational mechanics*, **44:** 631-649.

Korelc, J. (2010). "Automation of Computational Modeling by Automatic Differentiation". *IV European Conference on Computational Mechanics Palais des Congrès, Paris, France.*

Korelc, J. (2012). "AceGEN and AceFEM user manual". *www.fgg.uni-lj.si/symech/*

Korelc, J. and Kristanič, N. (2005). "Evaluation of design velocity field by direct differentiation of symbolically parameterized mesh, Onate E (ed) Plasticity: fundamentals and applications" *Proceedings of the eighth international conference on on computational plasticity, Swansea, CIMNE, Barcelona, Spain.* 380-383.

Larsen, U.D., O. Sigmund and S. Bouwstra, (1997). "Design and fabrication of compliant micromechanisms and structures with negative poisson's ratio". *J. Microelectromech. Syst.* **6:** 99- 106.

Lee, K. M. (1999). "On the Development of a Compliant Grasping Mechanism for On-line Handling of Live Objects, Part I: Analytical Model". *Int. Conference on Advanced Intelligent Mechatronics Proc. (AIM'99)*. 354-359.

Lee, T. (2009). "A contemporary engineering perspective on symbolic computation". *ICCAS-SICE, 2009*. 978-4-907764-34-0. 2379 – 2384.

Lemaitre, J. (1985). "A Continuum Damage Mechanics Model for Ductile Fracture," *J. of Engg. Mater. and Tech*. **107** 83-89.

Lemaitre, J. and Desmorat, R. (2005). "Engineering Damage Mechanics". *Berlin, Heidelberg, Germany, Springer-Verlag.*

Li, H., Ibrahim, R., and Cheng, K. (2011). "Design and principles of an innovative compliant fast tool servo for precision engineering". *Mechanical Science*, **2:** 139–146.

Li , X., Hristov, H. A., Yee A. and Gidley, D. W. (1995). "Influence of Cyclic Fatigue on the Mechanical Properties of Amorphous Polycarbonate". *Polymer,* **36(4):** 759-765.

Li, Y., Saito, K. and Kikuchi, N. (2002). "Design of heat-actuated compliant mechanism and its application to product-embedded disassembly". *Proc. 5th World Congress on Computational Mechanics (WCCM V), Vienna, Austria.*

Li, Z. and Kota, S. (2002). "Dynamic Analysis of Compliant Mechanisms". *Proceedings of the ASME Design Engineering Technical Conference.* **5:** 43-50.

Linthorne, N. P. (2000), "Energy loss in the pole vault take off and the advantage of flexible pole," *Sports Engineering, Blackwell Science Ltd, March.* 205-218.

Logg, A. (2007). "Automating the Finite Element Method". *Archives of Computational Methods in Engineering.* **14:** 93-138.

Lyon, S.M., Erickson, P.A., and Howell, L.L. (1999). "Prediction of the first modal frequency of compliant mechanisms using the Pseudo Rigid Body Model", *Journal of Mechanical Design Transactions of the ASME*, **121(2):** 309-313.

Lyon, S.M., Evans, M.S., Erickson, P.A. and Howell, L.L. (1997). "Dynamic Response of Compliant Mechanisms Using the Pseudo Rigid Body Model" *Proceedings of the 1997 ASME Design Engineering Technical Conferences*. DETC97/VIB-4177.

Mahmoud, W. E., Mansour, S. A., Hafez, M. and Salam, M. A. 2007. "On the Degradation and Stability of High Abrasion Furnace Black (HAF)/Acrylonitrile Butadiene Rubber (NBR) and High Abrasion Furnace Black (HAF)/Graphite/Acrylonitrile Butadiene Rubber (NBR) Under Cyclic Stress Strain", *Polym. Degrad. Stab*. **92:** 2011-15.

Mankame N. D., Ananthasuresh G. K. (2004). "Topology optimization for synthesis of contact-aided compliant mechanisms using regularized contact modeling". *Computers and Structures.* **82:** 1267–1290.

Mario, C. F., Richard, R. N. and Richard H. C. (2006). "The quasi-static response of compliant prosthetic sockets for transtibial amputees using finite element methods". *Medical Engineering & Physics 28 (2006)* 114–121.

Marvalova, B. (2006). "Application of Comsol Multiphysics 3.2 to finite strain viscoelasticity of an elastomeric solid". *Proceedings of the COMSOL Users Conference* 2006 Prague.

Mary, L. J., (2003). "On campus: Compliant mechanisms make braking news". *http://magazine.byu. edu/bym/2000sum/*

Mase, G. T.,Mase, G.E. (1999). "Continuum Mechanics for Engineers, 2nd Edition, CRC Press, New-York."

Mathisen, K. M.,Okstad, K. M.,Kvamsdal T.,Raknes, S. B. (2011). "Isogeometric analysis of finite deformation nearly incompressible solids". *Journal of Structural Mechanics*. **44(3):** 260 – 278.

Mattern, S., and Schweizerhof, K. (2010), "Software Supported Implementation of Efficient Solid-Shell Finite Elements". *Institute of Mechanics, Kaiserstr*. **12:** 1-16

Mitchell, D., (2003). "Compliant mechanism (Fourdegree of freedom compliant hinge mechanism) (GSC-13922-1)". *http://technology.nasa.gov/scripts/*

Mortensen, C.R., B.L. Weight, L.L. Howell and S.P. Magleby, (2000). "Compliant mechanism prototyping". *Proc. of DETC'00, ASME 2000 Design Engineering Technical Conferences & Computers & Information in Engineering Conference Baltimore, Maryland.*

Ogden*, R. W. (1997). "Non-Linear Elastic Deformations", Dover Publications*, New York.

Ouyang, P. R., Zhang, W. J. and Gupta, N. M. (2008). "A new compliant Amplifier Based on symmetric five-bar topology". *Journal of Mechanical Design, ASME.* **130**/104501-1.

Paláncz B. and Popper G. (2000). "Symbolic solution of boundary value problem via Mathematica". *Periodica polytechnica ser. Civ. Eng.* **44(1):** 89–97.

Papusha, Alexander N., Fedorov Ilya V., Shtrasser Victor V. (2009). "Symbolic Evaluation of Boundary Problems for Offshore Design Technology". *Mathematica Journal (2009)*. **11(1):** 107-128.

Passaglia, E. (1987). "Crazes and fracture in polymers". *J. Phys. Chem. Solids.* **48:** 1075-1100.

Pedersen, C.B.W., T. Buhl and O. Sigmund, (2001). "Topology synthesis of large-displacement compliant mechanisms". *Int. J. Numer. Meth. Engng*. **50:** 2683-2705.

Ping, J. J., Guang, M., Yi, S., and SongBo, X. (2003). "An Effective Continuum Damage Mechanics Model for Creep–Fatigue Life Assessment of a Steam Turbine Rotor", *International Journal of Pressure Vessels and Piping*. **80:** 389–396.

Pomeranz S. (2000). "Using a Computer Algebra System to Teach the Finite Element Method". *Int. J. Engng Ed.* 0949-149X/91. **16(4):** 362-368, 2000.

Rahmatalla, S. and Swan, C. C. (2005). "Sparse monolithic compliant mechanisms using continuum structural topology optimization". *International Journal of Numerical Methods in Engineering*. **62:** 1579–1605.

Rezaei, M., Tayefeh, M. and Bahrami, M. (2006). "Dynamic Behavior Analysis of Compliant Micromechanisms" *Journal of Physics: Conference Series*. **34:** 583–588.

Roach, G.M., (1998). "An investigation of compliant over-running ratchet and pawl clutches". *Thesis, Brigham Young University, Provo, Utah*.

Roach, G.M., S.M. Lyon and L.L. Howell, (1998). "A compliant, overrunning ratchet and pawl clutch with centrifugal throw-out". *Proc. of the 1998 ASME Design Engineering Technical Conf*. DETC98/MECH-5819.

Roach, G.M. and Howell, L.L. (1999). "Evaluation and comparison of alternative compliant overrunning clutch designs". *Proc. of the 1999 ASME Design Engineering Technical Conf.* DETC99/DAC-8619.

Saggere, L., Kota, S., (1997), "Synthesis of Diestributed Compliant Mechanims for Adaptive Structures Application: An Elasto-Kinematic Approach," DETC97/DAC-

3861, *Proceedings of the 1997 ASME Design Engineering Technical Conferences*, *Sacramento, CA.*

Sanders, M. B. (2003). "Novel compliant mechanisms could simplify, improve aircraft". http://www.afosr.af.mil/pdfs/

Saxena, A. and Ananthasuresh. G. K. (1998). "An optimality criteria approach for the topology synthesis of compliant mechanisms". *Proc. Of DETC'98, ASME Design, Engineering Technical Conf. (held in Atlanta, GA)*, DETC'98/MECH5937.

Saxena, A. and Ananthasuresh, G. K. (2000). "On an optimal property of compliant topologies". *Struct. Multidisc. Optim.* **19:** 36-49.

Schutz, W. (1996). "A history of fatigue". *Engineering Fracture Mechanics*. **54(2):** 263–300.

Shi, W., Hu, W., Zhang, M., and Meng, Q. (2011). "A damage mechanics model for fatigue life prediction of fiber reinforced polymer composite lamina" *Acta Mechanica Solida Sinica*. ISSN0894-9166. **24(5):**

Shuib, S., Yusoff, R., Hassan, A. Y., Ridzwan, M. I. Z. and Ibrahim, M. (2007). "A disposable compliant-forceps for HIV patients," *Journalof Medical Science*. **7(4):** 591 − 596.

Sidoroff, F. (1981). "Description of Anisotropic Damage Application to Eelasticity". *IUTAM Colloquium on Physical Nonlinearities in Structures (Edited by J. Hult and J. Lemaitre) Springer, Berlin.*. 237-244.

Sigmund, O., (1997). "On the design of compliant mechanisms using topology optimization". *Mech. Struct. & Machines.* **25:** 493-524.

Sigmund, O., (2000). "Topology optimisation: A tool for the tailoring of structures and materials". *Phil. Trans. R. Soc. Lond. A*. **358:** 211-227.

Sigmund, O. (2001). "Design of multiphysics actuators using topology optimization - Part I: One material structures". *Comput. Methods Appl. Mech. Engg*. . **190(49-50):** 6577 – 6604.

Sigmund, O. (2001). "Design of multiphysics actuators using topology optimization - Part II: Two material structures". *Comput. Methods Appl. Mech. Engg*. **190(49-50):** 6605 – 6627.

Solehuddin, S., Jamaluddin, A., Abd.Samad, M. and Nizam, A.M. (2002). "A novel design of a compliant one-piece nail clipper". *In: Proc. of the 2nd World Engineering Congress, 2002 WEC.*

Solid Works, (2008). "Understanding Nonlinear Analysis". *White Paper.*

Sorosiak, J., (2001). "Debunking the limits of MEMS. Interesting Articles". *Integrated Micro machines Incorporated (IMMI).*

Stolpe, M. and Svanberg, K. (2001), "On the Trajectories of Penalization Methods for Topology Optimisation". *Struct. Multidisc Optim.* **21:** 128-139.

Stolpe, M. and Svanberg, K. (2001). "An alternative interpolation scheme for minimum compliance topology optimization". *Struct. Multidisc. Optim.* **22:** 116-124.

Subaşi, L. (2005). "Synthesis of Compliant Bistable Four-Link Mechanisms for Two Positions". *Thesis, Middle East Technical University*.

Sugihara, G. (2010). "Nature is nonlinear". *Biodiversity. Kyoto Journal*. **75:** 56

Sun, W.,Chaikof, E. L. and Levenston, M. E. (2008). "Numerical Approximation of tangent Moduli for Finite Element Implementation of Nonlinear Hyperelastic material Models". *J Biomech Eng*. **130 (6):**

Swan, C. C. and Rahmatalla S. (2004). "Topological design and nonlinear control of path-following compliant mechanisms". *ASME 2004 Design Engineering*

Technical Conferences and Computers and Information in Engineering Conference, USA, DETC2004-57441.

Tang, C. Y. and Lee, W. B. (1995). "Damage Mechanics Applied to Elastic Properties of Polymers", *Engg Fracture Mech.anics*. **52(4):** 717-729.

Tang, C. Y., Tai, W. H. and Lee, W. B. (1996). "Modeling of damage behaviors of high impact polystyrene", *Engineering fracture mechanics. **55(4):** 583-591.

Tantanawat T., Li, Z., Kota, S., (2004). "Application of Compliant Mechanisms to Active Vibration Isolation Systems". *International Design Engineering Technical Conference September 28 – October 2, 2004 Salt Lake City, Utah*

Taylor, R. L. (2000). "A mixed-enhanced formulation for tetrahedral finite elements, International Journal for Numerical Methods in Engineering". **47:** 205 – 227.

Trehan, R. (2011). "Nonlinear Analysis". *Tips on SolidWorks products from the technical staff of CATI.*

Tsay, J., Chang, H. and Sung, C. (2005). "Design and experiments of fully compliant bistable micromechanisms," *Mechanism and Machine Theory*. **40:** 17–31.

Ugwuoke, I. C. (2008). "A Simplified Dynamic Model for Constant-Force Compression Spring". *Leonardo Journal of Sciences*. ISSN 1583-0233. **13:** 30-43.

Ugwuoke, I. C. (2009). "Stability Analysis for Compliant Constant-Force Compression Mechanisms". *Leonardo Journal of Sciences.* ISSN 1583-0233. **15:** 83-98.

Ugwuoke, I. C. (2009). "Dynamic Modeling and simulation of the compliant constant force mechanism using the pseudo rigid body modeling technique". *Ph D Thesis, Federal University of Technology Minna, Niger State, Nigeria.*

Ugwuoke, I. C., Abolarin, M. S. and Ogwuagwu, O. V. (2009). "Frequency Characteristics of the Compliant Constant-Force Mechanism Based on the Pseudo Rigid Body Model". *Assumption University Journal of Technology*. **12(3):** 193-198.

Upadhyaya, Y. S. and Sridhara, B. K. (2012). "Fatigue Crack Initiation and Propagation Life Prediction of Materials". *International Conference on Mechanical, Electronics and Mechatronics Engineering (ICMEME'2012), Bangkok.*

Vogel, S. (1998). "Cats' Paws and Catapults". *W. W. Norton and Company, New York, NY.*

Wang, B., Lu, H. and Kim, G. (2002). "A damage model for the fatigue life of elastomeric materials" *Mechanics of Materials*. **34:** 475–483.

Wang, M. Y. and Chen, S. (2009). "Compliant Mechanism Optimization: Analysis and Design with Intrinsic Characteristic Stiffness". *Mechanics Based Design of Structures and Machines: An International Journal.* **37(2):** 183 – 200.

Wang, Q. W., Berard, Y., Rathery, S., and Bathias, C. (1999). "High cycle fatigue crack initiation and propagation behaviour of high strength spring steel wires," *Fat. and Fract. of Engg. Mater. and Struct.* **22:** 673-677.

Wang, W. and Yu, Y. (2008). "Dynamic Anlysis of Compliant Mechanism using Finite Element Method". *Proceedings of IEEE/ASME International Conference on advanced Intelligent Mechatronics.China.* 247-251.

Wang, W. and Yu, Y. (2010). "Dynamic Analysis of Compliant Mechanisms Based on Finite Element Method". *Journal of Mechanical Engineering*. **46(9).**

Wei, P., Yang, Q. P., Salleh, M. R. and Jones B. (2007). "Symbolic Computation for Evaluation of Measurement Uncertainty". *Instrumentation and Measurement Technology 64.Conference - IMTC 2007 Warsaw, Poland, May 1-3.*

Wriggers, P., (2010). "Nonlinear Finite Element Methods". *Springer-Verlag New York, LLC*.

Wu, G., Datar, R. H., Hansen, K. M., Thundat, T., Cote, R. J., and Majumdar, A., (2001). "Bioassay of Prostate-specific Antigen (PSA) using Microcantilevers". *Nature Biotechnology*, **19(9):** 856 – 860.

Xian, D. Y., Ping, C. L., Hua, T. Q. and Jia, W. Z. (2009). "Topology synthesis of thermomechanical compliant mechanisms with geometrical nonlinearities using meshless method". *Advances in Engineering Software*. **40:** 315–322.

Yixian, D. and Liping, C. (2008). "Topology optimization for large-displacement compliant mechanisms using element free galerkin method". *International Journal of CAD/CAM*. **8(1):** 1-10.

Yu, Y., Howell, L. L. and Yue Y. (2005). "Dynamic Modeling of Compliant Mechanism Based on the Pseudo Rigid Body Model". *Journal of Mechine Design*. **127:** 760-765.

Zhang, X. and Hou, W. (2010). "Dynamic analysis of the precision compliant mechanisms considering thermal effect". *Precision Engineering*. **34:** 592–606.

Zienkiewicz, O. C. and Taylor, R. L. (2000). "The Finite Element Method". *Fifth Edition. Butterworth – Heinemann*.

APPENDIX A: HYPERELASTICITY AceGEN CODE GENERATION

```c
/***********************************************************

* AceGen     5.002 Windows (8 Mar 13)
*
*             Co. J. Korelc  2007              10 May 13
15:43:38*
************************************************************

User    :       Full professional version
Notebook:       Compliant Mechanisms Deformation Code
                (with both Nonlinearities).nb
Evaluation time     : 5 s
Mode                : Optimal
Number of formulae  : 207
Method              : Automatic
Subroutine          : SKR size :1679
Subroutine          : SPP size :1074
Total size of Mathematica code : 2753 subexpressions
Total size of C code            : 8864 bytes*/
#include "sms.h"

void SKR(double v[6385],ElementSpec *es,ElementData

*ed,NodeSpec **ns,NodeData **nd,double *rdata,int

*idata,double *p,double **s);

void SPP(double v[6385],ElementSpec *es,ElementData

*ed,NodeSpec **ns,NodeData **nd,double *rdata,int

*idata,double **gpost,double **npost);

int MMAInitialisationCode[]={

0,0

};

DLLEXPORT int SMTSetElSpec(ElementSpec *es,int *idata,int

ic,int ng)
```

```
{ int intc,nd,i;FILE *SMSFile;

   static int pn[11]={1, 2, 3, 4, 0, 1, 2, 3, 4, -1, 0};

   static int dof[4]={2, 2, 2, 2};

   static int nsto[4]={0, 0, 0, 0};

   static int ndat[4];

   static char *nid[]={"D","D","D","D"};

   static char *gdcs[]={"E -elastic modulus","$[Nu]$ -
Poisson ratio","t -thickness"};

   static double defd[]={21000e0,0.3e0,1e0,0e0};

   static char
*gpcs[]={"$[Sigma]$xx","$[Sigma]$xy","$[Sigma]$yx","$[Sig
ma]$yy","$[Sigma]$zz","Exx",

                      "Exy","Eyx","Eyy","Ezz","Mises
stress"};

   static char
*npcs[]={"DeformedMeshX","DeformedMeshY","u","v"};

   static char *sname[]={"E -elastic modulus","$[Nu]$ -
Poisson ratio"};

   static char *idname[]={""};

   static int idindex[1];

   static char *rdname[]={""};

   static char *cswitch[]={""};

   static int iswitch[1]={0};

   static double dswitch[2]={0.1e-7,0e0};

   static int rdindex[1];
```

```
static int nspecs[4];

static double version[3]={5.002,5.002,9.};

static double pnweights[4]={1e0,1e0,1e0,1e0};

static double rnodes[12]={-1e0,-1e0,0e0,1e0,-1e0,0e0,

1e0,1e0,0e0,-1e0,1e0,0e0};

es->ReferenceNodes=rnodes;

if(ng==-1) es->Data=defd;

es->id.NoGroupData=3;

es->Code="CMsWithHyperelasticity ";es->Version=version;

es->MainTitle="";

es->SubTitle="";

es-
>SubSubTitle="$bold$Postprocessing$bold$:$n2$$[Sigma]$ij

- small stress tensor$n2$Eij - small strain

tensor$nl$$bold$Real type domain

switches$bold$:$b1$SMTDomainData[dID,$Ap$DoubleSwitch$Ap$

,{$b2$1) tolerance for convergence of locally coupled

equations (default 10^-8)$b1$}].";

es->Bibliography="";

es->id.NoDimensions=2;es->id.NoDOFGlobal=8;es-
>id.NoDOFCondense=0;es->id.NoNodes=4;

es->id.NoSegmentPoints=10;es->Segments=pn;es-
>PostNodeWeights=pnweights;

es->id.NoIntSwitch=0;es->IntSwitch=iswitch;es-
>id.DemoLimitation=0;
```

```
es->id.NoDoubleSwitch=1;es->DoubleSwitch=dswitch;

es->id.NoCharSwitch=0;es->CharSwitch=cswitch;

es->DOFGlobal=dof;es->NodeID=nid;es-
>id.NoGPostData=11;es->id.NoNPostData=4;

es->id.SymmetricTangent=1;es->id.CreateDummyNodes=0;es-
>id.PostIterationCall=1;es->id.DOFScaling=0;

es->Topology="Q1";es->GroupDataNames=gdcs;es-
>GPostNames=gpcs;es->NPostNames=npcs;

es->AdditionalNodes="{}&";

es->AdditionalGraphics="{}&";

es->MMAInitialisation=MMAInitialisationCode;

es->MMANextStep="";

es->MMAStepBack="";

es->MMAPreIteration="";

es->IDataNames=idname;es->IDataIndex=idindex;es-
>RDataNames=rdname;es->RDataIndex=rdindex;

es->id.NoIData=0;es->id.NoRData=0;

es->id.ShapeSensitivity=0;es->id.NoSensNames=2;es-
>SensitivityNames=sname;es->NodeSpecs=nspecs;

es->user.SPP=SPP;es->user.SKR=SKR;

es->id.DefaultIntegrationCode=2;

if(ic==-1){intc=2;} else {intc=ic;};

es->id.IntCode=intc;

SMTMultiIntPoints(&intc,idata,&es->id.NoIntPoints,
```

```
      &es->id.NoIntPointsA,&es->id.NoIntPointsB,&es-
>id.NoIntPointsC,0);

  es->id.NoAdditionalData=(int)(0);

  es->id.NoTimeStorage=(int)((int)(es->id.NoIntPoints));

  es->id.NoElementData=(int)(0);

  nd=(int)(es-
>id.NoDimensions*idata[ID_NoShapeParameters]);for(i=0;i<4
;i++)ndat[i]=nd;

  es->NoNodeStorage=nsto;es->NoNodeData=ndat;

  if(1){

   return 0;

  }else{

   return 1;

  };

};

/****************** S U B R O U T I N E

********************/

void SKR(double v[6385],ElementSpec *es,ElementData

*ed,NodeSpec **ns

    ,NodeData **nd,double *rdata,int *idata,double

*p,double **s)

{

int

i1,i2,i94,i121,i122,i140,i154,b85,b86,b88,b111,b113,b130,

b150,b152;
```

```
FILE *SMSFile;

v[87]=es->DoubleSwitch[0];

b86=idata[ID_SkipTangent]==1e0;

v[53]=es->Data[2];

b85=(int)(idata[ID_SkipResidual])==1 ||

(int)(idata[ID_Iteration])==1;

v[23]=nd[3]->at[1];

v[22]=nd[3]->at[0];

v[21]=nd[2]->at[1];

v[20]=nd[2]->at[0];

v[19]=nd[1]->at[1];

v[18]=nd[1]->at[0];

v[17]=nd[0]->at[1];

v[16]=nd[0]->at[0];

v[15]=nd[3]->X[1];

v[14]=nd[3]->X[0];

v[13]=nd[2]->X[1];

v[12]=nd[2]->X[0];

v[11]=nd[1]->X[1];

v[10]=nd[1]->X[0];

v[9]=nd[0]->X[1];

v[8]=nd[0]->X[0];

v[4]=es->Data[1];

v[293]=2e0*v[4];

v[6]=1e0/(1e0+v[4]);
```

```
v[3]=es->Data[0];

v[7]=(v[3]*v[6])/2e0;

v[104]=((2e0/3e0)+v[293]/(1e0-v[293]))*v[7];

i1=(int)(es->id.NoIntPoints);

for(i2=1;i2<=i1;i2++){

 v[29]=es->IntPoints[4*(-1+i2)];

 v[38]=1e0-v[29];

 v[45]=-v[38]/4e0;

 v[36]=1e0+v[29];

 v[46]=-v[36]/4e0;

 v[30]=es->IntPoints[1+4*(-1+i2)];

 v[39]=1e0+v[30];

 v[47]=v[39]/4e0;

 v[34]=1e0-v[30];

 v[44]=-v[34]/4e0;

 v[48]=(v[12]-v[14])*v[47]+v[44]*(-v[10]+v[8]);

 v[49]=(v[13]-v[15])*v[47]+v[44]*(-v[11]+v[9]);

 v[50]=(v[10]-v[12])*v[46]+v[45]*(-v[14]+v[8]);

 v[51]=(v[11]-v[13])*v[46]+v[45]*(-v[15]+v[9]);

 v[52]=-(v[49]*v[50])+v[48]*v[51];

 v[54]=v[51]/v[52];

 v[72]=v[47]*v[54];

 v[64]=v[44]*v[54];

 v[55]=-(v[50]/v[52]);

 v[75]=v[47]*v[55];
```

```
v[66]=v[44]*v[55];

v[56]=-(v[49]/v[52]);

v[73]=v[45]*v[56];

v[68]=v[46]*v[56];

v[57]=v[48]/v[52];

v[76]=v[45]*v[57];

v[70]=v[46]*v[57];

v[62]=v[64]+v[73];

v[63]=v[66]+v[76];

v[65]=-v[64]+v[68];

v[67]=-v[66]+v[70];

v[69]=-v[68]+v[72];

v[71]=-v[70]+v[75];

v[74]=-v[72]-v[73];

v[6360]=0e0;

v[6361]=v[62];

v[6362]=0e0;

v[6363]=v[65];

v[6364]=0e0;

v[6365]=v[69];

v[6366]=0e0;

v[6367]=v[74];

v[6344]=v[62];

v[6345]=0e0;

v[6346]=v[65];
```

```
v[6347]=0e0;

v[6348]=v[69];

v[6349]=0e0;

v[6350]=v[74];

v[6351]=0e0;

v[77]=-v[75]-v[76];

v[6368]=0e0;

v[6369]=v[63];

v[6370]=0e0;

v[6371]=v[67];

v[6372]=0e0;

v[6373]=v[71];

v[6374]=0e0;

v[6375]=v[77];

v[6352]=v[63];

v[6353]=0e0;

v[6354]=v[67];

v[6355]=0e0;

v[6356]=v[71];

v[6357]=0e0;

v[6358]=v[77];

v[6359]=0e0;

v[82]=es->IntPoints[(-1+4*i2)]*v[52]*v[53];

if(b85){

 v[89]=ed->ht[i2-1];
```

```
  } else {

   v[89]=ed->hp[i2-1];

  };



v[90]=1e0+v[16]*v[62]+v[18]*v[65]+v[20]*v[69]+v[22]*v[74]

;

 v[91]=v[16]*v[63]+v[18]*v[67]+v[20]*v[71]+v[22]*v[77];

 v[92]=v[17]*v[62]+v[19]*v[65]+v[21]*v[69]+v[23]*v[74];



v[93]=1e0+v[17]*v[63]+v[19]*v[67]+v[21]*v[71]+v[23]*v[77]

;

 v[102]=-(v[91]*v[92])+v[90]*v[93];

 v[294]=v[102]*v[104];

 v[107]=(v[102]*v[102])*v[104]+v[7];

 for(i94=1;i94<=30;i94++){

  v[95]=1e0+v[89];

  v[105]=-1e0+v[102]*v[95];

  v[109]=-((v[105]*v[294]+v[7]*v[95])/v[107]);

  v[89]=v[109]+v[89];

  if(sqrt(Power(v[109],2))<v[87] || b85){

   ed->ht[i2-1]=v[89];

   if(!(b86)){

    v[115]=v[294]*v[95];

    v[296]=-(v[104]*v[105])-v[115];

    v[119]=v[295];
```

```
   v[6308]=v[296]*v[93];

   v[6309]=-(v[296]*v[92]);

   v[6310]=-(v[296]*v[91]);

   v[6311]=v[296]*v[90];

   v[120]=v[297];

   for(i121=1;i121<=4;i121++){

    i122=-1+i121;

    v[6312+i122]=v[6308+i122]/v[107];

   };/* end for */

   v[125]=v[6312];

   v[126]=v[6313];

   v[127]=v[6314];

   v[128]=v[6315];

  } else {

  };

 break;

} else {

};

if(i94==29){

 idata[ID_SubDivergence]=1e0;

 idata[ID_ErrorStatus]=2e0;

 if(idata[ID_NoMessages]<idata[ID_MaxMessages]){

 ++idata[ID_NoMessages];
```

```
    if(strcmp(es-

>OutFileName,"NONE")!=0){SMSFile=fopen(es-

>OutFileName,"a");if(SMSFile!=NULL){

    fprintf(SMSFile,"\n%s %g %s %g ","SUB-DIVERGENCE

element=",(double)idata[ID_CurrentElement]

      ,"int. point=",(double)i2);

    fclose(SMSFile);};}

     };

     break;

    } else {

    };

  };/* end for */

  v[135]=1e0+v[89];

  v[303]=v[102]*v[135];

  v[136]=(v[135]*v[135]);

  v[142]=-1e0+v[303];

  v[144]=v[104]*v[135]*v[142];

  v[143]=v[144]*v[90]+v[7]*v[93];

  v[145]=-(v[144]*v[91])+v[7]*v[92];

  v[146]=v[7]*v[91]-v[144]*v[92];

  v[147]=v[7]*v[90]+v[144]*v[93];

  v[6332]=v[147]*v[62]+v[146]*v[63];

  v[6333]=v[145]*v[62]+v[143]*v[63];

  v[6334]=v[147]*v[65]+v[146]*v[67];

  v[6335]=v[145]*v[65]+v[143]*v[67];
```

```
v[6336]=v[147]*v[69]+v[146]*v[71];

v[6337]=v[145]*v[69]+v[143]*v[71];

v[6338]=v[147]*v[74]+v[146]*v[77];

v[6339]=v[145]*v[74]+v[143]*v[77];

for(i140=1;i140<=8;i140++){

 v[157]=v[6343+i140]*v[82];

 v[158]=v[6351+i140]*v[82];

 v[159]=v[6359+i140]*v[82];

 v[160]=v[6367+i140]*v[82];

 v[161]=v[160]*v[90]-v[159]*v[91]-
v[158]*v[92]+v[157]*v[93];

 v[302]=v[104]*v[161];

 v[164]=v[136]*v[302];

 v[162]=v[302]*(v[142]+v[303]);


v[163]=v[144]*v[157]+v[128]*v[162]+v[160]*v[7]+v[164]*v[9
0];

 v[165]=-(v[144]*v[158])+v[127]*v[162]+v[159]*v[7]-
v[164]*v[91];

 v[166]=-(v[144]*v[159])+v[126]*v[162]+v[158]*v[7]-
v[164]*v[92];


v[167]=v[144]*v[160]+v[125]*v[162]+v[157]*v[7]+v[164]*v[9
3];

 v[6376]=v[167]*v[62]+v[166]*v[63];
```

```
v[6377]=v[165]*v[62]+v[163]*v[63];

v[6378]=v[167]*v[65]+v[166]*v[67];

v[6379]=v[165]*v[65]+v[163]*v[67];

v[6380]=v[167]*v[69]+v[166]*v[71];

v[6381]=v[165]*v[69]+v[163]*v[71];

v[6382]=v[167]*v[74]+v[166]*v[77];

v[6383]=v[165]*v[74]+v[163]*v[77];

if((int)(idata[ID_SkipResidual])==0){

 p[i140-1]+=v[6331+i140]*v[82];

} else {

};

if(b86){

 continue;

} else {

};

for(i154=i140;i154<=8;i154++){

 s[i140-1][i154-1]+=v[6375+i154];

};/* end for */

};/* end for */

};/* end for */

};

/****************** S U B R O U T I N E

********************/

void SPP(double v[6385],ElementSpec *es,ElementData

*ed,NodeSpec **ns
```

```
      ,NodeData **nd,double *rdata,int *idata,double

**gpost,double **npost)

{

int i170,i171;

FILE *SMSFile;

v[192]=nd[3]->at[1];

v[191]=nd[3]->at[0];

v[190]=nd[2]->at[1];

v[189]=nd[2]->at[0];

v[188]=nd[1]->at[1];

v[187]=nd[1]->at[0];

v[186]=nd[0]->at[1];

v[185]=nd[0]->at[0];

v[184]=nd[3]->X[1];

v[183]=nd[3]->X[0];

v[182]=nd[2]->X[1];

v[181]=nd[2]->X[0];

v[180]=nd[1]->X[1];

v[179]=nd[1]->X[0];

v[178]=nd[0]->X[1];

v[177]=nd[0]->X[0];

v[173]=es->Data[1];

v[304]=2e0*v[173];

v[175]=1e0/(1e0+v[173]);

v[172]=es->Data[0];
```

```
v[176]=(v[172]*v[175])/2e0;

v[279]=v[176]*((2e0/3e0)+v[304]/(1e0-v[304]));

i170=(int)(es->id.NoIntPoints);

for(i171=1;i171<=i170;i171++){

 v[198]=es->IntPoints[4*(-1+i171)];

 v[207]=1e0-v[198];

 v[214]=-v[207]/4e0;

 v[205]=1e0+v[198];

 v[215]=-v[205]/4e0;

 v[199]=es->IntPoints[1+4*(-1+i171)];

 v[208]=1e0+v[199];

 v[216]=v[208]/4e0;

 v[203]=1e0-v[199];

 v[213]=-v[203]/4e0;

 v[217]=(v[177]-v[179])*v[213]+(v[181]-v[183])*v[216];

 v[218]=(v[178]-v[180])*v[213]+(v[182]-v[184])*v[216];

 v[219]=(v[177]-v[183])*v[214]+(v[179]-v[181])*v[215];

 v[220]=(v[178]-v[184])*v[214]+(v[180]-v[182])*v[215];

 v[221]=-(v[218]*v[219])+v[217]*v[220];

 v[223]=v[220]/v[221];

 v[241]=v[216]*v[223];

 v[233]=v[213]*v[223];

 v[224]=-(v[219]/v[221]);

 v[244]=v[216]*v[224];

 v[235]=v[213]*v[224];
```

```
v[225]=-(v[218]/v[221]);

v[242]=v[214]*v[225];

v[237]=v[215]*v[225];

v[226]=v[217]/v[221];

v[245]=v[214]*v[226];

v[239]=v[215]*v[226];

v[231]=v[233]+v[242];

v[232]=v[235]+v[245];

v[234]=-v[233]+v[237];

v[236]=-v[235]+v[239];

v[238]=-v[237]+v[241];

v[240]=-v[239]+v[244];

v[243]=-v[241]-v[242];

v[246]=-v[244]-v[245];


v[254]=1e0+v[185]*v[231]+v[187]*v[234]+v[189]*v[238]+v[19
1]*v[243];


v[255]=v[185]*v[232]+v[187]*v[236]+v[189]*v[240]+v[191]*v
[246];


v[256]=v[186]*v[231]+v[188]*v[234]+v[190]*v[238]+v[192]*v
[243];

v[307]=(v[256]*v[256]);
```

```
v[257]=1e0+v[186]*v[232]+v[188]*v[236]+v[190]*v[240]+v[19

2]*v[246];

 v[308]=(v[257]*v[257]);

 v[277]=-(v[255]*v[256])+v[254]*v[257];

 v[258]=1e0+ed->ht[i171-1];

 v[263]=v[258]*v[277];

 v[280]=-1e0+v[263];

 v[306]=v[279]*v[280];

 v[305]=v[258]*v[306];

 v[266]=(v[254]*v[255]+v[256]*v[257])/2e0;

 v[281]=v[176]*v[254]+v[257]*v[305];

 v[282]=v[176]*v[255]-v[256]*v[305];

 v[286]=(v[254]*v[281]+v[255]*v[282])/v[263];

 v[287]=(v[256]*v[281]+v[257]*v[282])/v[263];

 v[288]=(v[277]*v[305]+v[176]*(v[307]+v[308]))/v[263];

 v[289]=(v[258]*(v[176]*v[258]+v[277]*v[306]))/v[263];

 v[290]=(-v[286]-v[288]-v[289])/3e0;

 gpost[i171-1][0]=v[286];

 gpost[i171-1][1]=v[287];

 gpost[i171-1][2]=v[287];

 gpost[i171-1][3]=v[288];

 gpost[i171-1][4]=v[289];

 gpost[i171-1][5]=(-1e0+(v[254]*v[254])+v[307])/2e0;

 gpost[i171-1][6]=v[266];

 gpost[i171-1][7]=v[266];
```

```
 gpost[i171-1][8]=(-1e0+(v[255]*v[255])+v[308])/2e0;

 gpost[i171-1][9]=(-1e0+(v[258]*v[258]))/2e0;

 gpost[i171-
1][10]=sqrt(0.15e1*(2e0*Power(v[287],2)+Power(v[286]+v[29
0],2)+Power(v[288]+v[290],2)
  +Power(v[289]+v[290],2)));

};/* end for */

npost[0][0]=v[185];

npost[1][0]=v[187];

npost[2][0]=v[189];

npost[3][0]=v[191];

npost[0][1]=v[186];

npost[1][1]=v[188];

npost[2][1]=v[190];

npost[3][1]=v[192];

npost[0][2]=v[185];

npost[1][2]=v[187];

npost[2][2]=v[189];

npost[3][2]=v[191];

npost[0][3]=v[186];

npost[1][3]=v[188];

npost[2][3]=v[190];

npost[3][3]=v[192];}
```

APPENDIX B: GEOMETRIC NONLINEAR MODEL AceGEN CODE GENARATION

```
/***********************************************************

* AceGen   5.002 Windows (8 Mar 13)
*
*           Co. J. Korelc  2007           10 May 13
15:40:49*
***********************************************************

User      : Full professional version
Notebook : Compliant Mechanisms Deformation Code (with
           only Geometric Nonlinear).nb
Evaluation time       : 8 s
Mode                  : Optimal
Number of formulae    : 365
Method                : Automatic
Subroutine            : SKR size :1457
Subroutine            : SSE size :2315
Subroutine            : SPP size :962
Total size of Mathematica  code : 4734 subexpressions
Total size of C code       : 14052 bytes*/
#include "sms.h"

void SKR(double v[4269],ElementSpec *es,ElementData

*ed,NodeSpec **ns,NodeData **nd,double *rdata,int

*idata,double *p,double **s);

void SSE(double v[4269],ElementSpec *es,ElementData

*ed,NodeSpec **ns,NodeData **nd,double *rdata,int

*idata,double *p);

void SPP(double v[4269],ElementSpec *es,ElementData

*ed,NodeSpec **ns,NodeData **nd,double *rdata,int

*idata,double **gpost,double **npost);
```

```
int MMAInitialisationCode[]={

0,0

};

DLLEXPORT int SMTSetElSpec(ElementSpec *es,int *idata,int

ic,int ng)

{ int intc,nd,i;FILE *SMSFile;

  static int pn[11]={1, 2, 3, 4, 0, 1, 2, 3, 4, -1, 0};

  static int dof[4]={2, 2, 2, 2};

  static int nsto[4]={0, 0, 0, 0};

  static int ndat[4];

  static char *nid[]={"D","D","D","D"};

  static char *gdcs[]={"E -elastic modulus","$[Nu]$ -

Poisson ratio","t -thickness"};

  static double defd[]={21000e0,0.3e0,1e0,0e0};

  static char

*gpcs[]={"Sxx","Sxy","Syx","Syy","Exx","Exy",

                    "Eyx","Eyy","Ezz","Mises stress"};

  static char

*npcs[]={"DeformedMeshX","DeformedMeshY","u","v"};

  static char *sname[]={"E -elastic modulus","$[Nu]$ -

Poisson ratio"};

  static char *idname[]={""};

  static int idindex[1];

  static char *rdname[]={""};

  static char *cswitch[]={""};
```

```
static int iswitch[1]={0};

static double dswitch[1]={0e0};

static int rdindex[1];

static int nspecs[4];

static double version[3]={5.002,5.002,9.};

static double pnweights[4]={1e0,1e0,1e0,1e0};

static double rnodes[12]={-1e0,-1e0,0e0,1e0,-1e0,0e0,

1e0,1e0,0e0,-1e0,1e0,0e0};

es->ReferenceNodes=rnodes;

if(ng==-1) es->Data=defd;

es->id.NoGroupData=3;

es->Code=" CMsWithGNL es->Version=version;

es->MainTitle="";

es->SubTitle="";

es->SubSubTitle="$bold$Postprocessing$bold$:$n2$Sij -
Cauchy stress tensor$n2$Eij - Green-Lagrange strain
tensor.";

es->Bibliography="";

es->id.NoDimensions=2;es->id.NoDOFGlobal=8;es-
>id.NoDOFCondense=0;es->id.NoNodes=4;

es->id.NoSegmentPoints=10;es->Segments=pn;es-
>PostNodeWeights=pnweights;

es->id.NoIntSwitch=0;es->IntSwitch=iswitch;es-
>id.DemoLimitation=0;

es->id.NoDoubleSwitch=0;es->DoubleSwitch=dswitch;
```

```
es->id.NoCharSwitch=0;es->CharSwitch=cswitch;

es->DOFGlobal=dof;es->NodeID=nid;es-
>id.NoGPostData=10;es->id.NoNPostData=4;

es->id.SymmetricTangent=1;es->id.CreateDummyNodes=0;es-
>id.PostIterationCall=0;es->id.DOFScaling=0;

es->Topology="Q1";es->GroupDataNames=gdcs;es-
>GPostNames=gpcs;es->NPostNames=npcs;

es->AdditionalNodes="{}&";

es->AdditionalGraphics="{}&";

es->MMAInitialisation=MMAInitialisationCode;

es->MMANextStep="";

es->MMAStepBack="";

es->MMAPreIteration="";

es->IDataNames=idname;es->IDataIndex=idindex;es-
>RDataNames=rdname;es->RDataIndex=rdindex;

es->id.NoIData=0;es->id.NoRData=0;

es->id.ShapeSensitivity=1;es->id.NoSensNames=2;es-
>SensitivityNames=sname;es->NodeSpecs=nspecs;

es->user.SPP=SPP;es->user.SSE=SSE;es->user.SKR=SKR;

es->id.DefaultIntegrationCode=2;

if(ic==-1){intc=2;} else {intc=ic;};

es->id.IntCode=intc;

SMTMultiIntPoints(&intc,idata,&es->id.NoIntPoints,
     &es->id.NoIntPointsA,&es->id.NoIntPointsB,&es-
>id.NoIntPointsC,0);
```

```
   es->id.NoAdditionalData=(int)(0);

   es->id.NoTimeStorage=(int)(0);

   es->id.NoElementData=(int)(0);

   nd=(int)(es-

>id.NoDimensions*idata[ID_NoShapeParameters]);for(i=0;i<4

;i++)ndat[i]=nd;

   es->NoNodeStorage=nsto;es->NoNodeData=ndat;

   if(1){

    return 0;

   }else{

    return 1;

   };

};

/****************** S U B R O U T I N E

********************/

void SKR(double v[4269],ElementSpec *es,ElementData

*ed,NodeSpec **ns

    ,NodeData **nd,double *rdata,int *idata,double

*p,double **s)

{

int i3,i4,i97,i110,b1,b2,b106,b108;

v[53]=es->Data[2];

v[25]=nd[3]->at[1];

v[24]=nd[3]->at[0];

v[23]=nd[2]->at[1];
```

```
v[22]=nd[2]->at[0];

v[21]=nd[1]->at[1];

v[20]=nd[1]->at[0];

v[19]=nd[0]->at[1];

v[18]=nd[0]->at[0];

v[17]=nd[3]->X[1];

v[16]=nd[3]->X[0];

v[15]=nd[2]->X[1];

v[14]=nd[2]->X[0];

v[13]=nd[1]->X[1];

v[12]=nd[1]->X[0];

v[11]=nd[0]->X[1];

v[10]=nd[0]->X[0];

v[6]=es->Data[1];

v[415]=2e0*v[6];

v[8]=1e0/(1e0+v[6]);

v[5]=es->Data[0];

v[9]=(v[5]*v[8])/2e0;

v[99]=2e0*v[9];

v[7]=(v[415]*v[9])/(1e0-v[415]);

v[128]=2e0*v[7]+v[99];

v[89]=v[99]/(v[7]+v[99]);

v[421]=v[89]/2e0;

b1=(int)(idata[ID_SkipResidual])==1;

b2=(int)(idata[ID_SkipTangent])==1;
```

```
i3=(int)(es->id.NoIntPoints);

for(i4=1;i4<=i3;i4++){

 v[29]=es->IntPoints[4*(-1+i4)];

 v[38]=1e0-v[29];

 v[45]=-v[38]/4e0;

 v[36]=1e0+v[29];

 v[46]=-v[36]/4e0;

 v[30]=es->IntPoints[1+4*(-1+i4)];

 v[39]=1e0+v[30];

 v[47]=v[39]/4e0;

 v[34]=1e0-v[30];

 v[44]=-v[34]/4e0;

 v[48]=(v[10]-v[12])*v[44]+(v[14]-v[16])*v[47];

 v[49]=(v[11]-v[13])*v[44]+(v[15]-v[17])*v[47];

 v[50]=(v[10]-v[16])*v[45]+(v[12]-v[14])*v[46];

 v[51]=(v[11]-v[17])*v[45]+(v[13]-v[15])*v[46];

 v[52]=-(v[49]*v[50])+v[48]*v[51];

 v[54]=v[51]/v[52];

 v[72]=v[47]*v[54];

 v[64]=v[44]*v[54];

 v[55]=-(v[50]/v[52]);

 v[75]=v[47]*v[55];

 v[66]=v[44]*v[55];

 v[56]=-(v[49]/v[52]);

 v[73]=v[45]*v[56];
```

```
v[68]=v[46]*v[56];

v[57]=v[48]/v[52];

v[76]=v[45]*v[57];

v[70]=v[46]*v[57];

v[62]=v[64]+v[73];

v[63]=v[66]+v[76];

v[65]=-v[64]+v[68];

v[67]=-v[66]+v[70];

v[69]=-v[68]+v[72];

v[71]=-v[70]+v[75];

v[74]=-v[72]-v[73];

v[4244]=0e0;

v[4245]=v[62];

v[4246]=0e0;

v[4247]=v[65];

v[4248]=0e0;

v[4249]=v[69];

v[4250]=0e0;

v[4251]=v[74];

v[4228]=v[62];

v[4229]=0e0;

v[4230]=v[65];

v[4231]=0e0;

v[4232]=v[69];

v[4233]=0e0;
```

```
v[4234]=v[74];

v[4235]=0e0;

v[77]=-v[75]-v[76];

v[4252]=v[63];

v[4253]=0e0;

v[4254]=v[67];

v[4255]=0e0;

v[4256]=v[71];

v[4257]=0e0;

v[4258]=v[77];

v[4259]=0e0;

v[4236]=0e0;

v[4237]=v[63];

v[4238]=0e0;

v[4239]=v[67];

v[4240]=0e0;

v[4241]=v[71];

v[4242]=0e0;

v[4243]=v[77];

v[78]=v[18]*v[62]+v[20]*v[65]+v[22]*v[69]+v[24]*v[74];

v[416]=2e0*v[78];

v[418]=v[416]+(v[78]*v[78]);

v[122]=2e0+v[416];

v[423]=v[122]*v[421];

v[79]=v[19]*v[62]+v[21]*v[65]+v[23]*v[69]+v[25]*v[74];
```

```
v[118]=1e0+v[79];

v[80]=v[18]*v[63]+v[20]*v[67]+v[22]*v[71]+v[24]*v[77];

v[117]=1e0+v[80];

v[81]=v[19]*v[63]+v[21]*v[67]+v[23]*v[71]+v[25]*v[77];

v[417]=2e0*v[81];

v[419]=v[417]+(v[81]*v[81]);

v[121]=2e0+v[417];

v[425]=v[121]*v[421];

v[82]=es->IntPoints[(-1+4*i4)]*v[52]*v[53];

v[83]=v[418]/2e0;

v[84]=(v[79]+v[118]*v[80])/2e0;

v[420]=v[84]*v[99];

v[85]=v[419]/2e0;

v[126]=v[7]*(v[418]+v[85])+v[83]*v[99];

v[120]=v[7]*(v[419]+v[83])+v[85]*v[99];

v[100]=v[118]*v[420];

v[101]=v[117]*v[420];

v[102]=v[120]*v[425];

v[103]=v[126]*v[423];

v[4216]=v[103]*v[62]+v[100]*v[63];

v[4217]=v[101]*v[62]+v[102]*v[63];

v[4218]=v[103]*v[65]+v[100]*v[67];

v[4219]=v[101]*v[65]+v[102]*v[67];

v[4220]=v[103]*v[69]+v[100]*v[71];

v[4221]=v[101]*v[69]+v[102]*v[71];
```

```
v[4222]=v[103]*v[74]+v[100]*v[77];

v[4223]=v[101]*v[74]+v[102]*v[77];

for(i97=1;i97<=8;i97++){

 v[113]=v[4227+i97]*v[82];

 v[127]=v[113]*v[423];

 v[114]=v[4235+i97]*v[82];

 v[129]=v[114]*v[425];

 v[115]=v[4243+i97]*v[82];

 v[116]=v[4251+i97]*v[82];

 v[119]=(v[115]*v[117]+v[116]*v[118])*v[99];

 v[428]=v[119]/2e0;


v[123]=(v[121]*(v[128]*v[129]+v[127]*v[7]))/2e0+v[114]*v[
120]*v[89];

 v[124]=v[115]*v[420]+v[118]*v[428];

 v[125]=v[116]*v[420]+v[117]*v[428];


v[130]=(v[122]*(v[127]*v[128]+v[129]*v[7]))/2e0+v[113]*v[
126]*v[89];

 v[4260]=v[130]*v[62]+v[124]*v[63];

 v[4261]=v[125]*v[62]+v[123]*v[63];

 v[4262]=v[130]*v[65]+v[124]*v[67];

 v[4263]=v[125]*v[65]+v[123]*v[67];

 v[4264]=v[130]*v[69]+v[124]*v[71];

 v[4265]=v[125]*v[69]+v[123]*v[71];
```

```
v[4266]=v[130]*v[74]+v[124]*v[77];

v[4267]=v[125]*v[74]+v[123]*v[77];

if(!(b1)){

 p[i97-1]+=v[4215+i97]*v[82];

} else {

};

if(b2){

 continue;

} else {

};

for(i110=i97;i110<=8;i110++){

 s[i97-1][i110-1]+=v[4259+i110];

};/* end for */

};/* end for */

};/* end for */

};

/****************** S U B R O U T I N E

******************/

void SSE(double v[4269],ElementSpec *es,ElementData

*ed,NodeSpec **ns

    ,NodeData **nd,double *rdata,int *idata,double *p)

{

int i133,i134,i135,i137,i138,i242,i245,b159,b244;

v[223]=es->Data[1];

v[261]=1e0-2e0*v[223];
```

```
v[440]=1e0/Power(v[261],2);

v[255]=1e0+v[223];

v[437]=1e0/Power(v[255],2);

v[222]=es->Data[0];

v[442]=v[222]*v[261];

v[429]=v[222]/v[255];

v[260]=v[223]*v[429];

v[441]=2e0*v[255]*v[260];

v[226]=v[429]/2e0;

v[224]=v[260]/v[261];

v[264]=v[224]+v[429];

v[443]=1e0/Power(v[264],2);

v[233]=(2e0*v[226])/v[264];

v[434]=v[233]*v[264];

v[192]=es->Data[2];

v[154]=nd[3]->at[1];

v[153]=nd[3]->at[0];

v[152]=nd[2]->at[1];

v[151]=nd[2]->at[0];

v[150]=nd[1]->at[1];

v[149]=nd[1]->at[0];

v[148]=nd[0]->at[1];

v[147]=nd[0]->at[0];

v[146]=nd[3]->X[1];

v[145]=nd[3]->X[0];
```

```
v[144]=nd[2]->X[1];

v[143]=nd[2]->X[0];

v[142]=nd[1]->X[1];

v[141]=nd[1]->X[0];

v[140]=nd[0]->X[1];

v[139]=nd[0]->X[0];

i133=(int)(idata[ID_SensIndex]);

i134=(int)(es->SensType[i133-1]);

i135=(int)(es->SensTypeIndex[i133-1]);

i137=(int)(es->id.NoIntPoints);

for(i138=1;i138<=i137;i138++){

 if(i134==2){

  v[160]=nd[0]->Data[(-1+i135)*idata[ID_NoDimensions]];

  v[161]=nd[0]->Data[1+(-1+i135)*idata[ID_NoDimensions]];

  v[162]=nd[1]->Data[(-1+i135)*idata[ID_NoDimensions]];

  v[163]=nd[1]->Data[1+(-1+i135)*idata[ID_NoDimensions]];

  v[164]=nd[2]->Data[(-1+i135)*idata[ID_NoDimensions]];

  v[165]=nd[2]->Data[1+(-1+i135)*idata[ID_NoDimensions]];

  v[166]=nd[3]->Data[(-1+i135)*idata[ID_NoDimensions]];

  v[167]=nd[3]->Data[1+(-1+i135)*idata[ID_NoDimensions]];

 } else {

  v[160]=0e0;

  v[161]=0e0;

  v[162]=0e0;

  v[163]=0e0;
```

```
 v[164]=0e0;

 v[165]=0e0;

 v[166]=0e0;

 v[167]=0e0;

};

v[168]=es->IntPoints[4*(-1+i138)];

v[177]=1e0-v[168];

v[184]=-v[177]/4e0;

v[175]=1e0+v[168];

v[185]=-v[175]/4e0;

v[169]=es->IntPoints[1+4*(-1+i138)];

v[178]=1e0+v[169];

v[186]=v[178]/4e0;

v[173]=1e0-v[169];

v[183]=-v[173]/4e0;

v[171]=es->IntPoints[3+4*(-1+i138)];

v[449]=v[171]*v[192];

v[187]=(v[139]-v[141])*v[183]+(v[143]-v[145])*v[186];

v[188]=(v[140]-v[142])*v[183]+(v[144]-v[146])*v[186];

v[189]=(v[139]-v[145])*v[184]+(v[141]-v[143])*v[185];

v[190]=(v[140]-v[146])*v[184]+(v[142]-v[144])*v[185];

v[191]=-(v[188]*v[189])+v[187]*v[190];

v[274]=1e0/Power(v[191],2);

v[193]=v[190]/v[191];

v[211]=v[186]*v[193];
```

```
v[203]=v[183]*v[193];

v[194]=-(v[189]/v[191]);

v[214]=v[186]*v[194];

v[205]=v[183]*v[194];

v[195]=-(v[188]/v[191]);

v[212]=v[184]*v[195];

v[207]=v[185]*v[195];

v[196]=v[187]/v[191];

v[215]=v[184]*v[196];

v[209]=v[185]*v[196];

v[201]=v[203]+v[212];

v[202]=v[205]+v[215];

v[204]=-v[203]+v[207];

v[206]=-v[205]+v[209];

v[208]=-v[207]+v[211];

v[210]=-v[209]+v[214];

v[213]=-v[211]-v[212];

v[216]=-v[214]-v[215];


v[217]=v[147]*v[201]+v[149]*v[204]+v[151]*v[208]+v[153]*v
[213];

v[430]=2e0*v[217];

v[432]=(v[217]*v[217])+v[430];

v[308]=2e0+v[430];

v[447]=v[308]/2e0;
```

```
v[218]=v[148]*v[201]+v[150]*v[204]+v[152]*v[208]+v[154]*v
[213];
 v[299]=1e0+v[218];


v[219]=v[147]*v[202]+v[149]*v[206]+v[151]*v[210]+v[153]*v
[216];
 v[301]=1e0+v[219];


v[220]=v[148]*v[202]+v[150]*v[206]+v[152]*v[210]+v[154]*v
[216];
 v[431]=2e0*v[220];
 v[433]=(v[220]*v[220])+v[431];
 v[303]=2e0+v[431];
 v[446]=v[303]/2e0;
 v[221]=v[191]*v[449];
 v[227]=v[432]/2e0;
 v[228]=(v[218]+v[219]*v[299])/2e0;
 v[435]=v[228]*v[429];
 v[229]=v[433]/2e0;
 v[310]=v[229]+v[432];
 v[309]=v[224]*v[310]+v[227]*v[434];
 v[305]=v[227]+v[433];
 v[304]=v[224]*v[305]+v[229]*v[434];
 v[231]=v[233]*v[309];
```

```
v[234]=v[233]*v[304];

v[248]=v[299]*v[435];

v[249]=v[301]*v[435];

v[250]=v[234]*v[446];

v[251]=v[231]*v[447];

v[4222]=v[202]*v[248]+v[201]*v[251];

v[4223]=v[201]*v[249]+v[202]*v[250];

v[4224]=v[206]*v[248]+v[204]*v[251];

v[4225]=v[204]*v[249]+v[206]*v[250];

v[4226]=v[210]*v[248]+v[208]*v[251];

v[4227]=v[208]*v[249]+v[210]*v[250];

v[4228]=v[216]*v[248]+v[213]*v[251];

v[4229]=v[213]*v[249]+v[216]*v[250];

v[241]=v[436];

for(i242=1;i242<=2;i242++){

 v[4203+i242]=0e0;

};/* end for */

v[243]=v[241];

if(i134==1){

 v[4203+i135]=1e0;

} else {

};

v[254]=v[4205];

v[256]=-(v[254]*v[437]);

v[439]=v[222]*v[256];
```

```
 v[257]=v[4204];

 v[438]=v[257]/v[255]+v[439];

 v[258]=v[438]/2e0;

 v[448]=2e0*v[258];



v[263]=(v[440]*(v[223]*v[261]*(v[257]+v[255]*v[439])+v[25
4]*(v[441]+v[442]))))/v[255];

 v[265]=-2e0*(-
(v[258]*v[264])+v[226]*(v[263]+v[438]))*v[443];

 v[266]=(v[160]-v[162])*v[183]+(v[164]-v[166])*v[186];

 v[267]=(v[161]-v[163])*v[183]+(v[165]-v[167])*v[186];

 v[268]=(v[160]-v[166])*v[184]+(v[162]-v[164])*v[185];

 v[269]=(v[161]-v[167])*v[184]+(v[163]-v[165])*v[185];

 v[270]=v[190]*v[266]-v[189]*v[267]-
v[188]*v[268]+v[187]*v[269];

 v[444]=v[270]*v[274];

 v[271]=v[269]/v[191]-v[190]*v[444];

 v[272]=v[186]*v[271];

 v[273]=v[183]*v[271];

 v[275]=-(v[268]/v[191])+v[189]*v[444];

 v[276]=v[186]*v[275];

 v[277]=v[183]*v[275];

 v[278]=-(v[267]/v[191])+v[188]*v[444];

 v[279]=v[184]*v[278];

 v[280]=v[185]*v[278];
```

```
v[281]=v[266]/v[191]-v[187]*v[444];

v[282]=v[184]*v[281];

v[283]=v[185]*v[281];

v[284]=v[273]+v[279];

v[285]=v[277]+v[282];

v[286]=-v[273]+v[280];

v[287]=-v[277]+v[283];

v[288]=v[272]-v[280];

v[289]=v[276]-v[283];

v[290]=-v[272]-v[279];

v[291]=-v[276]-v[282];


v[292]=v[147]*v[284]+v[149]*v[286]+v[151]*v[288]+v[153]*v
[290];
 v[311]=2e0*(1e0+v[217])*v[292];


v[293]=v[148]*v[284]+v[150]*v[286]+v[152]*v[288]+v[154]*v
[290];


v[294]=v[147]*v[285]+v[149]*v[287]+v[151]*v[289]+v[153]*v
[291];


v[295]=v[148]*v[285]+v[150]*v[287]+v[152]*v[289]+v[154]*v
[291];
 v[306]=2e0*(1e0+v[220])*v[295];
```

```
v[296]=v[311]/2e0;

v[297]=(v[294]*v[299]+v[293]*v[301])/2e0;

v[445]=v[297]*v[429]+v[228]*v[438];

v[298]=v[306]/2e0;

v[300]=v[293]*v[435]+v[299]*v[445];

v[302]=v[294]*v[435]+v[301]*v[445];

v[307]=v[234]*v[295]+v[446]*(v[265]*v[304]+v[233]*(v[263]
*v[305]+v[224]*(v[296]+v[306])
   +v[298]*v[434]+v[229]*v[448]));

v[312]=v[231]*v[292]+v[447]*(v[265]*v[309]+v[233]*(v[263]
*v[310]+v[224]*(v[298]+v[311])
   +v[296]*v[434]+v[227]*v[448]));


v[4230]=v[251]*v[284]+v[248]*v[285]+v[202]*v[300]+v[201]*
v[312];


v[4231]=v[249]*v[284]+v[250]*v[285]+v[201]*v[302]+v[202]*
v[307];


v[4232]=v[251]*v[286]+v[248]*v[287]+v[206]*v[300]+v[204]*
v[312];


v[4233]=v[249]*v[286]+v[250]*v[287]+v[204]*v[302]+v[206]*
v[307];
```

```
v[4234]=v[251]*v[288]+v[248]*v[289]+v[210]*v[300]+v[208]*

v[312];


v[4235]=v[249]*v[288]+v[250]*v[289]+v[208]*v[302]+v[210]*

v[307];


v[4236]=v[251]*v[290]+v[248]*v[291]+v[216]*v[300]+v[213]*

v[312];


v[4237]=v[249]*v[290]+v[250]*v[291]+v[213]*v[302]+v[216]*

v[307];

 for(i245=1;i245<=8;i245++){

  p[i245-

1]+=v[221]*v[4229+i245]+v[270]*v[4221+i245]*v[449];

 };/* end for */

};/* end for */

};

/****************** S U B R O U T I N E

*******************/

void SPP(double v[4269],ElementSpec *es,ElementData

*ed,NodeSpec **ns

     ,NodeData **nd,double *rdata,int *idata,double

**gpost,double **npost)

{
```

```
int i317,i318;

v[339]=nd[3]->at[1];

v[338]=nd[3]->at[0];

v[337]=nd[2]->at[1];

v[336]=nd[2]->at[0];

v[335]=nd[1]->at[1];

v[334]=nd[1]->at[0];

v[333]=nd[0]->at[1];

v[332]=nd[0]->at[0];

v[331]=nd[3]->X[1];

v[330]=nd[3]->X[0];

v[329]=nd[2]->X[1];

v[328]=nd[2]->X[0];

v[327]=nd[1]->X[1];

v[326]=nd[1]->X[0];

v[325]=nd[0]->X[1];

v[324]=nd[0]->X[0];

v[320]=es->Data[1];

v[450]=2e0*v[320];

v[322]=1e0/(1e0+v[320]);

v[319]=es->Data[0];

v[323]=(v[319]*v[322])/2e0;

v[451]=2e0*v[323];

v[321]=(v[323]*v[450])/(1e0-v[450]);

v[405]=1e0/(v[321]+v[451]);
```

```
v[403]=v[405]*v[451];

i317=(int)(es->id.NoIntPoints);

for(i318=1;i318<=i317;i318++){

 v[343]=es->IntPoints[4*(-1+i318)];

 v[352]=1e0-v[343];

 v[359]=-v[352]/4e0;

 v[350]=1e0+v[343];

 v[360]=-v[350]/4e0;

 v[344]=es->IntPoints[1+4*(-1+i318)];

 v[353]=1e0+v[344];

 v[361]=v[353]/4e0;

 v[348]=1e0-v[344];

 v[358]=-v[348]/4e0;

 v[362]=(v[324]-v[326])*v[358]+(v[328]-v[330])*v[361];

 v[363]=(v[325]-v[327])*v[358]+(v[329]-v[331])*v[361];

 v[364]=(v[324]-v[330])*v[359]+(v[326]-v[328])*v[360];

 v[365]=(v[325]-v[331])*v[359]+(v[327]-v[329])*v[360];

 v[366]=-(v[363]*v[364])+v[362]*v[365];

 v[368]=v[365]/v[366];

 v[386]=v[361]*v[368];

 v[378]=v[358]*v[368];

 v[369]=-(v[364]/v[366]);

 v[389]=v[361]*v[369];

 v[380]=v[358]*v[369];

 v[370]=-(v[363]/v[366]);
```

```
v[387]=v[359]*v[370];

v[382]=v[360]*v[370];

v[371]=v[362]/v[366];

v[390]=v[359]*v[371];

v[384]=v[360]*v[371];

v[376]=v[378]+v[387];

v[377]=v[380]+v[390];

v[379]=-v[378]+v[382];

v[381]=-v[380]+v[384];

v[383]=-v[382]+v[386];

v[385]=-v[384]+v[389];

v[388]=-v[386]-v[387];

v[391]=-v[389]-v[390];


v[392]=v[332]*v[376]+v[334]*v[379]+v[336]*v[383]+v[338]*v
[388];
 v[452]=2e0*v[392]+(v[392]*v[392]);


v[393]=v[333]*v[376]+v[335]*v[379]+v[337]*v[383]+v[339]*v
[388];


v[394]=v[332]*v[377]+v[334]*v[381]+v[336]*v[385]+v[338]*v
[391];

v[395]=v[333]*v[377]+v[335]*v[381]+v[337]*v[385]+v[339]*v
[391];
```

```
v[453]=2e0*v[395]+(v[395]*v[395]);

v[397]=v[452]/2e0;

v[398]=(v[393]+(1e0+v[393])*v[394])/2e0;

v[399]=v[453]/2e0;

v[401]=v[403]*(v[397]*v[451]+v[321]*(v[399]+v[452]));

v[402]=v[398]*v[451];

v[404]=v[403]*(v[399]*v[451]+v[321]*(v[397]+v[453]));

v[412]=-v[401]-v[404];

v[411]=v[412]/3e0;

gpost[i318-1][0]=v[401];

gpost[i318-1][1]=v[402];

gpost[i318-1][2]=v[402];

gpost[i318-1][3]=v[404];

gpost[i318-1][4]=v[397];

gpost[i318-1][5]=v[398];

gpost[i318-1][6]=v[398];

gpost[i318-1][7]=v[399];

gpost[i318-1][8]=-(v[321]*(v[397]+v[399])*v[405]);

gpost[i318-
1][9]=sqrt(0.15e1*(2e0*Power(v[402],2)+Power(v[401]+v[411
],2)+Power(v[404]+v[411],2)
  +Power(v[412],2)/9e0));

};/* end for */

npost[0][0]=v[332];

npost[1][0]=v[334];
```

```
npost[2][0]=v[336];

npost[3][0]=v[338];

npost[0][1]=v[333];

npost[1][1]=v[335];

npost[2][1]=v[337];

npost[3][1]=v[339];

npost[0][2]=v[332];

npost[1][2]=v[334];

npost[2][2]=v[336];

npost[3][2]=v[338];

npost[0][3]=v[333];

npost[1][3]=v[335];

npost[2][3]=v[337];

npost[3][3]=v[339];

};
```

APPENDIX C: LINEAR AceGEN CODE GENERATION

```
/**********************************************************

* AceGen    5.002 Windows (8 Mar 13)
*
*          Co. J. Korelc  2007            10 May 13
16:35:34*
**********************************************************

User        : Full professional version
Notebook    : Compliant Mechanisms Deformation Code (with
              both Linearities).nb
Evaluation time    : 14 s
Mode               : Optimal
Number of formulae : 309
Method             : Automatic
Subroutine         : SKR size :1124
Subroutine         : SSE size :2001
Subroutine         : SPP size :922
Total size of Mathematica code : 4047 subexpressions
Total size of C code           : 12313 bytes*/
#include "sms.h"

void SKR(double v[4269],ElementSpec *es,ElementData

*ed,NodeSpec **ns,NodeData **nd,double *rdata,int

*idata,double *p,double **s);

void SSE(double v[4269],ElementSpec *es,ElementData

*ed,NodeSpec **ns,NodeData **nd,double *rdata,int

*idata,double *p);
```

```
void SPP(double v[4269],ElementSpec *es,ElementData

*ed,NodeSpec **ns,NodeData **nd,double *rdata,int

*idata,double **gpost,double **npost);

int MMAInitialisationCode[]={

0,0

};

DLLEXPORT int SMTSetElSpec(ElementSpec *es,int *idata,int

ic,int ng)

{ int intc,nd,i;FILE *SMSFile;

  static int pn[11]={1, 2, 3, 4, 0, 1, 2, 3, 4, -1, 0};

  static int dof[4]={2, 2, 2, 2};

  static int nsto[4]={0, 0, 0, 0};

  static int ndat[4];

  static char *nid[]={"D","D","D","D"};

  static char *gdcs[]={"E -elastic modulus","$[Nu]$ -

Poisson ratio","t -thickness"};

  static double defd[]={21000e0,0.3e0,1e0,0e0};

  static char

*gpcs[]={"Sxx","Sxy","Syx","Syy","Exx","Exy",

                      "Eyx","Eyy","Ezz","Mises stress"};

  static char

*npcs[]={"DeformedMeshX","DeformedMeshY","u","v"};

  static char *sname[]={"E -elastic modulus","$[Nu]$ -

Poisson ratio"};

  static char *idname[]={""};
```

```
  static int idindex[1];

  static char *rdname[]={""};

  static char *cswitch[]={""};

  static int iswitch[1]={0};

  static double dswitch[1]={0e0};

  static int rdindex[1];

  static int nspecs[4];

  static double version[3]={3.001,3.001,7.};

  static double pnweights[4]={1e0,1e0,1e0,1e0};

  static double rnodes[12]={-1e0,-1e0,0e0,1e0,-1e0,0e0,

  1e0,1e0,0e0,-1e0,1e0,0e0};

  es->ReferenceNodes=rnodes;

  if(ng==-1) es->Data=defd;

  es->id.NoGroupData=3;

  es->Code=" CMsWithLinear";es->Version=version;

  es->MainTitle="";

  es->SubTitle="";

  es->SubSubTitle="$bold$Postprocessing$bold$:$n2$Sij -

Cauchy stress tensor$n2$Eij - Green-Lagrange strain

tensor.";

  es->Bibliography="";

  es->id.NoDimensions=2;es->id.NoDOFGlobal=8;es-
>id.NoDOFCondense=0;es->id.NoNodes=4;

  es->id.NoSegmentPoints=10;es->Segments=pn;es-
>PostNodeWeights=pnweights;
```

```
es->id.NoIntSwitch=0;es->IntSwitch=iswitch;es-
>id.DemoLimitation=0;

  es->id.NoDoubleSwitch=0;es->DoubleSwitch=dswitch;

  es->id.NoCharSwitch=0;es->CharSwitch=cswitch;

  es->DOFGlobal=dof;es->NodeID=nid;es-
>id.NoGPostData=10;es->id.NoNPostData=4;

  es->id.SymmetricTangent=1;es->id.CreateDummyNodes=0;es-
>id.PostIterationCall=0;

  es->Topology="Q1";es->GroupDataNames=gdcs;es-
>GPostNames=gpcs;es->NPostNames=npcs;

  es->AdditionalNodes="{}&";

  es->AdditionalGraphics="{}&";

  es->MMAInitialisation=MMAInitialisationCode;

  es->MMANextStep="";

  es->MMAStepBack="";

  es->MMAPreIteration="";

  es->IDataNames=idname;es->IDataIndex=idindex;es-
>RDataNames=rdname;es->RDataIndex=rdindex;

  es->id.NoIData=0;es->id.NoRData=0;

  es->id.ShapeSensitivity=1;es->id.NoSensNames=2;es-
>SensitivityNames=sname;es->NodeSpecs=nspecs;

  es->user.SPP=SPP;es->user.SSE=SSE;es->user.SKR=SKR;

  es->id.DefaultIntegrationCode=2;

  if(ic==-1){intc=2;} else {intc=ic;};

  es->id.IntCode=intc;
```

```
   SMTMultiIntPoints(&intc,idata,&es->id.NoIntPoints,

       &es->id.NoIntPointsA,&es->id.NoIntPointsB,&es-
>id.NoIntPointsC,0);

   es->id.NoAdditionalData=0;

   es->id.NoTimeStorage=0;

   es->id.NoElementData=0;

   nd=es-
>id.NoDimensions*idata[ID_NoShapeParameters];for(i=0;i<4;
i++)ndat[i]=nd;

   es->NoNodeStorage=nsto;es->NoNodeData=ndat;

   if(1){

    return 0;

   }else{

    return 1;

   };

};
/****************** S U B R O U T I N E

********************/

void SKR(double v[4269],ElementSpec *es,ElementData

*ed,NodeSpec **ns

     ,NodeData **nd,double *rdata,int *idata,double

*p,double **s)

{

int i3,i4,i97,i105,b1,b2,b101,b103;

v[53]=es->Data[2];
```

```
v[25]=nd[3]->at[1];

v[24]=nd[3]->at[0];

v[23]=nd[2]->at[1];

v[22]=nd[2]->at[0];

v[21]=nd[1]->at[1];

v[20]=nd[1]->at[0];

v[19]=nd[0]->at[1];

v[18]=nd[0]->at[0];

v[17]=nd[3]->X[1];

v[16]=nd[3]->X[0];

v[15]=nd[2]->X[1];

v[14]=nd[2]->X[0];

v[13]=nd[1]->X[1];

v[12]=nd[1]->X[0];

v[11]=nd[0]->X[1];

v[10]=nd[0]->X[0];

v[6]=es->Data[1];

v[380]=2e0*v[6];

v[8]=1e0/(1e0+v[6]);

v[5]=es->Data[0];

v[9]=(v[5]*v[8])/2e0;

v[99]=2e0*v[9];

v[7]=(v[380]*v[9])/(1e0-v[380]);

v[111]=2e0*v[7]+v[99];

v[89]=v[99]/(v[7]+v[99]);
```

```
b1=(int)(idata[ID_SkipResidual])==1;

b2=(int)(idata[ID_SkipTangent])==1;

i3=(int)(es->id.NoIntPoints);

for(i4=1;i4<=i3;i4++){

 v[29]=es->IntPoints[4*(-1+i4)];

 v[38]=1e0-v[29];

 v[45]=-v[38]/4e0;

 v[36]=1e0+v[29];

 v[46]=-v[36]/4e0;

 v[30]=es->IntPoints[1+4*(-1+i4)];

 v[39]=1e0+v[30];

 v[47]=v[39]/4e0;

 v[34]=1e0-v[30];

 v[44]=-v[34]/4e0;

 v[48]=(v[10]-v[12])*v[44]+(v[14]-v[16])*v[47];

 v[49]=(v[11]-v[13])*v[44]+(v[15]-v[17])*v[47];

 v[50]=(v[10]-v[16])*v[45]+(v[12]-v[14])*v[46];

 v[51]=(v[11]-v[17])*v[45]+(v[13]-v[15])*v[46];

 v[52]=-(v[49]*v[50])+v[48]*v[51];

 v[54]=v[51]/v[52];

 v[72]=v[47]*v[54];

 v[64]=v[44]*v[54];

 v[55]=-(v[50]/v[52]);

 v[75]=v[47]*v[55];

 v[66]=v[44]*v[55];
```

```
v[56]=-(v[49]/v[52]);

v[73]=v[45]*v[56];

v[68]=v[46]*v[56];

v[57]=v[48]/v[52];

v[76]=v[45]*v[57];

v[70]=v[46]*v[57];

v[62]=v[64]+v[73];

v[63]=v[66]+v[76];

v[65]=-v[64]+v[68];

v[67]=-v[66]+v[70];

v[69]=-v[68]+v[72];

v[71]=-v[70]+v[75];

v[74]=-v[72]-v[73];

v[4252]=v[62];

v[4253]=0e0;

v[4254]=v[65];

v[4255]=0e0;

v[4256]=v[69];

v[4257]=0e0;

v[4258]=v[74];

v[4259]=0e0;

v[77]=-v[75]-v[76];

v[4244]=0e0;

v[4245]=v[63];

v[4246]=0e0;
```

```
v[4247]=v[67];

v[4248]=0e0;

v[4249]=v[71];

v[4250]=0e0;

v[4251]=v[77];

v[4232]=v[63];

v[4233]=v[62];

v[4234]=v[67];

v[4235]=v[65];

v[4236]=v[71];

v[4237]=v[69];

v[4238]=v[77];

v[4239]=v[74];

v[82]=es->IntPoints[(-1+4*i4)]*v[52]*v[53];

v[83]=v[18]*v[62]+v[20]*v[65]+v[22]*v[69]+v[24]*v[74];

v[381]=2e0*v[83];

v[84]=(v[19]*v[62]+v[18]*v[63]+v[21]*v[65]+v[20]*v[67]+v[

23]*v[69]+v[22]*v[71]+v[25]*v[74]

 +v[24]*v[77])/2e0;

v[85]=v[19]*v[63]+v[21]*v[67]+v[23]*v[71]+v[25]*v[77];

v[382]=2e0*v[85];

v[87]=v[89]*(v[7]*(v[381]+v[85])+v[381]*v[9]);

v[90]=v[89]*(v[7]*(v[382]+v[83])+v[382]*v[9]);

v[4216]=v[62]*v[87];

v[4217]=v[63]*v[90];
```

```
v[4218]=v[65]*v[87];

v[4219]=v[67]*v[90];

v[4220]=v[69]*v[87];

v[4221]=v[71]*v[90];

v[4222]=v[74]*v[87];

v[4223]=v[77]*v[90];

for(i97=1;i97<=8;i97++){

 v[113]=v[4231+i97];

 v[386]=v[113]*v[99];

 v[108]=v[4243+i97]*v[82];

 v[109]=v[4251+i97]*v[82];

 v[110]=(v[108]*v[111]+v[109]*v[7])*v[89];

 v[112]=(v[109]*v[111]+v[108]*v[7])*v[89];

 v[4260]=v[112]*v[62];

 v[4261]=v[110]*v[63];

 v[4262]=v[112]*v[65];

 v[4263]=v[110]*v[67];

 v[4264]=v[112]*v[69];

 v[4265]=v[110]*v[71];

 v[4266]=v[112]*v[74];

 v[4267]=v[110]*v[77];

 if(!(b1)){

  p[i97-1]+=v[82]*(v[4215+i97]+v[386]*v[84]);

 } else {

 };
```

```
  if(b2){

   continue;

  } else {

  };

  for(i105=i97;i105<=8;i105++){

   s[i97-1][i105-

1]+=v[4259+i105]+(v[386]*v[4231+i105]*v[82])/2e0;

  };/* end for */

 };/* end for */

};/* end for */

};

/****************** S U B R O U T I N E

********************/

void SSE(double v[4269],ElementSpec *es,ElementData

*ed,NodeSpec **ns

    ,NodeData **nd,double *rdata,int *idata,double *p)

{

int i116,i117,i118,i120,i121,i225,i228,b142,b227;

v[206]=es->Data[1];

v[239]=1e0-2e0*v[206];

v[233]=1e0+v[206];

v[205]=es->Data[0];

v[388]=v[205]/v[233];

v[238]=v[206]*v[388];

v[209]=v[388]/2e0;
```

```
v[230]=v[388];

v[207]=v[238]/v[239];

v[242]=v[207]+v[230];

v[216]=(2e0*v[209])/v[242];

v[175]=es->Data[2];

v[137]=nd[3]->at[1];

v[136]=nd[3]->at[0];

v[135]=nd[2]->at[1];

v[134]=nd[2]->at[0];

v[133]=nd[1]->at[1];

v[132]=nd[1]->at[0];

v[131]=nd[0]->at[1];

v[130]=nd[0]->at[0];

v[129]=nd[3]->X[1];

v[128]=nd[3]->X[0];

v[127]=nd[2]->X[1];

v[126]=nd[2]->X[0];

v[125]=nd[1]->X[1];

v[124]=nd[1]->X[0];

v[123]=nd[0]->X[1];

v[122]=nd[0]->X[0];

i116=(int)(idata[ID_SensIndex]);

i117=(int)(es->SensType[i116-1]);

i118=(int)(es->SensTypeIndex[i116-1]);

i120=(int)(es->id.NoIntPoints);
```

```
for(i121=1;i121<=i120;i121++){

 if(i117==2){

  v[143]=nd[0]->Data[(-1+i118)*idata[ID_NoDimensions]];

  v[144]=nd[0]->Data[1+(-1+i118)*idata[ID_NoDimensions]];

  v[145]=nd[1]->Data[(-1+i118)*idata[ID_NoDimensions]];

  v[146]=nd[1]->Data[1+(-1+i118)*idata[ID_NoDimensions]];

  v[147]=nd[2]->Data[(-1+i118)*idata[ID_NoDimensions]];

  v[148]=nd[2]->Data[1+(-1+i118)*idata[ID_NoDimensions]];

  v[149]=nd[3]->Data[(-1+i118)*idata[ID_NoDimensions]];

  v[150]=nd[3]->Data[1+(-1+i118)*idata[ID_NoDimensions]];

 } else {

  v[143]=0e0;

  v[144]=0e0;

  v[145]=0e0;

  v[146]=0e0;

  v[147]=0e0;

  v[148]=0e0;

  v[149]=0e0;

  v[150]=0e0;

 };

 v[151]=es->IntPoints[4*(-1+i121)];

 v[160]=1e0-v[151];

 v[167]=-v[160]/4e0;

 v[158]=1e0+v[151];

 v[168]=-v[158]/4e0;
```

```
v[152]=es->IntPoints[1+4*(-1+i121)];

v[161]=1e0+v[152];

v[169]=v[161]/4e0;

v[156]=1e0-v[152];

v[166]=-v[156]/4e0;

v[154]=es->IntPoints[3+4*(-1+i121)];

v[397]=v[154]*v[175];

v[170]=(v[122]-v[124])*v[166]+(v[126]-v[128])*v[169];

v[171]=(v[123]-v[125])*v[166]+(v[127]-v[129])*v[169];

v[172]=(v[122]-v[128])*v[167]+(v[124]-v[126])*v[168];

v[173]=(v[123]-v[129])*v[167]+(v[125]-v[127])*v[168];

v[174]=-(v[171]*v[172])+v[170]*v[173];

v[252]=1e0/Power(v[174],2);

v[176]=v[173]/v[174];

v[194]=v[169]*v[176];

v[186]=v[166]*v[176];

v[177]=-(v[172]/v[174]);

v[197]=v[169]*v[177];

v[188]=v[166]*v[177];

v[178]=-(v[171]/v[174]);

v[195]=v[167]*v[178];

v[190]=v[168]*v[178];

v[179]=v[170]/v[174];

v[198]=v[167]*v[179];

v[192]=v[168]*v[179];
```

```
v[184]=v[186]+v[195];

v[185]=v[188]+v[198];

v[187]=-v[186]+v[190];

v[189]=-v[188]+v[192];

v[191]=-v[190]+v[194];

v[193]=-v[192]+v[197];

v[196]=-v[194]-v[195];

v[199]=-v[197]-v[198];

v[4238]=v[185];

v[4239]=v[184];

v[4240]=v[189];

v[4241]=v[187];

v[4242]=v[193];

v[4243]=v[191];

v[4244]=v[199];

v[4245]=v[196];

v[204]=v[174]*v[397];


v[210]=v[130]*v[184]+v[132]*v[187]+v[134]*v[191]+v[136]*v
[196];

v[390]=2e0*v[210];

v[211]=(v[131]*v[184]+v[130]*v[185]+v[133]*v[187]+v[132]*
v[189]+v[135]*v[191]+v[134]*v[193]

  +v[137]*v[196]+v[136]*v[199])/2e0;

v[398]=v[211]*v[230];
```

```
v[212]=v[131]*v[185]+v[133]*v[189]+v[135]*v[193]+v[137]*v
[199];
 v[389]=2e0*v[212];
 v[276]=v[210]+v[389];
 v[275]=v[207]*v[276]+v[209]*v[389];
 v[273]=v[212]+v[390];
 v[272]=v[207]*v[273]+v[209]*v[390];
 v[214]=v[216]*v[272];
 v[217]=v[216]*v[275];
 v[4222]=v[184]*v[214];
 v[4223]=v[185]*v[217];
 v[4224]=v[187]*v[214];
 v[4225]=v[189]*v[217];
 v[4226]=v[191]*v[214];
 v[4227]=v[193]*v[217];
 v[4228]=v[196]*v[214];
 v[4229]=v[199]*v[217];
 for(i225=1;i225<=2;i225++){
  v[4203+i225]=0e0;
 };/* end for */
 v[226]=v[224];
 if(i117==1){
  v[4203+i118]=1e0;
 } else {
```

```
  };

  v[232]=v[4205];

  v[234]=-(v[232]/Power(v[233],2));

  v[392]=v[205]*v[234];

  v[235]=v[4204];

  v[391]=v[235]/v[233]+v[392];

  v[236]=v[391]/2e0;

  v[237]=v[391];

v[241]=(v[232]*(2e0*v[233]*v[238]+v[205]*v[239])+v[206]*v

[239]*(v[235]+v[233]*v[392]))/

   (v[233]*Power(v[239],2));

  v[243]=(-2e0*(v[209]*(v[237]+v[241])-

v[236]*v[242]))/Power(v[242],2);

  v[244]=(v[143]-v[145])*v[166]+(v[147]-v[149])*v[169];

  v[245]=(v[144]-v[146])*v[166]+(v[148]-v[150])*v[169];

  v[246]=(v[143]-v[149])*v[167]+(v[145]-v[147])*v[168];

  v[247]=(v[144]-v[150])*v[167]+(v[146]-v[148])*v[168];

  v[248]=v[173]*v[244]-v[172]*v[245]-

v[171]*v[246]+v[170]*v[247];

  v[393]=v[248]*v[252];

  v[249]=v[247]/v[174]-v[173]*v[393];

  v[250]=v[169]*v[249];

  v[251]=v[166]*v[249];

  v[253]=-(v[246]/v[174])+v[172]*v[393];

  v[254]=v[169]*v[253];
```

```
v[255]=v[166]*v[253];

v[256]=-(v[245]/v[174])+v[171]*v[393];

v[257]=v[167]*v[256];

v[258]=v[168]*v[256];

v[259]=v[244]/v[174]-v[170]*v[393];

v[260]=v[167]*v[259];

v[261]=v[168]*v[259];

v[262]=v[251]+v[257];

v[263]=v[255]+v[260];

v[264]=-v[251]+v[258];

v[265]=-v[255]+v[261];

v[266]=v[250]-v[258];

v[267]=v[254]-v[261];

v[268]=-v[250]-v[257];

v[269]=-v[254]-v[260];

v[4254]=v[263];

v[4255]=v[262];

v[4256]=v[265];

v[4257]=v[264];

v[4258]=v[267];

v[4259]=v[266];

v[4260]=v[269];

v[4261]=v[268];

v[270]=v[130]*v[262]+v[132]*v[264]+v[134]*v[266]+v[136]*v
[268];
```

```
 v[394]=2e0*v[270];



v[271]=v[131]*v[263]+v[133]*v[265]+v[135]*v[267]+v[137]*v
[269];
 v[395]=2e0*v[271];
v[274]=v[243]*v[272]+v[216]*(v[241]*v[273]+v[236]*v[390]+
v[209]*v[394]+v[207]*(v[271]+v[394]));
v[277]=v[243]*v[275]+v[216]*(v[241]*v[276]+v[236]*v[389]+
v[209]*v[395]+v[207]*(v[270]+v[395]));
 v[4246]=v[214]*v[262]+v[184]*v[274];
 v[4247]=v[217]*v[263]+v[185]*v[277];
 v[4248]=v[214]*v[264]+v[187]*v[274];
 v[4249]=v[217]*v[265]+v[189]*v[277];
 v[4250]=v[214]*v[266]+v[191]*v[274];
 v[4251]=v[217]*v[267]+v[193]*v[277];
 v[4252]=v[214]*v[268]+v[196]*v[274];
 v[4253]=v[217]*v[269]+v[199]*v[277];
 for(i228=1;i228<=8;i228++){
  v[279]=v[4237+i228];
  p[i228-
1]+=v[248]*v[397]*(v[279]*v[398]+v[4221+i228])+v[204]*((v
[211]*v[237]+v[209]*
(v[131]*v[262]+v[130]*v[263]+v[133]*v[264]+v[132]*v[265]+
v[135]*v[266]+v[134]*v[267]+v[137]*v[268]+v[136]*v[269]))
*v[279]+v[4245+i228]+v[398]*v[4253+i228]);
```

```
 };/* end for */

};/* end for */

};

/****************** S U B R O U T I N E

********************/

void SPP(double v[4269],ElementSpec *es,ElementData

*ed,NodeSpec **ns

     ,NodeData **nd,double *rdata,int *idata,double

**gpost,double **npost)

{

int i282,i283;

v[304]=nd[3]->at[1];

v[303]=nd[3]->at[0];

v[302]=nd[2]->at[1];

v[301]=nd[2]->at[0];

v[300]=nd[1]->at[1];

v[299]=nd[1]->at[0];

v[298]=nd[0]->at[1];

v[297]=nd[0]->at[0];

v[296]=nd[3]->X[1];

v[295]=nd[3]->X[0];

v[294]=nd[2]->X[1];

v[293]=nd[2]->X[0];

v[292]=nd[1]->X[1];

v[291]=nd[1]->X[0];
```

```
v[290]=nd[0]->X[1];

v[289]=nd[0]->X[0];

v[285]=es->Data[1];

v[402]=2e0*v[285];

v[287]=1e0/(1e0+v[285]);

v[284]=es->Data[0];

v[288]=(v[284]*v[287])/2e0;

v[403]=2e0*v[288];

v[286]=(v[288]*v[402])/(1e0-v[402]);

v[370]=1e0/(v[286]+v[403]);

v[368]=v[370]*v[403];

i282=(int)(es->id.NoIntPoints);

for(i283=1;i283<=i282;i283++){

 v[308]=es->IntPoints[4*(-1+i283)];

 v[317]=1e0-v[308];

 v[324]=-v[317]/4e0;

 v[315]=1e0+v[308];

 v[325]=-v[315]/4e0;

 v[309]=es->IntPoints[1+4*(-1+i283)];

 v[318]=1e0+v[309];

 v[326]=v[318]/4e0;

 v[313]=1e0-v[309];

 v[323]=-v[313]/4e0;

 v[327]=(v[289]-v[291])*v[323]+(v[293]-v[295])*v[326];

 v[328]=(v[290]-v[292])*v[323]+(v[294]-v[296])*v[326];
```

```
v[329]=(v[289]-v[295])*v[324]+(v[291]-v[293])*v[325];

v[330]=(v[290]-v[296])*v[324]+(v[292]-v[294])*v[325];

v[331]=-(v[328]*v[329])+v[327]*v[330];

v[333]=v[330]/v[331];

v[351]=v[326]*v[333];

v[343]=v[323]*v[333];

v[334]=-(v[329]/v[331]);

v[354]=v[326]*v[334];

v[345]=v[323]*v[334];

v[335]=-(v[328]/v[331]);

v[352]=v[324]*v[335];

v[347]=v[325]*v[335];

v[336]=v[327]/v[331];

v[355]=v[324]*v[336];

v[349]=v[325]*v[336];

v[341]=v[343]+v[352];

v[342]=v[345]+v[355];

v[344]=-v[343]+v[347];

v[346]=-v[345]+v[349];

v[348]=-v[347]+v[351];

v[350]=-v[349]+v[354];

v[353]=-v[351]-v[352];

v[356]=-v[354]-v[355];
```

```
v[362]=v[297]*v[341]+v[299]*v[344]+v[301]*v[348]+v[303]*v
[353];
 v[404]=2e0*v[362];
v[363]=(v[298]*v[341]+v[297]*v[342]+v[300]*v[344]+v[299]*
v[346]+v[302]*v[348]+v[301]*v[350]
  +v[304]*v[353]+v[303]*v[356])/2e0;


v[364]=v[298]*v[342]+v[300]*v[346]+v[302]*v[350]+v[304]*v
[356];
 v[405]=2e0*v[364];
 v[366]=v[368]*(v[288]*v[404]+v[286]*(v[364]+v[404]));
 v[367]=v[363]*v[403];
 v[369]=v[368]*(v[288]*v[405]+v[286]*(v[362]+v[405]));
 v[377]=-v[366]-v[369];
 v[376]=v[377]/3e0;
 gpost[i283-1][0]=v[366];
 gpost[i283-1][1]=v[367];
 gpost[i283-1][2]=v[367];
 gpost[i283-1][3]=v[369];
 gpost[i283-1][4]=v[362];
 gpost[i283-1][5]=v[363];
 gpost[i283-1][6]=v[363];
 gpost[i283-1][7]=v[364];
 gpost[i283-1][8]=-(v[286]*(v[362]+v[364])*v[370]);
```

```
 gpost[i283-

1][9]=sqrt(0.15e1*(2e0*Power(v[367],2)+Power(v[366]+v[376

],2)+Power(v[369]+v[376],2)

  +Power(v[377],2)/9e0));

};/* end for */

npost[0][0]=v[297];

npost[1][0]=v[299];

npost[2][0]=v[301];

npost[3][0]=v[303];

npost[0][1]=v[298];

npost[1][1]=v[300];

npost[2][1]=v[302];

npost[3][1]=v[304];

npost[0][2]=v[297];

npost[1][2]=v[299];

npost[2][2]=v[301];

npost[3][2]=v[303];

npost[0][3]=v[298];

npost[1][3]=v[300];

npost[2][3]=v[302];

npost[3][3]=v[304]; };
```

APPENDIX D: AceFEM CODE FOR FEA OF CBMM

```
<< AceFEM`;

Ydisp = 5.000;

SMTInputData[];

SMTAddDomain["A", "CMsWithHyperelasticity", {"E *" ->
165.0*10^3(*N/mm^2*),

 "ν*" -> 0.4995, "t*" -> 3.5}];

SMTAddEssentialBoundary[Line[{{0.0000, 40.000}, {44.000,
40.000}}], 1 -> 0, 2 -> 0];

SMTAddEssentialBoundary[Line[{{0.0000, 93.000}, {44.000,
93.000}}], 1 -> 0, 2 -> 0];

SMTAddEssentialBoundary[Line[{{1293.700, 40.000},
{1337.700, 40.000}}], 1 -> 0, 2->0];

SMTAddEssentialBoundary[Line[{{1293.700, 93.000},
{1337.700, 93.000}}], 1 -> 0, 2->0];

SMTAddEssentialBoundary[Line[{{468.800, 107.200},
{868.800, 107.200}}], 2 -> -Ydisp];


(*Left Lower Anchor*)

SMTMesh["A", "Q1", {20, 20}, {{{44.000, 0.0000}, {44.000,
40.000}}, {{0.0000, 0.0000}, {0.0000, 40.000}}},
"InterpolationOrder" -> 4];
```

```
(*Right Lower Anchor*)

SMTMesh["A", "Q1", {20, 20}, {{{1337.7000, 0.0000},

{1337.700, 40.000}}, {{1293.700, 0.0000}, {1293.700,

40.000}}}, "InterpolationOrder" -> 4];


(*Left Upper Anchor*)

SMTMesh["A", "Q1", {20, 20}, {{{44.000, 93.000}, {44.000,

133.000}}, {{0.0000, 93.000}, {0.0000, 133.000}}},

"InterpolationOrder" -> 4];

(*Right Upper Anchor*)

SMTMesh["A", "Q1", {20, 20}, {{{1337.700, 93.000},

{1337.700, 133.000}}, {{1293.700, 93.000}, {1293.7000,

133.000}}}, "InterpolationOrder" -> 4];


(*Left Side Beam*)

SMTMesh["A", "Q1", {20, 20}, {{{24.000, 40.000}, {24.000,

65.500}}, {{20.000, 40.000}, {20.00, 65.500}}},

"InterpolationOrder" -> 4];

SMTMesh["A", "Q1", {20, 20}, {{{24.000, 65.500}, {24.000,

67.500}}, {{20.000, 65.500}, {20.000, 67.500}}},

"InterpolationOrder" -> 4];

SMTMesh["A", "Q1", {20, 20}, {{{24.000, 67.500}, {24.000,

93.000}}, {{20.000, 67.500}, {20.000, 93.000}}},

"InterpolationOrder" -> 4];
```

```
(*Right Side Beam*)

SMTMesh["A", "Q1", {20, 20}, {{{1317.700, 40.000},

{1317.700, 65.500}}, {{1313.700, 40.000}, {1313.700,

65.500}}}, "InterpolationOrder" -> 4];

SMTMesh["A", "Q1", {20, 20}, {{{1317.700, 65.500},

{1317.700, 67.500}}, {{1313.700, 65.500}, {1313.700,

67.500}}}, "InterpolationOrder" -> 4];

SMTMesh["A", "Q1", {20, 20}, {{{1317.7000, 67.500},

{1317.700, 93.000}}, {{1313.700, 67.500}, {1313.700,

93.000}}}, "InterpolationOrder" -> 4];


(*Left Outer Elastic Hinge*)

SMTMesh["A", "Q1", {20, 20}, {{{54.000, 66.300}, {54.000,

68.300}}, {{24.000, 65.500}, {24.000, 67.500}}},

"InterpolationOrder" -> 4];

(*Right Outer Elastic Hinge*)

SMTMesh["A", "Q1", {20, 20}, {{{1313.700, 65.500},

{1313.700, 67.500}}, {{1283.700, 66.300}, {1283.700,

68.300}}}, "InterpolationOrder" -> 4];


(*Left Coupler Link*)

SMTMesh["A", "Q1", {20, 20}, {{{438.900, 71.400},

{438.900, 76.400}}, {{54.000, 61.300}, {54.000,

66.300}}}, "InterpolationOrder" -> 4];
```

```
SMTMesh["A", "Q1", {20, 20}, {{{438.900, 76.400},

{438.900, 78.400}}, {{54.000, 66.300}, {54.000,

68.300}}}, "InterpolationOrder" -> 4];

SMTMesh["A", "Q1", {20, 20}, {{{438.900, 78.400},

{438.900, 83.400}}, {{54.000, 68.300}, {54.000,

73.300}}}, "InterpolationOrder" -> 4];


(*Right Coupler Link*)

SMTMesh["A", "Q1", {20, 20}, {{{1283.7000, 61.300},

{1283.700, 66.300}}, {{898.800, 71.400}, {898.800,

76.400}}}, "InterpolationOrder" -> 4];

SMTMesh["A", "Q1", {20, 20}, {{{1283.700, 66.300},

{1283.700, 68.300}}, {{898.800, 76.400}, {898.800,

78.400}}}, "InterpolationOrder" -> 4];

SMTMesh["A", "Q1", {20, 20}, {{{1283.700, 68.300},

{1283.700, 73.300}}, {{898.800, 78.400}, {898.800,

83.400}}}, "InterpolationOrder" -> 4];


(*Left Inner Elastic Hinge*)

SMTMesh["A", "Q1", {20, 20}, {{{468.800, 77.100},

{468.800, 79.100}}, {{438.900, 76.400}, {438.900,

78.400}}}, "InterpolationOrder" -> 4];

(*Right Inner Elastic Hinge*)
```

```
SMTMesh["A", "Q1", {20, 20}, {{{898.800, 76.400},
{898.800, 78.400}}, {{868.800, 77.100}, {868.800,
79.100}}}, "InterpolationOrder" -> 4];


(*Central Mass*)

SMTMesh["A", "Q1", {20, 20}, {{{868.800, 49.300},
{868.800, 77.100}}, {{468.800, 49.300}, {468.800,
77.100}}}, "InterpolationOrder" -> 4];

SMTMesh["A", "Q1", {20, 20}, {{{868.800, 77.100},
{868.800, 79.100}}, {{468.800, 77.100}, {468.800,
79.100}}}, "InterpolationOrder" -> 4];

SMTMesh["A", "Q1", {20, 20}, {{{868.800, 79.100},
{868.800, 107.200}}, {{468.800, 79.100}, {468.800,
107.200}}}, "InterpolationOrder" -> 4];

SMTAnalysis[];

SMTNextStep[1, 0.1];

While[While[step = SMTConvergence[10^(-8), 15, {Adaptive,
8, 0.01, 0.5, 1}], SMTNewtonIteration[]; ]; If[
!step[[1]],

        SMTShowMesh[DeformedMesh -> True, Field -> v,
Mesh -> False,

            Show -> Window | {Animation, Bending},
            BoundaryConditions -> True];

    If[step[[4]] === MinBound,

        SMTStatusReport[Error: Δλ < Δλmin]; ]; step[[3]],
```

```
      If[step[[1]], SMTStepBack[]; ]; SMTNextStep[1,

step[[2]]]];
```

APPENDIX E: AceFEM CODE FOR FEA OF CMA

```
<<AceFEM`;

Xdisp=0.1200; (*2 micrometer*)

SMTInputData[];

SMTAddDomain["A","CompMechAmpHyper",{"E

*"→1.034*10^9(*N/m^2*),"ν *"→0.4995, t*"→10.000}];

SMTAddEssentialBoundary[Line[{{0.000,0.000},{65.000,0.000

}}],1->0,2->0];

SMTAddEssentialBoundary[Line[{{0.000,5.000},{65.000,5.000

}}],1->0,2->0];

SMTAddEssentialBoundary[Line[{{9.500,9.000},{9.500,14.00}

}],1→-Xdisp];

SMTAddEssentialBoundary[Line[{{55.500,9.000},{55.500,14.0

0}}],1→Xdisp];


(*Base*)
SMTMesh["A","Q1",{20,20},{{{0.0,0.0},{65.0,0.0}},{{0.0,5.

0},{65.0,5.0}}},"InterpolationOrder"→4];


(*Left Column*)
SMTMesh["A","Q1",{20,20},{{{5.000,6.000},{5.000,10.500}},

{{0.000,6.000},{0.000,10.500}}},"InterpolationOrder"→4];
```

```
SMTMesh["A","Q1",{20,20},{{{5.000,10.500},{5.000,12.500}}

,{{0.000,10.500},{0.000,12.500}}},"InterpolationOrder"→4]

;

SMTMesh["A","Q1",{20,20},{{{5.000,12.500},{5.000,17.850}}

,{{0.000,12.500},{0.000,17.850}}},"InterpolationOrder"→4]

;

SMTMesh["A","Q1",{20,20},{{{5.000,17.850},{5.000,18.250}}

,{{0.000,17.850},{0.000,18.250}}},"InterpolationOrder"→4]

;

SMTMesh["A","Q1",{20,20},{{{5.000,18.250},{5.000,20.600}}

,{{0.000,18.250},{0.000,20.600}}},"InterpolationOrder"→4]

;

SMTMesh["A","Q1",{20,20},{{{5.000,20.600},{5.000,21.000}}

,{{0.000,20.600},{0.000,21.000}}},"InterpolationOrder"→4]

;

SMTMesh["A","Q1",{20,20},{{{5.000,21.000},{5.000,22.000}}

,{{0.000,21.000},{0.000,22.000}}},"InterpolationOrder"→4]

;


(*Right Column*)

SMTMesh["A","Q1",{20,20},{{{65.000,6.000},{65.000,10.500}

},{{60.000,6.000},{60.000,10.500}}},"InterpolationOrder"→

4];
```

```
SMTMesh["A","Q1",{20,20},{{{65.000,10.500},{65.000,12.500
}},{{60.000,10.500},{60.000,12.500}}},"InterpolationOrder
"→4];

SMTMesh["A","Q1",{20,20},{{{65.000,12.500},{65.000,17.850
}},{{60.000,12.500},{60.000,17.850}}},"InterpolationOrder
"→4];

SMTMesh["A","Q1",{20,20},{{{65.000,17.850},{65.000,18.250
}},{{60.000,17.850},{60.000,18.250}}},"InterpolationOrder
"→4];

SMTMesh["A","Q1",{20,20},{{{65.000,18.250},{65.000,20.600
}},{{60.000,18.250},{60.000,20.600}}},"InterpolationOrder
"→4];

SMTMesh["A","Q1",{20,20},{{{65.000,20.600},{65.000,21.000
}},{{60.000,20.600},{60.000,21.000}}},"InterpolationOrder
"→4];

SMTMesh["A","Q1",{20,20},{{{65.000,21.000},{65.000,22.000
}},{{60.000,21.000},{60.000,22.000}}},"InterpolationOrder
"→4];


(*Left Input Beam*)
SMTMesh["A","Q1",{20,20},{{{9.500,9.000},{9.500,10.500},{
9.500,12.500},{9.500,14.000}},{{6.000,9.000},{6.000,10.50
0},{6.000,12.500},{6.000,14.000}}},"InterpolationOrder"→4
];
```

(*Right Input Beam*)

SMTMesh["A","Q1",{20,20},{{{59.000,9.000},{59.000,10.500}

,{59.000,12.500},{59.000,14.000}},{{55.500,9.000},{55.500

,10.500},{55.500,12.500},{55.500,14.000}}},"Interpolation

Order"→4];

(*Shuttle*)

SMTMesh["A","Q1",{20,20},{{{37.500,12.000},{37.500,13.850

},{37.500,14.250},{37.500,16.600},{37.500,17.000},{37.500

,19.000}},{{27.500,12.000},{27.500,13.850},{27.500,14.250

},{27.500,16.600},{27.500,17.000},{27.500,19.000}}},"Inte

rpolationOrder"→4];

(*Left Outer Flexible links*)

SMTMesh["A","Q1",{20,20},{{{5.000,20.600},{8.000,20.067}}

,{{5.000,21.000},{8.000,20.467}}},"InterpolationOrder"→4]

;

SMTMesh["A","Q1",{20,20},{{{5.000,17.850},{8.000,17.317}}

,{{5.000,18.250},{8.000,17.717}}},"InterpolationOrder"→4]

;

(*Right Outer Flexible links*)

SMTMesh["A","Q1",{20,20},{{{57.000,20.067},{60.000,20.600

}},{{57.000,20.467},{60.000,21.000}}},"InterpolationOrder

"→4];

```
SMTMesh["A","Q1",{20,20},{{{57.000,17.317},{60.000,17.85}
},{{57.000,17.717},{60.000,18.250}}},"InterpolationOrder"
→4];
```

```
(*Left Rigid links*)
SMTMesh["A","Q1",{20,20},{{{24.500,13.458},{24.500,14.383
},{24.500,14.783},{24.500,15.708}},{{8.000,16.392},{8.000
,17.317},{8.000,17.717},{8.000,18.642}}},"InterpolationOr
der"→4];
SMTMesh["A","Q1",{20,20},{{{24.500,16.208},{24.500,17.133
},{24.500,17.533},{24.500,18.458}},{{8.000,19.142},{8.000
,20.067},{8.000,20.467},{8.000,21.392}}},"InterpolationOr
der"→4];
```

```
(*Right Rigid links*)
SMTMesh["A","Q1",{20,20},{{{57.000,16.392},{57.000,17.317
},{57.000,17.717},{57.000,18.642}},{{40.500,13.458},{40.5
00,14.383},{40.500,14.783},{40.500,15.708}}},"Interpolati
onOrder"→4];
SMTMesh["A","Q1",{20,20},{{{57.000,19.142},{57.000,20.067
},{57.000,20.467},{57.000,21.392}},{{40.500,16.208},{40.5
00,17.133},{40.500,17.533},{40.500,18.458}}},"Interpolati
onOrder"→4];
```

```
(*Left Inner Flexible links*)

SMTMesh["A","Q1",{20,20},{{{27.500,13.850},{27.500,14.250
}},{{24.500,14.383},{24.500,14.783}}},

"InterpolationOrder"→4];

SMTMesh["A","Q1",{20,20},{{{27.500,16.600},{27.500,17.000
}},{{24.500,17.133},{24.500,17.533}}},"InterpolationOrder
"→4];


(*Right Inner Flexible links*)

SMTMesh["A","Q1",{20,20},{{{40.500,14.383},{40.500,14.783
}},{{37.500,13.850},{37.500,14.250}}},"InterpolationOrder
"→4];

SMTMesh["A","Q1",{20,20},{{{40.500,17.133},{40.500,17.533
}},{{37.500,16.600},{37.500,17.000}}},"InterpolationOrder
"→4];


(*Upper Left Flexure Hinge*)

SMTMesh["A","Q1",{10,10},{{{5.000,12.500},{5.004,12.438},
{5.016,12.375},


{5.036,12.312},{5.067,12.250},{5.110,12.188},{5.169,12.12
5},{5.258,12.062},{5.499,12.000},{5.501,12.000},{5.742,12
.062},{5.831,12.125},{5.890,12.188},{5.933,12.250},{5.964
,12.312},{5.984,12.375},{5.966,12.438},{6.000,12.500}},{{
5.000,10.500},{5.004,10.562},{5.016,10.625},{5.036,10.688
```

},{5.067,10.750},{5.110,10.812},{5.169,10.875},{5.258,10.

938},{5.499,11.000},{5.501,11.000},{5.742,10.938},{5.831,

10.875},{5.890,10.812},{5.933,10.750},{5.964,10.688},{5.9

84,10.665},{5.966,10.562},{6.000,10.500}}},"Interpolation

Order"→4];

(*Upper Left Flexure Hinge*)

SMTMesh["A","Q1",{10,10},{{{59.000,12.500},{59.004,12.438

},{59.016,12.375},

{59.036,12.312},{59.067,12.250},{59.110,12.188},{59.169,1

2.125},{59.258,12.062},{59.499,12.000},{59.501,12.000},{5

9.742,12.062},{59.831,12.125},{59.890,12.188},{59.933,12.

250},{59.964,12.312},{59.984,12.375},{59.966,12.438},{60.

000,12.500}},{{59.000,10.500},{59.004,10.562},{59.016,10.

625},{59.036,10.688},{59.067,10.750},{59.110,10.812},{59.

169,10.875},{59.258,10.938},{59.499,11.000},{59.501,11.00

0},{59.742,10.938},{59.831,10.875},{59.890,10.812},{59.93

3,10.750},{59.964,10.688},{59.984,10.665},{59.966,10.562}

,{60.000,10.500}}},"InterpolationOrder"→4];

(*Lower Left Flexure Hinge*)

SMTMesh["A","Q1",{10,10},{{{1.500,5.000},{1.562,5.004},{1

.625,5.016},{1.688,5.036},{1.750,5.067},{1.812,5.110},{1.

875,5.169},{1.938,5.258},{2.000,5.499},{2.000,5.501},{1.9

38,5.742},{1.875,5.831},{1.812,5.890},{1.750,5.933},{1.68

8,5.964},{1.665,5.984},{1.562,5.966},{1.500,6.000}},{{3.5

00,5.000},{3.438,5.004},{3.375,5.016},{3.312,5.036},{3.25

0,5.067},{3.188,5.110},{3.125,5.169},{3.062,5.258},{3.000

,5.499},{3.000,5.501},{3.062,5.742},{3.125,5.831},{3.188,

5.890},{3.250,5.933},{3.312,5.964},{3.375,5.984},{3.438,5

.966},{3.500,6.000}}},"InterpolationOrder"→4];


```
(*Lower Right Flexure Hinge*)
SMTMesh["A","Q1",{10,10},{{{61.500,5.000},{61.562,5.004},
{61.625,5.016},{61.688,5.036},{61.750,5.067},{61.812,5.11
0},{61.875,5.169},{61.938,5.258},{62.000,5.499},{62.000,5
.501},{61.938,5.742},{61.875,5.831},{61.812,5.890},{61.75
0,5.933},{61.688,5.964},{61.665,5.984},{61.562,5.966},{61
.500,6.000}},{{63.500,5.000},{63.438,5.004},{63.375,5.016
},{63.312,5.036},{63.250,5.067},{63.188,5.110},{63.125,5.
169},{63.062,5.258},{63.000,5.499},{63.000,5.501},{63.062
,5.742},{63.125,5.831},{63.188,5.890},{63.250,5.933},{63.
312,5.964},{63.375,5.984},{63.438,5.966},{63.500,6.000}}}
,"InterpolationOrder"→4];
SMTAnalysis[];
SMTShowMesh["BoundaryConditions"→True]
SMTNextStep[1,.1];
While[
  While[step=SMTConvergence[10^-
8,15,{"Adaptive",8,.01,0.5,1}], SMTNewtonIteration[];];
```

```
   If[Not[step[[1]]],

SMTShowMesh["DeformedMesh"→True,"Field"→"v","Mesh"→Fals

e,"Show"→"Window"|{"Animation","Bending"},"BoundaryCondit

ions"→True];

    ];

   If[step[[4]]==="MinBound",SMTStatusReport["Error: Δλ <

Δλmin"];];

 step[[3]]

  ,If[step[[1]],SMTStepBack[];];

   SMTNextStep[1,step⬚2\[RightDoubleBracket]]  ];
```

APPENDIX F: AceFEM CODE FOR FEA OF CSA

```
<<AceFEM`;

Load=0.0015;

SMTInputData[];

SMTAddDomain["A","StrokeAmpMechanism",{"E *"-
>1103.61*10^6,"ν *"→0.4995, "t*"→0.001}];

SMTAddEssentialBoundary[Line[{{0.00000,0.00980},{0.00000,
0.01000}}],1->0,2->0];

SMTAddEssentialBoundary[Line[{{0.00590,0.00000},{0.00610,
0.00000}}],1->0,2->0];

SMTAddEssentialBoundary[Line[{{0.01000,0.00041},{0.01000,
0.00000}}],1->0];

SMTAddNaturalBoundary[Line[{{0.01000,0.00041},{0.01000,0.
00000}}],1->0,2→Load];

SMTMesh["A","Q1",{20,20},{{{0.00000,0.00980},{0.00898,0.0
0800}},{{0.00000,0.01000},{0.01000,0.00800}}},"Interpolat
ionOrder"→4];

SMTMesh["A","Q1",{20,20},{{{0.00071,0.00593},{0.01000,0.0
0800}},{{0.00023,0.00605},{0.00898,0.00800}}},"Interpolat
ionOrder"→4];
```

```
SMTMesh["A","Q1",{20,20},{{{0.00054,0.00573},{0.00794,0.0
0388}},{{0.00023,0.00605},{0.00804,0.00409}}},"Interpolat
ionOrder"→4];
SMTMesh["A","Q1",{20,20},{{{0.00000,0.00600},{0.00590,0.0
0000}},{{0.00023,0.00605},{0.00599,0.00019}}},"Interpolat
ionOrder"→4];
SMTMesh["A","Q1",{20,20},{{{0.00610,0.00000},{0.00795,0.0
0391}},{{0.00590,0.00000},{0.00776,0.00396}}},"Interpolat
ionOrder"→4];
SMTMesh["A","Q1",{20,20},{{{0.00795,0.00391},{0.01000,0.0
0000}},{{0.00805,0.00409},{0.01000,0.00036}}},"Interpolat
ionOrder"→4];
SMTAnalysis[];
SMTShowMesh["BoundaryConditions"→True]
SMTNextStep[1,.1];
While[
  While[step=SMTConvergence[10^-
8,15,{"Adaptive",8,.01,0.5,20}], SMTNewtonIteration[];];
  If[Not[step[[1]]],
SMTShowMesh["DeformedMesh"→True,"Field"→"v","Mesh"→Fals
e,"Show"→"Window"|{"Animation","Bending"},"BoundaryCondit
ions"→True];
    ];
```

```
    If[step[[4]]==="MinBound",SMTStatusReport["Error: Δλ <

Δλmin"];];

    step[[3]]

    ,If[step[[1]],SMTStepBack[];];

    SMTNextStep[1,stepΠ2\[RightDoubleBracket]]  ];
```

APPENDIX G: AceFEM CODE FOR FEA OF POLE VAULT

```
<<AceFEM`;

δ=0.50; (* 0.5 for non-dissipative model *)

β=((δ+0.5)/2)²;

Load=400;

SMTInputData[];

SMTAddDomain["A","PoleVaultHyperDynamic",{"E *"→26000,"ν

*"→0.4995, ,"δ*"→δ,"β*"→β}];

SMTAddEssentialBoundary[{ "Z"==0&,1->0,2->0,3->0},{

"X"□50.000 && "Z"□5000.000&,1->-100}];

SMTMesh["A","O1",{60,5,100},{{{{25.000,0.000,0.000},{37.5

00,3.350,0.000},{46.650,12.500,0.000},{50.000,25.000,0.00

0},{46.650,37.500,0.000},{37.500,46.650,0.000},{25.000,50

.000,0.000},{12.500,46.650,0.000},{3.350,37.500,0.000},{0

.000,25.000,0.000},{3.350,12.500,0.000},{12.500,3.350,0.0

00},{25.000,0.000,0.000}},{{25.000,12.500,0.000},{31.250,

14.170,0.000},{35.830,18.750,0.000},{37.500,25.000,0.000}

,{35.830,31.250,0.000},{31.250,35.830,0.000},{25.000,37.5

00,0.000},{18.750,35.830,0.000},{14.170,31.250,0.000},{12

.500,25.000,0.000},{14.170,18.750,0.000},{18.750,14.170,0

.000},{25.000,12.500,0.000}}},{{{25.000,0.000,5000.000},{
```

```
37.500,3.350,5000.000},{46.650,12.500,5000.000},{50.000,2
5.000,5000.000},{46.650,37.500,5000.000},{37.500,46.650,5
000.000},{25.000,50.000,5000.000},{12.500,46.650,5000.000
},{3.350,37.500,5000.000},{0.000,25.000,5000.000},{3.350,
12.500,5000.000},{12.500,3.350,5000.000},{25.000,0.000,50
00.000}},{{25.000,12.500,5000.000},{31.250,14.170,5000.00
0},{35.830,18.750,5000.000},{37.500,25.000,5000.000},{35.
830,31.250,5000.000},{31.250,35.830,5000.000},{25.000,37.
500,5000.000},{18.750,35.830,5000.000},{14.170,31.250,500
0.000},{12.500,25.000,5000.000},{14.170,18.750,5000.000},
{18.750,14.170,5000.000},{25.000,12.500,5000.000}}}}];

SMTAnalysis["Output"-
>"Deformation","PostOutput"→"BeamDynamic"];

SMTShowMesh["BoundaryConditions"→True]

SMTSave[ΔL,L,R];

f:=300; n:=20;

ω:=(2 Pi f n)/360;

Clear[λ];λ[t_]:=Sin[ω t];

Plot[λ[t],{t,0,1}]

SMTNextStep[0.01,λ];

While[

  While[step=SMTConvergence[10^-8,10,{"Adaptive

Time",8,0.001,1,1}], SMTNewtonIteration[];];

  If[Not[step[[1]]]

    ,force=(Plus@@ SMTResidual["Z"□5000.000&])[[2]];
```

```
    SMTPut[SMTRData["Time"],force,"TimeFrequency"→0.1];


SMTShowMesh["DeformedMesh"→True,"Field"→"u","Show"→"Win

dow"|{"Animation","column"},"BoundaryConditions"→True];];

  If[step[[4]]==="MinBound",SMTStatusReport["ΔT<ΔT_min"];];

  step[[3]]

  ,If[step[[1]],SMTStepBack[];];

  SMTNextStep[step [[2]] ,λ]  ];
```

APPENDIX H: AceFEM CODE FOR FEA OF FLEX-RUN

```
<<AceFEM`;

δ=0.50; (* 0.5 for non-dissipative model *)

β=((δ+0.5)/2)²;

SMTInputData[];

SMTAddDomain["A","FlexFootHYPERDynamic",{"E *"→26000,"ν

*"→0.4995,"t*"→22.22,"δ*"→δ,"β*"→β}];

SMTAddEssentialBoundary[Line[{{44.400,0.000},{44.400,6.67

0}}],1->0,2->0];

SMTAddNaturalBoundary["X"□95.460 && "Y"□197.580 &,2 ->

-Load];

SMTMesh["A","Q1",{85,5},{{{0.000,9.000},{21.749,2.273},{4

4.400,0.000},{58.610,2.500},{75.685,8.446},{94.009,17.109

},{113.549,29.859},{133.549,46.989},{150.486,66.782},{165

.483,91.199},{176.371,118.030},{182.040,142.080},{176.427

,166.358},{165.768,181.308},{147.117,193.606},{126.536,19

7.580},{95.460,197.580},{73.310,197.580}},{{2.597,15.144}

,{23.074,8.810},{44.400,6.67},{56.53,8.842},{73.168,14.62

3},{90.791,23.032},{109.773,35.217},{128.817,51.692},{145

.108,70.728},{159.532,94.211},{169.371,118.030},{175.367,

142.601},{170.431,163.437},{160.865,176.776},{144.639,187
```

```
.413},{126.536,190.910},{95.460,190.910},{73.310,190.910}
}}];

SMTAnalysis["Output"->"Deformation","PostOutput"→"
BeamDynamic"];

SMTShowMesh["BoundaryConditions"→True]

SMTSave[ΔL,L,R];

f:=300; n:=20;

ω:=(2 Pi f n)/360;

Clear[λ];λ[t_]:=Sin[ω t];

Plot[λ[t],{t,0,1}]

SMTNextStep[0.01,λ];

While[
  While[step=SMTConvergence[10^-8,10,{"Adaptive
Time",8,0.001,1,10}], SMTNewtonIteration[];];
  If[Not[step[[1]]]
    ,force=(Plus@@ SMTResidual["Y"□197.580&])[[2]];
    SMTPut[SMTRData["Time"],force,"TimeFrequency"→0.1];


SMTShowMesh["DeformedMesh"→True,"Field"→"Sxx","Show"→"W
indow"|{"Animation","column"},"BoundaryConditions"→True];


AppendTo[λucurve,{SMTData["Multiplier"],SMTPostData["v",{
73.310,197.580}]}];
```

```
   AppendTo[Misesv,SMTPostData[{"v","Mises

stress"},{73.310,197.580}]];

   ];

 If[step[[4]]==="MinBound",SMTStatusReport["ΔT<ΔT_min"];];

 step[[3]]

 ,If[step[[1]],SMTStepBack[];];

 SMTNextStep[stepΠ2\[RightDoubleBracket],λ] ];
```